Strength influencing parameters of iroko glued laminated timber

CIE5060-09: GRADUATION WORK

Written by: J.J. Hüpscher BSc

Student number: 1528599

Thesis committee:

prof.dr.ir. J.-W.G. van de Kuilen

dr.ir. G.J.P. Ravenshorst

dr.ir. P.C.J. Hoogenboom

TU Delft

Technische Universiteit Delft

Heko Spanten B.V.

Jesu Juva

Strength influencing parameters of iroko glued laminated timber

Scriptie

ter verkrijging van de graad van ingenieur
aan de Technische Universiteit Delft,
in het openbaar te verdedigen op
dinsdag 27 augustus om 14:00 uur

Door

Juval J. Hüpscher BSc

Preface

In completion of the Master Civil Engineering at the University of Technology Delft I present to you the thesis "Strength influencing parameters of iroko glued laminated timber". In the past two years I learned to review relevant literature, set up a programme for testing the strength of timber products and working towards a deadline. This report presents a theoretical background of the features that influence the strength of glued laminated timber, as well as its base material. Furthermore, tests in the laboratory have been conducted to examine bending strength of iroko glued laminated timber as well as tension strength of both iroko sawn timber and iroko finger joints. The experimental results were analysed, followed by several conclusions and recommendations.

I wish to express gratitude to prof.dr.ir. J.-W.G. van de Kuilen for offering me this interesting thesis subject and overseeing the thesis' process. I thank dr.ir. G.J.P. Ravenshorst for his feedback and providing the means to complete this report; also dr.ir. P.C.J. Hoogenboom his insight in the matter. I am very grateful to Mr L. van den Bosch for providing the iroko glued laminated beams and the unjointed and finger jointed lamellas. I am thankful for the people that assisted me in the process of completing this thesis: the employees of Heko Spanten B.V., the laboratory assistances at TU Delft, dr.ir. W. Gard and ir. P.A. de Vries from the Timber department and Prof. Dr.-Ing. F. Colling. He personally sent me one of his papers, which was very helpful as well as his dissertation on glulam bending strength.

This thesis is dedicated to my father, who studied Weg- en Waterbouwkunde at the HTS Utrecht and is therefore the most important civil engineer in my life. I am grateful for the faith-based life he lived; in this he will always be an example to me. His father studied Weg- en Waterbouwkunde at the TH Delft, and is therefore the second most important civil engineer in my life. He taught my father about Jesus of Nazareth, and so did my father to me. Papa, grandfather: thank you for who you are and for paving the way into this wonderful field of expertise.

Finally, my deepest gratitude belongs to the source of my life, the joy of my heart: Jesus of Nazareth. Ages ago he knew as a carpenter how to work with wood; and in these days He still inspires many people.

Abstract

As timber is being used for several millennia as construction material, glued laminated timber (glulam), a highly engineered timber product, exists for about hundred and fifty years. In Europe, it is nowadays common practise to make glulam from softwood species, though in the last few decades glulam made from different kinds of hardwoods emerged. Iroko glulam is part of this development, as iroko is a hardwood species from the African tropical regions.

The aim of this thesis is to investigate the bending strength of iroko glulam, as well as strength influencing features. From literature it is expected that the following features are of influence: density, modulus of elasticity, tension strength of the lamellas, finger joint strength and size. Several researches conducted in the past experiments to determine these mechanical and physical properties, focusing mainly on iroko sawn timber. Only few investigated iroko glulam, and none of those focused on finger jointed iroko glulam. In this lies the originality of this work: determining bending strength values of finger jointed iroko glulam, as well as density, modulus of elasticity and investigating mechanical and physical properties of the base material: iroko sawn timber and iroko finger joints. The laboratory experiments included the following: tension tests on 38 unjointed and 38 finger jointed lamellas, and four point bending tests on 12 glulam beams. Also density, modulus of elasticity and moisture content were determined.

The experimental results yield the following characteristic values: a lamella tension strength of 17 N/mm^2, a finger joint tension strength of 29 N/mm^2, and a glulam bending strength of 42 N/mm^2 (including size effect according to NEN-EN 1995, 2011).
The experimentally determined characteristic lamella tension strength is a little lower than values found in literature. This is due to a large scatter in the test results: a coefficient of variance equal to 0.37 was found. However, if the grain angle is equal or smaller than 5°, a higher lamella tension strength of 27 N/mm^2 is feasible. Grain angle is as expected a significant strength influencing parameter for iroko sawn timber. And it would suggest that the strength class is as expected D40 if the lamella bending strength equals 0.6 divided by the lamella tension strength.

The ratio of finger joint bending strength (30 N/mm^2) and tension strength (29 N/mm^2) on the characteristic level was found to be equal to 1.06. This is smaller than expected from theory: apparently the 1.4 ratio commonly assumed for softwood finger joint strength values does not hold for iroko finger joint strength values.

The investigated iroko glulam beams with depth 108 mm yielded a mean bending strength of 66 N/mm^2 and a characteristic bending strength of 42 N/mm^2. Due to the size effect and quasi-brittle failure this figures lie lower for full scale glulam beams, however, strength class GL24h is indeed a safe assumption for iroko glulam beams. These aspects explain the higher mean glulam bending strength compared to the mean finger joint tension strength of 40 N/mm^2.

A strong mathematical relationship between characteristic glulam bending strength and both lamella tension strength and finger joint strength was not found; however lamella and finger joint tension strength do influence the glulam bending strength. Furthermore, density does not influence any strength or stiffness property for both iroko sawn timber, finger joints, and glulam beams. Although there is a slight positive correlation with both dynamic and local modulus of elasticity of lamellas and its tension strength.

Nomenclature

The list below includes the symbols and abbreviations as they are used in this thesis. First Latin script letters are presented, followed by Greek script letters. The asterisk means that the unit depends on the considered quantity. In some cases, the same symbol is used to describe two parameters. However, the explanation in the text and the context in which the symbols are used will make the meaning of all symbols unambiguous.

Latin script

Symbol	Description	Unit
a	distance between support and nearest point load	mm
a	constant in lamination effect equation	N/mm^2
a	constant in regression line	*
b	width of lamella, glulam beam	mm
b	constant in lamination effect equation	-
b	constant in regression line	*
b_a	width of part a of batch II specimen	mm
b_b	width of part b of batch II specimen	mm
b_t	tip width (finger joint)	mm
b_{test}	width of test slice	mm
COV	coefficient of variance	*
E_{dyn}	dynamic modulus of elasticity	N/mm^2
E_{glob}	global modulus of elasticity	N/mm^2
$E_{glob,1}$	global modulus of elasticity due to LVDT 1	N/mm^2
$E_{glob,2}$	global modulus of elasticity due to LVDT 2	N/mm^2
E_{loc}	local modulus of elasticity	N/mm^2
$E_{loc,1}$	local modulus of elasticity due to LVDT 1	N/mm^2
$E_{loc,2}$	local modulus of elasticity due to LVDT 2	N/mm^2
$E_{loc,k}$	characteristic local modulus of elasticity	N/mm^2
$E_{loc,mean}$	mean local modulus of elasticity	N/mm^2
E_t	modulus of elasticity in tension	N/mm^2
$E_{t,1}$	modulus of elasticity in tension due to LVDT 1	N/mm^2
$E_{t,2}$	modulus of elasticity in tension due to LVDT 2	N/mm^2
$E_{t,k}$	characteristic modulus of elasticity in tension	N/mm^2
$E_{t,mean}$	mean modulus of elasticity in tension	N/mm^2
$E_{t,\alpha}$	modulus of elasticity in tension under angle α to grain	N/mm^2
f	least square function	
f_e	eigenfrequency	Hz
$f_{m,k}$	characteristic bending strength of sawn timber	N/mm^2
$f_{m,g}$	glulam bending strength	N/mm^2
$f_{m,g,k}$	characteristic glulam bending strength	N/mm^2
$f_{m,j,k}$	characteristic finger joint bending strength	N/mm^2
$f_{t,0}$	tension strength parallel to grain	N/mm^2
$f_{t,0,d}$	tension strength parallel to grain (design value)	N/mm^2
$f_{t,0,k}$	characteristic tension strength parallel to grain	N/mm^2
$f_{t,90}$	tension strength perpendicular to grain	N/mm^2
$f_{t,90,d}$	tension strength perpendicular to grain (design value)	N/mm^2

$f_{t,90,k}$	characteristic tension strength perpendicular to grain	N/mm^2
$f_{t,j}$	finger joint tension strength	N/mm^2
$f_{t,l}$	lamella tension strength	N/mm^2
$f_{t,l,k}$	characteristic lamella tension strength	N/mm^2
$f_{t,\alpha}$	tension strength under angle α to grain	N/mm^2
GLOB	global modulus of elasticity	N/mm^2
h_0	reference depth	mm
h	depth of lamella, glulam beam	mm
h_a	depth of part a of batch II specimen	mm
h_b	depth of part b of batch II specimen	mm
h_{test}	depth of test slice	mm
k_{disp}	factor to take into account stress distribution in top zone	-
k_h	size factor (involving depth)	-
k_l	size factor involving length	-
k_s (n)	statistical quantity	-
k_{vol}	volume factor	-
k_w	size factor involving width	-
l_0	reference length	mm
l_1	length over which local displacement is measured	mm
$l_{1,b}$	length over which local displacement is measured (LVDT 1)	mm
$l_{1,o}$	length over which local displacement is measured (LVDT 2)	mm
l	span length (with respect to bending test)	mm
l_{fj}	total width of finger joint	mm
l_j	finger length	mm
l_s	system length	mm
m_0	mass of test slice before drying	g
m_1	mass of test slice after drying	g
m	total mass of specimen	kg
max	maximum value of test results	*
MC	moisture content	%
MOE	modulus of elasticity	N/mm^2
MOR	modulus of rupture (bending strength)	N/mm^2
MUF	melamine-urea-formaldehydes	
min	minimum value of test results	*
m_k	characteristic bending or tension strength	N/mm^2
n	number of specimens	-
n	exponent	-
P	tension strength parallel to grain	N/mm^2
$P_{m,g}$	failure load in bending	kN
$P_{t,j}$	failure load in tension of finger jointed lamella	kN
$P_{t,l}$	failure load in tension of unjointed lamella	kN
PU	polyurethane	
p	pitch (finger joint)	mm
Q	tension strength perpendicular to grain	N/mm^2
R	resistance (strength, stiffness)	-
R^2	coefficient of determination	-
REF #	reference number	-
R_d	design value of resistance	-
R_k	characteristic value of resistance	-
S	solicitation (load)	-

S_d	design value of solicitation	-
S_k	characteristic value of solicitation	-
SoG	slope of grain	%
STAT	static bending	-
stdev	standard deviation	*
s_x	standard deviation	*
s_ρ	standard deviation of density	kg/m^3
t	least square function independent variable	
t_{test}	thickness of test slice	mm
w_0	reference width	mm
$\bar{x}$	mean value of test results	
x_i	a specimen's test result	
x_i	least square function independent variable	
y_i	least square function dependent variable	
Z	limit state function	-

Greek script

Symbol	Description	Unit
α	finger angle (finger joint)	°
α	grain angle	°
α	least square function parameter	
β	least square function parameter	
γ_M	material factor	-
γ_s	load factor	-
$\Delta P_{m,g}/\Delta w_{glob}$	slope of linear regression line of the load-global displacement curve of batch IV specimens	kN/mm
$\Delta P_{m,g}/\Delta w_{loc}$	slope of linear regression line of the load-local displacement curve of batch IV specimens	kN/mm
$\Delta P_{t,j}/\Delta w_t$	slope of linear regression line of the load-displacement curve of batch II specimens	kN/mm
$\Delta P_{t,l}/\Delta w_t$	slope of linear regression line of the load-displacement curve of batch I specimens	kN/mm
$\eta_{j,crack}$	percentage of finger joint failure	%
$\bar{\rho}$	mean value of density	kg/m^3
ρ	density	kg/m^3
ρ_k	characteristic density	kg/m^3
ρ_{mean}	arithmetic mean of density of the two parts of batch II specimen	kg/m^3
$\sigma_{t,0,d}$	timber tension stress under angle = 0° (design value)	N/mm^2
$\sigma_{t,90,d}$	timber tension stress under angle = 90° (design value)	N/mm^2
$\sigma_{t,\alpha,d}$	timber tension stress under angle = α (design value)	N/mm^2
φ	proportion of finger joint geometry	-
ω	moisture content	%

Table of contents

1. Introduction

1.1 Background of iroko timber

1.1.1 The iroko tree

Iroko (Figure 1, photograph taken in Togo) is a trade name for two tree species: *Milicia Excelsa* and closely related *Milicia Regia* (see NEN-EN 13556, 2003). The latter grows only in the tropical regions of west Africa; *M. Excelsa* however is widely spread over the tropical regions of the entire African continent. Its area of distribution ranges from Gambia, Senegal, Benin, central and east Africa to Mozambique (Figure 2).

Figure 1: Picture of an iroko tree (Togo).

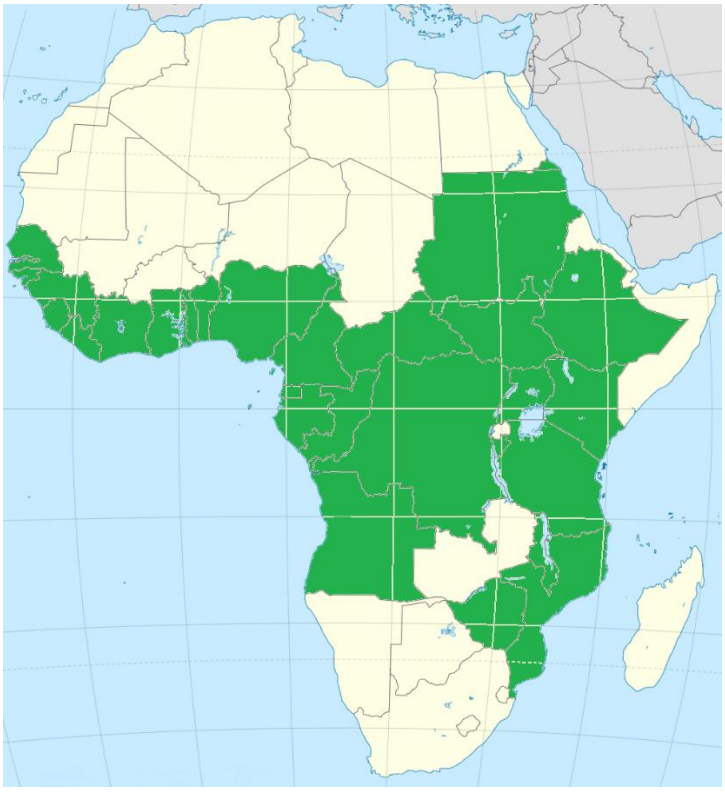

Figure 2: Area of distribution of M. Excelsa.

M. Excelsa is a deciduous tree with length 30-50 m, of which the first 20 m or more is without branches. Common trunk diameters are 2-10 m, with a straight and cylindrical trunk, and high, umbrella-like crown. The tree is ready to be harvested after 50 years, it provides high quality timber. It has been however excessively exploited because of this high quality; as of 2009 it is entitled as endangered (Orwa et al. 2009).

1.1.2 Iroko timber

Iroko timber is characterized by its great strength and durability, therefore it has many uses both indoors as outdoors. Examples are: construction work, furniture, boats, cabinet work, panelling, frames and floors. Freshly sawn planks have a colour range from colour of butter to brownish yellow, later on it darkens towards golden brown and dark brown (Figure 3).

Concerning its structural properties, NEN-EN 1912 (2012) assigns iroko timber to strength class D40 if graded according to BS 5756 (2007). This means among others a characteristic bending strength of 40 N/mm^2, a characteristic tension strength parallel to grain of 24 N/mm^2 and a mean modulus of elasticity in bending of 13000 N/mm^2.

Figure 3: Iroko planks.

1.1.3 Glued laminated iroko

In Europe, it is nowadays common practise to make glued laminated timber (in this thesis referred to as glulam) out of softwood species. European standard NEN-EN 14080 (2013) lists among others several types of spruce, fir, pine, and larch for which strength and stiffness requirements are defined. This standard covers only one hardwood species namely poplar. And in Germany, a national approval for beech glulam beams and hybrid (beech and softwood) glulam beams was assumed in recent years (Z-9.1-679, 2009); strength class up to GL48c is feasible with glulam. In a similar way, Technical Approval Z-9.1-577 (2015) recognizes glulam made of dark red meranti, a tropical hardwood species from South East Asia. If the lamellas meet certain conditions (regarding visual grade, dimensions, density, characteristic finger joint bending), the glulam beams are assigned to strength class GL24.
However, other hardwood glulam products are not covered (as of summer 2019) by any standard. For instance, glulam made of *Eucalyptus globulus* is currently under development in southern Europe: Spanish researchers investigated strength properties and concluded that strength class GL48c or higher is feasible when using *E. globulus* lamellas as base material (Lara-Bocanegra et al. 2017).
Another development is the production of glulam beams from iroko timber: Figure 4 shows a small convention centre consisting of iroko glued laminated columns, straight and curved beams. In the Netherlands, Heko Spanten B.V. is manufacturing these glulam beam for more than forty years. In this, strength class GL24h is assumed, however, it is not yet verified by research. Therefore the main goal of this thesis is to study the true strength profile of iroko glulam beams and what parameters influence its strength.

Figure 4: Iroko glued laminated structure.

1.2 Scope

This thesis will primarily focus on the following physical and mechanical properties of iroko sawn timber and glulam:

- density
- modulus of elasticity, both static and dynamic;
- bending strength of glulam beams;
- tension strength of sawn timber (lamellas);
- tension strength of finger joints;
- grain angle.

The reason behind this is as follows. NEN-EN 14080 (2013) states in clause 5.1.6.1 that in order to determine the glulam strength class by verification from full scale tests, density, modulus of elasticity and bending strength should be determined. This is also the case if one working with sawn timber (Table 2 from NEN-EN 408 (2016) suggests this). Moreover, the tension strength of lamellas is a lower bound value for the bending strength of glulam beams (see section 3.3 and subsection 5.2.4). The compression strength of sawn timber is not considered, as this property is less important than the tension strength: "the lamellas in the compression zone may have lower strength than the lamellas in the tension zone without affecting the load-bearing capacity of the glulam beams" (Colling, 1990).

The following strength and stiffness related features of iroko glulam beams will not be covered in this report: tension strength, compression strength, (rolling) shear strength, and (rolling) shear modulus. Also glueline quality, bond strength and adhesives are topics not covered in this thesis. Only for finger joints, two different kinds of adhesives are considered.
Concerning the influence of moisture content on mechanical properties this notion is made: the tension and bending strength and the modulus of elasticity of iroko sawn timber tends to decrease with increasing moisture content (Mvondo et al, 2017).

Regarding the quoted timber codes, this thesis assumes a European point of view. The timber codes widely used in European countries are identified with "EN" in the code's name. Furthermore, several national timber codes from European countries are occasionally quoted.

1.3 Research questions

For this thesis, the following main question is formulated:

- What defines the characteristic bending strength of iroko glulam beams, and which properties influence this bending strength?

Several sub questions arise from the main question, concerning both the glulam beams and its components:

- What is the relationship between the bending strength of iroko glulam beams on the one hand and the tension strength of lamellas and finger joints on the other hand?
- Of glulam beams: what is the relationship between the density/modulus of elasticity and the experimentally derived bending strength?
- Of lamellas: what is the relationship between the density/modulus of elasticity and the experimentally derived (finger joint) tension strength?

- How do visual features influence the lamella tension strength and glulam beam bending strength?
- Is the current strength class D40 as defined in NEN-EN 338 (2016) a proper choice for iroko lamellas?
- Is the assumed strength class GL24h as defined in NEN-EN 14080 (2013) a proper choice for iroko glulam beams?

1.4 Thesis structure

A flow chart of the thesis' structure is presented in Figure 5. Chapter 2 will discuss some statistics and the general concept of strength grading, for both sawn timber and glue laminated timber. Chapter 3 treats strength influencing parameters, such as density, stiffness, lamella tension strength, size and grain angle. Chapter 4 talks about mechanical and physical properties of iroko sawn timber and glulam, known from previous research programmes. Chapter 5 will extend this properties to an expected strength class for both sawn and glue laminated timber. Chapter 6 deals with how the test specimens were manufactured in the mill. Chapter 7 attends to how the experiments done on full scale iroko glulam beams and lamellas were performed. Chapter 8 presents the results from these experiments. Chapter 9 analyses the results; it addresses among others relationships between the stiffness, density and strength of both iroko lamellas and glulam beams. Chapter 10 brings the main study to an end with conclusions and recommendations.

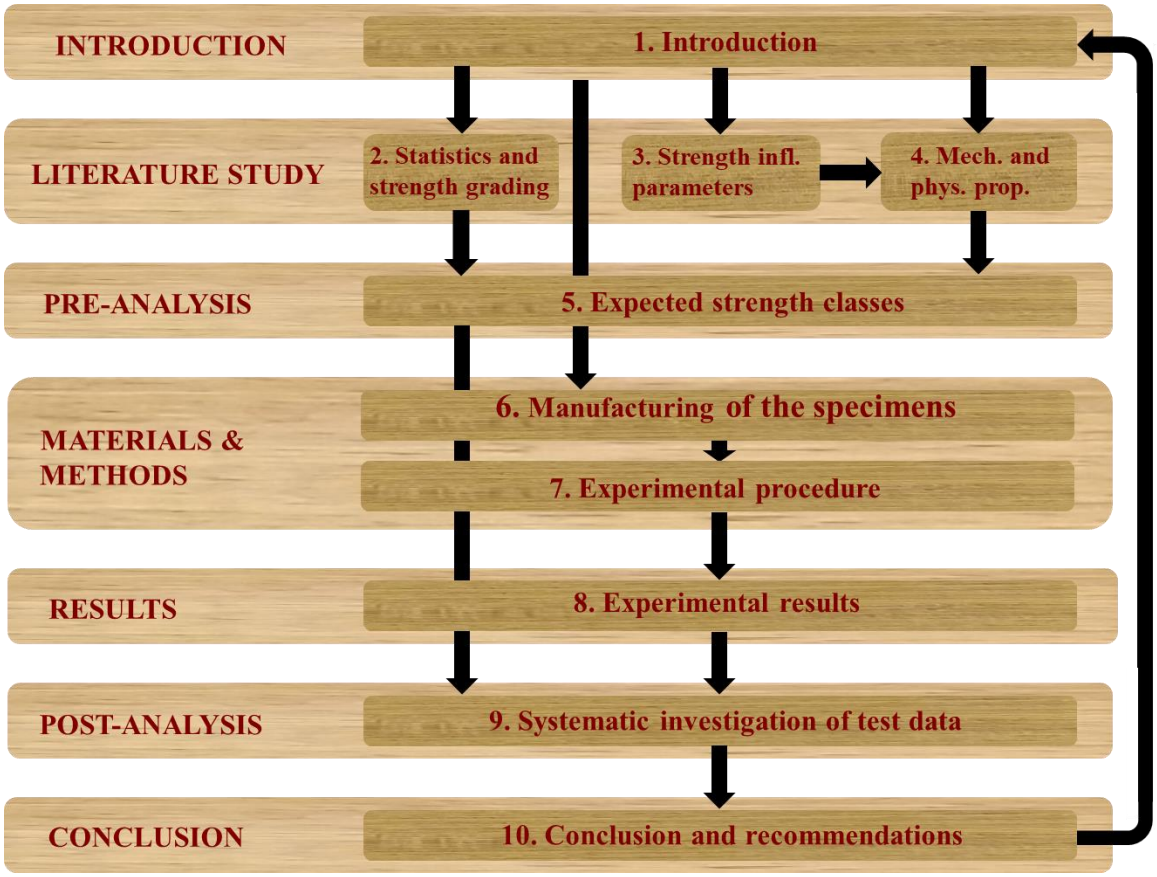

Figure 5: Flow chart thesis structure.

2. Statistics and strength grading of timber

2.1 Introduction

This chapter will deal with the concept of timber strength grading. To do so, the following two sections explain the background of probabilistic design, and how statistical quantities related to timber strength grading are determined. Section 2.4 will deal then with the reasons as to why timber in practise is strength graded, thereby different methods of strength grading will be elaborated on and an overview of current strength grades is given.

2.2 Probabilistic design of structures

When designing structures, the load in structural components should not exceed its strength. In algebraic terms this is expressed as: $Z = R - S \geq 0$, with Z being the limit state function, R the strength (resistance) of the material and S the load (solicitation) on the structure. As there is variability in both load and strength, in engineering practice one uses generally a semi-probabilistic approach as prescribed by the Eurocodes. This means that a certain probability distribution is assigned to both load and strength, usually a normal distribution. The fifth percentile then is called The characteristic value of a material property (strength, stiffness) R_k is then defined as the fifth percentile value; the characteristic value of the load S_k is defined as the 95th percentile. For a material property then the characteristic value is divided it by a material factor γ_M, for loads then the characteristic value is multiplied by a load factor. This results in the design value of material property and load, respectively:

$$R_d = R_k / \gamma_M$$
$$S_d = S_k \cdot \gamma_s$$

This is graphically shown in Figure 6 (Steenbergen, 2014). The material factor is implemented to take into account the following: uncertainties in the calculation model, scatter in dimensions and the difference between the structural component in a test setup and in a real structure. The load factor adjusts for (among others) uncertainties in the calculation model. The design value of the load then should not exceed the design value of the strength. This method is called a First Order Reliability Method, for details reference is made to existing literature on this topic (for instance Vrouwenvelder et al., 1982).

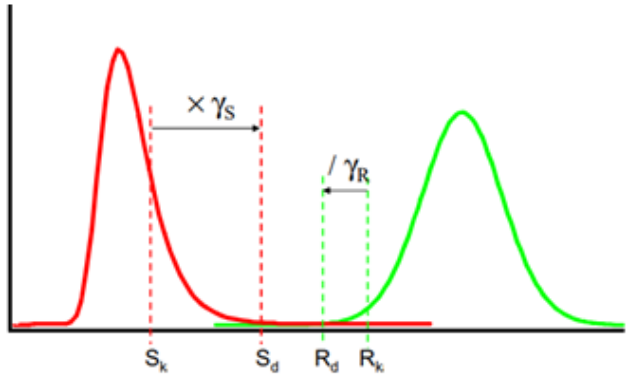

Figure 6: Solicitation and resistance function (Steenbergen, 2014).

From a probabilistic point of view this thesis will focus on characteristic values of material properties, as these define a so called strength grade of timber. The next subsection will therefore elaborate on how to determine certain statistical quantities, including these characteristic values.

2.3 Overview of statistical quantities

This section presents the statistical quantities that are used in these thesis. In all of the equations, the quantity *n* represents the number of specimens involved.

Sample mean (in this thesis generally referred to as "mean"):

$$\bar{x} = \frac{\sum_{i=1}^{n} x_i}{n}$$

Standard deviation according to NEN-EN 14358 (2016):

$$s_x = \max \begin{cases} \sqrt{\frac{\sum_{i=1}^{n} \left(x_i - \bar{x}\right)^2}{n-1}} \\ 0.05\bar{x} \end{cases}$$

Coefficient of variance:

$$COV = \frac{s_x}{\bar{x}}$$

Characteristic value of bending strength (glulam beams) and tension strength (lamellas, finger joints) according to NEN-EN 14358 (2016) and NEN-EN 384 (2016):

$$m_k = \frac{\bar{x} - k_s(n) \cdot s_x}{k_h}$$

$$k_s(n) = \frac{6.5n + 6}{3.7n - 3}$$

$$k_h = \min \begin{cases} (150/b)^{0.2} \\ 1.3 \end{cases} \qquad \text{sawn timber}$$

$$k_h = 1.0 \qquad \text{finger jointed lamellas}$$

$$k_h = \min \begin{cases} \left(\frac{600}{h}\right)^{0.1} \\ 1.1 \end{cases} \qquad \text{glulaminated timber}$$

Characteristic value of density according to NEN-EN 14358 (2016):

$$\rho_k = \overline{\rho} - k_s(n) \cdot s_\rho$$
$$k_s(n) = \frac{6.5n + 6}{3.7n - 3}$$

Least square method to determine linear regression curve (determined by EXCEL):

$$f = \alpha t + \beta$$
$$\beta = \frac{n\sum_{i=1}^{n} x_i y_i - \left(\sum_{i=1}^{n} x_i\right)\left(\sum_{i=1}^{n} y_i\right)}{n\sum_{i=1}^{n} x_i^2 - \left(\sum_{i=1}^{n} x_i\right)^2}$$
$$\alpha = \overline{x}_n - \beta \overline{y}_n$$

In which x is the independent variable and y is the dependent variable.

Coefficient of determination (f_i are the modelled value; determined by EXCEL or MAPLE):

$$R^2 = 1 - \frac{\sum_{i=1}^{n}(x_i - f_i)^2}{\sum_{i=1}^{n}(x_i - \overline{x})^2}$$

2.4 Strength grading and strength classes

2.4.1 Sawn timber

Concerning the building material timber, it stems from trees who greatly differ in species, growth area and environmental conditions during growth. These trees then are cut in varies ways and sizes to end up with sawn timber. All this factors induce a great variability in timber properties: even between boards cut from the same tree great variety occurs. It may even be so that within a timber species the strongest specimen is ten times stronger than the weakest specimen (Blaß et al., 2017). To utilise then timber economically, one uses so called strength grades. By introducing strength grades the variability within the classes is greatly reduced, see Figure 7 (Glos, 1995).

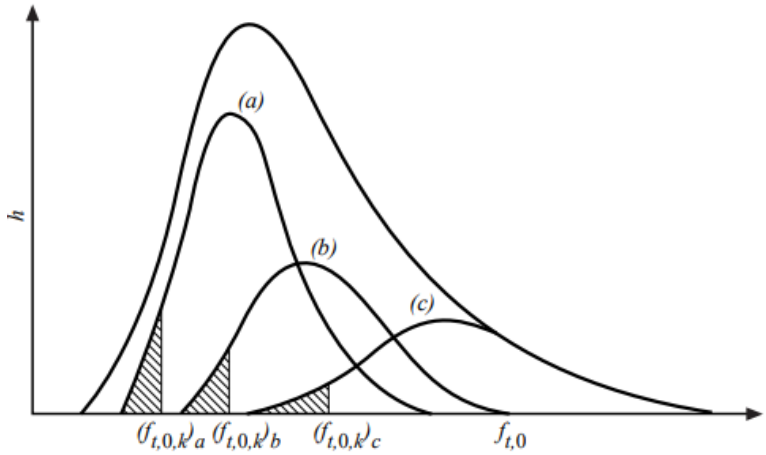

Figure 7: Graded timber assigned to three grades a, b and c, reducing the variability (Glos, 1995).

However, some overlap is present as a result of the accuracy of the grading method. For the strength of an individual specimen is unknown, this must be determined by a strength grading method: visual grading or mechanical grading.

Visual grading aims at deriving strength and stiffness properties on the basis of visual features of timber specimens such as knot size or ratio, grain angle or slope of grain, pith, growth rings, fissures and distortions like bow, spring, twist and cup. Different grades then have different limitations on these features: the higher the grade, the more strict these limitations are. Visual grades generally vary per country, therefore NEN-EN 14081-1 (2016) prescribes certain minimum requirements for national visual grading rules. NEN-EN 1912 (2012) then assigns these national grades combined with timber species to the strength classes listed in NEN-EN 338 (2016). A strength class is then a cluster of mechanical and physical properties to be used in engineering practice: among the listed properties per strength class are bending, tension and compression strength parallel and perpendicular to the grain, modulus of elasticity, shear modulus, and density. NEN-EN 338 (2016) lists three types of strength classes: C-classes for softwood species in bending, T-classes for softwood species in tension and D-classes for hardwood species. Kovryga et al. (2016) proposes even so called DT-classes: tension classes for hardwood species, based on temperate hardwood species such as maple and ash.

Three examples are presented of visual grades and designated strength classes:

- The German visual strength grading code for hardwoods DIN 4074-5 (2008) distinguishes three grades: LS 7, LS 10 and LS 13. For instance, one of the limitations given is that the slope of grain cannot be greater than 12% for grade LS 10. NEN-EN 1912 (2012) assigns oak that meets the requirements of LS 10 to strength class D30. This strength class then involves a characteristic bending strength of 30 N/mm^2, a mean modulus of elasticity of 11000 N/mm^2 and a characteristic density of 530 kg/m^3.
- The British visual strength grading code for hardwoods BS 5756 (2007) distinguishes five grades: HS for tropical hardwood species, and TH1, TH2, THA and THB for temperate hardwood species. NEN-EN 1912 (2012) assigns iroko that meets the requirements of HS to strength class D40.
- The Dutch visual strength grading code for hardwoods NEN 5493 (2011) distinguishes three grades: C3 STH for tropical hardwood species, and both C3 EHA and C3 EHB for European hardwood. NEN-EN 1912 (2012) assigns azobé that meets the requirements of C3 STH to strength class D70.

Machine grading aims to measure mechanical and/or physical properties like modulus of elasticity (static or dynamic) and density by a grading machine. These properties correlate then to bending strength values, by which the specimens can be assigned to strength classes: indicating properties are characteristic bending strength, mean local modulus of elasticity and characteristic density.

Furthermore, NEN-EN 14081-1 prescribes some visual override inspection requirements for machine graded timber.

Combining visual and machine grading may increase correlation with strength (Glos, 1995). For example, Ehrhart et al. (2016) describes strength grading procedures of beech lamellas, in order to produce glulam beams. These lamellas were graded with regard to knot size and dynamic modulus of elasticity: combining these grading parameters led to a greater yield. These researchers defined new tension strength classes exceeding the existing ones given in NEN-EN 338 (2016).

2.4.2 Glued laminated timber

NEN-EN 14080 (2013) defines strength classes for glulam beams made of softwoods. This standard distinguishes between homogeneous glulam and combined glulam. This refers to the lay-up of the glulam beams: the lamellas in homogeneous glulam are from the same (tension) strength class, the lamellas in combined glulam have different strength. Typically combined glulam is more efficient in bending, as the outer lamellas are of higher strength compared to the inner lamellas.
In Germany this way of designing is extended and legalized for beech glulam by means of Technical Approval Z-9.1-679 (2009). In this strength classes are defined with characteristic bending strengths exceeding those of NEN-EN 14080 (2013): GL28h and GL32c till GL48c. Requirements for two types of beech glulam beams are given: combined glulam beams entirely made of beech lamellas, and hybrid glulam beams in which the outer lamella are made of beech and the inner lamellas made of softwood.

3. Strength influencing parameters of glued laminated timber

3.1 Introduction

Glulam is a highly engineered timber product made of sawn timber (lamellas), finger joints and adhesive(s). These components all have influence on the strength of glued laminated timber. Frese et al. (2006) reports that the strength influencing parameters for beech glulam are: finger joint bending strength and lamella tension strength; the latter depends on knot ratio values and dynamic modulus of elasticity. And Brandner et al. (2008) reports the following parameters which influence the strength of glulam beams (assuming softwood): knots, density, modulus of elasticity, lamellas in the tension zone, finger joints and size. Moreover, the grain angle influences the tension strength of lamellas, therefore it will be considered as well. The following sections elaborate on these parameters, with the exception of knots. For although they are a strength reducing factor both in sawn timber and glulam, their occurrence is very rare in iroko timber and therefore not considered in this report. The sections of this chapter will also include how these parameters were implemented into European (building) standards.

3.2 Density, modulus of elasticity and lamellas in the tension zone

The base material of sawn timber, the tree trunk, consists of woody cells at the microscopic level. The cell wall thickness governs the strength and stiffness of the cells. Assuming that the amount of cell wall material determines both strength and stiffness of small clear wood, this suggests a relationship between density and modulus of elasticity on the gross level. Ravenshorst (2015) points out indeed a linear relationship between density and bending strength and between density and modulus of elasticity for clear wood.

As for glulam, Colling (1990) reports that with increasing quality of the outer lamellas in the tension zone, the strength of the glulam beam increases. In this, quality means not only appearance but also density and modulus of elasticity: lamellas with a high MOE in the tension zone are very beneficial to the bearing capacity. If indeed the density of the tension zone lamellas increases, so will its bending strength and related to the bending strength the tension strength.

The stress state of a bending beam is triangular shaped when assuming linear elastic material properties (in reality some nonlinear behaviour will occur). With increasing beam depth, the stress state in the outer lamella will approach a pure tension stress state, see Figure 8. Therefore the lamella tension strength is a lower limit for the glulam bending strength. This is also why the glulam bending strength increases with increasing lamella tension strength. From tests, it appears that the glulam bending strength is usually greater than the lamella tension strength. This will be discussed in the next section.

From Tables 3-5 in NEN-EN 14080 (2013) it is clear that with increasing strength class (bending strength), modulus of elasticity and density generally increase as well. (In spite of the fact that NEN-EN 14080 (2013) is not valid for glue laminated tropical hardwood.)

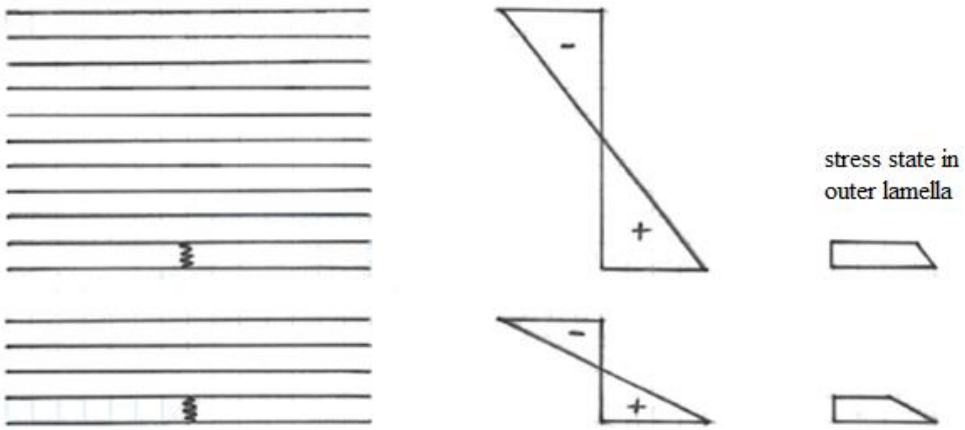

Figure 8: Bending stress state of two glulam beams with different depths.

3.3 Laminating effect

Glulam beams consist of lamellas, which usually possess a tension strength smaller than the bending strength of the glulam beam. This is the so-called laminating effect, caused by three distinct, though interrelated, physical effects: the effect of the tension test procedure, there is reinforcement of defects and dispersion of low-strength timber (Falk ea. 1995).

3.3.1 Effect of tension test procedure

Defects such as knots present outside of the centre of the member or areas of asymmetrical density can induce lateral bending stresses. For the European standard NEN-EN 408 does not prescribe lateral restrains during tension tests (see Figure 9). If these bending stresses are combined with tension stresses (which are obviously present during a tension test), they will reduce the measured tension strength. On the contrary, in glulam beams these lateral bending stresses are negligible since these defects are restrained by the nearly rigid glue lines. This is one reason why the measured tension strength of lamellas is smaller than the bending tension strength of glulam beams.

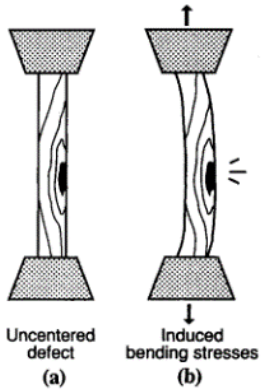

Figure 9: Induced bending stresses in standard tension tests: (a) no defect; (b) with off-centred defect (Falk ea. 1995).

Factors influencing this difference are the beam depth and the length of the specimen. The tension lamella in a shallow beam is subjected to both tension and bending stresses, in a deep beam mainly to tension stresses. Furthermore, as the specimen length increases, the probability of an excentric defect also increases.

3.3.2 Reinforcement of defects

In a glulam beam, defects and other low-stiffness areas are reinforced by adjacent lamellas, at least at one side. This provides alternative paths for stresses to flow around the defect through adjacent areas with greater stiffness. In other words, redistribution of stresses is possible in glulam through the clear wood of neighbouring lamellas (see Figure 10) which increases the capacity of the cross section with a defect.

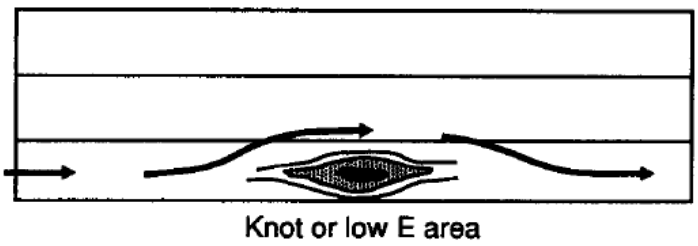

Figure 10: Redistribution of stresses around defect or low density area (Falk ea. 1995).

3.3.3 Dispersion of low-strength timber

In a population of tension specimens, the lower strength pieces will be represented in the characteristic tension strength $f_{t,l,k}$. If this same tension specimens however were put into a glulam beam, the probability that the lowest strength pieces would be positioned at a high-stressed location that initiate failure is lessened. A quote from Falk et al. (1995): ”Therefore, because low-strength timber pieces are distributed throughout the glulam beam volume, there is a decreased probability that the lowest strength timber piece will initiate beam failure.”

3.3.4 Relevance of the laminating effect

As mentioned, the laminating effect is the phenomenon that the glulam bending strength is greater than the lamella tension strength. Falk et al. (1995) reports laminating factors (ratio glulam bending strength / lamella tension strength) for European glulam beams between 1.06 and 1.56, and for North American glulam between 0.95 and 2.51. Considering iroko timber, it is likely however that this ratio will be greater than 1.00. Although iroko timber shows hardly any defects such as knots, grain angle does occur and finger joints generally weaken the cross section. Despite the high quality of the base material in glulam iroko beams, the tension strength of the lamella is a lower bound value for the glulam bending strength.

3.3.5 Models of the lamination effect and its implementation in standards

Brandner et al. (2008) gives an extensive overview of research done within a time frame of almost twenty years (focus in this paper is on spruce glulam; no requirements for finger joints are mentioned). Reported are 19 equations relating the characteristic glulam bending strength with the characteristic lamella tension strength, of which 16 are linear (with varying reference dimensions):

$$f_{m,g,k} = a + b \cdot f_{t,l,k}$$

In which *a* ranges from 3.5 to 12 and *b* ranges from 1 to 1.4. Also 3 power functions were given:

$$f_{m,g,k} = \left(2.7 - 0.04 \cdot f_{t,l,k}\right) f_{t,l,k}$$

$$f_{m,g,k} = \left(2.35 - 0.035 \cdot f_{t,l,k}\right) f_{t,l,k}$$

$$f_{m,g,k} = 2.7\, f_{t,l,k}^{0.8}$$

Figure 11 gives a graphical representation of 13 equations (10 unique linear relationships and 3 power functions), without adjusting to reference dimensions and size factors.

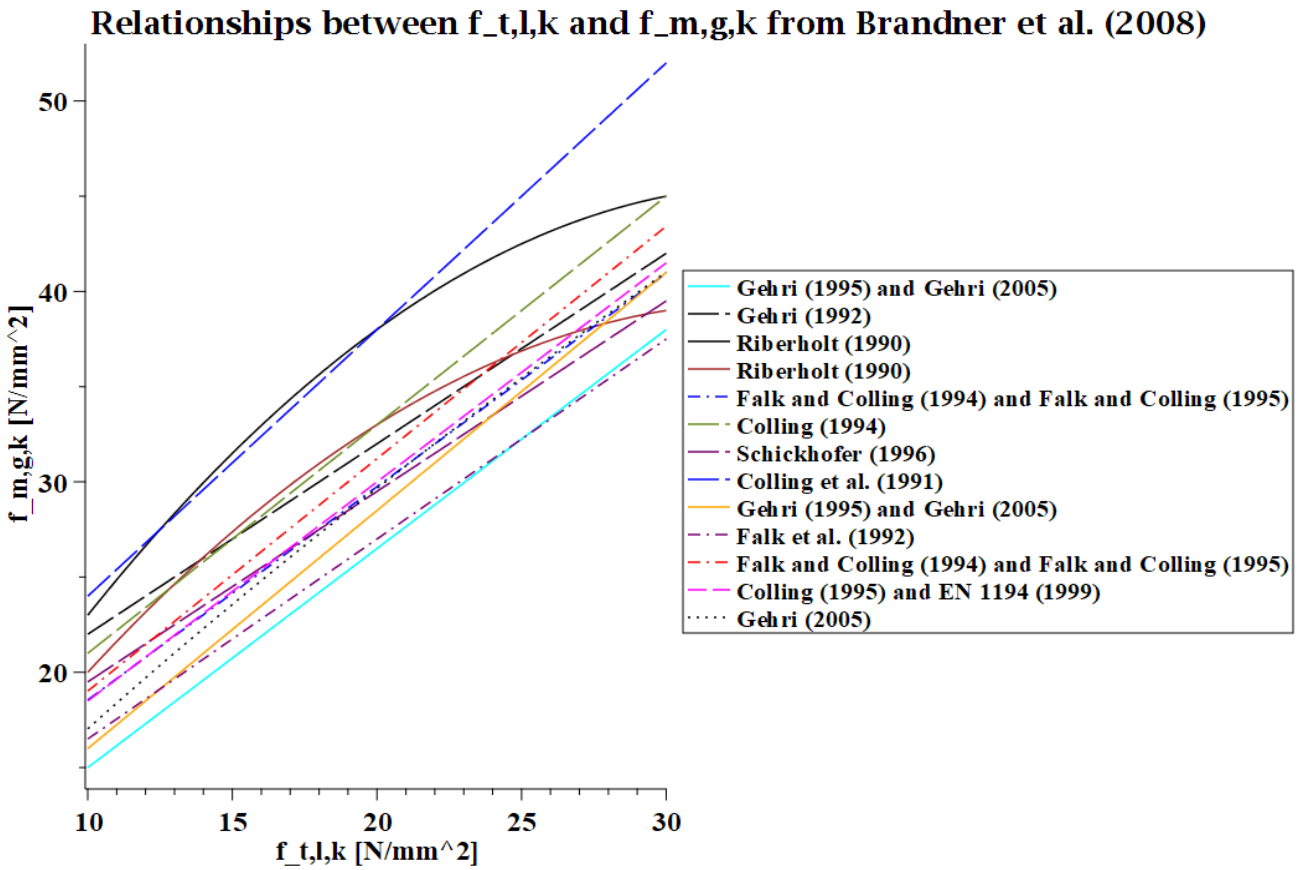

Figure 11: Relationships between the characteristic lamella tension strength ($f_{t,0,l,k}$) and the characteristic glulam bending strength ($f_{m,g,k}$), unadjusted to reference dimensions and size factors (Brandner et al, 2008).

The equation given in NEN-EN 1194 (1999) is included in the graph of Figure 11:

$$f_{m,g,k} = 7 + 1.15 f_{t,l,k}$$

Note that the influence of finger joints is taken account in none of the above mentioned relationships. Subsection 3.4.3 will deal with models including the finger joint strength.

3.4 Finger joints

3.4.1 Introduction

By means of finger joints, the lamellas can be extended and therefore the length of a glulam beam may exceed the length of the base material, the planks. There are mainly two types of finger joints: regular finger joints (Figure 12) and large finger joints (Figure 13). Large finger joints are used as moment resisting joints in e.g. frame corners of three-hinged frames. This topic will not be further elaborated in this thesis.

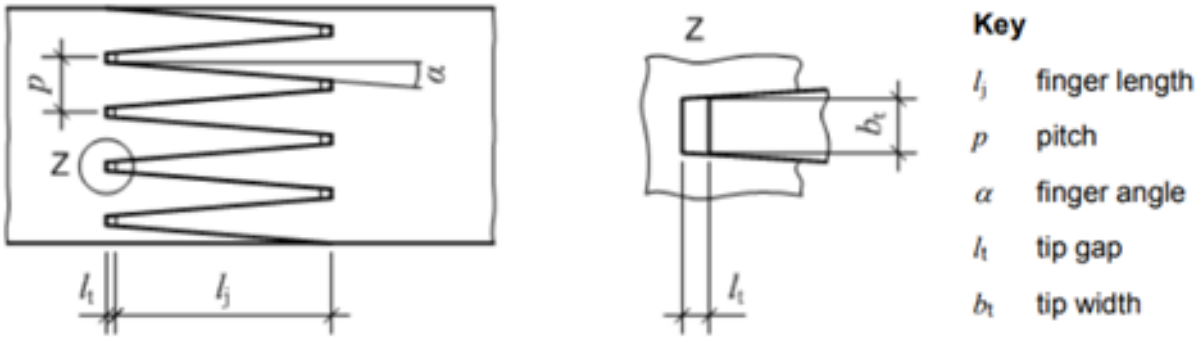

Figure 12: Regular finger joints (NEN-EN 14080, 2013).

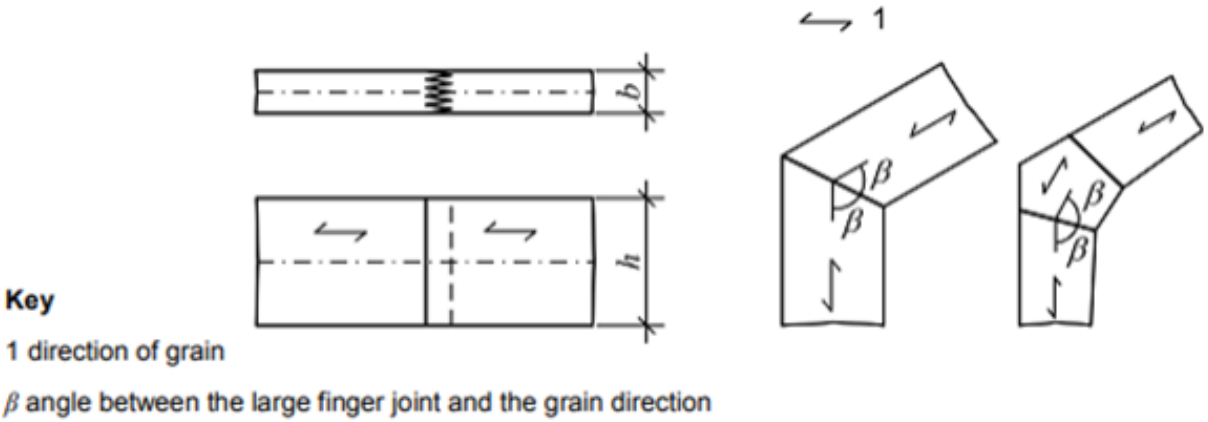

Figure 13: Large finger joints (NEN-EN 14080, 2013).

Furthermore, it is worth noticing their predecessor: the scarf joint (Figure 14). This kind of joint is hardly used nowadays; Colling (1990) reports that they are stronger but more difficult to manufacture compared to finger joints. Moreover, they are not very efficient regarding material usage, for it requires the horizontal length of the joint from both lamellas to create it. Despite this, scarf joints will be briefly mentioned again in Chapter 4.

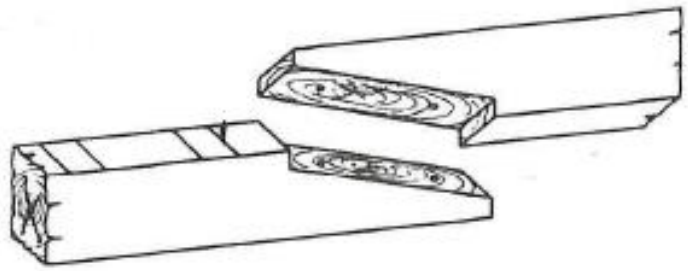

Figure 14: Scarf joint (Goldstein, 1999).

3.4.2 Overview of strength influencing parameters

Regarding the finger joint strength, one distinguishes between the tension strength and the bending strength. Glulam beams are generally loaded in bending, though the stress state in the outer lamella approaches the stress state of pure tension (as mentioned earlier in section 3.2 and shown in Figure 8). Thus the stress state in a finger joint in the outer lamella approaches pure tension.
In a finger joint without glue, the tension strength is equal to zero, but its bending strength can be greater than zero due to interlocking of the fingers. The tension test is therefore the basic case in which wood failure can also occur. For quality control purposes in factories, one uses a four point bending test setup to determine the bending strength of finger joints. This is because these tests are relatively easy to perform: no clamping of the specimens is necessary and a lower force is required.

Colling (1990) investigated the finger joint strength, although not always specifically making this distinction between bending and tension. He mentioned among others the following strength influencing factors (focused on softwoods, mostly spruce):

Density and modulus of elasticity
Colling's performed research on 845 finger joints loaded in bending pointed out a coefficient of determination of 0.25 between density/modulus of elasticity and finger joint bending strength.

Geometry
The proportion $\varphi = 2l_j/p$ is a measure for the glue surface per unit width for the transfer of forces. As this ratio increases, the finger joint strength increases: this holds for values up to $\varphi \approx 8$ concerning the timber species sitka spruce. Furthermore, with increasing tip width b_t the finger joint strength decreases, because there is no transfer of forces possible through the gap between fingertip and wood. The forces need to be rerouted, which induces additional peak stresses around the gap area. Colling's research seemed to confirm these findings: the 205 finger joints with nominal finger length of 15 mm and mean φ equal to 7.1 were on average stronger than the 640 finger joints with nominal finger length of 20 mm and mean φ equal to 6.0 (although in this the definition $\varphi = 2l_j / (p \cos \alpha)$ was used).

Production factors
The following production factors can influence the finger joint strength negatively: inadequate adhesive injectors, poor clamp pressure, too high or too much varying moisture content, non-uniformly adhesive flow, blunt grinders (therefore regularly sharpening of the grinder is required for a high finger joint quality).

To conclude, the probability of beam fracture induced by finger joint failure increases with increasing quality of the lamellas in the tension zone. This is of particular interest for glulam beams made of high quality timber such as iroko glulam. Therefore the finger joint strength may serve as an upper limit of the glulam bending strength (if there would be no lamination effect).

3.4.3 Implementation in standards
Frese et al. (2006) and Frese et al. (2009a) introduced models in which the glulam bending strength is related to both the lamella tension strength and the finger joint bending strength, for beech and spruce glulam beams, respectively. These are quadratic functions, the equation found for spruce glulam was (the empirically found relation for beech glulam was similar, though with other constants):

$$\begin{cases} f_{m,g,k} = 3.454 + 0.7125 \cdot f_{m,j,k} - 0.01078 \cdot f_{m,j,k}^2 - \\ 0.001632 \cdot f_{t,l.k}^2 + 0.02558 \cdot f_{m,j,k} \cdot f_{t,l,k} \end{cases} \qquad 13\,N/mm^2 \le f_{t,l,k} \le 21\,N/mm^2$$

$$\begin{cases} f_{m,g,k} = -17.39 + 1.636 \cdot f_{m,j,k} - 0.01644 \cdot f_{m,j,k}^2 + \\ 0.008169 \cdot f_{m,j,k} \cdot f_{t,l,k} \end{cases} \qquad 22\,N/mm^2 \le f_{t,l,k} \le 35\,N/mm^2$$

These equations assume that $f_{m,j,k} / f_{t,j,k} = 1.4$, according to NEN-EN 14080 and stem from finite element simulations and were experimentally verified (see also Frese et al., 2009b).
Even earlier, in 2005 the successor of NEN-EN 1194 (1999) was presented as the new norm NEN-EN 14080. The most recent update of this is the 2013 version, it includes unlike NEN-EN 1194 (1999) a relationship between the glulam bending strength on the one hand and the lamella tension strength and the finger joint bending strength on the other. However, this expression is somewhat different than those presented by Frese et al. (2006) and Frese et al. (2009a), though it is valid for numerous softwoods and poplar:

$$f_{m,g,k} = -2.2 + 2.5 f_{t,l,k}^{0.75} + 1.5\left(f_{m,j,k} / 1.4 - f_{t,l,k} + 6 \right)^{0.65}$$

This power function is only valid if the finger joint bending strength is in the following range:

$$1.4 f_{t,l,k} \leq f_{m,j,k} \leq 1.4 f_{t,j,k} + 12$$

It appears that the NEN-EN 14080 (2013) expression yields in general higher values than the expression from Frese et al. (2009a): Figure 15 shows the curves for $f_{m,j,k}$ ranging from 30 to 50 N/mm^2 in steps of 10 N/mm^2. In this the dashed lines represent the Eurocode formula and the solid lines represent the quadratic formulae from Frese et al. (2009a).

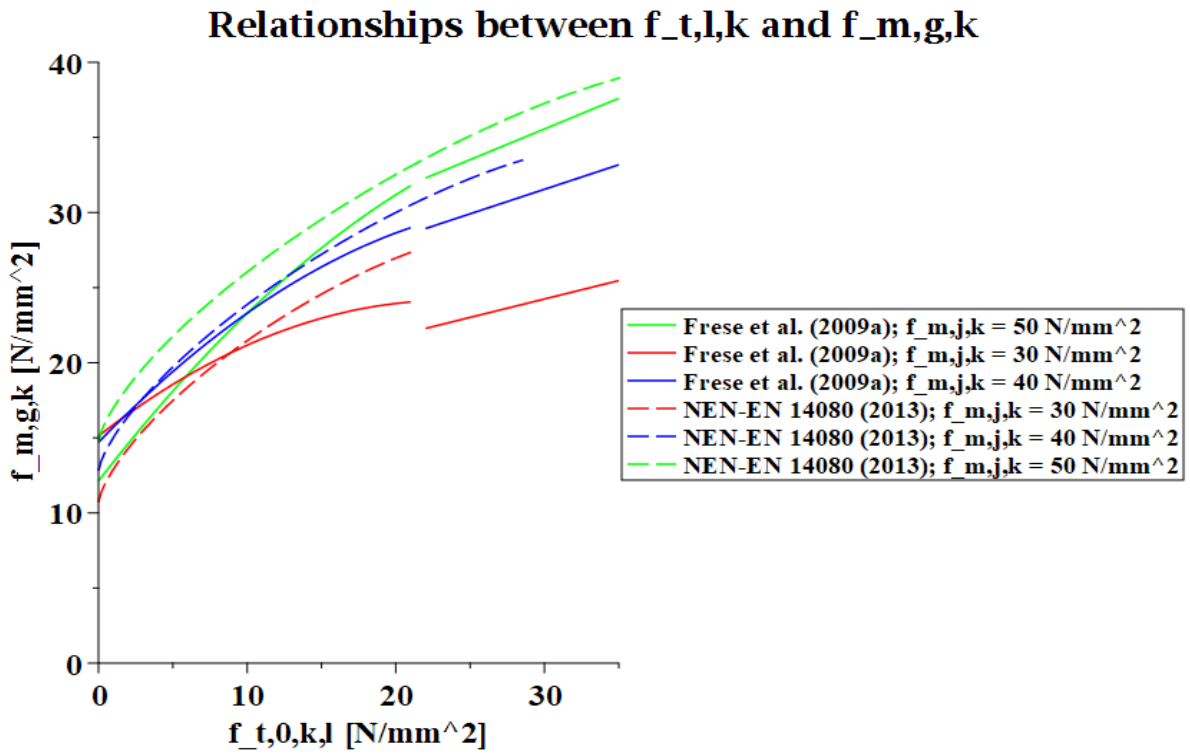

Figure 15: Relationships between the characteristic lamella tension strength ($f_{t,l,k}$) and the characteristic glulam bending strength ($f_{m,g,k}$);solid lines by Frese et al. (2009a) and dashed lines from NEN-EN 14080 (2013).

3.5 Size effect

Timber loaded in tension fails in a brittle way. Therefore, the size effect should be taken into account. This means in short that the strength decreases as the stressed volume increases. It is based on the weakest link theory: a chain loaded in tension is as strong as its weakest link, developed by Weibull and others. In Eurocode 5 (NEN-EN 1995-1-1) the following expression is used to take into account the size effect for sawn timber loaded in tension or bending:

$$k_h = \min \begin{cases} \left(\frac{150}{h} \right)^{0.2} \\ 1.3 \end{cases}$$

In which *h* is the depth in case of bending, and the width in case of tension. One should notice however that the stress state of bending is a combination of compression and tension. Therefore the weakest

link theory is debatable when applied to bending, and research results show discrepancy in the case of bending (Rouger, 1995). This Eurocode expression is therefore a compromise.

For glulam beams, the influence of the size effect is less compared to sawn timber, as the lamination effect increases the strength. Furthermore, in case of bending with constant span to depth ratio (as is prescribed by NEN-EN 408, 2012), the size effect is depended on the depth of the beam. Eurocode 5 gives the following, again simplified expression:

$$k_h = \min \begin{cases} \left(\frac{600}{h}\right)^{0.1} \\ 1.1 \end{cases}$$

Figure 16 shows this expression as function of *h*, as well as without the truncation of 1.1. For depth beams smaller than about 231 mm, the size factor would increase rapidly without this truncation.

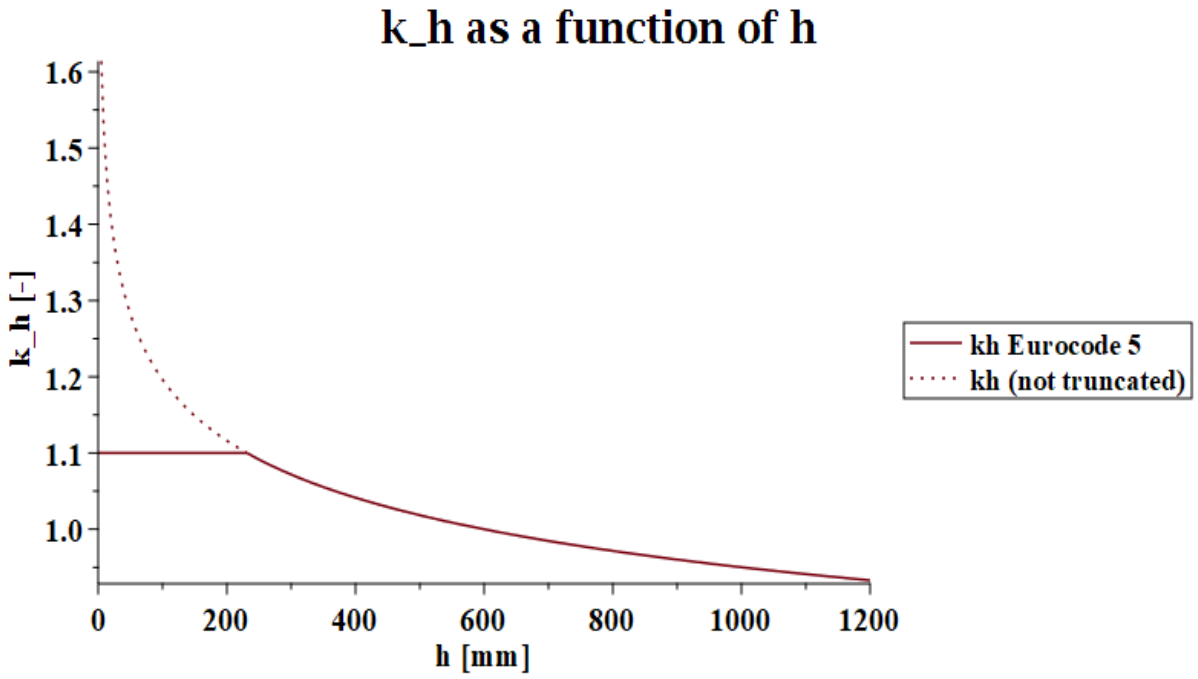

Figure 16: k_h *as a function of* h.

The exponent of 0.1 in this expression is based on several studies and it assumes a reference depth of 600 mm. This formula though is being discussed, as the determination of the size factor depends on the way of grading and testing conditions. Moreover, bending is not a purely brittle failure mode for timber (as mentioned). What is more, for timber beams with a depth greater than 600 mm, the material factor γ_M has to compensate for the decrease in strength when constructing according to NEN-EN 1995-1-1 (2011). Literature however agrees on one thing: the size effect does occur for timber beams. For instance, the computer simulations done by Frese et al. (2009a) indicates that a size factor of 0.85 applies for a beam depth of 1800 mm, and a size factor of 1.09 for a beam depth of 300 mm or less.

In the case of iroko glulam beams, it is unknown how the size effect will manifest itself. For the Eurocode 5 formula holds for all species that meet the requirements of NEN-EN 14080 (2013) which consists only of softwood species and poplar), and the mentioned research was conducted on the basis of data taken from spruce beams. Yet the results from the bending tests will most likely yield a higher characteristic bending strength than the beams with greater depth used in practice.

3.6 Grain angle

Softwoods loaded in tension commonly fail at the knot (Van der Have, 2013). However, as knots are usually not present in iroko timber, loaded in tension it may fail due to slope of grain (SoG). According to Wiselius (1994) iroko's grain is characterized as straight till interlocked (Figure 17), and occasionally wavy grain (Figure 18) may occur.

Figure 17: Interlocked grain.

Figure 18: Wavy grain.

Concerning the timber feature "grain angle", codes usually speak of "slope of grain" rather than grain angle. Slope of grain may be presented as a proportion (for example 1:10) or a percentage. The two designations slope of grain and grain angle refer however to the same feature and are related as follows:

$$\text{Slope of grain} = \tan(\text{grain angle}) \qquad \text{SoG represented as proportion}$$

$$\text{Slope of grain} = 100\% \times \tan(\text{grain angle}) \qquad \text{SoG represented as percentage}$$

Hankinson proposed in 1921 an equation to describe the strength of timber with an angle α (0° to 90°) between the direction of the load and the grain angle:

$$f_{t,\alpha} = \frac{f_{t,0}}{\frac{f_{t,o}}{f_{t,90}} \sin^2 \alpha + \cos^2 \alpha}$$

This means that from an angle of about 5° between direction of the load and the slope of grain the strength decreases rapidly. This is shown in Figure 19 for a beam with strength class D40, in which $f_{t,0,k}$ is equal to 24 N/mm^2 and $f_{t,90,k}$ equal to 0.6 N/mm^2.

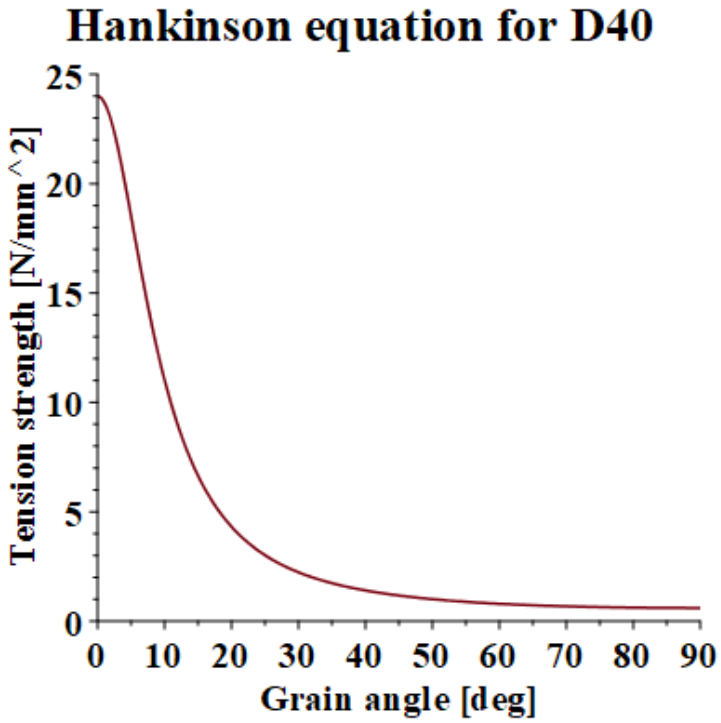

Figure 19: Hankinson equation for a D40 beam.

A generalization of the Hankinson equation is as follows (according to Bodig et al. (1982), quoted in Green et al, 1999):

$$f_{t,\alpha} = \frac{PQ}{P\sin^n \alpha + Q\cos^n \alpha}$$

In which n = 1.5-2 and Q/P = 0.04-0.07. These equations will be used to validate its applicability for iroko lamellas. As for the Eurocode 5, it does not include the case of loading under an angle. The Dutch National Annex however does mention this load case (NEN-EN 1995-1-NA, subsection 6.2.5, 2013), and states a requirement derived from the original Hankinson equation:

$$\frac{\sigma_{t,0,d}}{f_{t,0,d}} + \frac{\sigma_{t,90,d}}{k_{vol} \cdot k_{disp} \cdot f_{t,90,d}} \leq 1$$

$$\sigma_{t,0,d} = \sigma_{t,\alpha,d} \cdot \cos^2 \alpha$$

$$\sigma_{t,90,d} = \sigma_{t,\alpha,d} \cdot \sin^2 \alpha$$

Based on the above statements, it is expected that the iroko lamellas loaded in pure tension with a grain angle will fail at a lower stress than lamellas with straight grains.

4. Mechanical and physical properties of iroko timber

4.1 Literature review on iroko sawn timber

4.1.1 Introduction

In the past, several studies were conducted to determine the bending strength, modulus of elasticity and density of iroko sawn timber. Some are from decades ago, some are conducted quite recently. This section presents found values of density, modulus of elasticity, tension and bending strength of iroko sawn timber, with both smaller and greater dimensions. Mean, standard deviation and characteristic values were calculated from the available data. Also coefficient of determination R^2 was calculated at several instances, to investigate the correlation between bending strength and modulus of elasticity/density. (See section 2.3 for an overview of the statistical equations applied.)

4.1.2 Clear wood specimens (small sizes)

Houtinstituut TNO (1961) reports three point bending tests conducted on 36 small clear wood specimens with length 700 mm, width 50 mm and depth 50 mm (values for density based on 34 specimens). Moisture content was between 22% and 93%, so all specimens had a moisture content around or above fibre saturation point equal to 23% (Gérard et al., 1998; Tropix 7, 2012). Values for density, bending strength and modulus of elasticity are given in Table 1.

Property	Unit	Mean value	Standard deviation	Characteristic value
Density	kg/m^3	566 (wet)	61	466
Bending strength	N/mm^2	76.1	11.8	54.4
MOE in bending	N/mm^2	10192	1542	7655

Table 1: Summary results Houtinstituut TNO (1961) of small clear wood specimens data.

A medium to fairly high correlation was found between (global) modulus of elasticity and bending strength (R^2 = 0.59), see Figure 20.

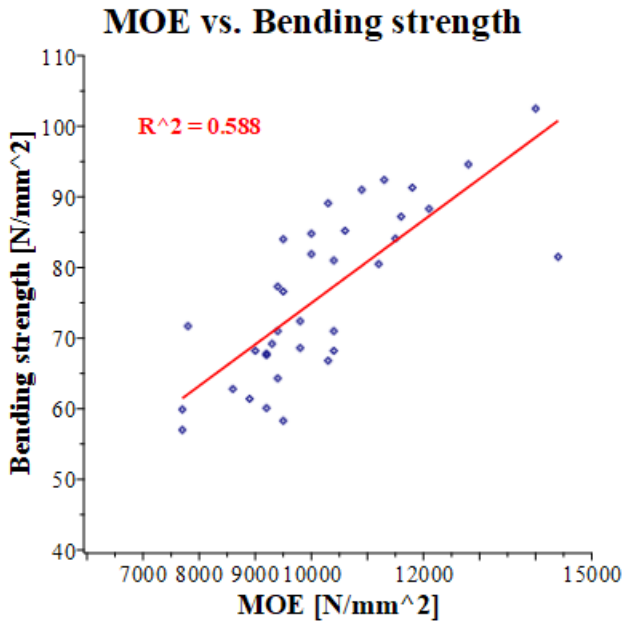

Figure 20: Bending strength vs. modulus of elasticity of small clear wood specimens (Houtinstituut TNO 1961).

However, a lower correlation was found between density and bending strength ($R^2 = 0.31$), see Figure 21.

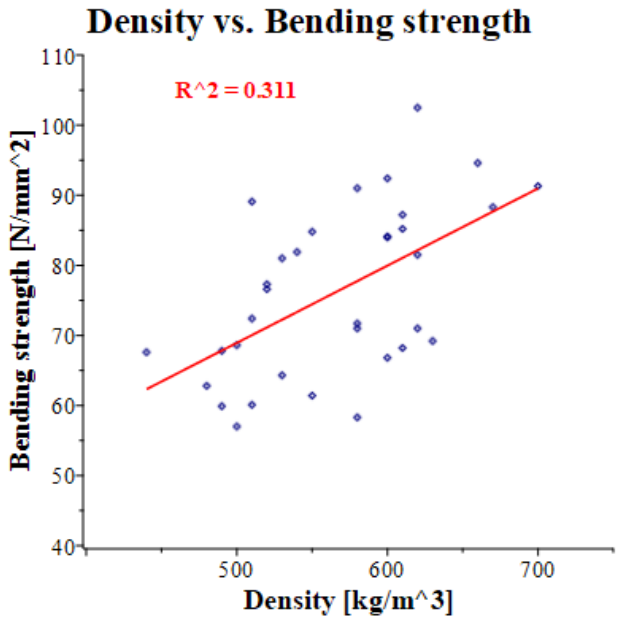

Figure 21: Bending strength vs. density of small clear wood specimens (Houtinstituut TNO 1961).

As the moisture content of all specimens was around or above the fibre saturation point, the mechanical properties in dry condition could have been 10-30% higher. On the other hand, tests on specimens of structural sizes will usually give lower results (size effect), which is indeed shown by the results on specimens with structural size (see subsection 4.1.3).
More researchers report mechanical and physical properties of iroko small clear wood specimens: Table 2 shows minima and maxima of mean values of density, bending strength and modulus of elasticity. Also the moisture content (MC) is given and the reference number in brackets (see Appendix 2). Some researchers however did not report modulus of elasticity, moisture content and/or dimensions. Thereby the figures are not adjusted for size and moisture content.

Property	Unit	Mean value min	MC [Reference]	Mean value max	MC [Reference]
Density	kg/m^3	496	10 [36]	760	12 [34]
Bending strength	N/mm^2	64	12 [32]	117.6	10 [1]
MOE in bending	N/mm^2	8600	12 [8]	15300	15 [10]

Table 2: Density, bending strength and modulus of elasticity of small clear wood specimens.

Also graphical representations of these figures are given. The mean values of density found are presented in Figure 22, sorted from lowest to highest value. Mean values of bending strength (green bars) and modulus of elasticity (red bars) are presented in Figure 23, sorted on bending strength from lowest to highest value. On the horizontal axis of these charts the reference numbers are shown, see Appendix 2. Also on the horizontal axis the moisture content is given in straight brackets; most of the specimens had a moisture content below fibre saturation point.
Note 1: references 1-25 are presented in Houtinstituut TNO (1961).
Note 2: in a few cases the dimensions of the specimens are unknown, though the sources suggest that the data is obtained from small, clear wood specimens. Appendix 2 reports also the dimensions of the specimens.
Note 3: in Figure 23 the left vertical axis corresponds to values for bending strength, and the right vertical axis corresponds to values for modulus of elasticity (units: N/mm^2).

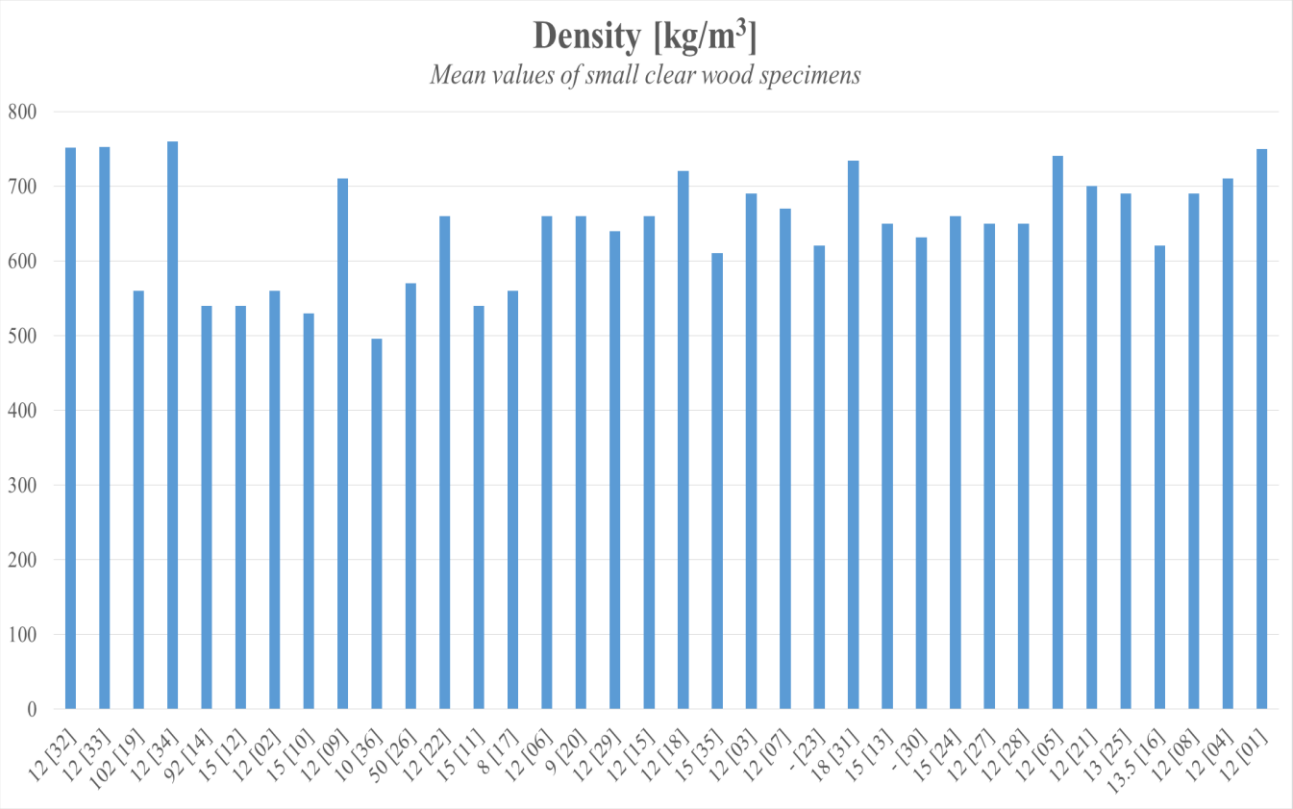

Figure 22: Mean density of small clear wood specimens.

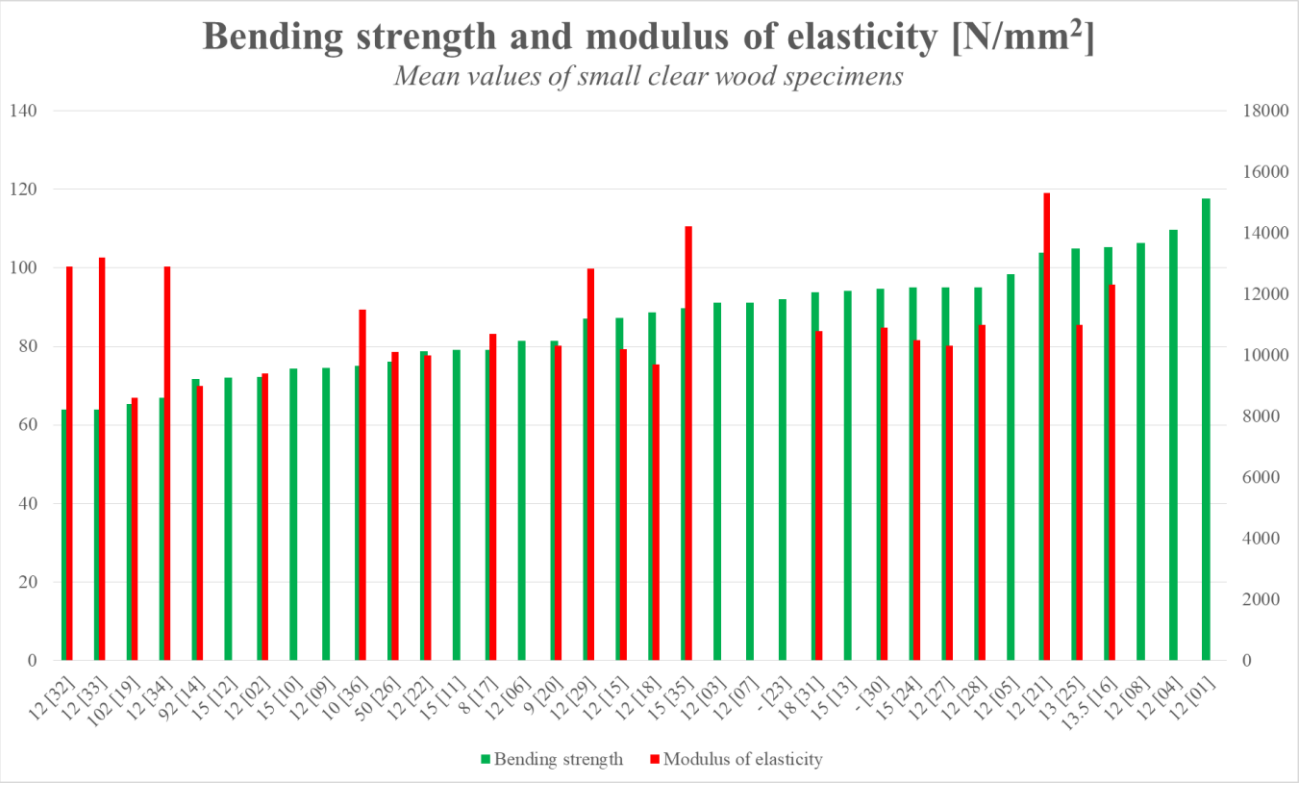

Figure 23: Mean bending strength (green) and modulus of elasticity (red) of small clear wood specimens.

As with the data from Houtinstituut TNO (1961), the relationship between mean bending strength and modulus of elasticity was investigated of those specimens with a moisture content below the fibre saturation point (MC between 8% and 18%). It appeared that there was no correlation at all: an R^2 equal to 0.00 was found, see Figure 24. This is probably due to the differences in testing conditions

like specimen dimensions, test setup (either three point bending test or four point bending test) and moisture content.

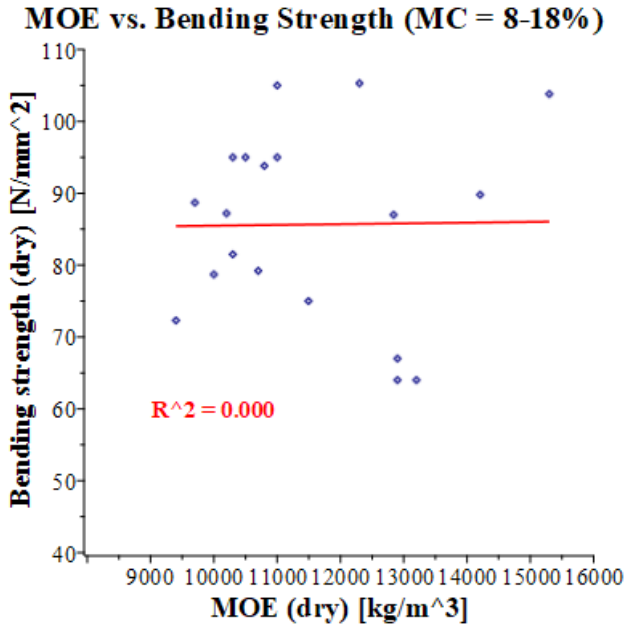

Figure 24: Bending strength vs. density of small clear wood specimens, MC between 8-18%.

To conclude this subsection, tension strength values from Bucci et al. (2016) are reported. This research included 21 iroko lamellas with testing length of 280 mm, width 50 mm and depth 15 mm. Values for density, bending strength and modulus of elasticity are given in Table 3.

Property	Unit	Mean value	Standard deviation	Characteristic value
Density	kg/m^3	622	-	-
Tension strength	N/mm^2	38.3	5.6	27.5
MOE in tension	N/mm^2	13014	1507	10140

Table 3: Density, tension strength and modulus of elasticity of small specimens (Bucci, 2016).

The relationship between tension strength and modulus of elasticity in tension was investigated; a reasonable high correlation was found ($R^2 = 0.69$), see Figure 25.

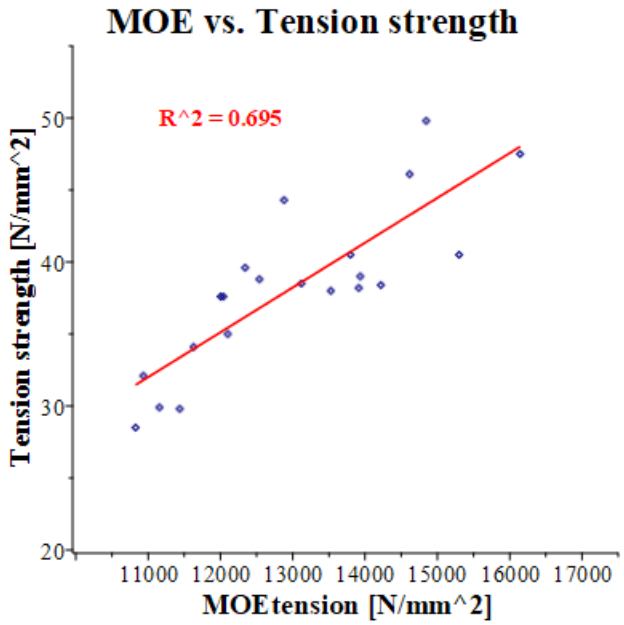

Figure 25: Tension strength vs. modulus of elasticity (Bucci, 2016).

The same research included 20 tension tests on scarf-jointed specimens with testing length of 180 mm, width 50 mm and depth 15 mm. Values for density, bending strength and modulus of elasticity are given in Table 4.

Property	Unit	Mean value	Standard deviation	Characteristic value
Density	kg/m^3	616	-	-
Tension strength	N/mm^2	37.0	6.0	25.5
MOE in tension	N/mm^2	12707	1381	10062

Table 4: Density, tension strength and modulus of elasticity of small, scarf-jointed specimens (Bucci, 2016).

The relationship between scarf joint tension strength and modulus of elasticity in tension was investigated; a reasonable high correlation was found ($R^2 = 0.53$), see Figure 26.

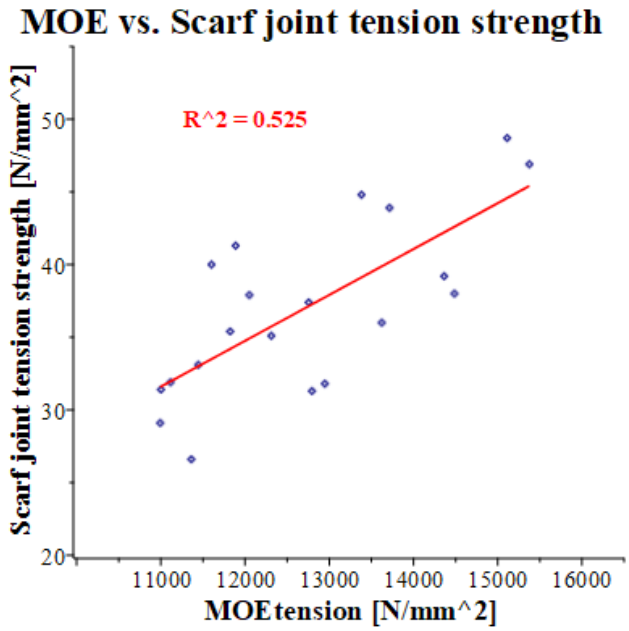

Figure 26: Scarf joint tension strength vs. modulus of elasticity (Bucci, 2016).

4.1.3 Structural sizes

Houtinstituut TNO (1961) reports also four-point bending tests conducted on 39 structural size planks with length 3000 mm, width 50 mm and depth 150 mm. Moisture content was between 29% and 101%, so all specimens had a moisture content above the fibre saturation point. Mean and characteristic density, bending strength and modulus of elasticity are given in Table 5.

Property	Unit	Mean value	Standard deviation	Characteristic value
Density	kg/m^3	566	66	445
Bending strength	N/mm^2	58.8	9.4	41.5
MOE in bending	N/mm^2	11074	1351	8593

Table 5: Summary results Houtinstituut TNO (1961) of structural size specimens data.

Obviously, these figures may increase when considering planks with a moisture content below the fibre saturation point. A coefficient of determination of 0.41 was found relating the bending strength with the modulus of elasticity. Compared with the small clear wood specimens, these structural size specimens yielded a lower mean bending strength. This can be explained by the size of the specimens: smaller sizes yield generally higher strengths, and by the test setup differed: a four point bending test setup generates lower values, because a larger region is under peak stress by which the size effect is playing a role.

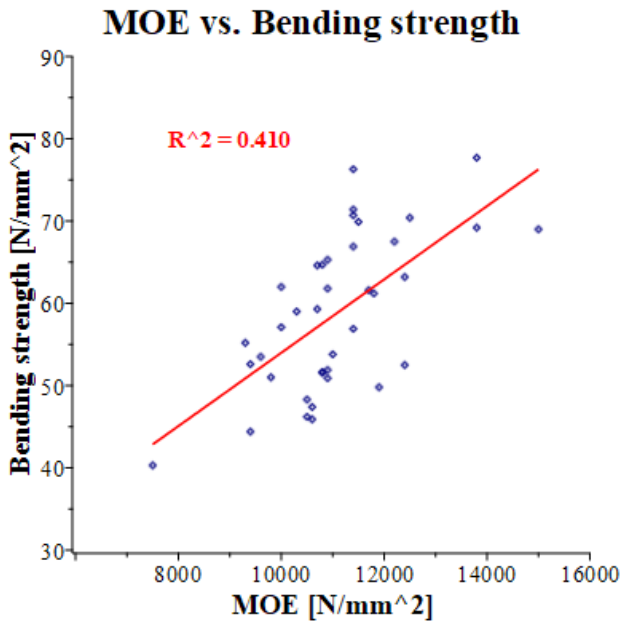

Figure 27: Bending strength vs. modulus of elasticity of structural size specimens (Houtinstituut TNO 1961).

4.2 Literature review on iroko glued laminated timber

4.2.1 Introduction

This section will focus on the bending strength of iroko glulam beams and bending strength of finger joints. Research has been conducted by TNO in corporation with TU Delft, both based in The Netherlands, as to investigate the bending strength and modulus of elasticity of glued laminated iroko without finger joints. Also two Italian universities, those of Messina and Trieste, were involved in testing glued laminated iroko. They considered beams with scarf joints to be applied in a wooden sailboat, referring to the largest wooden yacht S/Y Dream Symphony that was built from glued laminated iroko (Shinell et al., 2012). It must be noted however that both the Dutch and Italian

research programs do not represent structural glued laminated iroko as used to build for instance roofbeams or rafters. However, it may give an indication of its strength.

This section will conclude with finger joint bending strength data provided by Heko Spanten. As these figures are part of their internal quality control system, they are representative for the actual finger joint strength in their manufactured glulam beams. Though the finger joint tension strength is even more representative, as explained in subsection 3.4.2.
Just like iroko sawn timber in the previous section, the following quantities were calculated from the available data: mean, standard deviation and characteristic values. Also coefficient of determination R^2 was calculated at several instances, to investigate the correlation between bending strength and modulus of elasticity/density. (See section 2.3 for an overview of the statistical equations applied.)

4.2.2 Dutch research – glulam beams without joints

De Jong et al. (2011) reports of tests conducted on 6 glulam beams with length 2000 mm, width 80 mm and depth 80 mm. It involved a four-point test setup. Note that these beams were without any joints, only lamellas glued on top of each other. The beams consisted of 8 lamellas with thickness of 10 mm each. Mean and characteristic density, bending strength and local modulus of elasticity are given in Table 6.

Property	Unit	Mean value	Standard deviation	Characteristic value
Density	kg/m^3	635	23	583
Bending strength	N/mm^2	73.9	3.5	65.8
MOE in bending (local)	N/mm^2	12494	768	10692

Table 6: Summary results De Jong et al. (2011) glulam beams without joints.

This resulting mean bending strength should be considered as a first upper bound value for the following two reasons. Firstly, there are as stated no joints present (except the glue). And secondly the lamellas have a small depth of 10 mm, which may yield higher values for the bending strength because of the size effect. No correlation was found between bending strength and local modulus of elasticity (R^2 = 0.00) and between bending strength and density (R^2 = 0.09).

4.2.3 Italian research – glulam beams with and without scarf joints

The research reported by Corigliano et al. (2016) involved three point bending tests on 16 iroko glulam beams. These beams were manufactured from three lamellas, with total of length 900 mm, width 90 mm and depth 45 mm; the lamella depth was 15 mm. In this 8 beams had no joints and 8 consisted of two scarf joints in the outer lamellas, see Figure 28. Moisture content was reported as 16%; density, bending strength and modulus of elasticity values are given in Table 7 (glulam beams without scarf joints) and Table 8 (glulam beams with scarf joints). Note that in this research the modulus of elasticity stems from static measurements (global), and shear influence was cancelled out by means of the variable span method.

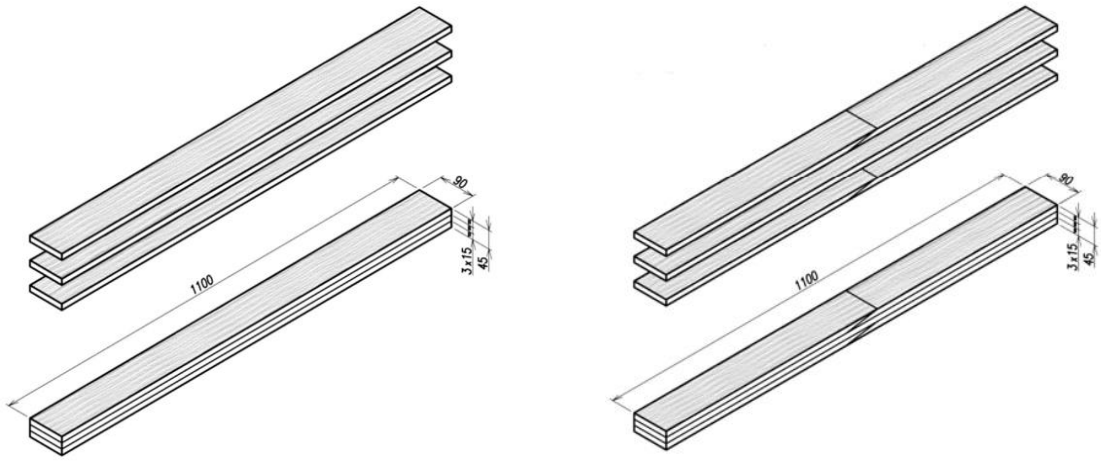

Figure 28: Glued laminated test specimen with (left) and without (right) scarf joints (Corigliano ea. 2016).

Without scarf joints				
Property	**Unit**	**Mean value**	**Standard dev.**	**Char. value**
Density	kg/m^3	626	-	-
Bending strength	N/mm^2	90.4	9.7	69.2
MOE in bending	N/mm^2	16465	2144	11790

Table 7: Summary of Italian data on glulam beams without scarf joints (Corigliano, 2016).

With scarf joints				
Property	**Unit**	**Mean value**	**Standard dev.**	**Char. value**
Density	kg/m^3	630	-	-
Bending strength	N/mm^2	67.1	10.5	44.2
MOE in bending	N/mm^2	16500	1940	12270

Table 8: Summary of Italian data on glulam beams with scarf joint (Corigliano, 2016).

It is apparent that the glulam beams without scarf joints yielded a higher characteristic bending strength than both glulam beams with scarf joints, and the glulam beams tested by means of a four point bending test in the mentioned Dutch programme (De Jong et al., 2011). This agrees with the findings of Bucci et al. (2016) in subsection 4.1.2, as they report that the lamella tension strength is greater than the scarf joint tension strength.
No correlation (R^2 = 0.00) was found between bending strength and modulus of elasticity for the glulam beams with scarf joints. However, a reasonable high correlation (R^2 = 0.77) was found between bending strength and modulus of elasticity for the glulam beams without scarf joints.

Kuisch et al. (2007) reports that scarf joints create end joints with higher bending strengths than finger joints (based on tests done on two Surinamese tropical hardwood species, glued with both PRF and PU): a ratio of 1.01-1.60 was found. One could therefore conclude that the given mean bending strength of the glulam beams with scarf joints is an upper bound values for finger jointed iroko glulam beams.

4.2.4 Finger joint data
For quality control purposes, Heko Spanten B.V. has been testing the finger joint bending strength of iroko lamellas by means of a four point bending test setup. The acquired data stems from the year 2005 till early 2019. 69 data points for finger joints glued with a one-component polyurethane adhesive (PU) and 38 data points were given for iroko finger joints glued with melamine-urea-formaldehyde (MUF). Spatial dimensions are shown in Table 9, the depth to span ratio was for all cases 1:15.

		PU (69)		*MUF (38)*	
	Unit	**max**	**max**	**min**	**max**
Width	mm	90	300	100	245
Depth	mm	25	50	22	52
Span	mm	375	750	330	780

Table 9: Iroko finger joint dimensions.

Distinction was made in the type of failure of the specimens, see Table 10. Data of 69 PU jointed and 37 MUF jointed specimens were given. A great part of the specimens failed at the finger joint, meaning that the wood was stronger than the joint. This is unfavourable, as the capacity of the wood remained greatly untouched.

	Finger joint failure	**Wood failure**	**Combination**
PU (69)	80%	4%	16%
MUF (37)	92%	3%	5%
PU + MUF (106)	84%	4%	12%

Table 10: Finger joint failure type.

The finger joint bending strength properties are given in Table 11. It is apparent that the characteristic values for PU, MUF and combined data of PU and MUF finger joint are almost equal: around 30 to 31 N/mm^2. However, the characteristic bending strength for the PU finger joints equal to 30.22 N/mm^2 is considered an upper bound value for the characteristic bending strength of iroko glulam beams. This is because in this thesis PU is used to glue the finger joints.

Property	**Unit**	**Mean value**	**Standard deviation**	**Characteristic value**
Bending strength *PU*	N/mm^2	50.00	10.98	30.22
Bending strength *MUF*	N/mm^2	55.38	12.99	31.50
Bending strength *PU + MUF*	N/mm^2	51.89	11.95	30.56

Table 11: Summary finger joint test data (Heko Spanten B.V.).

5. Expected strength class of iroko sawn and glued laminated timber

5.1 Introduction

This chapters deals with expected values of the following mechanical and physical properties of iroko sawn timber and iroko glulam beams, see Table 12.

Material	Property
Sawn timber	Density
	Modulus of elasticity
	Tension strength
Glulam beams	Density
	Modulus of elasticity
	Bending strength
Finger joints	Bending strength

Table 12: Materials and properties.

The test series shall have to verify most of these properties. Also expected strength classes are proposed, for both sawn iroko timber and iroko glulam beams.

5.2 Expected values of mechanical and physical properties

5.2.1 Density

From the literature review in Chapter 4 it appears that the density of sawn iroko timber varies between 530 and 760 kg/m^3. The data on iroko glulam (see section 4.2) reports mean values of 635 and 630 kg/m^3. Therefore, a mean density of around 630 kg/m^3 is expected for both iroko planks and glulam beams. To estimate a characteristic value, the following assumptions are made:

- Coefficient of variance equals 0.1 (see JCSS, 2006);
- Number of test specimens equals 40.

With these assumptions, a characteristic value for density becomes 630 – 0.1·630·1.8345 = 514 kg/m^3.

5.2.2 Modulus of elasticity

As mentioned, the mean values of the modulus of elasticity of sawn timber ranges from 8600 to 15300 N/mm^2. However, in this literature review the type of modulus of elasticity was not in every case known. This is clarified in Appendix 2 and indicated in Table 43. For those values known as being the mean global modulus of elasticity, values between 10797 N/mm^2 and 13200 N/mm^2 were found. Ravenshorst et al. (2009) investigated the relationship between E_{loc}, E_{glob} and E_{dyn}, resulting in:

$$E_{glob} = 0.81E_{dyn}$$

$$E_{loc} = 1.16E_{glob} \text{ (for tropical hardwoods)}$$

$$E_{loc} = 0.92E_{dyn}$$

For glulam beams De Jong (2011) reports mean values of 12494 N/mm^2 (E_{loc}) and 13306 N/mm^2 (E_{dyn}). It appears that these findings are quite consistent with the findings of Ravenshorst et al. (2009) for sawn tropical hardwood: 12494 / 13306 = 0.94. Corigliano et al. (2016) reports a mean value of 16495 N/mm^2, however, this value was found by means of a three point bending setup and applying the variable span method.

Expectations for the mean modulus of elasticity are therefore:

- E_{loc} for sawn timber: 12000·1.16 = 13920 N/mm^2;
- E_{glob} for sawn timber: 12000 N/mm^2;
- E_{dyn} for sawn timber: 12000 / 0.81 = 14800 N/mm^2;
- E_{loc} for glulam beams: 12500 N/mm^2;
- E_{glob} for glulam beams: 12500 / 1.16 = 10800 N/mm^2;
- E_{dyn} for glulam beams: 12500 / 0.92 = 13500 N/mm^2.

It must be noted however that Ravenshorst et al. (2009) reports ratios for sawn timber, not for glulam beams. Therefore, these expected values are at most indications.

5.2.3 Bending strength of sawn timber

Presented values in subsection 4.1.2 are results of tests on clear wood specimens, therefore these are in principle not applicable to specimens of structural size. However, as Houtinstituut TNO (1961) presents values taken from both clear wood specimens as for specimens of structural size, a ratio of 0.77 was found between mean bending strengths of both batches. Values for characteristic bending strength were thus calculated on the basis of the lowest and highest mean bending strength presented in Table 2, assuming 40 specimens and a coefficient of variation of 0.15 (JCSS, 2006):

$$f_{m,k} = 0.77 \cdot (64 - 1.83 \cdot 64 \cdot 0.15) / 1.3 = 27.6 \; N/mm^2 \qquad \text{LOW}$$

$$f_{m,k} = 0.77 \cdot (117.6 - 1.83 \cdot 117.6 \cdot 0.15) / 1.3 = 50.7 \; N/mm^2 \qquad \text{HIGH}$$

5.2.4 Tension strength of sawn timber

The tension strength of lamellas may serve as a lower bound value of the glulam bending strength, due to the lamination effect (section 3.3). As mentioned in subsection 4.1.2, a characteristic value for the tension strength was calculated by means of the research reported by Bucci et al. (2016): 22.1 N/mm^2.

5.2.5 Finger joint strength

The finger joint tension strength is the governing factor for the glulam bending strength, it serves therefore as an upper bound value. Heko Spanten provided data on finger joint bending strength values reported in subsection 4.2.4: the calculated characteristic finger joint bending strength is 30.22 N/mm^2.

Frese et al. (2009a) reports an empirical relation to estimate the percentage of wood failure of spruce glulam beams:

$$\eta_{j,crack} \approx 93.5 - 2.35 \cdot f_{m,j,k} + 2.29 \cdot f_{t,l,k}$$

An estimated characteristic lamella tension strength is 22.1 N/mm^2 (subsection 5.2.5), this yields a finger joint failure of about 73%. The finger joint data (subsection 4.2.4) suggests a higher finger joint failure of 80%.

The finger joint tension strength is assumed as being equal to the finger joint bending strength divided by 1.4: $f_{m,j,k} = f_{t,j,k} / 1.4 = 21.59$ N/mm^2.

5.3 Expect strength classes

5.3.1 Sawn timber

The obtained data presented in subsections 5.2.1 till 5.2.3 suggest a strength class of sawn iroko timber between D27 and D50, disregarding density and modulus of elasticity. If the modulus of elasticity is taken into account, a strength class not higher than D45 is expected. Taken into account characteristic density would result in strength D27.

5.3.2 Glued laminated timber

As to estimate a characteristic glulam bending strength, there will be four methods used. All of these methods are based on glulam made of softwood, not tropical hardwood. The resulting characteristic bending strengths are therefore indicative. The input parameters are presented in Table 13.

Input parameter	Unit	Value
Char. lamella tension strength	N/mm^2	22.1
Char. finger joint bending strength	N/mm^2	30.22
Mean modulus of elasticity (glulam beam)	N/mm^2	12500
Mean modulus of elasticity (sawn timber)	N/mm^2	13920
Char. density	kg/m^3	514

Table 13: Input parameters to estimate glulam bending strength.

The four methods are:

1. The curves presented in Colling (1995), see Figure 29.

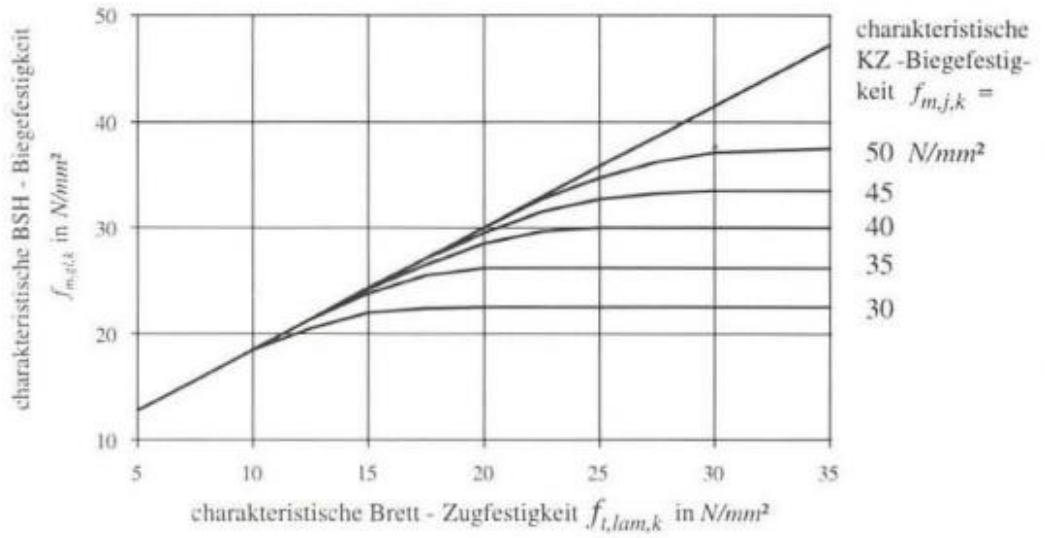

Figure 29: Characteristic glulam bending strength depending on the characteristic lamella tension strength and characteristic finger joint bending strength (Colling, 1995).

2. Equation 7 from Frese et al. (2009a):

$$f_{m,g,k} = 3.454 + 0.7125 \cdot f_{m,j,k} - 0.01078 \cdot f_{m,j,k}^2 - 0.01632 \cdot f_{t,l,k}^2 + 0.02558 \cdot f_{m,j,k} \cdot f_{t,l,k}$$

3. Tables 1 and 3 from NEN-EN 14080 (2013).

4. The formula given in Table 6 from NEN-EN 14080 (2013):

$$f_{m,g,k} = -2.2 + 2.5 \cdot f_{t,l,k}^{0.75} + 1.5 \cdot \left(f_{m,j,k} / 1.4 + 6 \right)^{0.65}$$

By means of these estimated characteristic glulam bending strengths, the glulam strength class is determined (Table 5 from NEN 14080, 2013). The results are presented in Table 14, including the limiting factor.

Method no.	$f_{m,g,k}$ [N/mm^2]	Glulam strength class	Limiting factor
1	23	GL 22h	finger joint bending strength
2	24.3	GL 24h	glulam bending strength
3	24	GL 24h	finger joint bending strength
4	36.2	GL 26h	mean modulus of elasticity

Table 14: Estimation of characteristic glulam bending strength.

The following can be observed:

- For method 1 the individual curves per characteristic finger joint bending strength turn eventually horizontally, after a certain value of the characteristic lamella tension strength. Given a characteristic finger joint bending strength of around 30 N/mm^2, there is no benefit in using lamellas with characteristic tension strength greater than 15 N/mm^2.
- In method 3 the conditions are met for strength class T22 (Table 1 from NEN-EN 14080, 2013): characteristic lamella density is equal or greater than 390 kg/m^3 and mean modulus of elasticity (E_{loc}) is equal or greater than 13000 N/mm^2. Then from Table 3 glulam the strength class GL 24h is chosen, because the characteristic finger joint bending strength is the limiting factor. This time there is no benefit in using lamellas with characteristic tension strength greater than 14 N/mm^2 which is obviously close to the value of 15 N/mm^2 of method 1.
- Using method 4 it appears that just the mean modulus of elasticity is the limiting factor.

From this analyse a glulam strength class of at least GL 22h and at most GL 26h is expected. The estimation of GL 24h fits perfectly in between these values. The experimental results will indicate whether these calculation methods are valid for iroko glulam (see Chapter 8).

6. Manufacturing of the glued laminated beams

6.1 Introduction

This chapter describes the manufacturing of the glulam beams at the factory of Heko Spanten B.V. The operation procedure was as follows:

- preparation:
  - sawing (cutting in half);
  - selecting of planks;
  - measuring of properties;
- finger jointing;
- determining beam lay up;
- gluing of planks into glulam beams.

This steps will be elaborated in the next section.

6.2 Preparation of the planks

Starting point is the raw material, consisting of about 30 sawn planks (Figure 30) from Cameroon with the following dimensions: width about 200 mm, depth about 30-35 mm, and lengths between ca. 2.85 m to 3.55 m. With the band saw these planks were cut in half, see Figure 31.

Figure 30: Raw material of 30 sawn planks.

Figure 31: Cutting the planks in half.

After cutting a rough visual grading was performed with the following criteria:

- straightness (curved planks were rejected);
- imperfections (planks with holes were rejected);
- depth (planks with depth smaller than 32 mm were rejected).

34 planks were found suitable to produce glulam beams from. Some physical and mechanical properties of these planks were measured, see section 7.3.

6.3 Finger jointing

After the measurements, the planks were put in the production line to be finger jointed. Firstly, the moisture content of the planks was automatically measured (Figure 32), then they were cut by an automatic mitre saw (see also Figure 32), after which they were transported to the finger joint machine (Figure 33). Here the ends of two planks were cut in the right shape (length 15 mm; Figure 34), glued with PU (160 g/cm^2) and pressed into each other with a pressure of at least 0.8 N/mm^2. By this procedure 24 lamellas with a length of 4.2 m were created, see Figure 35.

Figure 32: Automatic moisture meter, with the mitre saw in the back.

Figure 33: Finger joint machine.

Figure 34: Finger joint.

Figure 35: 24 finger jointed lamellas.

6.4 Gluing the lamellas

Then a beam lay up for all the 6 beams (with 4 lamellas per beams) was introduced, such that there would be a finger joint in the critical zone (Figure 36) for all of the glulam beams with final length of 2.1 m. The lamellas were planed to a depth of 27 mm by the thicknessing machine (Figure 37), whereupon the lamellas were glued with MUF with an amount of 400 g/cm^2, see Figure 38 for the binder and hardener curtain.

Figure 36: Boards stacked in right layup.

Figure 37: Planing of the boards.

Figure 38: Gluing of the lamellas.

Next, the lamellas were placed in the pressing device (Figure 39 and Figure 40), such that the right beam layup is obtained. A pressure of 0.9 N/mm^2 was applied and held in place for at least 4 hours. See subsection 8.3.3 (Figure 74 till Figure 85) for the beam layup of the final 12 glulam beams. Nearby climate sensors indicated a temperature of 21.7°C and a relative humidity of 42%.

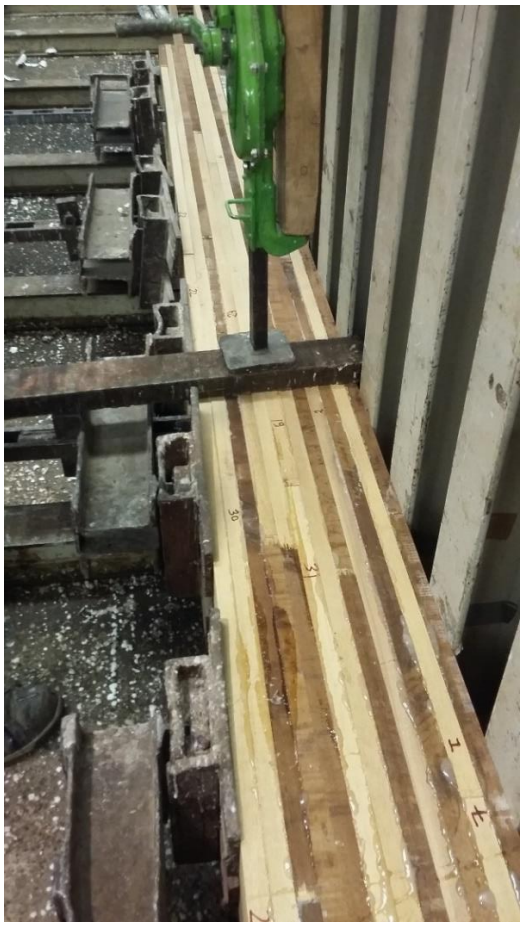

Figure 39: Pressing of the boards (a).

Figure 40: Pressing of the boards (b).

Finally, the 6 glulam beams were planed and cut in half, resulting in 12 beams of length 2.1 m.

7. Experimental procedure

7.1 Description of the batches

As to investigate the strength profile of glued laminated iroko beams, four batches of timber were used and their properties were determined. The four batches I-IV are briefly described below.

- Batch I consists of 38 lamellas (sawn timber) with lengths varying between 1243 mm and 1257 mm, mean width of 91.33 mm and mean depth of 26.98 mm. See Figure 41. It is used to investigate the tension strength of the base material from which the glulam beams are made. Appendix 3 shows pictures of batch I specimens after failure.
- Batch II consists of 38 finger jointed lamellas with lengths varying between 1241 mm and 1251 mm, mean width of 89.96 mm and mean depth of 27.15 mm. See Figure 42. It is used to investigate the tension strength of the finger joints, as there are finger joints used to make the glulam beams. Appendix 4 shows pictures of batch II specimens after failure.
- Batch III consists of the 34 lamellas (sawn timber) mentioned in section 6.2; see Figure 43). Before finger jointing the dimensions were as follows: length varying between 2831 mm and 3550 mm, mean width of 100.3 mm and mean depth of 34.81 mm.

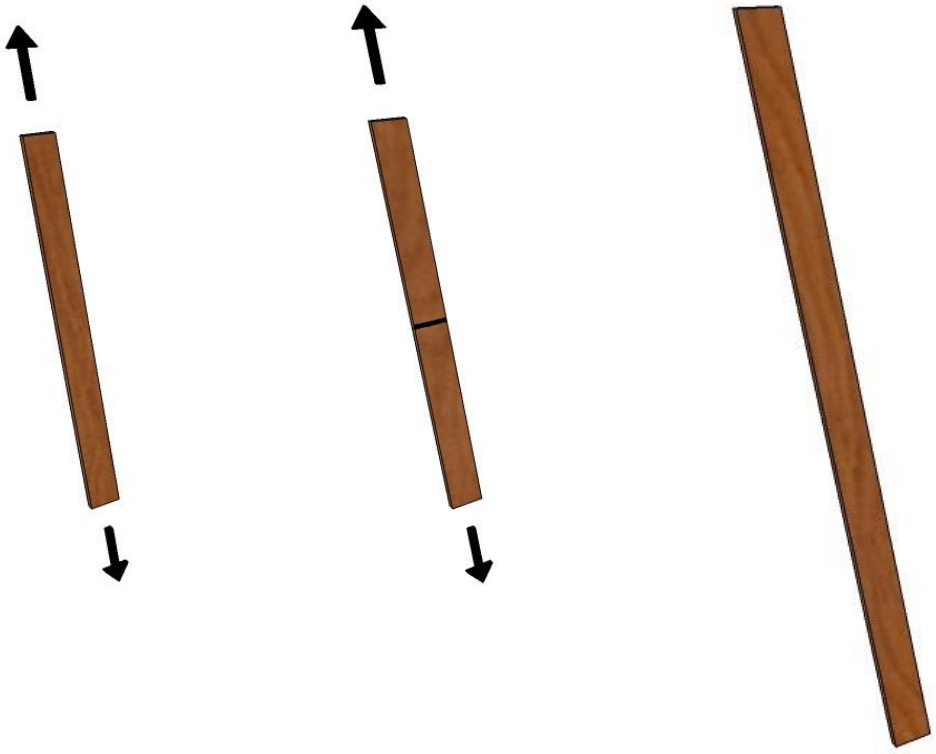

Figure 41: Batch I specimen. *Figure 42: Batch II specimen* *Figure 43: Batch III specimen.*

- Batch IV consists of 12 glulam beams (4 lamellas each) with lengths varying between 2093 mm and 2102 mm, mean width of 89.90 mm and mean depth of 109.4 mm; see Figure 44. These beams consist of the batch III lamellas randomly put in place. It is used to investigate the bending strength of glulam iroko beams. Appendix 5 shows pictures of batch IV specimens after failure.

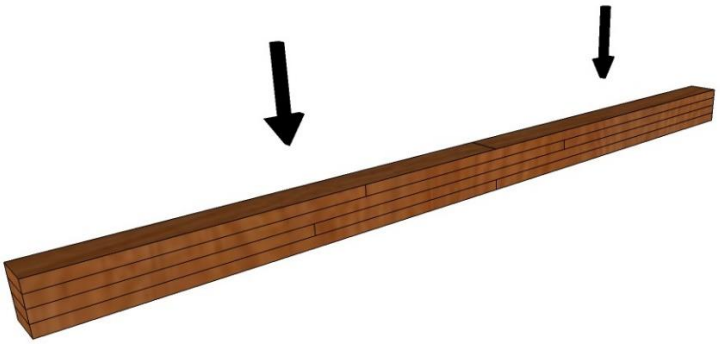

Figure 44: Batch IV specimen.

7.2 Conditioning of the specimens

After manufactured at Heko Spanten's facility, the specimens were transported to Delft and placed in the climate chamber of the Stevin II laboratory of Technische Universiteit Delft, see Figure 45 (batch I and II) and Figure 46 (batch IV). In this climate chamber, with temperature of about 20°C and about 59% relative humidity, the batch I and II specimens were conditioned for at least one week and the batch IV specimens for at least two weeks. NEN-EN 408 (2012) clause 8 requires furthermore that the specimens attain constant mass, which means that "two successive weightings, carried out at an interval of 6 hours, do not differ by more than 0.1 %". Appendix 6-9 shows the results of these weightings, and proves that constant mass was attained for all specimens of batch I, II and IV. See also subsection 7.3.3.

Figure 45: Specimens of batch I and II in climate chamber.

Figure 46: Specimens of batch IV in climate chamber.

7.3 Measured quantities

7.3.1 Working method

The measurements for batch III were done at Heko Spanten's facility in Ede, and the measurements and tests on batches I, II and IV were done at the Stevin II laboratory of Technische Universiteit Delft. The following quantities were measured:

- Spatial dimensions of the specimens, consisting of:
  - System length
  - Width
  - Depth
- Mass of the specimens
- Mass of test slices (batch I, II and IV only)
- Spatial dimensions of test slices (batch I, II and IV only)
- Eigenfrequency
- Moisture content (batch III only)
- Failure load in tension (batch I and II only)
- Angle of failure (batch I and II only)
- Displacement of lamellas (batch I and II only)
- Failure load in bending (batch IV only)
- Global and local beam displacement (batch IV only)

The following subsections describe the working how these quantities were obtained.

7.3.2 Spatial dimensions of the specimens

The system length, depth and width of lamellas and glulam beams were measured with either a tape measure (Figure 47) or a vernier capiler (Figure 48). NEN-EN 408 (2012), clause 5 states that an accuracy of 1% is required. This accuracy or relative error is equal to 100% × measurement error / measured value. Table 15 shows the measurement tool used per quantity, measurement error per tool and relative error for the lamellas; Table 16 shows this for the glulam beams. It is apparent that the stated requirement concerning relative error is met for measuring the spatial dimensions of both the lamellas and glulam beams.

Figure 47: Measuring with the tape measure..

Figure 48: Measuring with the vernier caliper.

Quantity	Measurement tool	Measurement error tool [mm]	Smallest measured value [mm]	Relative error
System length	Tape measure	1.0	1250	0.08%
Depth	Vernier capiler	0.01	27	0.04%
Width	Vernier capiler	0.01	90	0.01%

Table 15: Relative error lamellas.

Quantity	Measurement tool	Measurement error tool [mm]	Smallest measured value [mm]	Relative error
System length	Tape measure	1.0	2100	0.05%
Depth	Vernier capiler	0.01	108	0.01%
Width	Vernier capiler	0.01	90	0.01%

Table 16: Relative error glulam beams.

7.3.3 Mass of the specimens

The mass of the specimens was measured by an electronic balance. At Heko Spanten's facility in Ede this was done by a portable balance (calibrated at the Stevin II laboratory in Delft); the specimens of batch III were attached by strings to the portable balance (Figure 49).

Figure 49: Mass measurement of batch III specimen.

At the Stevin II laboratory in Delft this was done by a (heavy) balance (Figure 50), for the specimens of batch I, II and IV. This balance was also used to ensure constant mass (section 7.2) of the batch IV specimens.

Figure 50: (Heavy) balance, used to weigh specimens of batch I, II and IV.

7.3.4 Mass of the test slices (batch I, II and IV only)

As to calculate the moisture content for batch I, II and IV, the procedures of NEN-EN 13183-1 (2002) clause 5 and NEN-EN 408 (2012) clause 6 were followed, this is the oven-dry method. Test slices with thicknesses of around 25-40 mm were cut from the specimens after the tension/bending test, at a distance generally not closer than 300 mm from the ends and as close as possible to the fracture

(Figure 51). The batch II lamellas consisted of two finger jointed, distinctive planks, therefore the test slices of batch were cut from both planks (both sides of the finger joints).


Figure 51: Cutting of the test slices from the specimens.

These test slices were "free from resin wood and features such as bark, knots and resin pockets". After cutting, the mass of the test slices was measured by means of the small balance (Figure 52, accurately balanced to 0.01 g) and labelled with a marker. Subsequently, they were put in the oven at a temperature of 103 °C (with a margin of 2°). The test slices were weighed with an interval of 1-3 days. Within two weeks, all test slices attained constant mass, i.e. the moment when the difference of two successive measurements was less than 0.1 %.

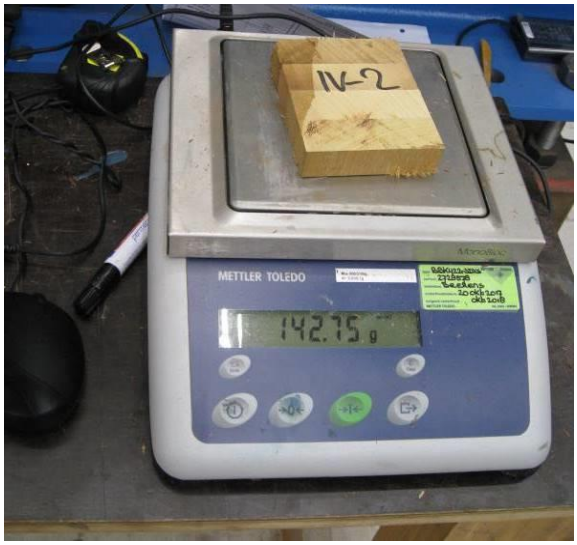

Figure 52: Small balance; weighing of the test slices.

7.3.5 Spatial dimensions of test slices (batch I, II and IV only)

After the test slices attained constant mass, the thickness of the test slices was measured with a vernier capiler (Figure 53). This was done in order to be able to calculate the density.

Figure 53: Measuring the thickness of a test slice with the vernier caliper.

In general, the width and depth of the test slice was assumed equal to the width and depth of the specimens, respectively. Incidentally, the width and depth of a test slice was measured with a vernier capiler. For in these cases it was from visual observation clear that the test slice's width or depth deviated significantly from the specimen's width or depth.

7.3.6 Eigenfrequency

The eigenfrequency of the specimens was measured by a Brookhuis © MTG handheld timber grader (Figure 54). This device initiates a longitudinal stress wave, and measures the vibration in less than 0.2 seconds. The eigenfrequency or first natural frequency is determined from this vibration measurements. The lamellas and glulam beams were supported on two (small) wooden strips before the measurements took place.

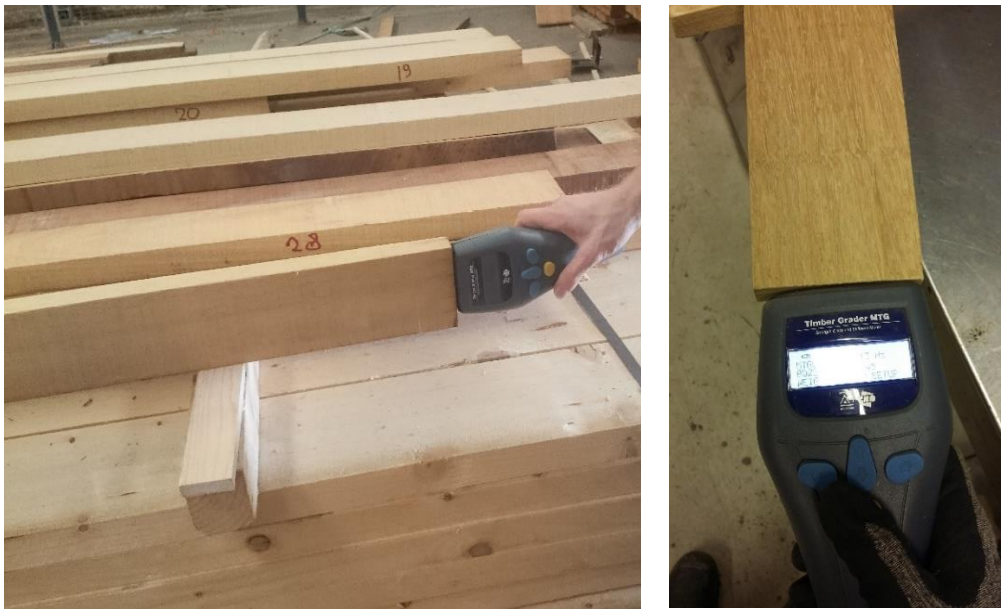

Figure 54: Timber grader handheld: initiating stress wave and measuring vibrations.

7.3.7 Moisture content (batch III only)

The moisture content of the specimens of batch III was estimated by a Brookhuis © capacitive moisture meter (Figure 55), as prescribed by NEN-EN 13183-3 (2005) The specimen area were "free from features affecting the measurement such as bark, knots, resin pockets, wetted surface or checks". At a distance not closer than 300 mm from the ends, the handheld was placed to the plank's surface. The settings for the device were: density 0.650 g/cm^3, measurement depth 20 mm.

Figure 55: Estimating the moisture content of batch III.

7.3.8 Failure load in tension (batch I and II only)

The failure load in tension of the lamellas was measured by means of a short-term displacement-controlled test. The specimens were placed in clamps (Figure 56), which generated a pressure of about 8.0 N/mm^2. With a bubble level it was assured that the specimens were vertically placed in the clamps (Figure 57). A hydraulic cylinder beneath generated the tension force, at a speed of 0.015 mm/s. The distance between the clamps (i.e. the free testing length) was not individually measured for all test specimens. The tension test machine was always returned to its original position, therefore allowing an equal free testing length of 856 mm for all batch I and II specimens. NEN-EN 408 (2012) clause 13 requires a free testing length of at least nine times the width; the testing length was about 9.5 times the width, thus this condition was met.

Figure 56: Lamella clamped in tension testing machine.

Figure 57: Levelling the lamella.

7.3.9 Angle of failure (batch I)

The angle at which failure of the lamella occurred, was measured with a protractor after the specimen failed (Figure 58). Also before failure grain angle was measured: in some instances these angles matched.

Figure 58: Measuring the angle at which failure occurred.

7.3.10 Displacement of lamellas (batch I and II only)

The displacement in tension of the lamellas was measured by means of two LVDT's: one on both sides of the lamellas. The LVDT's were placed in a brace (Figure 59), such that they would measure the displacement parallel to the axis of the lamella. To place the braces at the right location, holes were drilled in advance. The length between two holes l_1 was measured, it was around 430 mm. This is about equal to 5 times the width (450 mm) prescribed by NEN-EN 408 (2012) clause 13.

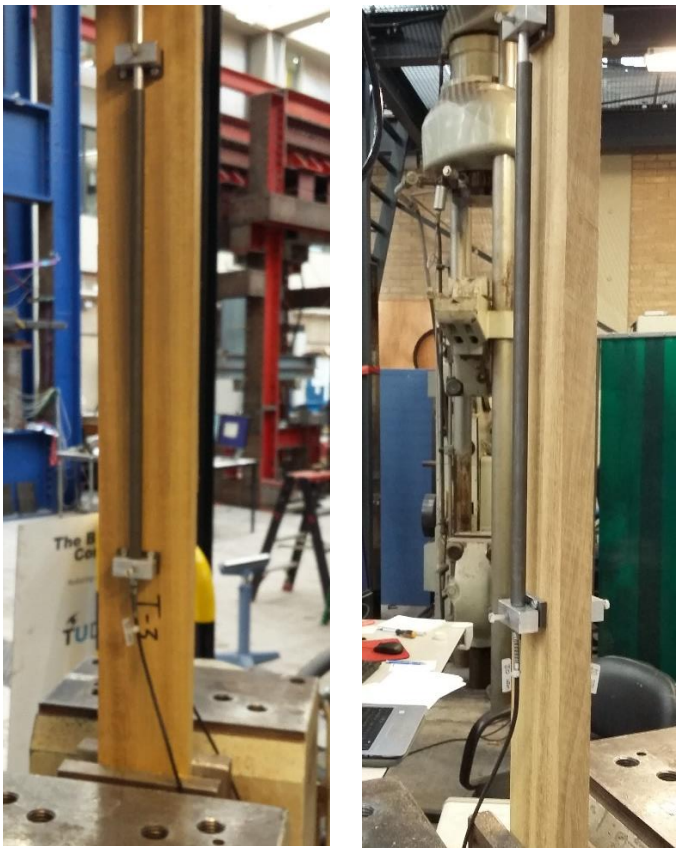

Figure 59: LVDT's in place.

Note: at first instance, the LVDT's were held in place till failure. It occurred then that at certain moment during testing the displacements went beyond their range. Also, in the last test 14 series of

batch II one LVDT broke. The test series were continued thereafter with one LVDT, and it was removed when the load reached about 60 kN (which is about 60% of the expected failure load). Subsection 8.2.1 elaborates more on this issue.

7.3.11 Failure load in bending (batch IV only)

The failure load in bending of the glulam beams was measured by means of a short-term displacement-controlled test, in a four point bending setup. This resulted in a pure bending zone (shear free) between the two concentrated loads. The span was 1900 mm, which is about 18 times the depth; the distance between the supports and the centre of action of the nearest point load *a* was equal to 635 mm: about 6 times the depth. The latter is in accordance with NEN-EN 408 (2012) clause 19. This distance *a* between point of action of the concentrated loads and supports was not individually measured for all specimens. The supports were placed at fixed position and the points of actions of the concentrated were also fixed in advance. Therefore the properties *a* and *l* (span) are all the same for every specimen of batch IV. A small overlength of about 100 mm was applied on both sides. The beam was placed such that between the two loads there is a finger joint in the outer tension zone (i.e. the bottom side of the beam). See Figure 60 (scheme) and Figure 61 (reality).

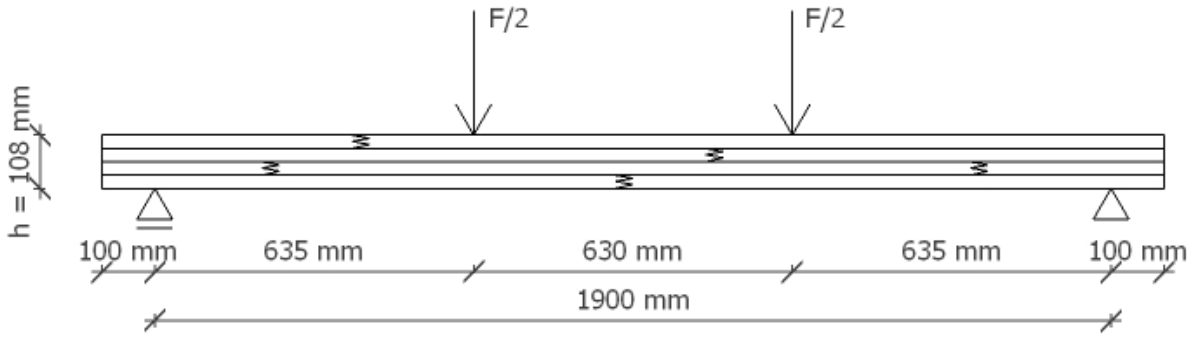

Figure 60: Four point bending test setup (scheme).

Figure 61: Four point bending test setup (reality).

7.3.12 Global and local beam displacement (batch IV only)

The displacement of the batch IV specimens was measured in two ways: locally and globally.

Local measurement of the displacement means measurement in the shear free area between the two concentrated loads. This is done by placing braces on both sides of each specimen which hold the LVDT's (see Figure 62). To place the braces at the right location, holes were drilled in advance. The length between two holes l_1 is equal to 510 mm, which is about equal to 5 times the depth (540 mm) prescribed by NEN-EN 408 (2012) clause 9.2. The purpose of this measurement is to determine the local modulus of elasticity.

Figure 62: LVDT's placed in braces upon the test beam.

Global measurement of the displacement means measurement of the displacement of the bottom side at midspan of each specimen. This was done by means of built-in lasers, see Figure 63. The purpose of this measurement was to determine the global modulus of elasticity, in which shear deflection is incorporated. Reference is made to NEN-EN 408 (2012) clause 10 for the prescribed procedure to determine the global modulus of elasticity.

Figure 63: Lasers as to determine the global displacements.

8. Experimental results

8.1 Measurement results

Table 17 presents a summary of the (principal) measured values of the following quantities of lamellas and glulam beams, listed with their symbols:

- System length l_s
- Width b (batch II: part a and b)
- Depth h (batch II: part a and b)
- Total mass of the specimen m
- Eigenfrequency f_e
- Moisture content ω (batch III only)
- Failure load in tension $P_{t,l}$ and $P_{t,j}$ (batch I and II only)
- Failure load in bending $P_{m,g}$ (batch IV only)
- Time to failure (batch I, II and IV only)

Summary measured values of batch I-IV										
Batch I # 38	***l*$_s$ [mm]**	***b*** **[mm]**		***h*** **[mm]**		***m*** **[kg]**		***f*$_e$ [Hz]**	***P*$_{t,l}$ [kN]**	***Time to failure* [s]**
min	1243.6	88.29		26.07		1.817		1137	51.2	128.54
max	1257.0	94.82		27.76		2.283		2240	307.3	833.87
mean	1247.9	91.33		26.98		2.031		1907	145.7	344.98
stdev		1.42		0.35		0.099		209	53.9	144.10
Batch II # 38	***l*$_s$ [mm]**	***b* (a) [mm]**	***b* (b) [mm]**	***h* (a) [mm]**	***h* (b) [mm]**	***m*** **[kg]**		***f*$_e$ [Hz]**	***P*$_{t,j}$ [kN]**	***Time to failure* [s]**
min	1241.0	88.35	87.85	26.40	26.32	1.872		1571	54.9	150.74
max	1251.5	94.80	92.97	28.53	27.94	2.235		2123	120.6	323.23
mean	1247.1	90.99	90.76	27.22	27.07	2.034		1829	95.9	237.41
stdev	2.2	1.43	1.29	0.56	0.40	0.087		130	13.9	37.68
Batch III # 34	***l*$_s$ [mm]**	***b*** **[mm]**		***h*** **[mm]**		***m*** **[oz]**	***ω*** **[%]**	***f*$_e$ [Hz]**		
min	2831	97.89		32.78		202.0	6.0	654		
max	3550	103.22		39.04		288.0	9.2	849		
mean	3263	100.3		34.81		249.3	7.7	730		
stdev		1.03		1.58		20.3	0.8	52		
Batch IV # 12	***l*$_s$ [mm]**	***b*** **[mm]**		***h*** **[mm]**		***m*** **[kg]**		***f*$_e$ [Hz]**	***P*$_{m,g}$ [kN]**	***Time to failure* [s]**
min	2093	89.09		108.51		12.250		1108	28.7	90.04
max	2102	91.15		109.84		13.235		1171	44.2	263.27
mean	2099	89.90		109.04		12.794		1146	36.8	141.17
stdev	2.97	0.57		0.40		0.32		22	5.27	52.29

Table 17: Summary measured values of batch I-IV.

All results of spatial dimensions, total mass of specimens, mass of test slices before and after drying (m_1 and m_2, respectively), eigenfrequencies, and failure loads (both in tension and bending) are presented in Appendix 6-9, as well as calculated physical and mechanical quantities. Load-displacement curves of all specimens of batches I, II and IV are presented in Appendix 10-12.

8.2 Calculation of physical and mechanical quantities

8.2.1 Used formulae

The relevant physical and mechanical quantities to be calculated and the formulae of how to calculate these are presented in Table 18.

Symbol	Quantity	Formula	Applies to batch no.
ρ	Density	$\rho = \frac{b_{test} \cdot h_{test} \cdot t}{m_1}$	I, II, IV
ρ	Density	$\rho = \frac{l_s \cdot b \cdot h}{m}$	III
E_{dyn}	Dynamic modulus of elasticity	$E_{dyn} = \frac{m}{b \cdot h \cdot l_s} \cdot \left(2 \cdot f_e \cdot l_s\right)^2$	I, III, IV
E_{dyn}	Dynamic modulus of elasticity	$E_{dyn} = \rho_{\text{mean}} \cdot \left(2 \cdot f_e \cdot l_s\right)^2$ $\rho_{\text{mean}} = \frac{m}{\text{mean}\left(b_a, b_b\right) \cdot \text{mean}\left(h_a, h_b\right) \cdot l_s}$	II
ω	Moisture content	$\omega = \frac{m_1 - m_0}{m_0} \times 100$	I, II, IV
$f_{t,l}$	Lamella tension strength	$f_{t,l} = \frac{P_{t,l}}{b \cdot h}$	I
$f_{t,j}$	Finger joint tension strength • Finger joint failure • Wood failure • Combination	$f_{t,j} = \frac{P_{t,j}}{l_{fj} \cdot \min\left(h_a, h_b\right)}$ $f_{t,j} = \frac{P_{t,j}}{b_i \cdot h_i} \quad i = a \text{ or } b$ $f_{t,j} = \frac{P_{t,j}}{\max\left(b_a, b_b\right) \cdot \max\left(h_a, h_b\right)}$	II
E_t	Modulus of elasticity in tension	$E_t = \frac{l_1}{bh} \frac{\Delta P_{t,l}}{\Delta w_t}$	I
E_t	Modulus of elasticity in tension	$E_t = \frac{l_1}{\text{mean}\left(b_a, b_b\right) \cdot \text{mean}\left(h_a, h_b\right)} \frac{\Delta P_{t,j}}{\Delta w_t}$	II
$f_{m,g}$	Glulam bending strength	$f_{m,g} = \frac{3P_{m,g} \cdot a}{b \cdot h^2}$	IV
E_{loc}	Local modulus of elasticity	$E_{loc} = \frac{a l_1^2}{16 \cdot \frac{1}{12} b h^3} \frac{\Delta P_{m,g}}{\Delta w_{loc}}$	IV
E_{glob}	Global modulus of elasticity	$E_{glob} = \frac{3l^2 - 4a^3}{4bh^3} \frac{\Delta P_{m,g}}{\Delta w_{glob}}$	IV

Table 18: Relevant physical and mechanical quantities and their formulae.

As to determine characteristic values, the formulae mentioned in section 4.1 are used. Regarding the static moduli of elasticity (tension, local and global), one should notice the following:

1) For batch I, the slope of the linear regression line of the load-displacement curve between $0.1 \cdot P_{t,l,max}$ and $0.4 \cdot P_{t,l,max}$ (denoted as $\Delta P_{t,l} / \Delta w$) was used to calculate the modulus of elasticity in tension. In this regression analysis a coefficient of determination R^2 greater than 0.99 is required by NEN-EN 408 (2012) clause 12.3. It appeared that all of the 76 displacement measurements (38 specimens, 2 displacement measurements per lamella) met this requirement.
2) For batch II, the slope of the linear regression line of the load-displacement curve between $0.1 \cdot P_{t,j,max}$ and $0.4 \cdot P_{t,j,max}$ (denoted as $\Delta P_{t,j} / \Delta w$) was used to calculate the modulus of elasticity in tension. In this regression analysis a coefficient of determination R^2 greater than 0.99 is required by NEN-EN 408 (2012) clause 12.3. It appeared that all of the 62 displacement measurements (38 specimens, 2 displacement measurements per lamella for specimens II-1 till II-24) met this requirement.
3) Regarding the tension tests, LVDT 1 failed during testing of the batch II specimens. From the load-displacements curves presented in Appendix 10 and 11, it is clear that the results from LVDT 1 deviate in some cases very much from the results from LVDT 2. That is, in some cases the load-displacement curve resulting from both LVDT's did not coincide very well. This was the case with e.g. specimens I-15, I-30, I-37, II-11 and II-22; see Figure 237, Figure 252, Figure 259, Figure 271, and Figure 282, respectively.
   After failure of specimen II-24, the LVDT 1 was calibrated manually. It appeared that its results were inaccurate, therefore the results from LVDT 1 in the tension tests of both batch I and II are disregarded in further calculations.
4) For batch IV, the slope of the linear regression line of the load-displacement curve between $0.1 \cdot P_{m,g,max}$ and $0.4 \cdot P_{m,g,max}$ (denoted as $\Delta P_{m,g} / \Delta w$) was used to calculate both the local and global modulus of elasticity. In this regression analysis a coefficient of determination R^2 greater than 0.99 is required by NEN-EN 408 (2012) clause 9.3 and 10.3. It appeared that out of the 48 displacement measurements (12 beams, 4 displacement measurements per beam), only 2 measurements failed to achieve this requirement: $w_{glob,1}$ (output of Laser 1) for beam 7 and 12 achieved an R^2 between 0.98 and 0.99.

8.2.2 Results of the calculations

Table 19 summarizes the results of the calculations of the physical and mechanical quantities mentioned in section 7.1, for batch I to IV.

One comment about the tension strength values of batch I: it shows a large scatter (COV = 0.37), however, compared to some literature values on softwood species (Stapel et al., 2013: COV between 0.39-0.50) this is rather low.

Summary calculation results of batch I-IV								
Batch I # 38	**ω [%]**		**ρ [kg/m^3]**		**$f_{t,l}$ [N/mm^2]**	**E_{dyn} [N/mm^2]**	**E_t [N/mm^2]**	
min	7.8		576.65		20.41	5545	9923	
max	10.0		806.86		122.99	20472	21368	
mean	9.1		660.31		59.23	15101	15076	
stdev	0.6		44.74		22.02	3034	2752	
COV			0.07		0.37	0.20	0.18	
Char. val.			578.05		17.05	9523	10016	
Batch II # 38	**ω (a) [%]**	**ω (b) [%]**	**ρ (a) [kg/m^3]**	**ρ (b) [kg/m^3]**	**$f_{t,j}$ [N/mm^2]**	**E_{dyn} [N/mm^2]**	**E_t [N/mm^2]**	
min	6.7	8.0	550.31	581.92	22.70	10344	9708	
max	11.2	17.6	788.50	736.71	48.83	18862	17409	
mean	9.7	9.9	653.88	659.89	39.54	13799	13242	
stdev	1.3	1.6	50.07	42.85	5.93	1934	1862	
COV			0.08	0.06	0.15	0.14	0.14	
Char. val.			561.82	581.10	28.64	10244	9818	
Batch III # 34	**m [kg]**		**ρ [kg/m^3]**			**E_{dyn} [N/mm^2]**		
min	5.7		556.44			11138		
max	8.2		717.01			16778		
mean	7.1		623.07			14221		
stdev	0.6		41.10			1377		
COV			0.07			0.10		
Char. val.			547.09			11676		
Batch IV # 12	**ω [%]**		**ρ [kg/m^3]**		**$f_{m,g}$ [N/mm^2]**	**E_{dyn} [N/mm^2]**	**E_{loc} [N/mm^2]**	**E_{glob} [N/mm^2]**
min	8.9		587.45		50.25	13085	13481	12731
max	10.3		649.61		79.45	15397	15824	15195
mean	9.5		619.81		65.50	14407	14878	13659
stdev			18.98		9.3	696	738	776
COV			0.03		0.14	0.05	0.05	0.06
Char. val.			581.30		42.30	12994	13380	12085

Table 19: Summary calculation results batch I-IV.

8.3 Failure modes

This section reports in what way the specimens of batches I, II and IV failed (i.e. failure modes).

8.3.1 Failure modes of batch I

Most of the specimens of batch I failed at the grain angle, as expected. Only two specimens (specimen I-21, failure load of 136.01 kN; specimen I-26, failure load of 128.06 kN) failed at the clamps, meaning that there actual strength is higher than recorded. See also Figure 125, Figure 126, Figure 135 and Figure 136 in Appendix 3. In further calculations, the assumed angle of failure of these two specimens is 0°. This is justified by observing the grain angle of the two specimens before testing: both specimens had a grain angle parallel to the beam axis. Figure 64 shows a plot of the tension

strength vs. the angle of failure. Generally, the tension strength decreases with increasing angle of failure, as is expected from theory. Figure 65 shows a plot of the modulus of elasticity in tension vs. the angle of failure

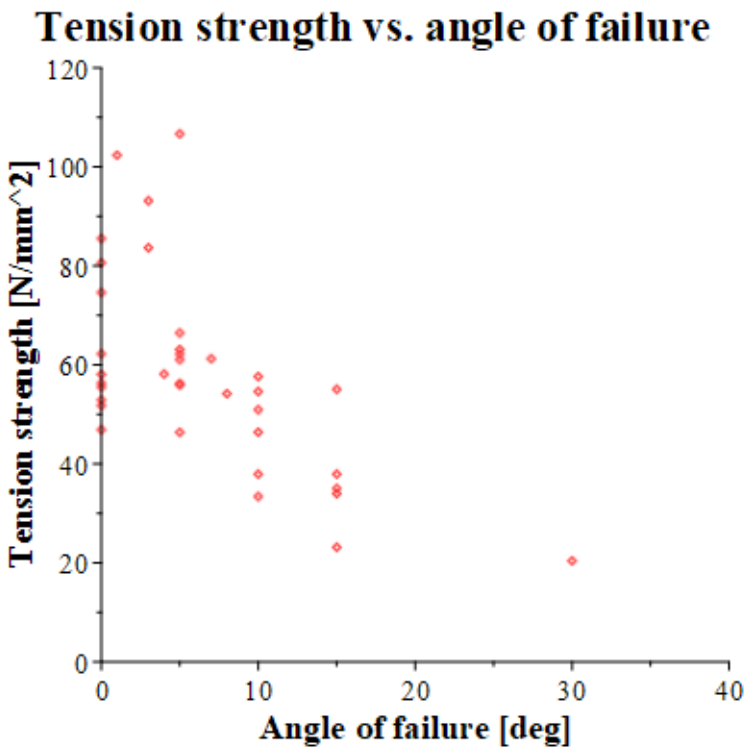

Figure 64: Batch I: tension strength vs. angle of failure.

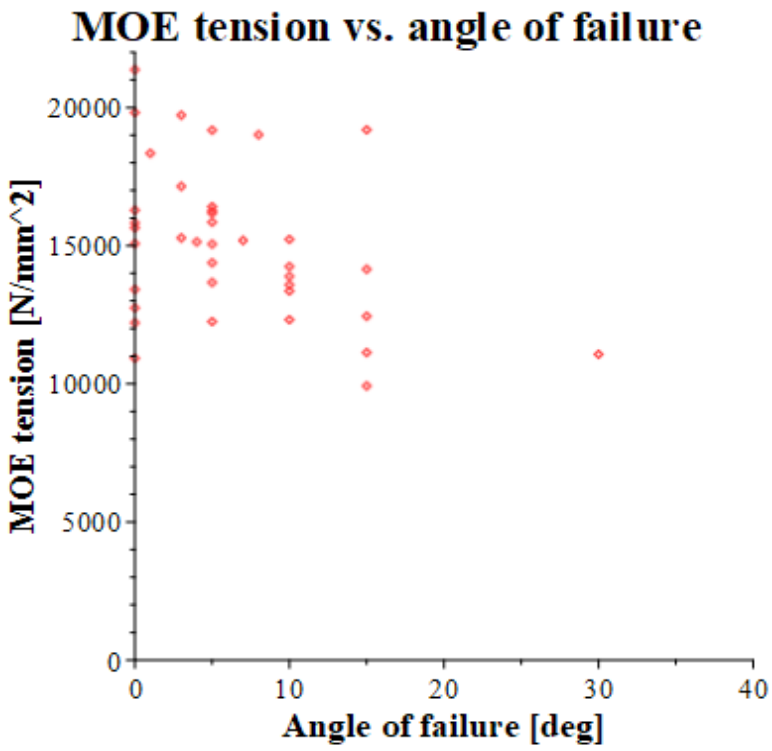

Figure 65: Batch I: modulus of elasticity in tension vs. angle of failure.

8.3.2 Failure modes of batch II

The batch II specimens showed in general three failure modes: failure of the finger joint, failure of the wood (Figure 70) and a combination of both (Figure 66). Failure of finger joint can be subdivided into failure of the fingers (Figure 67), failure of the glue (Figure 68) and a combination of both (Figure 71). See Figure 66 for a flow chart.

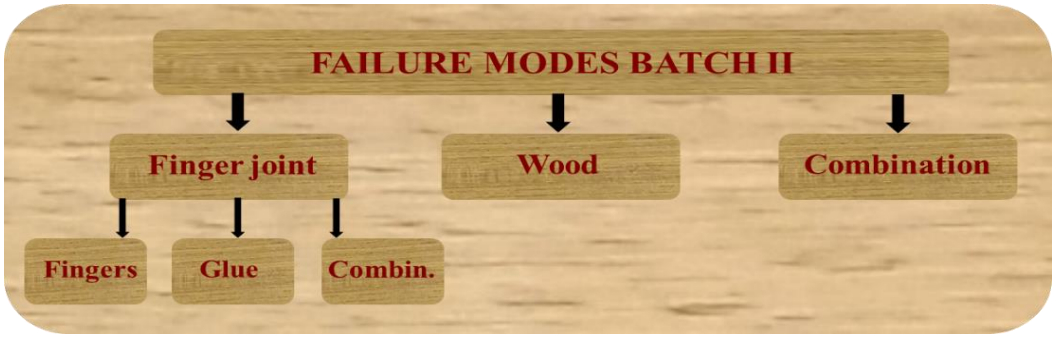

Figure 66: Failure modes of batch II.

Figure 67: Finger failure (II-32).

Figure 68: Glue failure (II-31).

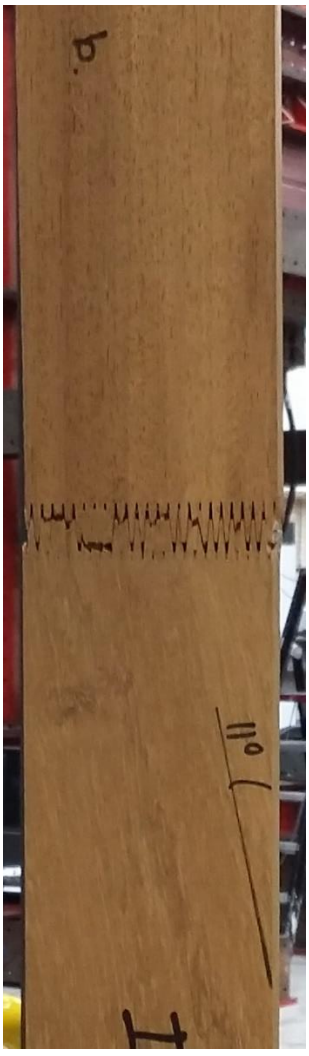

Figure 69: Failure of both fingers and glue (II-24).

Figure 70: Wood failure (II-30).

Figure 71: Failure of both wood and finger joint (II-29).

63% of all specimens failed at the finger joint; wood failure was 24% of all specimens and in 13% of the cases the failure mode was a combination of finger joint failure and wood failure. Detailed information on the failure modes of all batch II specimens can be found in Table 67 (Appendix 7).

8.3.3 Failure modes of batch IV

Two failure modes are distinguished for the batch IV specimens: finger joint failure and wood failure. Generally, it appeared that 75% of the specimens failed at the finger joint and 25% of the specimens failed at the wood. However, in some cases of finger joint failure the failure mode was in fact a combination of finger joint failure and wood failure. Table 20 lists the failure modes of all specimens.

No.	Failure type	Comment
1	Wood	Crack in lamella no. III-9 and III-21.
2	Finger joint	Finger joint partly broken; crack in lamella no. III-14.
3	Finger joint	
4	Finger joint	
5	Wood	Crack in lamella no. III-11 and III-10.
6	Wood	Crack in lamella no. III-7 and III-7.
7	Finger joint	
8	Finger joint	Finger joint partly broken; crack in lamella no. III-29 and unknown lamella.
9	Finger joint	
10	Finger joint	
11	Finger joint	Finger joint partly broken; crack in lamella no. III-11 and III-18.
12	Finger joint	Finger joint partly broken; crack in lamella no. III-4 and III-23.

Table 20: Failure modes of batch IV specimens.

It is apparent that wood failure of specimens in some cases coincided with the grain angle: see Figure 72 for specimen IV-5 and Figure 73 for specimen IV-6.


Figure 72: Failure of specimen IV-5.


Figure 73: Failure of specimen IV-6.

Figure 74 till Figure 85 show the beam layup of the 12 glulam beams, including the crack formation indicated with a red line. The length of each individual lamella is given in mm, as well as its label. Each lamella is part of batch III; the data of batch III before laminating is presented in Appendix 8. In the longitudinal direction, the lamellas are connected with finger joints, indicated with a vertical line |. Some lamellas of the glulam beams were not traceable, these lamellas are indicated with a "U" (unknown).

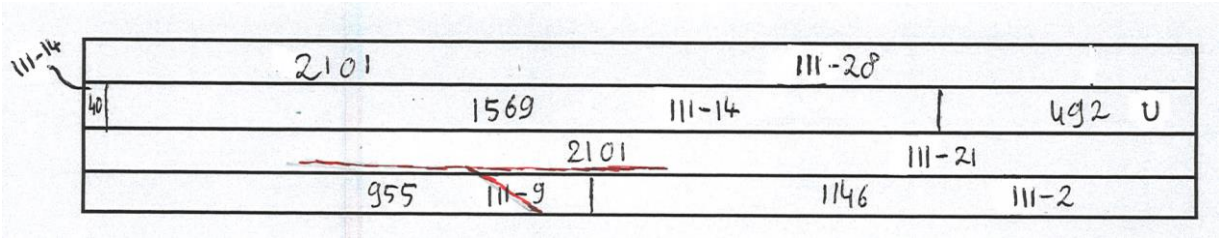

Figure 74: Beam layup and crack formation of specimen IV-1.

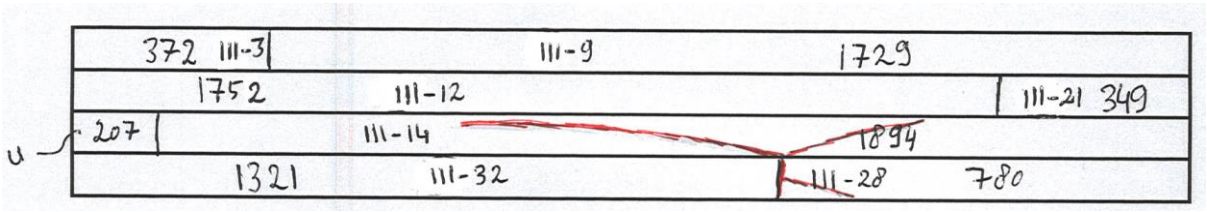

Figure 75: Beam layup and crack formation of specimen IV-2.

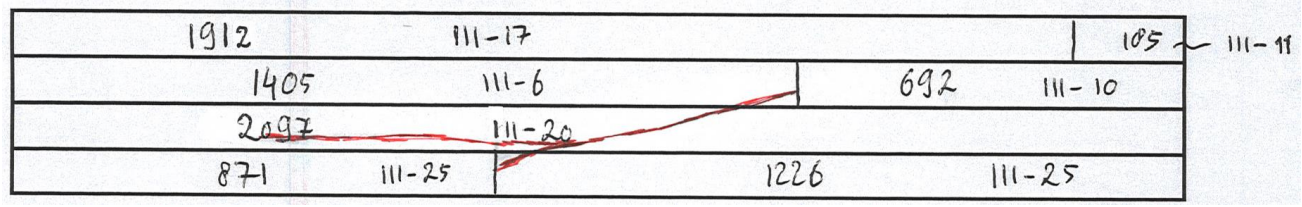

Figure 76: Beam layup and crack formation of specimen IV-3.

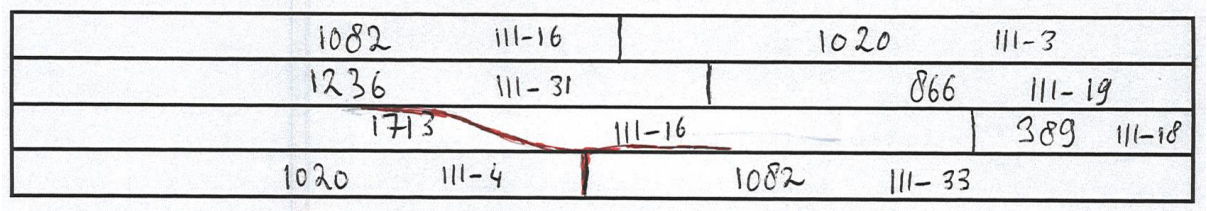

Figure 77: Beam layup and crack formation of specimen IV-4.

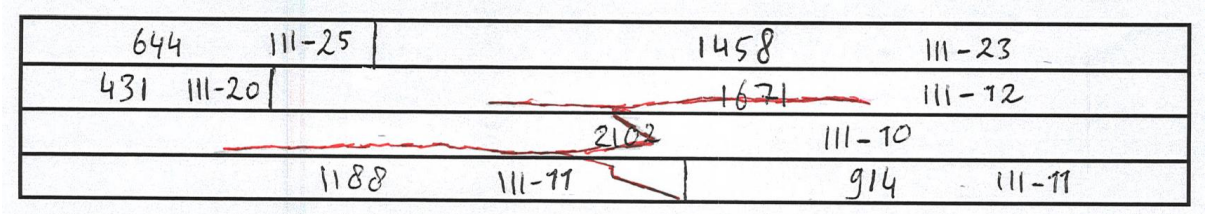

Figure 78: Beam layup and crack formation of specimen IV-5.

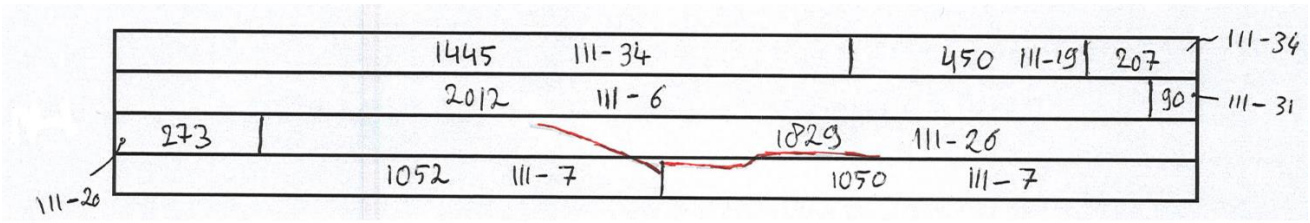

Figure 79: Beam layup and crack formation of specimen IV-6.

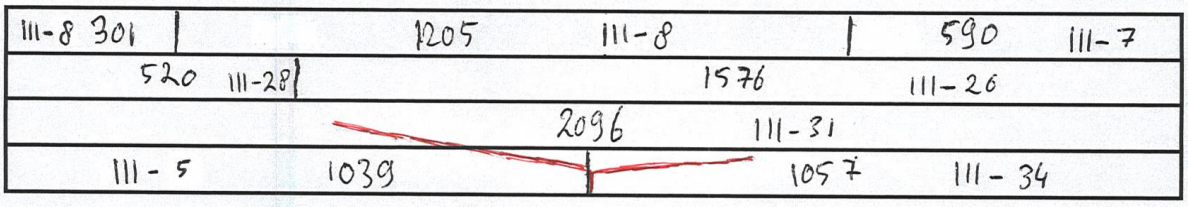

Figure 80: Beam layup and crack formation of specimen IV-7.

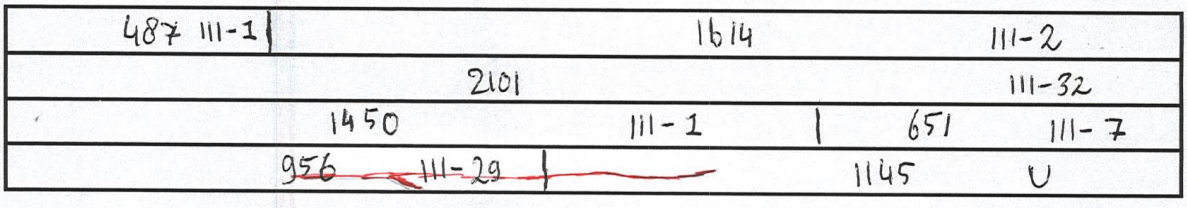

Figure 81: Beam layup and crack formation of specimen IV-8.

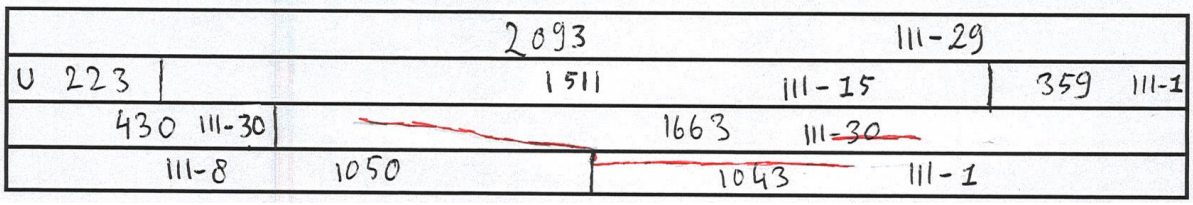

Figure 82: Beam layup and crack formation of specimen IV-9.

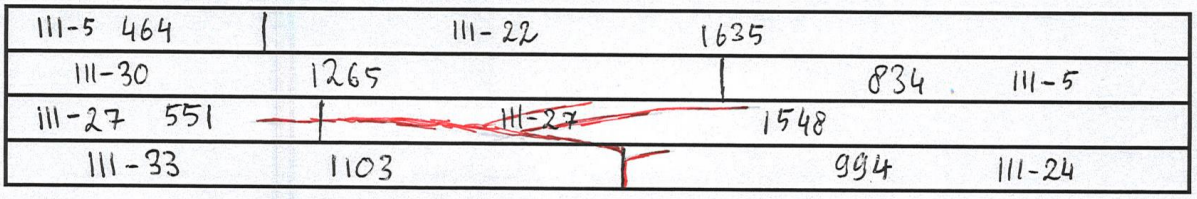

Figure 83: Beam layup and crack formation of specimen IV-10.

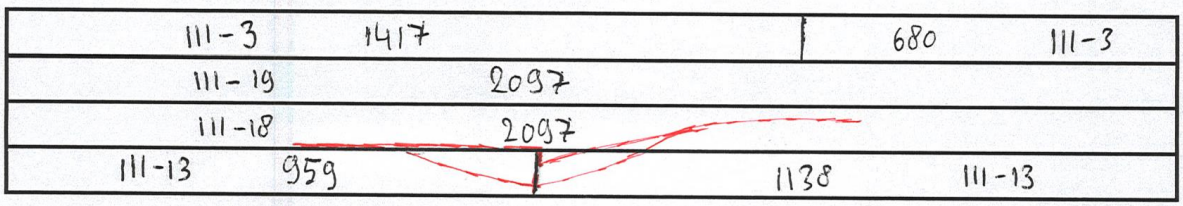

Figure 84: Beam layup and crack formation of specimen IV-11.

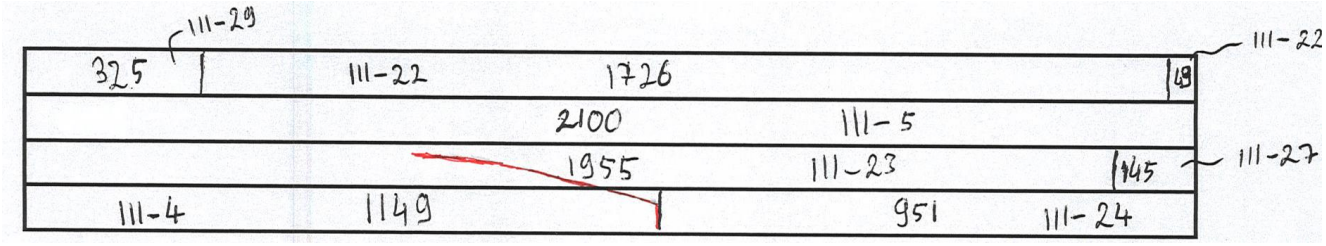

Figure 85: Beam layup and crack formation of specimen IV-12.

9. Systematic investigation of test data

9.1 General remarks on the test results

Table 21 repeats part of the calculated results presented in Table 19.

Summary calculation results of batch I-IV						
Batch I # 38	**ρ [kg/m^3]**		**$f_{t,l}$ [N/mm^2]**	**E_{dyn} [N/mm^2]**	**E_t [N/mm^2**	
mean	660.31		59.23	15101	15076	
COV	0.07		0.37	0.20	0.18	
Char. val.	578.05		17.05	9523	10016	
Batch II # 38	**ρ (a) [kg/m^3]**	**ρ (b) [kg/m^3]**	**$f_{t,j}$ [N/mm^2]**	**E_{dyn} [N/mm^2]**	**E_t [N/mm^2**	
mean	653.88	659.89	39.54	13799	13242	
COV	0.08	0.06	0.15	0.14	0.14	
Char. val.	561.82	581.10	28.64	10244	9818	
Batch III # 34	**ρ [kg/m^3]**			**E_{dyn} [N/mm^2]**		
mean	623.07			14221		
COV	0.07			0.10		
Char. val.	547.09			11676		
Batch IV # 12	**ρ [kg/m^3]**		**$f_{m,g}$ [N/mm^2]**	**E_{dyn} [N/mm^2]**	**E_{loc} [N/mm^2]**	**E_{glob} [N/mm^2]**
mean	619.81		65.50	14407	14878	13659
COV	0.03		0.14	0.05	0.05	0.06
Char. val.	581.30		42.30	12994	13380	12085

Table 21: Calculated test results (parts of it).

It appears from the test results that the mean values of density are in the range of 620-660 kg/m^3, which is a rather close range and agrees very well with mean values from literature presented in Chapter 4.

Comparing the results for dynamic modulus of elasticity of batch I and III, the latter shows a smaller COV and thus less scatter. However, mean values lie very close (15101 N/mm^2 and 14221 N/mm^2, respectively). This agrees very well with literature values, if assuming $E_{dyn} = E_{glob} / 0.81$ (see subsection 5.2.2 and Ravenshorst et al., 2009).

About the finger joint tension strength results, differentiating these strength values with respect to the failure modes finger joint, wood and combination shows that at both mean and characteristic level the strength values do not deviate very much (Table 22).

[N/mm²]	Finger joint	Wood	Combination	All
min	22.70	28.99	31.55	22.70
max	48.83	48.61	44.53	48.83
mean	40.41	39.00	36.32	39.54
stdev	5.74	6.73	5.17	5.93
COV	0.14	0.17	0.14	0.15
Char. val.	29.85	26.62	26.82	28.64

Table 22: Finger joint strength values differentiated with respect to failure mode.

The mean lamella tension strength is equal to 59.2 N/mm^2, the mean finger joint tension strength 39.5 N/mm^2 and the mean glulam bending strength 65.5 N/mm^2. It was however expected that the glulam bending strength would not exceed the finger joint tension strength. This can be explained by the Weibull size effect as mentioned in section 3.5: beams with small depth will yield higher bending strengths compared to beams with greater depth. In addition to this, finite element models have explained this phenomenon by assuming quasi-brittle behaviour of the glulam beams (Blank et al., 2017). Taken both aspects into account, it is very likely that iroko glulam beams with depths of structural size will show lower bending strengths than reported in this thesis.

Blank et al. (2017) reports measured mean bending strength of glulam beam of depth 100 mm and 1000 mm of 49.5 N/mm^2 and 28.3 N/mm^2, respectively, while the specimens fitted strength class GL24. The investigated spruce glulam beams had a length to depth ratio of about 18, which is about equal to the iroko glulam beams investigated in this thesis. Therefore, a size factor of 1.75 is postulated for structural size glulam beams. This results in a mean bending strength for iroko glulam beam with structural sizes of 37.4 N/mm^2, which agrees very well with the mean finger joint tension strength. It should be noted however that the mentioned spruce glulam beams with depth of 100 mm were not finger jointed. As finger jointed glulam beam will most likely yield lower bending strengths (as is the case with scarf jointed glulam beams: see Corigliano et al., 2016), this postulated size factor of 1.75 could be a little lower.

Considering the glulam bending strength / lamella tension strength on the mean level, its ratio equals 1.11, and on the characteristic level its ratio equals 2.48. It was observed that the specimens loaded in tension did not bend laterally (see subsection 3.3.1). Reinforcement of defects (grain angle, finger joints) and dispersion of low strength timber did most likely occur during the bending tests, which can explain the lamination factor being greater than 1.0.

9.2 Regression analyses

9.2.1 Visual grading and Hankinson (batch I)

BS 5657 (2007) requires for strength grade HS a maximum slope of grain equal to 1 in 11, that is equal to a grain angle not greater than 5.2° (see also subsection 2.4.1 and section 3.6). Assuming then that the grain angle equals the angle of failure, one can make the following distinction: lamellas with an angle of failure of 5° or less, and with an angle of failure greater than 5°. This would result in the mechanical and physical characteristics presented in Table 23.

		all α (38 specimens)		α ≤ 5° (24 specimens)	
Symbol	**Unit**	**Mean**	**Char. value**	**Mean**	**Char. value**
$f_{t,l}$	N/mm^2	59.23	17.05	68.71	26.91
ρ	kg/m^3	660	578	661	588
E_t	N/mm^2	15076	10016	15756	10843
E_{dyn}	N/mm^2	15101	9523	15871	9765

Table 23: Mechanical and physical characteristics of batch I – distinguished on the basis of grain angle.

From this, it can be concluded that the grain angle has a profound influence on the tension strength: the smaller this angle is, the stronger the material. This is as expected from theory. Furthermore, it appears that with small grain angles the stiffness is only a little greater; regarding density this positive influence is even smaller.
Regression analyses seem to conform this. Referring to literature, Van der Have (2013) presents models relating the tension strength to the angle of failure and the modulus of elasticity to the angle of failure. Models that fit this data into a form of the Hankinson-equation, concerning tension strength and modulus of elasticity in tension are presented:

$$f_{t,\alpha} = \frac{P}{\frac{P}{Q}\sin^n \alpha + \cos^n \alpha}$$

$$E_{t,\alpha} = \frac{P}{\frac{P}{Q}\sin^n \alpha + \cos^n \alpha}$$

The reading of these symbols is shown in Table 24.

Symbol	Quantity	Unit	Value
$f_{t,\alpha}$	tension strength at angle α	N/mm^2	
$E_{t,\alpha}$	modulus of elasticity in tension at angle α	N/mm^2	
P ($f_{t,0}$)	mean tension strength parallel to grain of which α = 0°	N/mm^2	62.44
P (E_t)	mean modulus of elasticity in tension, parallel to grain of which α = 0°	N/mm^2	15329
Q ($f_{t,90}$)	tension strength perpendicular to grain	N/mm^2	
Q ($E_{t,90}$)	modulus of elasticity in tension, perpendicular to grain	N/mm^2	
α	angle of failure	°	
n	exponent	-	

Table 24: Quantities associated with Hankinson-type equation.

Five analyses regarding tension strength were performed, of which four with initial values mentioned in Bodig et al. (1982). Table 25 shows the input and output values of the nonlinear regression and Figure 86 shows the curves of the regression models. Also, three analyses regarding modulus of elasticity in tension were performed, of which two with initial values mentioned in Bodig et al. (1982). Table 26 shows the input and output values of the nonlinear regression and Figure 87 shows the curves of the regression models.

Input and output nonlinear regression analysis (tension strength)					
	Initial values		Results		
No.	Q	n	Q	n	Q/P
1	0.04×P	1.5	1.956127	2.728662	0.031328
2	0.04×P	2	1.68498	2.814383	0.026986
3	0.07×P	1.5	1.612385	2.838232	0.025823
4	0.07×P	2	1.473842	2.851024	0.023604
5	none	none	2.219344	2.659631	0.035544

Table 25: Input and output nonlinear regression analysis regarding tension strength.

Input and output nonlinear regression analysis (MOE)					
	Initial values		Results		
No.	***Q***	***n***	***Q***	***n***	***Q/P***
1	0.04×P	2.0	5242.080605	2.0187449	0.341960505
2	0.12×P	2.0	5119.337167	2.0335491	0.333953492
3	none	none	5184.878566	2.0253773	0.338229003

Table 26: Input and output nonlinear regression analysis regarding modulus of elasticity in tension.

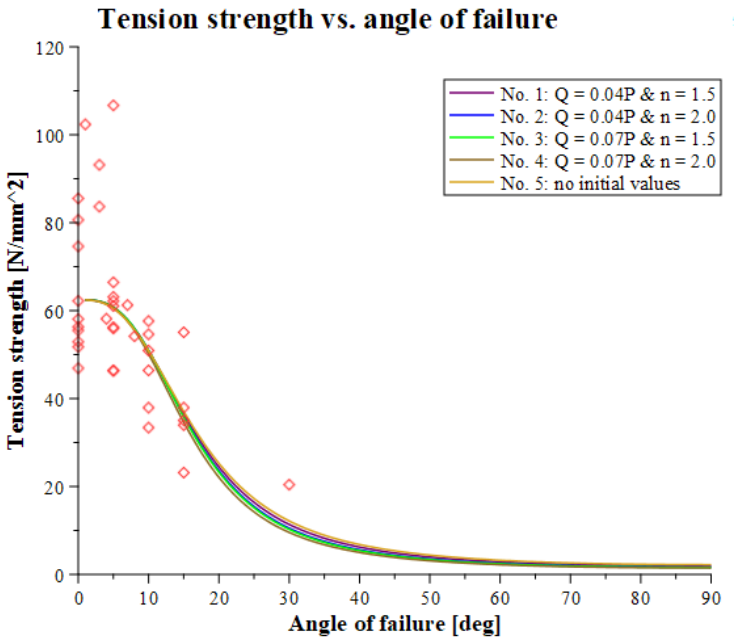

Figure 86: Batch I: nonlinear models of tension strength vs. angle of failure.

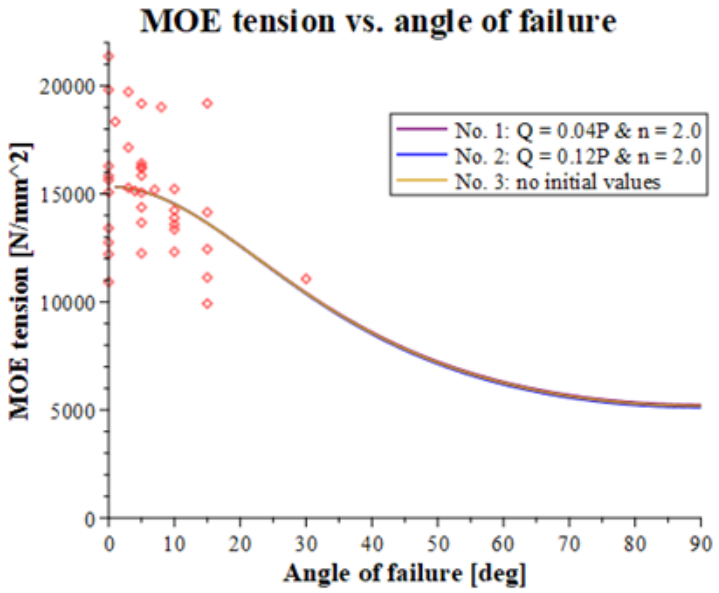

Figure 87: Batch I: nonlinear models of modulus of elasticity in tension vs. angle of failure.

It appears that the five and two models for tension strength and modulus of elasticity in tension respectively, lie very close to each other. Regarding tension strength: model 5 gives output parameters which are closest to the literature values. Regarding modulus of elasticity in tension: the fits seem to be less accurate than those for tension strength. It should be noted however that the data upon which

these curves are based is limited, as the greatest failure angle taken into account is 30°. Therefore, more research is required to verify these regression lines beyond a failure angle of 30°.

9.2.2 Relationships between mechanical and physical properties

This subsection reports of relationships between several mechanical and physical properties of the specimens of batch I, II and IV; see Table 27, Table 28 and Table 29, respectively. In these Tables the first column shows the investigated pairs of related properties; the second column presents the slope of the linear regression line; the third column presents the intercept and the last column the coefficient of determination. Appendix 13-15 presents the corresponding scatterplots: 5 plots in batch I, 11 plots in batch II and 10 plots in batch IV.

Batch I properties	a	b	R^2
$\rho - E_{dyn}$	-7.724	20201.327	0.013
$\rho - E_t$	-6.904	19634.830	0.013
$\rho - f_{t,l}$	-0.002	60.620	0.000
$E_{dyn} - f_{t,l}$	0.004	-1.099	0.303
$E_t - f_{t,l}$	0.005	-10.148	0.331
$E_{dyn} - E_t$	0.423	8692.297	0.217

Table 27: Batch I: relationships between mechanical and physical properties.

Batch II properties	a	b	R^2
ρ **(part a)** $- E_{dyn}$	6.365	9637.456	0.027
ρ **(part b)** $- E_{dyn}$	-2.091	15179.145	0.002
ρ **(mean a,b)** $- E_{dyn}$	4.791	10652.118	0.008
ρ **(part a)** $- E_t$	5.875	9400.533	0.025
ρ **(part b)** $- E_t$	-4.197	16011.666	0.009
ρ **(mean a,b)** $- E_t$	2.776	11418.508	0.003
ρ **(part a)** $- f_{t,j}$	0.009	33.413	0.006
ρ **(part b)** $- f_{t,j}$	0.019	26.673	0.020
ρ **(mean a,b)** $- f_{t,j}$	0.023	24.142	0.020
$E_{dyn} - f_{t,j}$	0.001	24.931	0.119
$E_t - f_{t,j}$	0.001	28.041	0.074
$E_{dyn} - E_t$	0.887	1002.245	0.848

Table 28: Batch II: relationships between mechanical and physical properties.

Batch IV properties	a	b	R^2
$\rho - E_{dyn}$	9.157	8731.696	0.062
$\rho - E_{loc}$	4.175	12290.762	0.012
$\rho - E_{glob}$	6.699	9506.636	0.027
$E_{glob} - E_{loc}$	0.769	4372.164	0.653
$E_{dyn} - E_{loc}$	0.612	6061.515	0.333
$E_{dyn} - E_{glob}$	0.860	1270.362	0.596
$\rho - f_{m,g}$	-0.074	111.109	0.022
$E_{dyn} - f_{m,g}$	0.001	53.437	0.004
$E_{loc} - f_{m,g}$	0.000	69.085	0.000
$E_{glob} - f_{m,g}$	-0.002	97.739	0.038

Table 29: Batch IV: relationships between mechanical and physical properties.

From these results, the following can be observed and concluded:

- Density does not influence any strength or stiffness property, for both iroko sawn timber, finger joints, and glulam beams. For sawn timber, this is in contrary what would be expected from theory as presented in previous chapters. For glulam beams however, literature suggests indeed that there is no correlation between bending strength and both density and modulus of elasticity.
- Stiffness does not seem to be a very good predictor for strength properties either, again for both iroko sawn timber and glulam. Concerning sawn timber however (batch I), when disregarding one outlier (specimen I-19) the coefficient of determination with respect to E_{dyn} and $f_{t,l}$ becomes 0.616 instead of 0.303. Even so, the coefficient of determination with respect to E_t and $f_{t,l}$ becomes 0.541 instead of 0.331 when disregarding two outliers (specimen I-30 and I-37).
- Considering the glulam beams, a slight correlating exists between E_{dyn} and E_{loc}; and the pairs E_{glob} and E_{loc}, and E_{dyn} and E_{glob} seem to be reasonably well correlated.

9.2.3 Relationships between glulam bending strength and lamella strength and stiffness

For all batch IV specimens, it holds that failure occurred in the outer lamellas of the tension zone. This subsection compares the bending stresses in the glulam beams with the lamella and finger joint tension strength. Also, it aims to relate the stiffness of the batch III specimens with the occurring bending stresses in the tension zone of the batch IV specimens.

Subsection 8.3.3 presented the failure modes of all 12 batch IV specimens, see Table 20. Now this table is extended in Table 30 with the corresponding stiffness of the (batch III) lamellas that failed during the bending test series. Also, the bending strength is repeated in this table.

No.	Failure mode	Failed outer lamella(s)		Failed inner lamella	Corresponding E_{dyn} [N/mm^2]			$f_{m,g}$ [N/mm^2]
1	Wood	III-9		III-21	12093		12766	52.41
2	Finger joint	III-32	III-28	III-14	16591	15611	12798	71.08
3	Finger joint	III-25	III-25	III-20	16532	16532	13051	71.22
4	Finger joint	III-4	III-33	III-16	13529	13075	13162	79.45
5	Wood	III-11		III-10	12285		11138	63.20
6	Wood	III-7	III-7		16778	16778		70.40
7	Finger joint	III-5	III-34	III-31	15920	14379	15423	66.35
8	Finger joint	III-29	unknown		13453			64.81
9	Finger joint	III-8	III-1	III-30	13575	13442	15190	50.25
10	Finger joint	III-33	III-24	III-27	13075	15225	15756	72.93
11	Finger joint	III-13	III-13	III-18	14231	14231	14619	71.65
12	Finger joint	III-4		III-23	13529		14561	52.24

Table 30: Failure modes batch IV with corresponding stiffness of failed (batch III) lamellas.

Figure 88 shows a scatterplot of the dynamic modulus of elasticity of the failed outer lamellas and corresponding glulam bending strength. A poor correlation (R^2-value of 0.180) was found when considering the dynamic modulus of elasticity of the batch III specimens listed in the third column of Table 30 and the bending strength of the corresponding specimens of batch IV. This could be due to the high number of finger joint failures of the glulam beams.

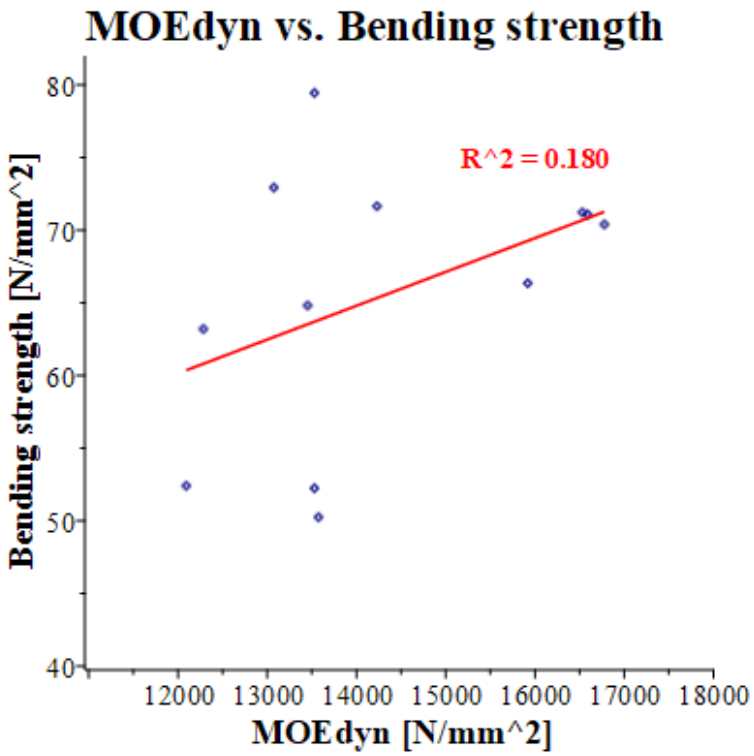

Figure 88: Dynamic modulus of elasticity of outer lamellas vs. glulam bending strength.

9.2.4 Multivariate linear regression analysis

To take into account the finger joint tension strength in predicting the glulam bending strength, a multivariate linear regression analysis was performed. The procedure was as followed:

1. Sort from low to high every single dynamic modulus of elasticity value of batch I, II and IV.
2. Sort the tension strength values, finger joint tension strength values and bending strength values after their respective ranking of dynamic modulus of elasticity (see step 1).
3. Delete from batch I and II the lowest two values of tension strength and finger joint strength values. Result is 36 values for tension strength, 36 values for finger joint tension strength.
4. Create 4 groups per batch and thus 12 groups in total.
5. Based upon the ranking resulting from steps 1-3, fill the groups with strength values. This results in 9 tension strength values per group for batch I and II, and 3 bending strength values for batch IV (Table 31).

Batch // Group	1	2	3	4
I	9	9	9	9
II	9	9	9	9
IV	3	3	3	3

Table 31: Number of specimens per MVLRA Group.

6. Calculate per group the characteristic strength value.
7. Perform an automated linear regression with the 12 characteristic strength values.

Table 32 shows the result of the multivariate linear regression analysis.

Results multivariate linear regression analysis				
Model: $f_{m,g,k}$ = 28.477414 + 4.2731220 × f_{tlk} - 3.3391044 × f_{tjk}				
	Estimate	**Std. Error**	**t-value**	**P (>|t|)**
Parameter 1	28.4774	55.6344	0.5119	0.6988
Parameter 2	4.2731	3.2582	1.3115	0.4147
Parameter 3	-3.3391	4.2808	-0.7800	0.5783
R^2: 0.7816; adjusted R^2: 0.3448				

Table 32: Results multivariate linear regression analysis.

The standard error is an estimate of the standard error of the calculated parameters. The t-value is the quotient of parameter value and standard error. Both these quantities are relatively high. This is therefore not a very accurate model.

9.3 Strength predicting models from literature

The four strength prediction models mentioned in subsection 5.3.2 are validated with the test data. All of these methods are based on glulam made of softwood, not tropical hardwood (as mentioned). The input parameters are presented in Table 33.

Input parameter	Unit	Value
Char. lamella tension strength	N/mm^2	26.05
Char. finger joint bending strength	N/mm^2	30.22
Mean modulus of elasticity (glulam beam)	N/mm^2	14878
Mean modulus of elasticity (sawn timber)	N/mm^2	14087
Char. density	kg/m^3	578

Table 33: Input parameters to validate strength prediction models.

In this the finger joint bending strength from previous tests at Heko Spanten's facility is used (see also subsection 4.2.4), instead of the for this thesis experimentally determined finger joint tension strength. The first reason is that all this four methods depend on the finger joint bending strength. Another reason is that a finger joint bending strength equal to 1.4 times the finger joint tension strength is assumed in the counterpart of method 2 and in method 4. However, the test data suggests a ratio of 1.06 (= 30.22/28.64) rather than 1.4 for iroko finger joints.

The four methods are:

1. The curves presented in Colling (1995), see Figure 29 in subsection 5.3.2.
2. Equation 7 from Frese et al. (2009a):

$$f_{m,g,k} = 3.454 + 0.7125 \cdot f_{m,j,k} - 0.01078 \cdot f_{m,j,k}^2 - 0.01632 \cdot f_{t,l,k}^2 + 0.02558 \cdot f_{m,j,k} \cdot f_{t,l,k}$$

3. Tables 1 and 3 from NEN-EN 14080 (2013).
4. The formula given in Table 6 from NEN-EN 14080 (2013):

$$f_{m,g,k} = -2.2 + 2.5 \cdot f_{t,l,k}^{0.75} + 1.5 \cdot \left(f_{m,j,k} / 1.4 + 6 \right)^{0.65}$$

By means of these estimated characteristic glulam bending strengths, the glulam strength class is determined (Table 5 from NEN 14080, 2013). The results are presented in Table 34, including the limiting factor (in which the characteristic glulam bending strength is the main limiting factor).

Method no.	$f_{m,g,k}$ [N/mm^2]	Glulam strength class	Limiting factor
1	23	GL 22h	finger joint bending strength
2	24.1	GL 24h	glulam bending strength
3	24	GL 24h	finger joint bending strength
4	40.3	GL 32h	system of strength classes

Table 34: Validation of strength prediction models.

It is apparent that the first three methods yield very conservative bending strength values of iroko glulam; the method from NEN-EN 14080 (2013) fits the test data quite well as the characteristic glulam bending strength from the tests is equal to 42.30 N/mm^2.

9.4 Combined visual and mechanical grading of unjointed lamellas

In subsection 9.2.1, the specimens of batch I were visually graded: distinction was made on the basis of the grain angle. The batch I specimens can be further graded based on both grain angle and dynamic modulus of elasticity. This is called combined visual and mechanical grading; Table 35 presents the results with four classes for the dynamic modulus of elasticity, and Table 36 presents the results with two classes for the dynamic modulus of elasticity. The entries of these tables show the number of specimens in the different classes, and in brackets the characteristic tension strength is shown. Note: not all the specimens are taken into account in this analysis, because a few batch I specimens have a dynamic modulus of elasticity lower than 10000 N/mm^2.

E_{dyn} [N/mm^2]	$\alpha \leq 5°$	$\alpha > 5°$	#
≥ 17500	5 [46.56]	0 [n/a]	5
≥ 15000	16 [43.74]	4 [25.09]	15
≥ 12500	21 [32.51]	11 [27.22]	12
≥ 10000	21 [n/a]	13 [<0]	2
#	21	13	34

Table 35: Combined visual and mechanical grading; dynamic modulus of elasticity with 4 classes.

E_{dyn} [N/mm^2]	$\alpha \leq 5°$	$\alpha > 5°$	#
≥ 15000	16 [32.44]	4 [25.09]	20
≥ 10000	21 [32.51]	13 [18.07]	14
#	21	13	34

Table 36: Combined visual and mechanical grading; dynamic modulus of elasticity with 2 classes.

It appears that applying combined visual and mechanical grading with two visual classes (grain angle) and four mechanical classes (dynamic modulus of elasticity) gives a high yield for the tension strength of unjointed lamellas; even so applying four mechanical classes based on dynamic modulus of elasticity gives the highest yield.

9.5 Ratios for moduli of elasticity

Table 37 presents both literature values as mean test values for moduli of elasticity ratios.

Type	MOE	Literature	Tests
Sawn timber	E_t / E_{dyn}	0.92	1.05
Glulam beams	E_{glob} / E_{dyn}	0.81	0.92
	E_{loc} / E_{dyn}	0.92	1.03
	E_{loc} / E_{glob}	1.16	1.09

Table 37: Moduli of elasticity ratios.

It appears that literature values do not apply on the test data. However, literature presents sawn timber data which do not need to apply for glulam beams.

9.6 Strength classes

9.5.1 Introduction

From the mechanical and physical properties derived from the test results, one can propose strength classes for iroko sawn timber and glulam beams. The second subsection presents feedback on the values of mechanical and physical properties found in literature, as shown in Chapters 4 and 5. The last subsection presents the proposed strength classes.

9.5.2 Feedback on literature review of mechanical and physical properties

Table 38 presents a comparison of values of mechanical and physical properties of both iroko sawn timber and glulam beams, from literature and test results.

			MEAN		CHAR. VALUE	
Type	**Property**	**Unit**	**Literature**	**Tests**	**Literature**	**Tests**
Sawn timber	Density	kg/m^3	530-760	623-660		
	Local MOE	N/mm^2	13920 [1)]	15076		
	Dynamic MOE	N/mm^2	14800 [2)]	15101		
	Tension strength	N/mm^2	38.3	59.2	22.1	17.1 (26.9)
Glulam beams	Density	kg/m^3	630	620		
	Local MOE	N/mm^2	12494	14878	10692	13380
	Bending strength	N/mm^2	73.9	65.5	59.8	42.3
	Bending strength	N/mm^2	50.0		30.2	
Finger joints	Tension strength	N/mm^2	39.5		28.6	21.6 [3)]
Notes						
1)	Taken as 1.16×E_{glob}					
2)	Taken as E_{glob} / 0.81					
3)	Taken as $f_{t,j,k}$ / 1.4					

Table 38: Comparison mechanical and physical properties from literature and tests.

It is apparent that iroko sawn timber seems to be stronger and stiffer than literature values imply (assuming however that $\alpha \leq 5°$). The test results of glulam beams show a stiffer behaviour, though the strength is lower. This can be very well explained by the fact that the literature bending strength values are based on glulam beams without finger joints. On the characteristic level, the finger joint tension strength resulting from tests is greater than the expected finger joint bending strength divided by 1.4.

9.5.3 Proposed strength classes

From the experimental results and the previous analyses, one can propose to grade iroko sawn timber and iroko glulam beams as listed in Table 39.

Type	Strength class	Indicating properties	Conditions and/or assumptions	Reference
Sawn timber	T16	$f_{t,l,k}$, $E_{t,mean}$, ρ_k	none	NEN-EN 338 (2016)
Sawn timber	T26	$f_{t,l,k}$, $E_{t,mean}$, ρ_k	$\alpha \leq 5°$	NEN-EN 338 (2016)
Sawn timber	DT25	$f_{t,l,k}$, $E_{t,mean}$, ρ_k	$\alpha \leq 5°$	Kovryga et al (2016)
Sawn timber	DT30	$f_{t,l,k}$, $E_{t,mean}$, ρ_k	$\alpha \leq 5°$; $E_{dyn} > 12500$ N/mm^2	Kovryga et al (2016); section 9.4
Sawn timber	D27	ρ_k	$f_{m,k} = f_{t,l,k}/0.6$; $E_{loc,mean} = E_{t,mean}$	NEN-EN 338 (2016)
Sawn timber	D40	ρ_k	$\alpha \leq 5°$; $f_{m,k} = f_{t,l,k}/0.6$; $E_{loc,mean} = E_{t,mean}$	NEN-EN 338 (2016)
Glulam beams	GL32h	$f_{m,g,k}$, $E_{loc,mean}$, ρ_k	none	NEN-EN 14080 (2013)
Glulam beams	GL36c	$f_{m,g,k}$, $E_{loc,mean}$, $E_{loc,k}$	no knot ratio values	Frese et al. (2005)

Table 39: Proposed strength classes for iroko sawn timber and glulam beams.

However, no bending tests on iroko sawn timber were performed for this thesis. Therefore, proposed strength classes for sawn timber based on bending strength (D27 and D40) are indicative only.

10. Conclusions and recommendations

In this thesis, parameters that influence the strength of glue laminated iroko beams have been investigated: strength tests have been conducted on 12 glulam beams, 38 unjointed lamellas and 38 finger jointed lamellas. The main question and sub questions are repeated here from section 1.3, followed by its answers; the Chapter closes with a list of recommendations.

Main question

The main question is:

What defines the characteristic bending strength of iroko glulam beams, and which properties influence this bending strength?

The characteristic bending strength of iroko glulam beams is calculated from multiple maximum bending stresses following from four point bending tests conducted on these beams. Requirements hold for depth to span ratio and reference depth. Influencing properties on the bending strength are mean finger joint tension strength and mean lamella tension strength. Thereby, size effect and quasi-brittle failure play an important role: the beam bending strength decreases with increasing depth. Also the lamination effect has its part to play: the glued lamellas reinforce weaker sections in the lamellas and if lower strength pieces are randomly distributed over the beam, there is reduced probability that these pieces will initiate beam failure.

Sub questions

The sub question are:

What is the relationship between the bending strength of iroko glulam beams on the one hand and the tension strength of lamellas and finger joints on the other hand?

A strong mathematical relationship between characteristic glulam bending strength and both lamella tension strength and finger joint strength was not found. However, about 75% of the beams failed at the finger joint in the tension zone, which confirms that the finger joint is a strength influencing parameter. The wood failure of the glulam beams is (partially) due to failure on the grain angle.

Of glulam beams: what is the relationship between the density/modulus of elasticity and the experimentally derived bending strength?

Density nor modulus of elasticity has a profound influence on the bending strength of iroko glulam beams, on the contrary what was expected from theory. Only a slight to reasonable correlation was found between local, global and dynamic modulus of elasticity.

Of lamellas: what is the relationship between the density/modulus of elasticity and the experimentally derived (finger joint) tension strength?

Density nor modulus of elasticity has a profound influence on the tension strength of iroko finger jointed lamellas. Also, density does not influence the tension strength of iroko unjointed lamellas. However, there is a slight influence of the dynamic modulus of elasticity and the modulus of elasticity in tension of lamellas on its tension strength: it increases with increasing modulus of elasticity. R^2-values of about 0.3 were found, though with omitting outliers these would increase.

How do visual features influence the lamella tension strength and glulam beam bending strength?

Grain angle is a significant strength influencing parameter for the lamella tension strength. Distinguishing between specimens with a grain angle lower or equal than and greater than 5 degrees has a significant influence on the characteristic tension strength and a slight influence on the stiffness; specimens with low value grain angle yield higher strength and stiffness values. As for glulam beams, glued lamellas may fail at the grain angle. However, theory suggests a significant failure on the finger joint for glulam beams, which is confirmed by the experiments.

Is the current strength class D40 as defined in NEN-EN 338 (2016) a proper choice for iroko lamellas?

Iroko lamellas may be graded into strength class D40, on the condition that the grain angle is equal or lower than 5 degrees, and assuming that the characteristic bending strength equals the characteristic tension strength divided by 0.6. If the grain angle is greater than 5 degrees, strength class D27 would be appropriated. Iroko lamellas may also be graded into tension strength class T16; if the grain angle is lower or equal than 5 degrees, strength class T26 is feasible.

Is the assumed strength class GL24h as defined in NEN-EN 14080 (2013) a proper choice for iroko glulam beams?

The experimentally derived characteristic bending strength of glulam iroko beams is 42 N/mm^2, yet with a beam depth of 108 mm. This is higher than the presumed bending strength resulting from strength class GL24h. As stated however, due to the size effect and quasi-brittle failure of glulam beams, the bending strength of glulam beams decreases with increasing depth. If a size factor of 1.75 (instead of 1.1) holds, the characteristic bending strength would become: 42.3 N/mm^2 / 1.59 = 27 N/mm^2. Therefore, at the very least glulam strength class GL24h is indeed a proper choice for iroko glulam beams. Strength models from literature would suggest strength class GL32h (NEN-EN 14080, 2013) and GL36c (Frese et al, 2005).

Recommendations

The following features are recommended:

- Invest in sustainable timber production in the tropical regions of Africa where iroko trees grow in nature, to counteract the overexploitation of the species.
- Investigate the possibility of developing tree farming for *M. Excelsa* and *M. Regia*.
- Investigate how the source of the iroko timber influences its strength properties, i.e. take for the next iroko research programme specimens from its entire distribution area.
- As iroko is a strong, durable though endangered wood species, hybrid glulam beams may form an efficient bearing system. The outer lamellas of this hybrid beams are iroko lamellas, and the inner lamellas may consist of lower quality timber like spruce or other softwood species. Research is required to investigate its technological and economic feasibility, as well as its mechanical and physical properties.
- Investigate how to increase the finger joint strength, As the finger joint strength seems to govern the glulam bending strength. One of the aspects to be investigated should be the influence of the finger joint geometry on the finger joint tension strength.
- Investigate the size effect for glue laminated hardwoods i.e. set up a test programme glulam beams with different heights (and related spans).
- Investigate the influence of warp on the lamella tension strength.
- Use lamellas with a higher grain angle ($> 5°$) in lower stressed zones i.e. inner zone of glulam beams.
- Use lamellas with high dynamic modulus of elasticity and low grain ($\leq 5°$) in high stressed zones of glulam beams.

References

Literature

Ansell M. ea. (2015). *Wood composites*, Ch. 7 by C.B. Ong. Elsevier Ltd.

Blank L., Fink G., Jockwer R., Frangi A. (2017). *Quasi-brittle behaviour and size effect of glued laminated timber beams*. Eur. J. Wood Prod. (2017) 75:667-681.

Blaß H.J., Sandhaas C. (2017). *Timber Engineering – Principles for design.* Printed book. Karlsruher Institut für Technologie, Germany.

Bodig J., Jayne B.A. (1982) *Mechanics of wood and wood composites*. Van Nostrand Reinhold Company, New York, USA. Quoted from Green et al. (1999).

Brandner R., Schickhofer G. (2008) *Glued laminated timber in bending: new aspects concerning modelling.* Wood Science and Technology (2008) 42:401–425.

Bucci V., Corigliano P., Crupi V., Epasto G., Guglielmino E., Marinò A. (2016). *Experimental investigation on Iroko wood used in shipbuilding.* Proc. IMechE Part C: Journal of Mechanical Engineering Science 2017, Vol. 231(1) 128–139.

Colling F. (1990) *Tragfähigkeit von Biegeträgern aus Brettschichtholz in Abhängigkeit von den festigkeitsrelevanten Einflussgrößen*. PhD thesis. Universität Karlsruhe, Karlsruhe, Germany (in German).

Colling F. (1995) Brettschichtholz unter Biegebeanspruchung Step 3. Fachverlag Holz der Arbeitsgemeinschaft Holz e.V., Düsseldorf, Germany (in German).

De Jong J.D., De Richmont S.A.J., Ravenshorst G.J.P., De Vries P.A. (2011). *Research on the strength and durability characteristics of glued laminated iroko to be used in a wooden sailing ship – Phase 1*. Unpublished report by TNO. Delft, The Netherlands.

Ehrhart T., Fink G., Steiger R., Frangi A. *Strength grading of European beech lamellas for the production of GLT & CLT*. Proceedings of INTER—Meeting Forty-Nine, Graz, Austria, pp 29-43.

Falk, R.H. and Colling, F. (1995) *Laminating effect in glued-laminated timber beams*. Journal of Structural Engineering 1995.121:1857-1863.

Frese M., Blaß H.J. (2005). *Beech glulam strength classes.* CIB-W18 Meeting thirty-eight. Universität Karlsruhe, Karlsruhe, Germany.

Frese M., Blaß H.J. (2006). *Characteristic bending strength of beech glulam*. Materials and Structures (2006) 40:3–13.

Frese M., Blaß H.J. (2009a). *Bending strength of spruce glulam*. European Journal of Wood and Wood Products (2009) 67:277-286.

Frese M., Hunger F., Blaß H.J., Glos P. (2009b) *Verifikation von Festigkeitsmodellen für die Brettschichtholz-Biegefestigkeit*. European Journal of Wood and Wood Products (2010) 68:99-108.

Gérard J., Edi Kouassi A., Daigremont C., Détienne P., Fouquet D., Vernay M. (1998). *Synthèse sur les caractéristiques technologiques de référence des principaux bois commerciaux africains* (Overview of the technological reference characteristics of the main African commercial timbers). CIRAD-Forêt, Montpellier, France. (in French)

Glos P. (1995) *STEP lecture A6: Strength grading.* Timber Engineering STEP 1, edited by H.J. Blaß et al. First Edition, Centrum Hout, The Netherlands.

Goldstein E.W. (1999) Timber construction for architects and builders. McGraw-Hill, New York, USA.

Green D.W., Winandy J.E., Kretschmann D.E. (1999). *Chapter 4: Mechanical Properties of Wood.* Wood handbook: Wood as an engineering material. Forest Products Laboratory, Madison, USA.

Houtinstituut TNO (1961) *Buig- en drukproeven bij iroko van handelskwaliteit en afmetingen en bijbehorend foutvrij hout* (Bending and compression tests of structural size and clear wood iroko). Rapport H-61-147. Houtinstituut TNO. Delft, The Netherlands. (in Dutch)

JCSS: Joint Committee on Structural Safety (2006) *Probabilistic Model Code Part III: Resistance models, section 3.5 Properties of Timber.* See https://www.jcss.byg.dtu.dk/Publications/Probabilistic_Model_Code.

Kovryga, A., Stapel, P., Van de Kuilen, J.W.G. (2016). *Tensile strength classes for hardwoods.* INTER Proceedings Meeting 49. Graz, Austria.

Kuisch, H.P., Ravenshorst, G.J.P., Sailer, M. (2007). *The effect of moisture content and joint geometry on the bending strength of end-joints in 2 Surinamese wood species.*

Lara-Bocanegra A. J., Majano-Majano A., Crespo J., Guaita M. (2017). *Finger-jointed Eucalyptus globulus with 1C-PUR adhesive for high performance engineered laminated products.* Construction and Building Materials 135 (2017) 529-537.

Lehringer, C., Gabriel, J., 2014. *Review of recent research activities on one-component PUR-adhesives for engineered wood products*. In: Aicher, S., Reinhardt, H.-W., Garrecht, H. (Eds.), Materials and Joints in Timber Structures. In: RILEM Book Series, vol. 9. Springer, pp. 405–420.

Mvondo, R.R.N., Meukam P., Jeong J., De Sousa Meneses D., Nkeng E.G. (2017). *Influence of water content on the mechanical and chemical properties of tropical wood species.* Results in Physics, Volume 7, 2017, 2096-2103.

Orwa C., A Mutua, Kindt R., Jamnadass R., Anthony S. (2009) *Agroforestry Database: a tree reference and selection guide version 4.0.* See http://www.worldagroforestry.org/sites/treedbs/treedatabases.asp.

Ravenshorst G.J.P. (2015) *Species independent strength grading of structural timber*. PhD thesis. Technische Universiteit Delft, Delft, The Netherlands.

Ravenshorst, G. J. P., van de Kuilen J.W.G. (2009). Relationships between local, global and dynamic modulus of elasticity for soft- and hardwoods. In s.n. (Ed.), CIB-W18 Meeting forty-two (pp. 1-11). Universität Karlsruhe, Karlsruhe, Germany.

Rouger F. (1995) *STEP lecture B1: Volume and stress distribution effects.* Timber Engineering STEP 1, edited by H.J. Blaß et al. First Edition, Centrum Hout, The Netherlands.

Shinell A., Tison T., Have H.P. (2012) *Structural design of s/y Dream Symphony: the largest wooden ship ever built*. 22nd international HISWA symposium on Yacht design and Yacht construction, Amsterdam, 12-13 November 2012, pp.1e13. Edited by P.W. de Heer.

Stapel P., van de Kuilen J.W.G (2013) *Efficiency of visual strength grading of timber with respect to origin, species, cross section, and grading rules: a critical evaluation of the common standards.* Holzforschung 2014; 68(2): 203–216, Technische Universität München, München, Germany.

Steenbergen R.D.J.M. (2014). *CIE4130: Probabilistic design* (lecture slides). MSc course at Technische Universiteit Delft, Delft, The Netherlands.

Tropix 7 (2012). *Iroko's datasheet.* CIRAD. See https://tropix.cirad.fr/FichiersComplementaires/EN/Africa/IROKO.pdf

Van de Have, R. (2013). *De invloed van de vezelrichting op de mechanische eigenschappen van hout.* Bachelor Thesis. Technische Universiteit Delft, Delft, The Netherlands (in Dutch).

Vrouwenvelder A.C.W.M., Vrijling, J.K. (1982). *Probabilistisch ontwerpen.* TU Delft, Section Hydraulic Engineering (in Dutch). See http://resolver.tudelft.nl/uuid:ff7487f4-6b23-4032-a0a3-490a9c70143b.

Wiselius S. I. (1994) *Houtvademecum* (Wood vademecum). Kluwer, Deventer, The Netherlands (in Dutch).

Standards

BS 5756 (2007). Visual grading of hardwood-Specification- Determination of characteristic values of mechanical properties and density. BSI

DIN 4074-5 (2008) Sortierung von Holz nach der Tragfähigkeit – Teil 5: Laubschnittholz (in German).

NEN 5493 (2011) Kwaliteitseisen voor loofhout in grond-, weg- en waterbouwkundige werken en andere constructieve toepassingen (Quality requirements for hardwoods in civil engineering works and other structural applications) (in Dutch).

NEN-EN 338 (2016) Structural timber - Strength classes

NEN-EN 384 (2016) Structural timber - Determination of characteristic values of mechanical properties and density

NEN-EN 408 (2012). Timber Structures-Structural Timber and Glued Laminated timber Determination of some physical and mechanical properties. Brussels. CEN

NEN-EN 1194 (1999) Timber structures - Glued laminated timber - Strength classes and determination of characteristic values.

NEN-EN 1912 EN 1912 (2012). Structural Timber - Strength classes - Assignment of visual grades and species. Brussels. CEN.

NEN-EN 13183-1 (2002) Moisture content of a piece of sawn timber - Part 1: Determination by oven dry method.

NEN-EN 13183-3 (2005) Moisture content of a piece of sawn timber - Part 3: Estimation by capacitance method.

NEN-EN 13556 (2003) Round and sawn timber - Nomenclature of timbers used in Europe.

NEN-EN 14080 (2013) Timber structures - Glued laminated timber and glued solid timber – Requirements

NEN-EN 14081-1 (2016) Timber structures - Strength graded structural timber with rectangular cross section - Part 1: General requirements

NEN-EN 14358 (2016) Timber structures - Calculation and verification of characteristic values.

NEN-EN 1995-1-1 (2011). Eurocode 5. Design of timber structures - Part 1-1: General Common rules and rules for buildings. Delft. NEN.

Z-9.1-679 (2009) *Allgemeine Bauaufsichtliche Zulassung; BS-Holz aus Buche und BS-Holz Buche Hybridträger*. Studiengemeinschaft Holzleimbau e.V.; Wuppertal, Germany (in German).

Z-9.1-577 (2015) *Allgemeine Bauaufsichtliche Zulassung; Brettschichtholz aus Dark Red Meranti.* Deutsches Institut für Bautechnik, Berlin, Germany (in German).

Appendix 1: Data used to create Figure 11

This Appendix shows the data used to create Figure 11, mentioned in Chapter 3. Brandner et al. (2008) reports the following equations listed in Table 40 (linear) and Table 41 (nonlinear), relating the characteristic lamella tension strength to the characteristic glulam bending strength.

Linear equations		
Author reference	**Reference dimensions, size factors**	**Bearing model for GLT in bending**
Colling et al. (1991)	h_0 = 300 mm	$f_{m,g,k} = 10 + 1.4 f_{t,l,k}$
Falk et al. (1992)	h_0 = 600 mm w_0 = 150 mm	$f_{m,g,k} = 6 + 1.05 f_{t,l,k}$
Gehri (1992)	h_0 = 600 mm k_h = 0.20	$f_{m,g,k} = 12 + f_{t,l,k}$
Falk and Colling (1994)	h_0 = 305 mm w_0 = 150 mm l_0 = 533 mm k_h = 0.10 k_w = 0.10 k_l = 0.10	$f_{m,g,k} = 6.82 + 1.22 f_{t,l,k}$
Falk and Colling (1994)	h_0 = 600 mm k_h = 0.20	$f_{m,g,k} = 10 + 1.4 f_{t,l,k}$
Colling (1994) pr EN 1194 (1994)	h_0 = 600 mm	$f_{m,g,k} = 9 + 1.20 f_{t,l,k}$
Gehri (1995)	h_0 = 600 mm w_0 = 150 mm	Low COV-$f_{t,l}$: $f_{m,g,k} = 3.5 + 1.15 f_{t,l,k}$ High COV-$f_{t,l}$: $f_{m,g,k} = 3.5 + 1.25 f_{t,l,k}$
Falk and Colling (1995)	h_0 = 305 mm w_0 = 150 mm l_0 = 533 mm k_h = 0.10 k_w = 0.10 k_l = 0.10	$f_{m,g,k} = 6.82 + 1.22 f_{t,l,k}$ $f_{m,g,k} = 7.35 + 1.15 f_{t,l,k}$
Colling (1995)	h_0 = 600 mm k_h = 0.10	$f_{m,g,k} = 7 + 1.15 f_{t,l,k}$
pr EN 1194 (1995)	h_0 = 600 mm	$f_{m,g,k} = 9 + 1.20 f_{t,l,k}$
Schickhofer (1996)	h_0 = 600 mm k_h = 0.10	$f_{m,g,k} = 9.5 + f_{t,l,k}$
EN 1194 (1999)	h_0 = 600 mm w_0 = 150 mm k_h = 0.10 k_w = 0.05 k_l = 0.10	$f_{m,g,k} = 7 + 1.15 f_{t,l,k}$
Gehri (2005)	h_0 = 600 mm k_h = 0.10	Low COV-$f_{t,l}$: $f_{m,g,k} = 3.5 + 1.15 f_{t,l,k}$ High COV-$f_{t,l}$: $f_{m,g,k} = 3.5 + 1.25 f_{t,l,k}$

Table 40: Overview of linear relationships between characteristic lamella tension strength and characteristic glulam bending strength listed in Brandner et al. (2008).

Nonlinear equations		
Author reference	**Reference dimensions, size factors**	**Bearing model for GLT in bending**
Riberholt (1990)	h_0 = 300 mm k_h = 0.20	$f_{m,g,k} = \left(2.7 + 0.04 \cdot f_{t,l,k}\right) f_{t,l,k}$
Riberholt (1990)	h_0 = 600 mm k_h = 0.20zzz	$f_{m,g,k} = \left(2.35 + 0.035 \cdot f_{t,l,k}\right) f_{t,l,k}$
Gehri (2005)	h_0 = 600 mm k_h = 0.10	$f_{m,g,k} = 2.7\, f_{t,l,k}^{0.8}$

Table 41: Overview of nonlinear relationships between characteristic lamella tension strength and characteristic glulam bending strength listed in Brandner et al. (2008).

The author references listed in Table 40 and Table 41 are expanded in Table 42.

Reference	
Riberholt (1990)	Riberholt H. (1990) *Glued laminated timber - strength classes and determination of characteristic properties.* CIB-W18/23-12-4, 1-9. Lisbon, Portugal.
Colling et al. (1991)	Colling F., Ehlbeck J., Görlacher R. (1991) *Glued laminated timber - contribution to the determination of the bending strength of glulam beams*. CIB-W18/24-12-1, 1–17. Oxford, United Kingdom.
Falk et al. (1992)	Falk R.H., Solli K., Aasheim E. (1992) *The performance of glued laminated beams manufactured from machine stress graded norwegian spruce.* Norwegian Institute of Wood Technology, Publ. 77 [referenced by Gehri (1995)]
Gehri (1992)	Gehri E. (1992) *Determination of characteristic bending values of glued laminated timber - EN-approach and reality*. CIB-W18/25-12-1, 1–10. Åhus, Sweden.
Falk and Colling (1994)	Falk R.H., Colling F. (1994) *Glued-laminated timber: laminating effects.* PTEC 94,618–625, Gold Coast Australia, Australia.
Colling (1994)	Colling F. (1994) *Annexes to new draft of prEN 1194* [Ref. by Gehri 1995]
Gehri (1995)	Gehri E. (1995) *Determination of characteristic bending strength of glued laminated timber.* CIB-W18/28- 12-1, 1–4. Copenhagen, Denmark.
Falk and Colling (1995)	Falk R.H., Colling F. (1995) *Laminating effects in glued-laminated timber beams.* J Struct Eng 121/12/ 1857–1863
Colling (1995)	Colling F. (1995) *Brettschichtholz unter Biegebeanspruchung.* Informationsdienst Holz; Holzbauwerke; STEP 3: Holzbauwerke nach Eurocode 5: Grundlagen, Entwicklungen, Ergänzungen 5/1–18. Arbeitsgemeinschaft Holz e.V., Düsseldorf, Germany.
Schickhofer (1996)	Schickhofer G. (1996) *Development of efficient glued laminated timber*. CIB-W18/29-12-1, 1–17. Bordeaux, France
EN 1194 (1999)	EN 1194:1999 - Timber structures - Glued laminated timber - Strength classes and determination of characteristic values.
Gehri (2005)	Gehri E. (2005) *Zur Erfassung des Biegewiderstandes von Brettschichtholz - Gedanken im Hinblick auf die Überarbeitung der EN 1194.* Internes Paper, 1-9. Rüschlikon, Schweiz.

Table 42: References of Table 40 and Table 41.

Appendix 2: Data used to create Figure 22 and Figure 23

This Appendix shows the data used in Figure 22 and Figure 23, mentioned in Chapter 4. Table 43 shows subsequently the reference number, density, bending strength, modulus of elasticity, type of modulus of elasticity, moisture content, and the spatial dimensions of the specimens length, width, depth if known. The used abbreviations are:

REF #	Reference number
MOR	Modulus of rupture (bending strength)
MOE	Modulus of elasticity
GLOB	Global modulus of elasticity
STAT	Static bending
MC	Moisture content

The dash (-) means that this information is not given. The question mark (?) means that this information is uncertain.

Comments about the spatial dimensions:

- Houtinstituut TNO (1961) (REF # 26) suggests that the specimens width and depth were 50 mm of the specimens of which mechanical and physical properties are given in reference numbers 14-22.
- SKH (2009) (REF # 28) reports as a general comment that most bending strength values are obtained from "small (…) test pieces".
- Aguwa et al. (2012) (REF # 31) reports that 200 specimens were cut from five iroko planks with length 3.6 m. This clearly suggests small sizes of the specimens. It is also reported that the dimensions of the specimens are in accordance with BS 373. Amaoh et al. (2012) (REF # 32-34) reports the same and specifies the dimensions of the specimens, therefore the mentioned dimensions are assumed.

Comments about the type of modulus of elasticity:

- Houtinstituut TNO (1961) (REF # 26) reports displacements at proportion stress and failure stress. Therefore it is clear that static bending took place and most likely that the global modulus of elasticity was calculated from the measurements.
- Gérard e.a. (1998) (REF # 27) report that the modulus of elasticity was measured from static bending, suggesting therefore local or global modulus of elasticity.
- SKH (2009) (REF # 28) indicates that the modulus of elasticity was calculated "from the force executed in a bending test, the thereby occurring bending, the length of the span and the x-section of the timber to be tested." This suggests clearly that the modulus of elasticity from a static bending test was calculated.
- Aguwa e.a. (2012) (REF # 31) reports a load-displacement chart, from which a global modulus of elasticity can be calculated corresponding with the figures reported.
- The formula to calculate the modulus of elasticity in Amaoh et al. (2012) (REF # 32-34) is a rough version of the global modulus of elasticity, without the influence of shear deflection taken into account.
- The bending tests reported by Bucci et al. (2016) (REF # 35) were executed as three point bending tests. From these results the modulus of elasticity was calculated by means of the variable span method, to cancel out shear influence.

REF #	Density [kg/m^3]	MOR [N/mm^2]	MOE [N/mm^2]	MOE type	MC [%]	Length [mm]	Width [mm]	Depth [mm]
1	750	117.6	-	-	12	-	20	20
2	560	72.3	9400	-	12	-	20	20
3	690	91.2	-	-	12	-	20	20
4	710	109.7	-	-	12	-	20	20
5	740	98.4	-	-	12	-	20	20
6	660	81.4	-	-	12	-	20	20
7	670	91.2	-	-	12	-	20	20
8	690	106.3	-	-	12	-	20	20
9	710	74.6	-	-	12	-	20	20
10	530	74.3	-	-	15	-	20	20
11	540	79.2	-	-	15	-	20	20
12	540	72.1	-	-	15	-	20	20
13	650	94.1	-	-	15	-	20	20
14	540	71.7	9000	-	92	-	50?	50?
15	660	87.2	10200	-	12	-	50?	50?
16	620	105.3	12300	-	13.5	-	50?	50?
17	560	79.2	10700	-	8	-	50?	50?
18	720	88.7	9700	-	12	-	50?	50?
19	560	65.4	8600	-	102	-	50?	50?
20	660	81.5	10300	-	9	-	50?	50?
21	700	103.8	15300	-	12	-	50?	50?
22	660	78.7	10000	-	12	-	50?	50?
23	620	92	-	-	-	-	-	-
24	660	95	10500	-	15	-	-	-
25	690	105	11000	-	13	-	-	-
26	570	58.8	10100	STAT	50	700	50	50
27	650	95	10300	STAT	12	340	20	20
28	550-750	95	11000	STAT	12	MOR: “usually values determined from small, defect free test pieces.”		
29	640	87	12840	-	12	-	-	-
30	631	94.7	10897	GLOB	-	1000	80	25
31	734	93.81	10797	GLOB	18	300?	20?	20?
32	751	64	12900	GLOB	12	300	20	20
33	752	64	13200	GLOB	12	300	20	20
34	760	67	12900	GLOB	12	300	20	20
35	610	89.8	14208	STAT	15	420	80	25
36	496	75	11495	GLOB	10	360	20	20

Table 43: Data used to create charts of Figure 22 and Figure 23, including information on dimensions of the specimens.

References	
1-9	Sallenave, P. (1955). *Propriétés physiques et mécaniques des bois tropicaux de l'Union française.* Centre Technique Forestier Tropical, Nogent sur Marne.
10-13	Fouarge, J., G. Gerard et E. Sacrés (1953). *Bois du Congo.* Laboratoire forestier, Institut National pour l'étude agronomique du Congo Beige, Gembloux.
14-15	Armstrong, F. H. (1960). *The strength properties of timber.* Bulletin 45, For. Prod. Res. Lab., Princes Risborough.
16	*Timbers from the Gold Coast*. Bulletin Imperial Institute XXIV, 1926, pages 434 et seq.
17-18	*Results of the examination of Nigeria Timbers*. Bulletin Imperial Institute, XXI, 1923, pages 458 et seq.
19-20	Kynoch W., Norton N.A (1938). *Mechanical properties of certain tropical woods*, chiefly from South America. Bulletin 7 University of Michigan School of Forestry and Conservation.
21	Cooper G. P., Record S.J. (1931). *The evergreen forests of Liberia*. Bulletin 31 Yale University School of Forestry.
22	Brush W.D., (1943). *Iroko.* Leaflet Forest Service U.S. Dept. of Agriculture.
23	Jentsoh F., Appel E. (1936). *Beschreibung tropischer Hölzer aus dem Urwalde Kameruns. Holzforschungsbericht des Instituts für auslandische und koloniale/Forstliche Hochschule Tharandt.* Zeitschrift für Weltforstwirtschaft 1936, page 336.
24	Iroko (1936). *Merkblätter über koloniale Nutzhölzer für die Praxis No. 3.* Zeitschrift für Weltforstwirtschaft, page 336.
25	Keylwerth R. (1952) Iroko. *Holzeigenschaftstafel Holz als Roh- und Werkstoff,* page 225.
26	Houtinstituut TNO (1961) B*uig- en drukproeven bij iroko van handelskwaliteit en afmetingen en bijbehorend foutvrij hout* (Bending and compression tests of structural size and clear wood iroko). Rapport H-61-147. Houtinstituut TNO. Delft, The Netherlands. (in Dutch)
27	Gérard J., Edi Kouassi A., Daigremont C., Détienne P., Fouquet D., Vernay M. (1998). *Synthèse sur les caractéristiques technologiques de référence des principaux bois commerciaux africains* (Overview of the technological reference characteristics of the main African commercial timbers). CIRAD-Forêt, Montpellier, France. (in French)
28	SKH, Stichting Keurmerk Hout (2009). *Timber information sheet IROKO.*
29	Tropix 7 (2012). *Iroko's datasheet.* CIRAD.
30	De Jong J.D., De Richmont S.A.J., Ravenshorst G.J.P., De Vries P.A. (2011). *Research on the strength and durability characteristics of glued laminated iroko to be used in a wooden sailing ship – Phase 1*. Unpublished report by TNO. Delft, The Netherlands.
31	Aguwa J. I., Sadiku S. (2012). *Reliability Studies on Timber Data from Nigerian Grown Iroko Tree (Chlorophora excelsa) as Bridge Beam Material.* International Journal of Engineering Research in Africa, ISSN: 1663-4144, Vol. 8, pp 17-35.
32-34	Amoah M., Appiah-Yeboahand J., Okai R. (2012). *Characterization of Physical and Mechanical Properties of Branch, Stem and Root Wood of Iroko and Emire Tropical Trees.* Research Journal of Applied Sciences, Engineering and Technology 4(12): 1755-1761.
35	Bucci V., Corigliano P., Crupi V., Epasto G., Guglielmino E., Marinò A. (2016). *Experimental investigation on Iroko wood used in shipbuilding.* Proc. IMechE Part C: J Mechanical Engineering Science 2017, Vol. 231(1) 128–139.
36	Rwondo R.R.N., Meukam P., Jeong J., De Sousa Meneses D., Nkeng E.G. (2017). *Influence of water content on the mechanical and chemical properties of tropical wood species.* Results in Physics 7, 2096-2103. DOI:10-1016/j.rinp.2017.06.025

Table 44: References of the data in Table 43.

Appendix 3: Pictures of batch I specimens

This Appendix shows pictures of the 38 batch I specimens at failure, see Figure 89 till Figure 160.

Figure 89: Failure of specimen I-1.

Figure 90: Failure of specimen I-2.

Figure 91: Failure of specimen I-3 (front side).

Figure 92: Failure of specimen I-3 (flipside).

Figure 93: Failure of specimen I-4 (front side).

Figure 94: Failure of specimen I-4 (flipside).

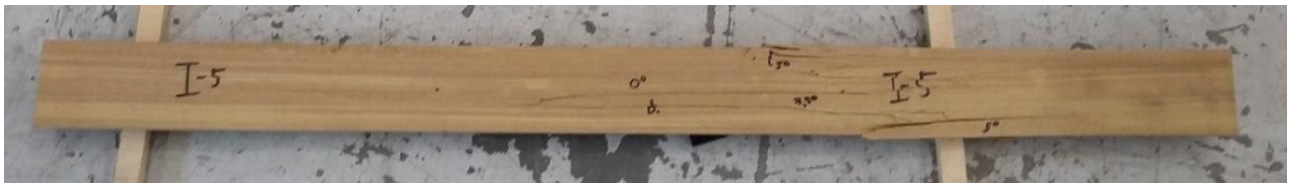

Figure 95: Failure of specimen I-5 (front side).


Figure 96: Failure of specimen I-5 (flip side).

Figure 97: Failure of specimen I-6.

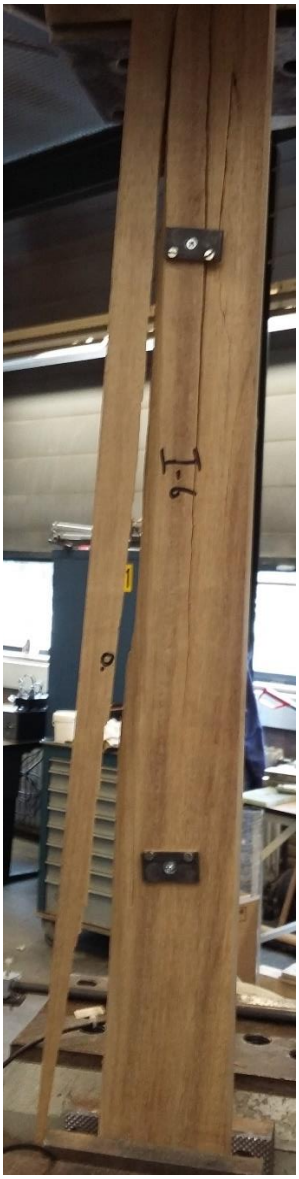

Figure 98: Failure of specimen I-7.

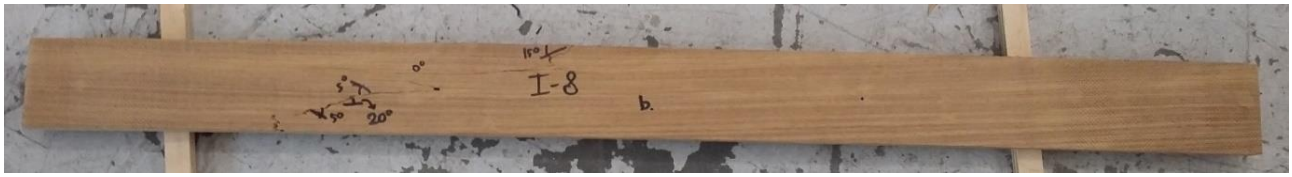

Figure 99: Failure of specimen I-8 (front side).

Figure 100: Failure of specimen I-8 (flipside).

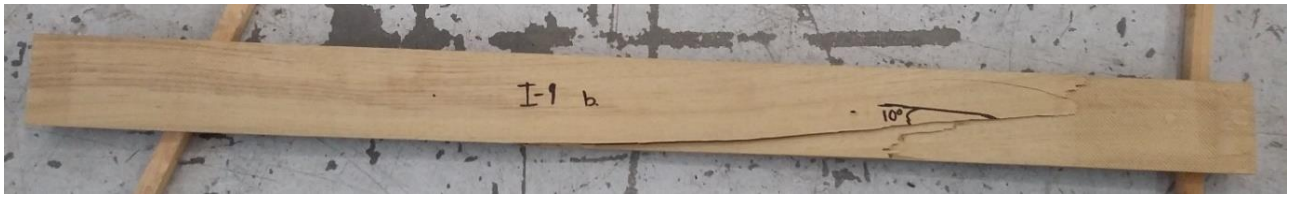

Figure 101: Failure of specimen I-9 (front side).

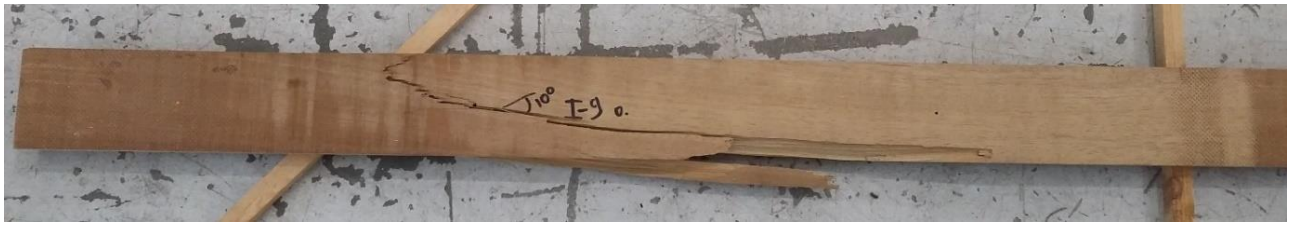

Figure 102: Failure of specimen I-9 (flipside).

Figure 103: Failure of specimen I-10 (front side).

Figure 104: Failure of specimen I-10 (flipside).

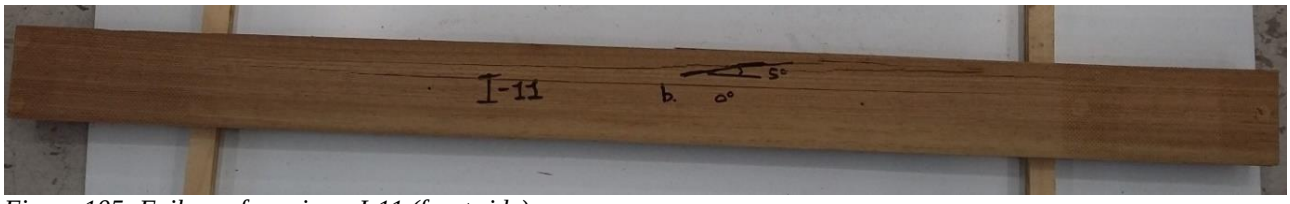

Figure 105: Failure of specimen I-11 (front side).

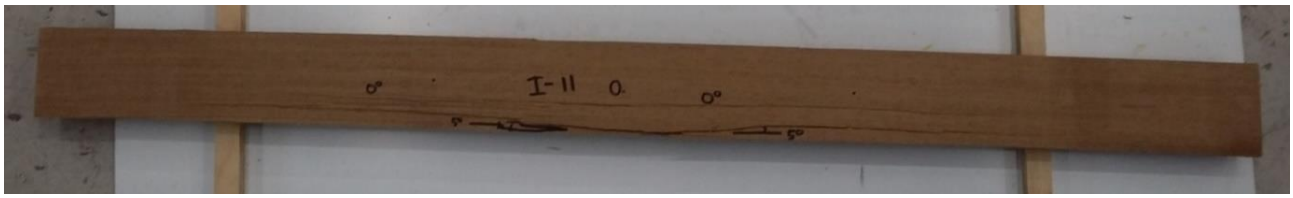

Figure 106: Failure of specimen I-11 (flipside).

Figure 107: Failure of specimen I-12 (front side).

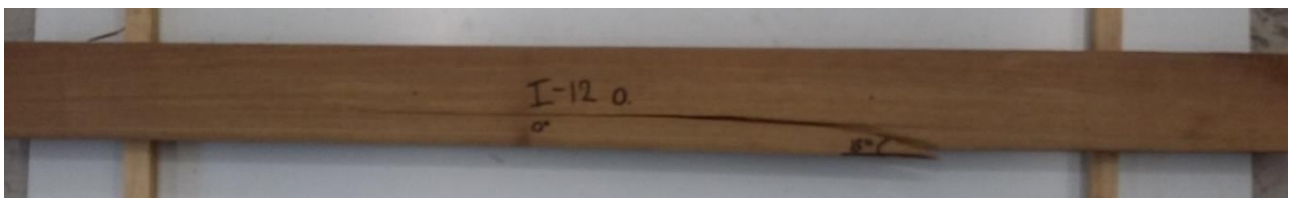

Figure 108: Failure of specimen I-12 (flipside).

Figure 109: Failure of specimen I-13 (front side).

Figure 110: Failure of specimen I-13 (flipside).

Figure 111: Failure of specimen I-14 (front side).

Figure 112: Failure of specimen I-14 (flip side).

Figure 113: Failure of specimen I-15 (front side).

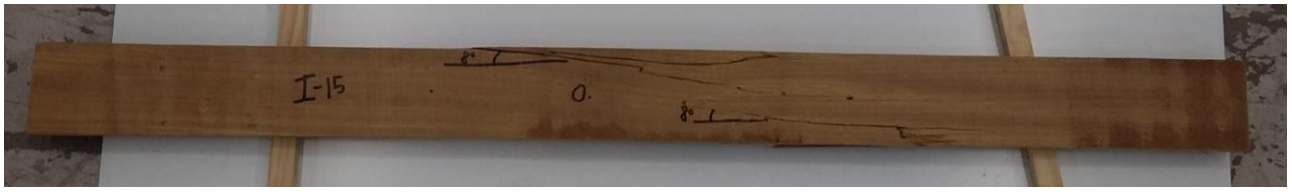

Figure 114: Failure of specimen I-15 (flipside).

Figure 115: Failure of specimen I-16 (front side).

Figure 116: Failure of specimen I-16 (flipside).

Figure 117: Failure of specimen I-17 (front side).

Figure 118: Failure of specimen I-17 (flipside).

Figure 119: Failure of specimen I-18 (front side).

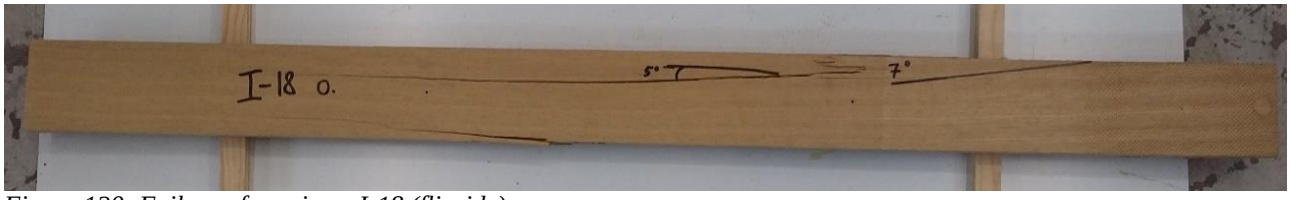

Figure 120: Failure of specimen I-18 (flipside).

Figure 121: Failure of specimen I-19 (front side).

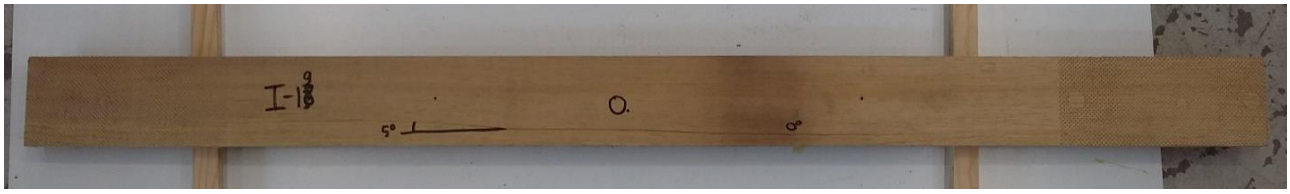

Figure 122: Failure of specimen I-19 (flipside).

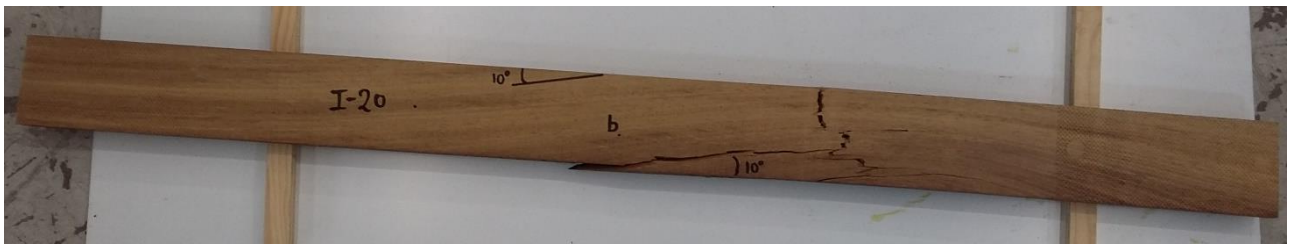

Figure 123: Failure of specimen I-20 (front side).

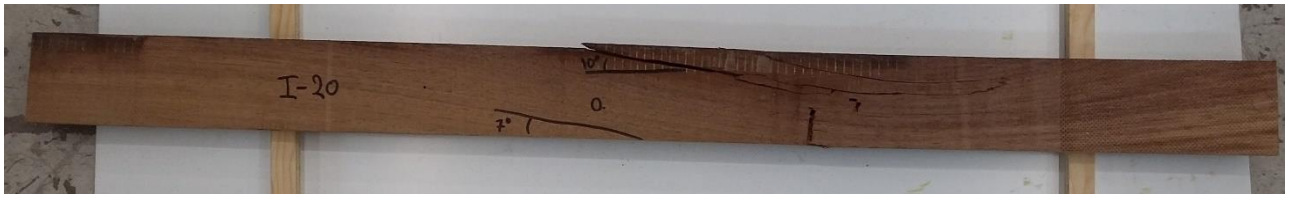

Figure 124: Failure of specimen I-20 (flipside).

Figure 125: Failure of specimen I-21 (front side).

Figure 126: Failure of specimen I-21 (flipside).

Figure 127: Failure of specimen I-22 (front side).

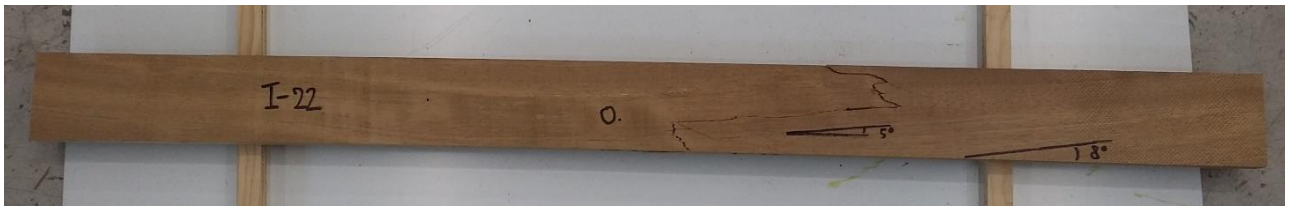

Figure 128: Failure of specimen I-22 (flipside).

Figure 129: Failure of specimen I-23 (front side).

Figure 130: Failure of specimen I-23 (flipside).

Figure 131: Failure of specimen I-24 (front side).

Figure 132: Failure of specimen I-24 (flipside).

Figure 133: Failure of specimen I-25 (front side).


Figure 134: Failure of specimen I-25 (flipside).

Figure 135: Failure of specimen I-26 (front side).

Figure 136: Failure of specimen I-26 (flipside).

Figure 137: Failure of specimen I-27 (front side).

Figure 138: Failure of specimen I-27 (flipside).

Figure 139: Failure of specimen I-28 (front side).

Figure 140: Failure of specimen I-28 (flipside).

Figure 141: Failure of specimen I-29 (front side).


Figure 142: Failure of specimen I-29 (flipside).

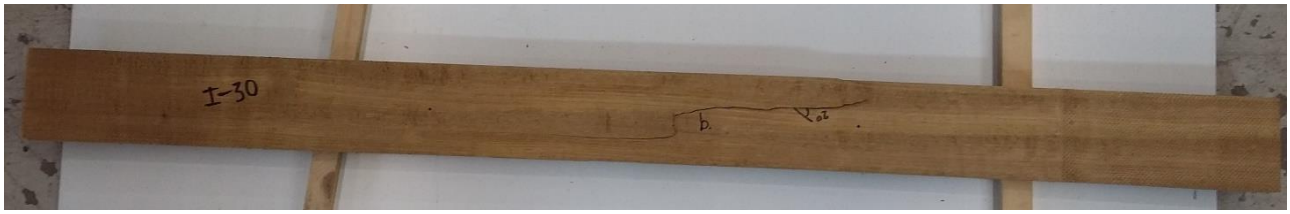

Figure 143: Failure of specimen I-30 (front side).

Figure 144: Failure of specimen I-30 (flipside).

Figure 145: Failure of specimen I-31 (front side).

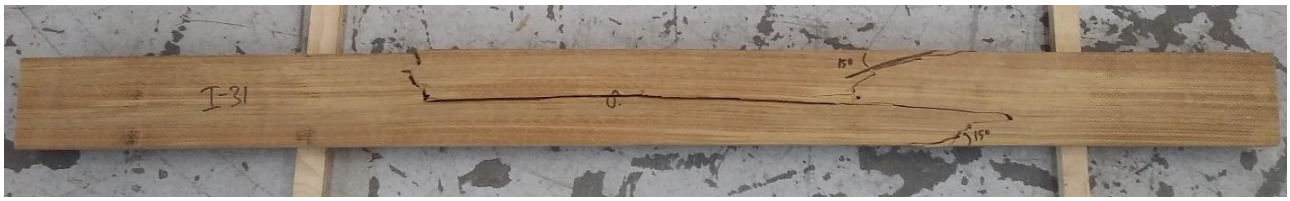

Figure 146: Failure of specimen I-31 (flipside).

Figure 147: Failure of specimen I-32 (front side).

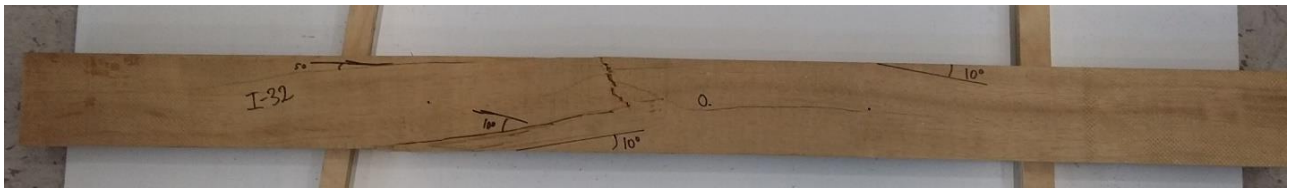

Figure 148: Failure of specimen I-32 (flipside).

Figure 149: Failure of specimen I-33 (front side).

Figure 150: Failure of specimen I-33 (flipside).

Figure 151: Failure of specimen I-34 (front side).

Figure 152: Failure of specimen I-34 (flipside).

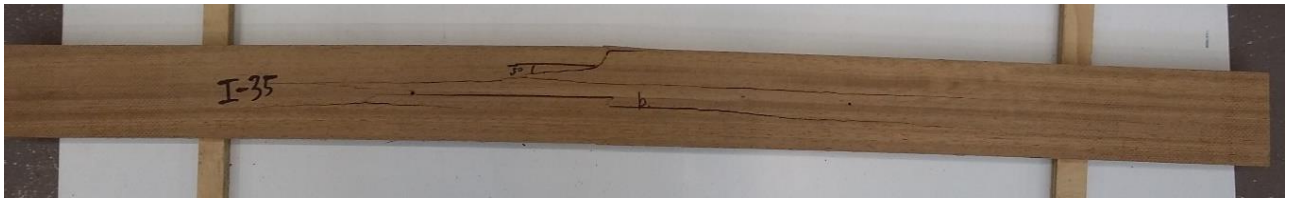

Figure 153: Failure of specimen I-35 (front side).

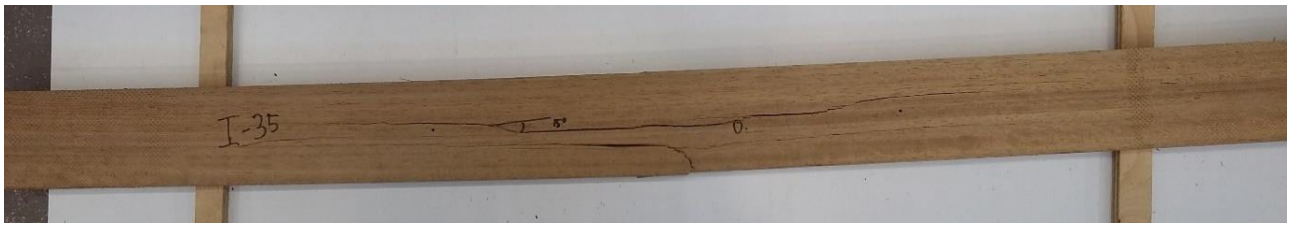

Figure 154: Failure of specimen I-35 (flipside).

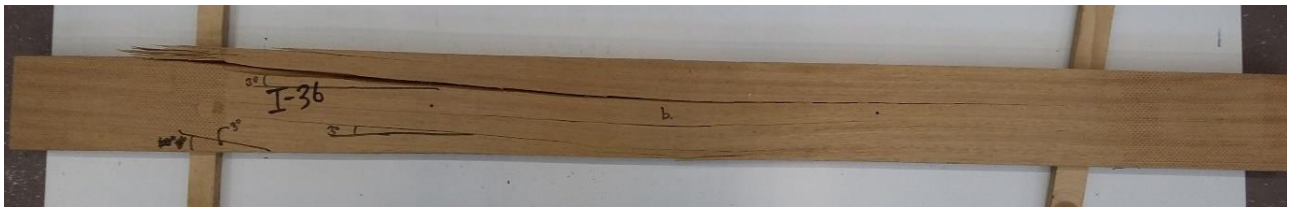

Figure 155: Failure of specimen I-36 (front side).

Figure 156: Failure of specimen I-36 (flipside).

Figure 157: Failure of specimen I-37 (front side).

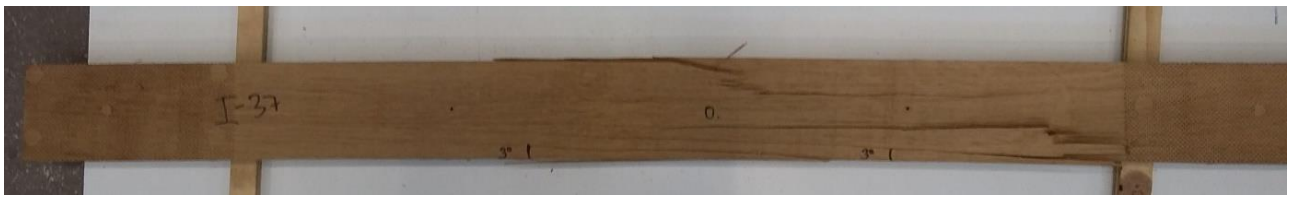

Figure 158: Failure of specimen I-37 (flipside).

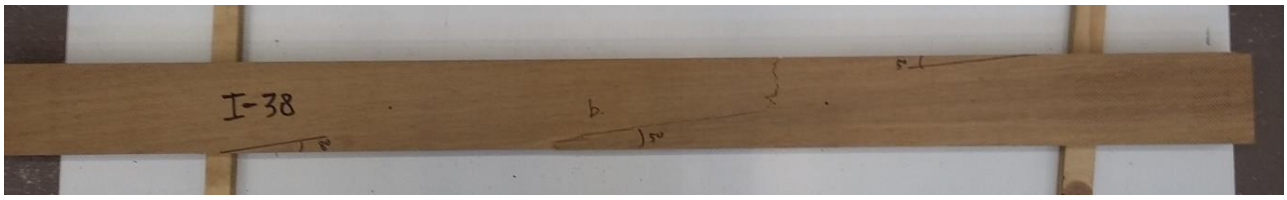

Figure 159: Failure of specimen I-38 (front side).

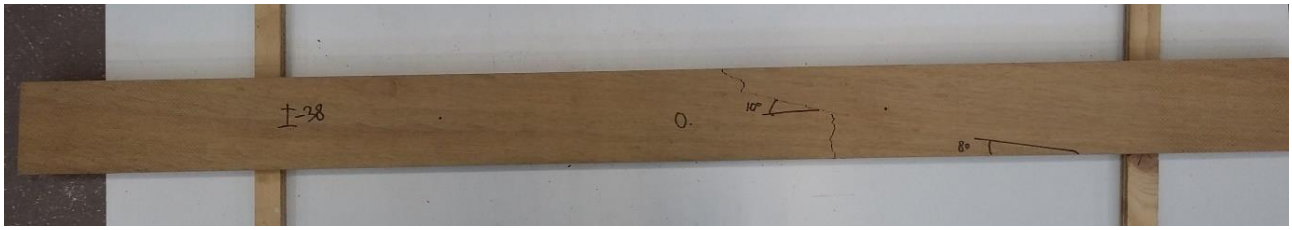

Figure 160: Failure of specimen I-38 (flipside).

Appendix 4: Pictures of batch II specimens

This Appendix shows pictures of the 38 batch I specimens at failure, see Figure 161 till Figure 198.

Figure 161: Failure of specimen II-1.

Figure 162: Failure of specimen II-2.

Figure 163: Failure of specimen II-3.

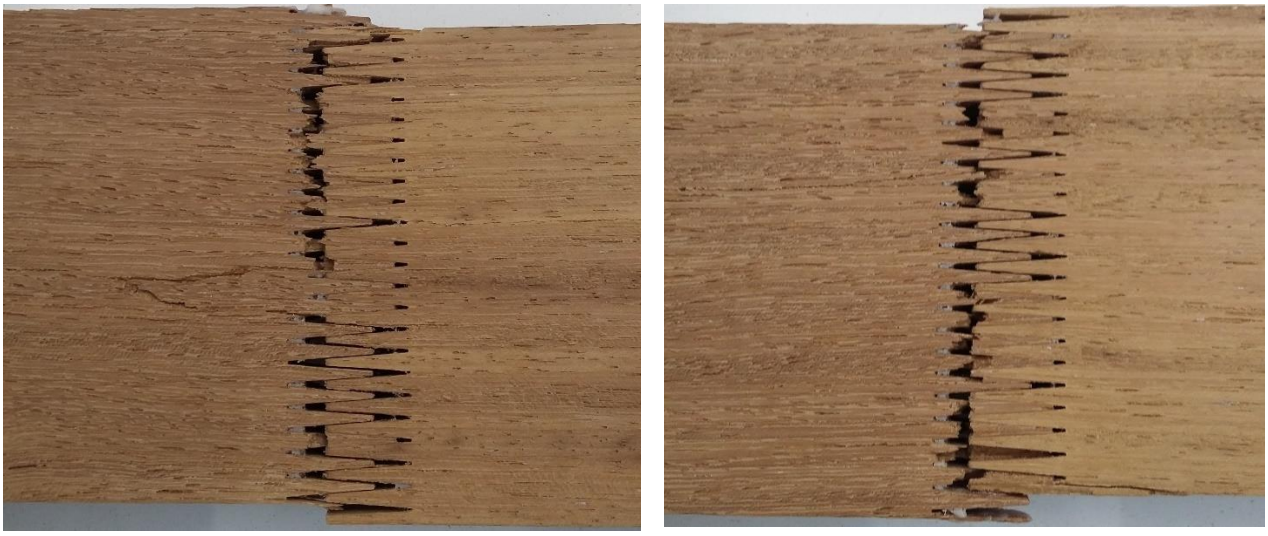

Figure 164: Failure of specimen II-4.

Figure 165: Failure of specimen II-5.

Figure 166: Failure of specimen II-6.

Figure 167: Failure of specimen II-7.

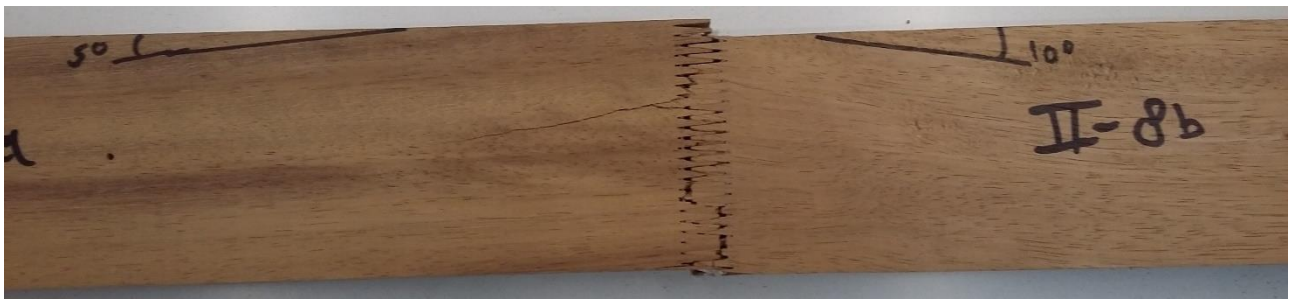

Figure 168: Failure of specimen II-8.


Figure 169: Failure of specimen II-9.

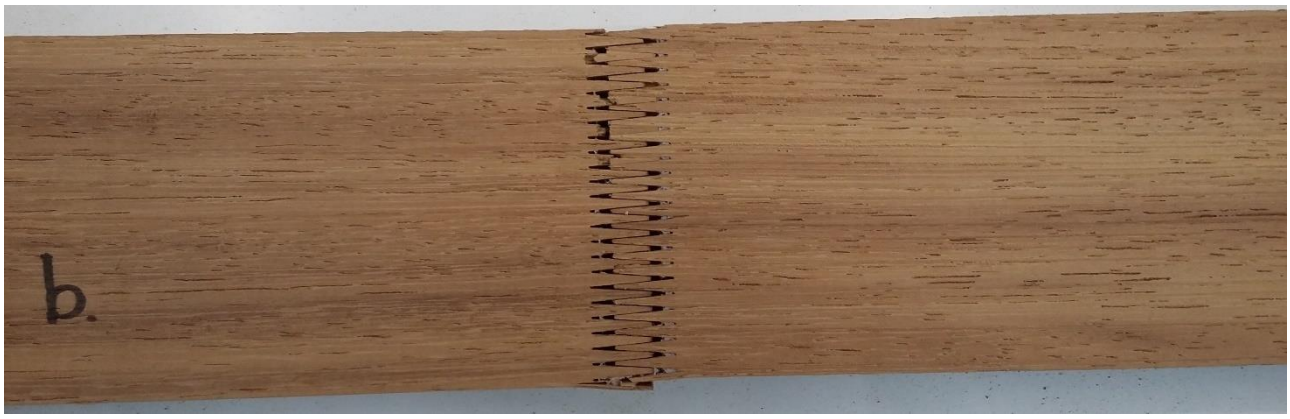

Figure 170: Failure of specimen II-10.

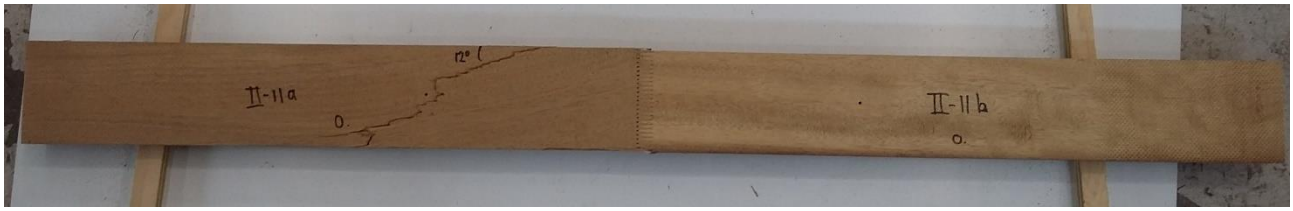

Figure 171: Failure of specimen II-11.

Figure 172: Failure of specimen II-12.


Figure 173: Failure of specimen II-13.

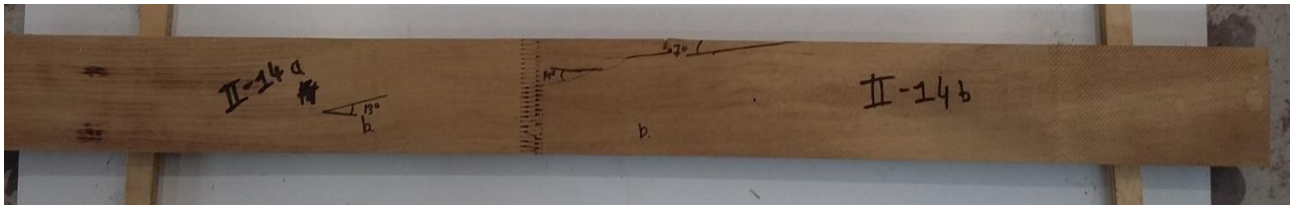

Figure 174: Failure of specimen II-14.

Figure 175: Failure of specimen II-15.

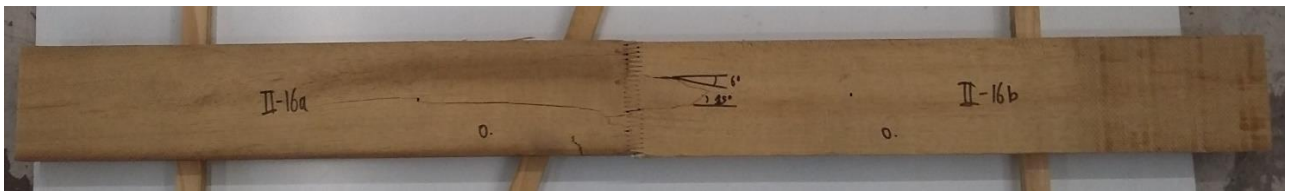

Figure 176: Failure of specimen II-16.

Figure 177: Failure of specimen II-17.

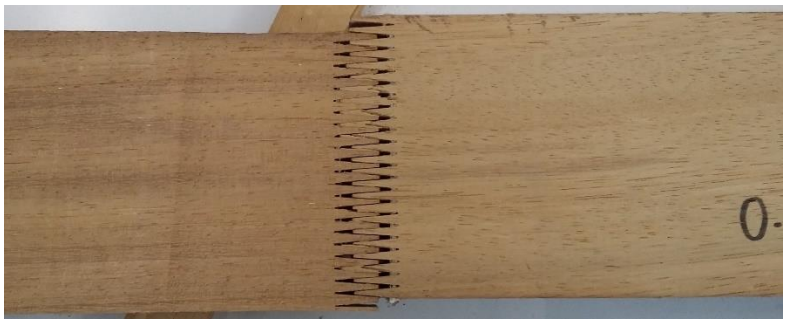

Figure 178: Failure of specimen II-18.

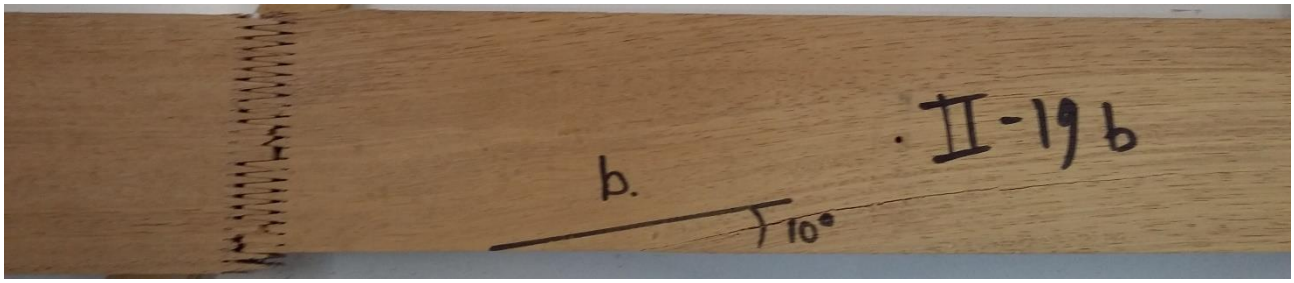

Figure 179: Failure of specimen II-19.

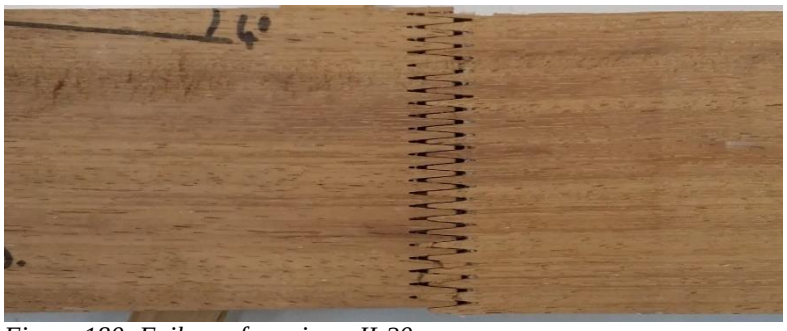

Figure 180: Failure of specimen II-20.

Figure 181: Failure of specimen II-21.

Figure 182: Failure of specimen II-22.

Figure 183: Failure of specimen II-23.

Figure 184: Failure of specimen II-24.

Figure 185: Failure of specimen II-25.

Figure 186: Failure of specimen II-26.

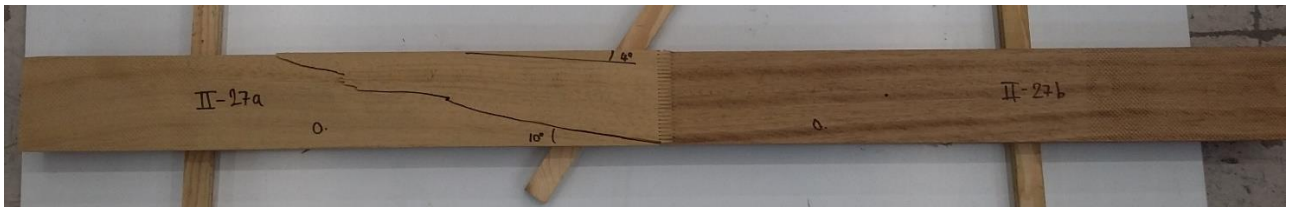

Figure 187: Failure of specimen II-27.

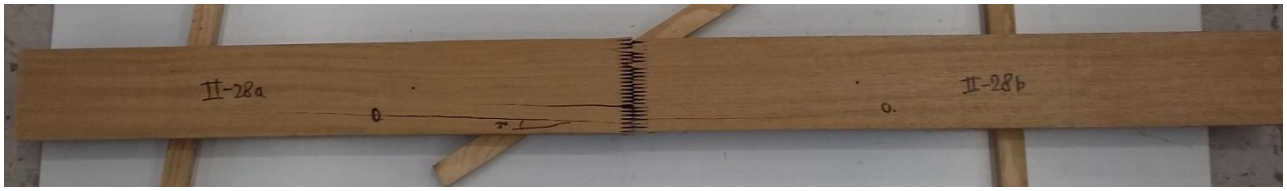

Figure 188: Failure of specimen II-28.

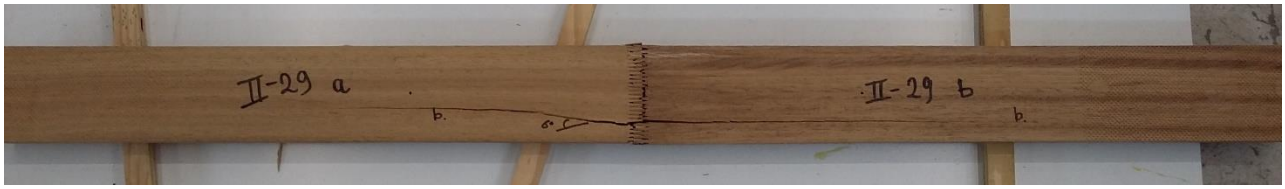

Figure 189: Failure of specimen II-29.

Figure 190: Failure of specimen II-30.

Figure 191: Failure of specimen II-31.

Figure 192: Failure of specimen II-32.

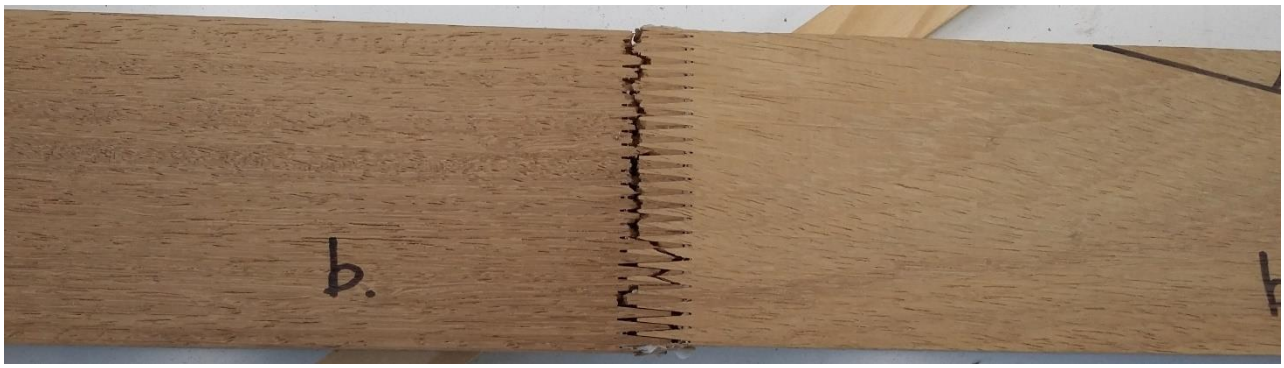

Figure 193: Failure of specimen II-33.

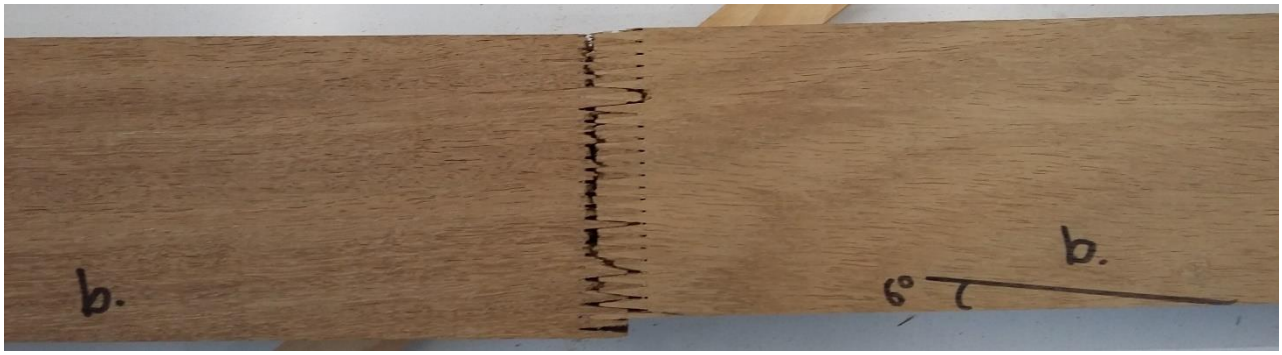

Figure 194: Failure of specimen II-34.

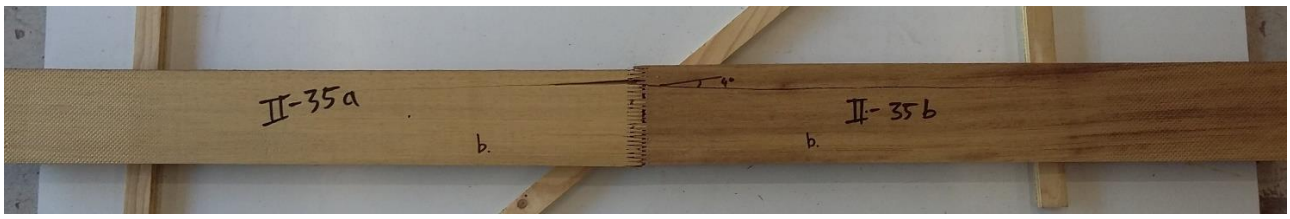

Figure 195: Failure of specimen II-35.

Figure 196: Failure of specimen II-36.

Figure 197: Failure of specimen II-37.

Figure 198: Failure of specimen II-38.

Appendix 5: Pictures of batch IV specimens

This Appendix shows pictures of the 12 batch IV specimens at failure, see Figure 199 till Figure 222.

Figure 199: Failure of specimen IV-1.

Figure 200: Failure of specimen IV-1 (crack detail).

Figure 201: Failure of specimen IV-2.

Figure 202: Failure of specimen IV-2 (crack detail).

Figure 203: Failure of specimen IV-3.

Figure 204: Failure of specimen IV-3 (crack detail).

Figure 205: Failure of specimen IV-4.


Figure 206: Failure of specimen IV-4 (crack detail).


Figure 207: Failure of specimen IV-5.

Figure 208: Failure of specimen IV-5 (crack detail).

Figure 209: Failure of specimen IV-6.

Figure 210: Failure of specimen IV-6 (crack detail).

Figure 211: Failure of specimen IV-7.


Figure 212: Failure of specimen IV-7 (crack detail).

Figure 213: Failure of specimen IV-8.

Figure 214: Failure of specimen IV-8 (crack detail).

Figure 215: Failure of specimen IV-9.

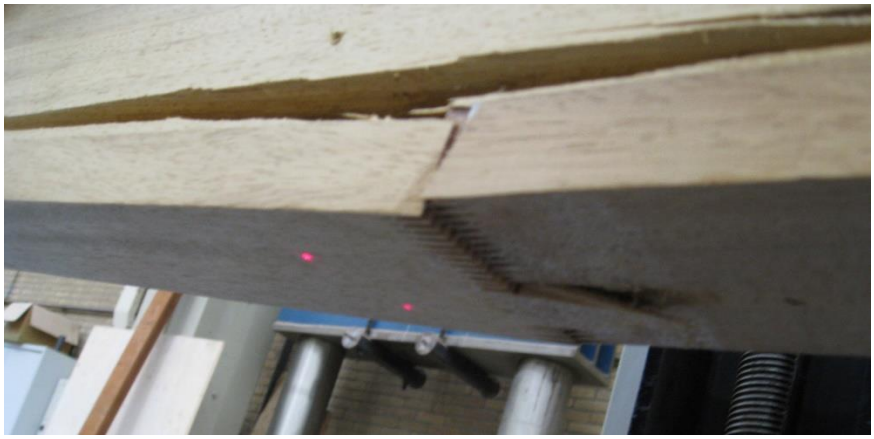

Figure 216: Failure of specimen IV-9 (crack detail).

Figure 217: Failure of specimen IV-10.


Figure 218: Failure of specimen IV-10 (crack detail).

Figure 219: Failure of specimen IV-11.

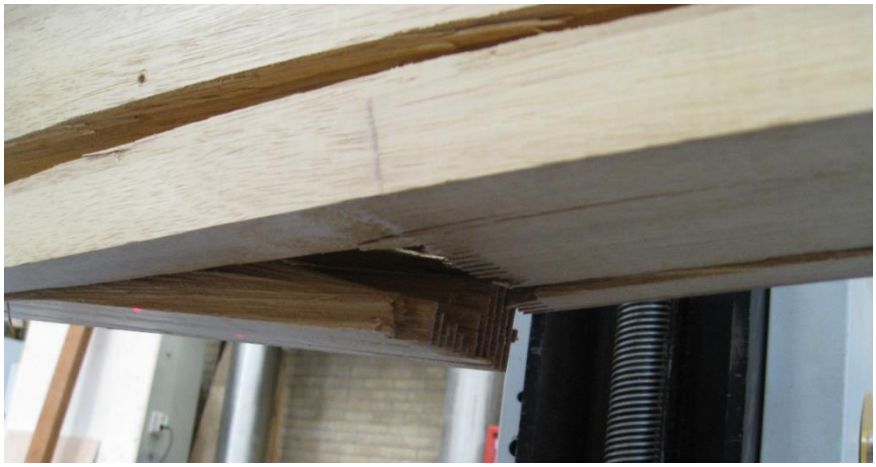

Figure 220: Failure of specimen IV-11 (crack detail).

Figure 221: Failure of specimen IV-12.

Figure 222: Failure of specimen IV-12 (crack detail).

Appendix 6: Data of batch I

This Appendix presents measured and calculated data of batch I; the light grey highlighted data are calculated values. The successive weightings of the specimens (before cutting) are shown in Table 45 (specimens 1-35) and Table 46 (specimens 36-38). The last column shows that the requirement of a relative difference of less than 0.1% is met.

No.	*m* [kg] 1 Mar	*m* [kg] 5 Mar	*m* [kg] 7 Mar	*m* [kg] 8 Mar	rel. diff. 1 and 8 Mar [%]
1	2.120	2.126	2.128	2.127	-0.05%
2	2.198	2.209	2.211	2.209	-0.09%
3	2.058	2.068	2.069	2.068	-0.05%
4	2.262	2.268	2.270	2.270	0.00%
5	2.213	2.129	2.131	2.129	-0.09%
6	2.186	2.197	2.199	2.198	-0.05%
7	2.241	2.249	2.251	2.250	-0.04%
8	2.186	2.193	2.196	2.194	-0.09%
9	2.057	2.065	2.067	2.067	0.00%
10	2.080	2.087	2.090	2.089	-0.05%
11	2.127	2.134	2.136	2.135	-0.05%
12	2.281	2.287	2.290	2.289	-0.04%
13	2.122	2.129	2.132	2.131	-0.05%
14	2.048	2.056	2.057	2.057	0.00%
15	2.231	2.239	2.241	2.240	-0.04%
16	2.167	2.174	2.176	2.175	-0.05%
17	2.185	2.193	2.196	2.195	-0.05%
18	2.255	2.261	2.263	2.263	0.00%
19	2.228	2.230	2.231	2.230	-0.04%
20	2.097	2.104	2.107	2.106	-0.05%
21	1.973	1.977	1.978	1.977	-0.05%
22	2.119	2.127	2.129	2.128	-0.05%
23	2.185	2.191	2.193	2.192	-0.05%
24	2.147	2.153	2.156	2.155	-0.05%
25	2.306	2.310	2.311	2.310	-0.04%
26	2.110	2.110	2.111	2.110	-0.05%
27	2.267	2.275	2.277	2.276	-0.04%
28	2.472	2.474	2.476	2.475	-0.04%
29	2.248	2.255	2.257	2.257	0.00%
30	2.138	2.146	2.149	2.148	-0.05%
31	2.105	2.112	2.114	2.114	0.00%
32	2.131	2.137	2.139	2.139	0.00%
33	2.315	2.320	2.323	2.321	-0.09%
34	2.249	2.250	2.252	2.251	-0.04%
35	2.236	2.241	2.243	2.242	-0.04%

Table 45: Successive weightings specimens 1-35 batch I.

No.	*m* [kg] 1 Mar	*m* [kg] 5 Mar	*m* [kg] 7 Mar	*m* [kg] 8 Mar	rel. diff. 1 and 8 Mar [%]
36	2.251	2.257	2.259	2.258	-0.04%
37	2.380	2.385	2.388	2.386	-0.08%
38	2.420	2.423	2.425	2.424	-0.04%

Table 46: Successive weightings specimens 36-38 batch I.

The measured values of spatial dimensions, mass of specimens (after cutting), eigenfrequency and failure load in tension are shown in Table 47 (specimens 1-32) and Table 48 (specimens 33-38).

No.	l_s [mm]	$l_{1,b.}$ [mm]	$l_{1,o.}$ [mm]	b [mm]	h [mm]	m [kg]	f_e [Hz]	$P_{t,l,max}$ [kN]
1	1250.1	430	430	88.99	26.71	1.965	2240	221.419873
2	1248.2	430	430	90.85	27.04	2.044	1669	56.883743
3	1243.6	430	430	88.29	26.98	1.902	2098	177.726000
4	1246.0	469	431	91.22	26.64	2.098	1806	112.672900
5	1250.4	430	430	88.80	26.87	1.971	2006	148.334840
6	1246.5	431	430	90.84	26.37	2.039	1825	151.176469
7	1246.5	430	430	91.69	26.84	2.077	2094	251.897351
8	1247.0	430	430	92.04	27.76	2.024	2035	132.211092
9	1248.4	430	430	93.08	26.64	1.906	1976	142.892420
10	1249.8	430	430	93.50	26.97	1.925	1972	117.001082
11	1246.1	431	430	92.01	27.17	1.964	2001	201.557257
12	1247.8	431	429	92.16	27.20	2.107	1752	145.590052
13	1247.0	429	430	92.32	27.25	1.958	1869	95.440686
14	1247.2	430	430	90.75	26.84	1.904	1972	136.273690
15	1247.0	430	429	92.24	27.47	2.065	2025	137.257983
16	1248.5	430	430	92.68	27.55	2.000	2011	96.845869
17	1248.0	430	430	92.40	27.16	2.028	2118	166.744773
18	1246.2	430	430	91.22	26.88	2.080	1996	137.871406
19	1247.5	430	430	89.09	26.94	2.063	1137	205.242623
20	1245.5	430	430	91.32	26.89	1.932	1810	134.130130
21	1246.9	430	430	89.72	27.31	1.817	1928	136.008348
22	1248.0	430	430	90.13	26.90	1.956	1889	80.972950
23	1249.8	430	431	92.49	27.11	2.027	1542	51.169257
24	1246.2	430	430	91.59	27.10	1.986	2001	152.034107
25	1246.0	430	432	94.82	26.41	2.131	1547	85.068659
26	1245.5	430	430	91.30	26.52	1.942	1708	128.062028
27	1247.5	431	430	91.88	26.55	2.099	2015	137.378457
28	1249.2	430	430	90.24	27.12	2.283	1669	134.777262
29	1249.2	430	432	91.51	27.45	2.079	1986	146.082470
30	1247.5	432	432	92.53	27.11	1.988	2001	87.839402
31	1248.0	430	431	91.83	26.07	1.953	2001	148.923487
32	1248.5	431	431	92.14	26.92	1.974	1859	126.323072

Table 47: Spatial dimensions, mass, eigenfrequency, failure load of specimens 1-32 batch I.

No.	l_s [mm]	$l_{1,b.}$ [mm]	$l_{1,o.}$ [mm]	b [mm]	h [mm]	m [kg]	f_e [Hz]	$P_{t,l,max}$ [kN]
33	1249.5	430	431	92.03	26.73	2.148	2118	262.426740
34	1248.5	431	431	88.53	27.02	2.097	1996	146.017875
35	1249.2	429	430	92.13	26.87	2.077	1815	116.092886
36	1246.0	430	432	91.18	27.41	2.090	2123	209.052944
37	1249.5	432	432	91.27	27.38	2.222	2133	307.344930
38	1257.0	431	430	89.68	27.20	2.242	1713	113.017162
max	1243.6			88.29	26.07	1.817	1137	51.169257
min	1257.0			94.82	27.76	2.283	2240	307.344930
mean	1247.9			91.33	26.98	2.031	1907	145.730586
stdev				1.42	0.35	0.099	209	53.857869
COV				0.02	0.01	0.05	0.11	0.37

Table 48: Spatial dimensions, mass, eigenfrequency, failure load of specimens 33-38 batch I.

The data of the successive weightings of the test slices is shown in Table 49 (specimens 1-22) and Table 50 (specimens 23-38), in order to determine the moisture content of the beams. The last column of both Tables show that the requirement of a relative difference of less than 0.1% (see NEN-EN 13183-1, 2002) is met.

No.	m_{test} [kg] (13-3)	m_{test} [kg] (14-3)	m_{test} [kg] (15-3)	m_{test} [kg] (18-3)	m_{test} [kg] (19-3)	m_{test} [kg] (25-3)	m_{test} [kg] (27-3)	m_{test} [kg] (28-3)	rel. diff. 13 and 25 Mar [%]
1	40.90	37.22	37.24	37.23	37.28	37.23	37.26	37.25	-0.027
2	43.58	39.98	40.01	40.01	40.07	40.05	40.08	40.08	0.000
3		46.09	42.27	42.25	42.32	42.26	42.30	42.29	-0.024
4		44.54	40.50	40.48	40.55	40.52	40.55	40.54	-0.025
5		41.31	37.86	37.83	37.89	37.81	37.85	37.84	-0.026
6		48.99	44.71	44.68	44.73	44.69	44.72	44.72	0.000
7		55.59	51.07	50.98	51.07	50.99	51.01	51.00	-0.020
8		39.82	36.32	36.29	36.37	36.30	36.34	36.32	-0.055
9		39.96	37.05	37.01	37.08	36.98	36.99	36.99	0.000
10		44.01	40.75	40.71	40.77	40.69	40.72	40.70	-0.049
11		43.70	39.74	39.75	39.80	39.73	39.77	39.76	-0.025
12		35.69	32.88	32.88	32.92	32.88	32.90	32.89	-0.030
13		48.47	44.79	44.78	44.83	44.75	44.77	44.75	-0.045
14			61.06	55.44	55.52	55.47	55.51	55.51	0.000
15			61.75	56.44	56.49	56.44	56.49	56.47	-0.035
16			58.64	53.40	53.47	53.43	53.48	53.45	-0.056
17			60.38	55.30	55.38	55.33	55.36	55.35	-0.018
18			57.55	52.51	52.58	52.55	52.58	52.59	0.019
19			62.80	57.16	57.23	57.18	57.22	57.23	0.017
20			55.80	50.70	50.79	50.69	50.73	50.73	0.000
21			44.01	40.40	40.10	40.10	40.13	40.12	-0.025
22			58.34	53.83	53.90	53.84	53.88	53.88	0.000

Table 49: Successive weightings test slices of specimens 1-22 batch I.

No.	m_{test} [kg] (13-3)	m_{test} [kg] (14-3)	m_{test} [kg] (15-3)	m_{test} [kg] (18-3)	m_{test} [kg] (19-3)	m_{test} [kg] (25-3)	m_{test} [kg] (27-3)	m_{test} [kg] (28-3)	rel. diff. 13 and 25 Mar [%]
23			57.80	53.30	53.34	53.30	53.36	53.32	-0.075
24				52.93	48.20	48.18	48.23	48.22	-0.021
25				66.05	60.41	60.41	60.47	60.47	0.000
26				56.27	51.43	51.42	51.47	51.47	0.000
27				64.28	58.86	58.81	58.88	58.56	-0.543
28				66.22	61.16	61.16	61.23	61.21	-0.033
29				62.71	57.71	57.65	57.73	57.70	-0.052
30				58.38	53.79	53.56	53.61	53.60	-0.019
31				57.01	52.51	52.45	52.51	52.49	-0.038
32				59.13	54.87	54.80	54.85	54.84	-0.018
33					60.43	55.18	55.25	55.23	-0.036
34					64.17	58.46	58.52	58.50	-0.034
35					61.18	55.76	55.83	55.81	-0.036
36					63.11	57.65	57.71	57.69	-0.035
37					61.24	56.02	56.08	56.05	-0.053
38					64.74	54.82	59.87	59.87	0.000

Table 50: Successive weightings test slices of specimens 23-38 batch I.

The data of the width, depth, thickness, and mass before drying of test slices is shown in Table 51 (1-19) and Table 52 (20-38), in order to determine the density of the lamellas.

No.	b_{test} [mm]	h_{test} [mm]	t_{test} [mm]	m_1 [g]
1	88.99	26.71	29.84	40.90
2	78.21	27.04	25.54	43.58
3	88.29	26.98	29.25	46.09
4	91.22	26.64	27.44	44.54
5	88.80	26.87	26.08	41.31
6	90.84	26.37	29.94	48.99
7	91.69	26.84	33.03	55.59
8	92.04	27.76	24.57	39.82
9	93.08	26.64	25.51	39.96
10	93.50	26.97	28.49	44.01
11	92.01	27.17	26.99	43.70
12	92.16	27.20	20.97	35.69
13	92.32	27.25	31.22	48.47
14	90.75	26.84	37.69	61.06
15	92.24	27.47	36.24	61.75
16	92.68	27.55	37.68	58.64
17	92.40	27.16	37.31	60.38
18	91.22	26.88	36.76	57.55
19	89.09	26.94	39.28	62.80

Table 51: Width, depth, thickness and mass before drying of test slices 1-19 batch I.

No.	b_{test} [mm]	h_{test} [mm]	t_{test} [mm]	m_1 [g]
20	91.32	26.89	36.45	55.80
21	75.74	27.31	36.41	44.01
22	90.13	26.90	36.60	58.34
23	92.49	27.11	35.56	57.80
24	91.59	27.10	33.85	52.93
25	94.82	26.41	38.61	66.05
26	91.30	26.52	35.71	56.27
27	91.88	26.55	37.13	64.28
28	90.24	27.12	36.68	66.22
29	91.51	27.45	37.80	62.71
30	92.53	27.11	35.47	58.38
31	91.83	26.07	38.60	57.01
32	92.14	26.92	37.87	59.13
33	92.03	26.73	36.48	60.43
34	88.53	27.02	38.36	64.17
35	92.13	26.87	39.76	61.18
36	91.18	27.41	37.10	63.11
37	91.27	27.38	34.16	61.24
38	89.68	27.20	35.44	64.74

Table 52: Width, depth, thickness and mass before drying of test slices 20-38 batch I.

Table 53 (1-16) and Table 54 (17-38) show the calculated slope of the load-displacement curves, the related coefficient of determination R^2, the modulus of elasticity in tension 1 and 2, and the relative difference between modulus of elasticity in tension 1 and 2.

No.	Slope $E_{t,1}$	Slope $E_{t,2}$	R^2 $E_{t,1}$	R^2 $E_{t,2}$	$E_{t,1}$ [N/mm^2]	$E_{t,2}$ [N/mm^2]	rel. diff. $E_{t,1}$ and $E_{t,2}$ [%]
1	102.85855	109.01057	0.999873	0.999851	18608	19721	5.6
2	69.82449	63.58838	0.999543	0.999617	12222	11130	9.8
3	95.54123	90.20910	0.999811	0.999889	17247	16284	5.9
4	64.41698	81.07282	0.999365	0.999743	12432	14379	13.5
5	81.72195	90.19723	0.999816	0.999806	14727	16255	9.4
6	73.00244	76.14825	0.999906	0.999910	13135	13669	3.9
7	84.00781	104.97191	0.999933	0.999760	14679	18342	20.0
8	94.12476	89.55491	0.999784	0.999771	15841	15072	5.1
9	80.89324	82.13233	0.999862	0.999859	14028	14243	1.5
10	81.94272	89.29593	0.999804	0.999843	13973	15227	8.2
11	81.62529	91.97566	0.999899	0.999795	14073	15820	11.0
12	69.72674	74.48685	0.999899	0.999855	11989	12748	6.0
13	70.50794	82.76963	0.999720	0.999633	12024	14147	15.0
14	74.52617	92.97498	0.999868	0.999689	13157	16414	19.8
15	74.87294	112.30875	0.999588	0.999365	12706	19015	33.2
16	81.06652	80.66781	0.999678	0.999674	13652	13585	0.5

Table 53: Slope load-displacement curve, related R^2 and modulus of elasticity in tension of specimens 1-16 batch I.

No.	Slope $E_{t,1}$	Slope $E_{t,2}$	R^2 $E_{t,1}$	R^2 $E_{t,2}$	$E_{t,1}$ [N/mm^2]	$E_{t,2}$ [N/mm^2]	rel. diff. $E_{t,1}$ and $E_{t,2}$ [%]
17	102.39447	92.49486	0.999811	0.999843	17545	15848	10.7
18	92.09135	85.86548	0.999813	0.999829	16150	15058	7.3
19	89.04696	119.26578	0.999870	0.999790	15954	21368	25.3
20	57.72725	70.35124	0.999841	0.999819	10109	12319	17.9
21	73.15058	76.43674	0.999870	0.999867	12837	13414	4.3
22	74.44395	78.30448	0.999643	0.996602	13203	13888	4.9
23	61.01359	64.39203	0.999446	0.999446	10463	11068	5.5
24	88.46365	87.68040	0.999830	0.999845	15326	15190	0.9
25	58.55853	57.52315	0.999774	0.999779	10055	9923	1.3
26	61.22338	61.51176	0.999873	0.999872	10873	10924	0.5
27	79.16674	112.42359	0.999723	0.999616	13987	19817	29.4
28	69.93990	70.82347	0.999858	0.999881	12289	12444	1.2
29	95.03323	88.01230	0.999813	0.999844	16268	15136	7.5
30	74.07502	111.44950	0.999579	0.999374	12757	19193	33.5
31	85.21700	86.87578	0.999834	0.999819	15306	15640	2.1
32	76.98799	76.87173	0.999808	0.999809	13378	13357	0.2
33	96.94341	109.45805	0.999919	0.999885	16946	19178	11.6
34	80.46340	89.78835	0.999795	0.999848	14498	16178	10.4
35	74.23038	70.27727	0.999821	0.999900	12865	12208	5.4
36	100.64731	99.19464	0.999830	0.999852	17317	17146	1.0
37	119.05568	88.38417	0.999596	0.999780	20581	15279	34.7
38	68.50245	69.50139	0.999873	0.999880	12104	12252	1.2
min					10055	9923	0.2
max					20581	21368	34.7
mean					14087	15076	10.1
stdev					2384	2752	9.9
COV					0.17	0.18	0.98

Table 54: Slope load-displacement curve, related R^2 and modulus of elasticity in tension of specimens 8-38 batch I.

Table 55 (1-7) and Table 56 (8-38) present the speed of the test, the recorded time to failure, the angle of failure, and the calculated moisture content, density, dynamic modulus of elasticity and the tension strength.

No.	*Speed* [mm/s]	*Time to failure* [s]	α [°]	ω [%]	ρ [kg/m^3]	E_{dyn} [N/mm^2]	$f_{t,l}$ [N/mm^2]
1	0.012	833.87	3	9.8	576.6	20742	93.15
2	0.020	128.54	15	8.7	806.9	11572	23.16
3	0.017	344.35	0	9.0	661.5	17483	74.61
4	0.015	261.50	5	9.9	667.9	14034	46.37
5	0.015	324.10	5	9.2	663.8	16626	62.17
6	0.015	366.09	5	9.5	683.1	14135	63.11
7	0.015	628.80	1	9.0	683.9	18452	102.36

Table 55: Speed, time to failure, angle of failure, moisture content, density, dynamic modulus of elasticity, tension strength of specimens 1-7 batch I.

No.	*Speed* [mm/s]	*Time to failure* [s]	α [°]	ω [%]	ρ [kg/m^3]	E_{dyn} [N/mm^2]	$f_{t,l}$ [N/mm^2]
8	0.015	279.81	0	9.6	634.3	16363	51.75
9	0.015	322.41	10	8.0	631.7	14987	57.63
10	0.015	270.61	10	8.1	612.6	14841	46.40
11	0.015	470.22	0	9.9	647.7	15679	80.63
12	0.015	366.65	0	8.5	678.9	12877	58.08
13	0.015	233.46	15	8.3	617.1	13561	37.94
14	0.015	305.74	5	10.0	665.1	15165	55.95
15	0.015	295.26	8	9.4	672.5	16669	54.17
16	0.015	224.80	10	9.7	609.5	15820	37.93
17	0.015	340.33	5	9.1	644.9	18096	66.44
18	0.015	295.83	5	9.4	638.5	16847	56.23
19	0.015	481.72	0	9.7	666.1	5545	85.51
20	0.015	355.24	10	10.0	623.4	12841	54.62
21	0.015	327.01	*	9.7	584.4	13748	55.51
22	0.015	199.26	10	8.3	657.5	14371	33.40
23	0.015	150.44	30	8.4	648.2	9609	20.41
24	0.015	344.15	7	9.8	630.0	15970	61.25
25	0.015	268.88	15	9.2	683.1	10150	33.97
26	0.015	346.96	*	9.3	650.8	11657	52.89
27	0.015	258.89	0	9.8	709.7	17433	56.32
28	0.015	347.49	15	8.2	737.7	12984	55.07
29	0.015	322.86	4	8.7	660.4	16312	58.16
30	0.015	172.90	15	8.9	656.1	15834	35.02
31	0.015	330.64	0	8.6	616.9	16306	62.21
32	0.015	315.76	10	7.8	629.5	13735	50.93
33	0.015	560.67	5	9.4	673.4	19577	106.68
34	0.015	325.57	5	9.7	699.3	17442	61.04
35	0.015	283.40	0	9.6	621.6	13811	46.90

Table 56: Speed, time to failure, angle of failure, moisture content, density, dynamic modulus of elasticity, tension strength of specimens 8-38 batch I.

Appendix 7: Data of batch II

This Appendix presents measured and calculated data of batch II; the light grey highlighted data are calculated values. The successive weightings of the specimens (before cutting) are shown in Table 57 (specimens 1-35) and Table 58 (specimens 36-38). The last column shows that the requirement of a relative difference of less than 0.1% is met.

No.	*m* [kg] 1 Mar	*m* [kg] 5 Mar	*m* [kg] 7 Mar	*m* [kg] 8 Mar	rel. diff. 1 and 8 Mar [%]
1	2.268	2.271	2.273	2.272	-0.04%
2	2.086	2.093	2.095	2.093	-0.10%
3	2.143	2.149	2.152	2.151	-0.05%
4	2.285	2.287	2.290	2.288	-0.09%
5	2.156	2.162	2.164	2.163	-0.05%
6	2.277	2.281	2.283	2.281	-0.09%
7	2.194	2.198	2.200	2.199	-0.05%
8	2.171	2.178	2.180	2.179	-0.05%
9	2.025	2.028	2.029	2.028	-0.05%
10	2.109	2.110	2.113	2.112	-0.05%
11	2.099	2.105	2.108	2.107	-0.05%
12	2.256	2.260	2.261	2.260	-0.04%
13	2.316	2.319	2.320	2.319	-0.04%
14	2.067	2.074	2.076	2.075	-0.05%
15	2.340	2.342	2.344	2.342	-0.09%
16	2.115	2.122	2.125	2.123	-0.09%
17	2.423	2.431	2.433	2.431	-0.08%
18	2.211	2.215	2.218	2.217	-0.05%
19	2.109	2.109	2.111	2.109	-0.09%
20	2.237	2.238	2.240	2.237	-0.13%
21	2.156	2.156	2.157	2.156	-0.05%
22	2.062	2.061	2.063	2.061	-0.10%
23	2.257	2.257	2.258	2.257	-0.04%
24	2.328	2.331	2.333	2.331	-0.09%
25	2.151	2.156	2.158	2.157	-0.05%
26	2.055	2.056	2.058	2.056	-0.10%
27	2.108	2.111	2.113	2.111	-0.09%
28	2.274	2.279	2.281	2.280	-0.04%
29	2.184	2.187	2.189	2.187	-0.09%
30	2.265	2.266	2.268	2.266	-0.09%
31	2.269	2.270	2.271	2.269	-0.09%
32	2.149	2.154	2.156	2.155	-0.05%
33	2.328	2.330	2.331	2.329	-0.09%
34	2.342	2.348	2.350	2.348	-0.09%
35	2.158	2.164	2.166	2.164	-0.09%

Table 57: Successive weightings specimens 1-35 batch II.

No.	*m* [kg] 1 Mar	*m* [kg] 5 Mar	*m* [kg] 7 Mar	*m* [kg] 8 Mar	rel. diff. 1 and 8 Mar [%]
36	2.255	2.259	2.261	2.260	-0.04%
37	2.242	2.248	2.249	2.248	-0.04%
38	2.204	2.205	2.206	2.205	-0.05%

Table 58: Successive weightings specimens 36-38 batch II.

The measured values of spatial dimensions are shown in Table 59 (specimens 1-32) and Table 60 (specimens 33-38).

No.	l_s [mm]	$l_{1,b}$.[mm]	$l_{1,o}$.[mm]	*part a b* [mm]	*part b*	l_{fj} [mm]	*part a h* [mm]	*part b*
1	1247.0	430	430	89.16	89.42	88.81	27.04	27.84
2	1248.5	431	430	88.66	90.08	89.93	27.54	27.18
3	1248.0	431	430	93.42	92.40	90.94	27.22	26.58
4	1246.5	432	430	89.73	87.85	86.67	27.25	27.59
5	1246.5	431	431	92.26	92.78	91.23	26.67	27.24
6	1247.0	432	430	90.53	89.70	88.01	27.63	27.73
7	1247.0	432	431	91.88	92.16	90.58	27.09	27.58
8	1245.2	431	432	91.64	90.85	87.00	27.00	27.03
9	1249.5	430	432	92.14	89.40	85.85	27.58	27.06
10	1245.5	431	431	90.42	91.42	89.38	27.21	27.03
11	1250.5	431	430	92.35	92.21	92.10	28.40	27.06
12	1251.0	431	432	88.35	90.55	87.69	26.40	27.12
13	1247.0	431	432	89.97	90.09	88.34	28.24	26.32
14	1246.5	431	431	92.58	91.57	91.56	26.55	26.62
15	1248.2	430	431	90.43	89.89	89.65	27.06	26.75
16	1244.5	431	431	91.45	92.68	90.31	27.86	26.55
17	1248.0	433	431	90.63	89.71	88.64	27.27	27.12
18	1248.5	431	432	90.83	91.98	86.18	28.08	26.46
19	1246.5	432	432	92.65	88.86	85.93	26.45	26.87
20	1246.0	432	431	89.40	88.60	85.16	26.59	26.85
21	1245.5	432	431	91.69	91.30	90.78	27.18	26.77
22	1244.1	432	432	90.56	91.61	90.07	26.74	26.92
23	1249.9	431	432	90.47	90.67	88.83	27.69	26.63
24	1246.5	431	430	92.44	90.50	89.68	27.40	27.29
25	1246.5	431	432	91.94	91.01	90.71	27.24	27.04
26	1249.1	431	432	88.93	92.78	90.68	26.55	26.84
27	1248.5	431	432	92.00	91.56	90.76	27.40	26.76
28	1243.2	432	431	91.63	92.06	91.42	27.07	27.45
29	1250.0	431	431	91.55	92.05	90.25	26.91	27.63
30	1241.0	432	448	89.65	90.31	88.90	26.73	26.87
31	1245.0	432	431	89.95	89.35	88.88	26.74	26.93
32	1245.5	431	431	92.37	90.06	89.60	26.72	27.27

Table 59: Spatial dimensions of specimens 1-32 batch II.

No.	l_s [mm]	$l_{1,b}$.[mm]	$l_{1,o}$.[mm]	part a b [mm]	part b	l_{fj} [mm]	part a h [mm]	part b
33	1246.5	431	431	92.16	89.76	89.33	26.97	27.94
34	1248.5	431	431	94.80	90.75	90.66	28.53	26.74
35	1246.5	431	470	89.29	92.97	88.94	26.40	27.82
36	1251.5	431	431	89.78	89.43	88.87	27.75	27.16
37	1248.5	431	431	89.93	90.06	87.80	27.62	26.94
38	1245.5	430	431	90.10	90.37	87.86	27.66	27.21
min	1241.0	430	430	88.35	87.85	85.16	26.40	26.32
max	1251.5	433	470	94.80	92.97	92.10	28.53	27.94
mean	1247.1	431	433	90.99	90.76	89.16	27.22	27.07
stdev	2.2			1.43	1.29	1.74	0.56	0.40

Table 60: Spatial dimensions of specimens 33-38 batch II.

The measured values of mass of specimens (after cutting), eigenfrequency and failure load in tension are shown in Table 61.

No.	m [kg]	f [Hz]	$P_{t,j}$ [kN]	No.	m [kg]	f [Hz]	$P_{t,j}$ [kN]
1	2.091	1952	94.864418	**20**	2.085	2011	93.971145
2	1.931	1825	95.226985	**21**	1.981	1976	94.626971
3	1.978	1708	54.877333	**22**	1.888	1913	97.937825
4	2.106	1801	108.785304	**23**	2.092	1635	113.006424
5	1.991	1991	115.682693	**24**	2.146	1732	89.056952
6	2.096	1571	72.511007	**25**	2.001	2006	116.871479
7	2.025	1928	109.038424	**26**	1.912	1830	105.935168
8	2.003	1859	81.523823	**27**	1.949	1806	98.952260
9	1.872	1776	90.561363	**28**	2.107	2123	120.583598
10	1.943	1869	96.196785	**29**	2.014	1864	87.707977
11	1.947	1796	96.715539	**30**	2.087	1635	75.955888
12	2.087	1976	97.363645	**31**	2.085	1918	77.949386
13	2.138	1625	105.968577	**32**	1.986	1810	107.127426
14	1.903	1889	109.731742	**33**	2.143	1703	86.393504
15	2.154	1742	117.094043	**34**	2.165	1659	98.844028
16	1.961	1864	85.371008	**35**	1.994	1845	87.344914
17	2.235	1688	94.929638	**36**	2.088	1615	98.680749
18	2.042	1962	100.573815	**37**	2.076	1801	84.354006
19	1.957	1889	78.554950	**38**	2.025	1893	102.472863
min	1.872	1571	54.877333				
max	2.235	2123	120.583598				
stdev	0.087	130	13.904646				
COV	0.04	0.07	0.15				

Table 61: Mass, eigenfrequency, failure load of batch II.

The data of the width, depth, thickness, and mass before drying of test slices is shown in Table 62, in order to determine the density of the lamellas.

No.	part a b_{test} [mm]	part b	part a h_{test} [mm]	part b	part a t_{test} [mm]	part b	part a m_{test} [g]	part b
1	89.16	89.42	27.04	27.84	39.86	36.81	67.49	59.61
2	88.66	90.08	27.54	27.18	20.60	39.09	27.68	65.64
3	93.42	92.40	27.22	26.58	34.22	30.80	57.44	47.53
4	89.73	87.85	27.25	27.59	33.63	32.44	59.16	55.66
5	92.26	92.78	26.67	27.24	33.14	34.14	56.46	50.82
6	90.53	89.70	27.63	27.73	36.44	33.11	62.70	52.47
7	91.88	92.16	27.09	27.58	35.95	34.76	58.86	56.12
8	91.64	90.85	27.00	27.03	36.93	32.54	59.56	50.19
9	92.14	89.40	27.58	27.06	35.07	35.07	56.18	49.37
10	77.85	91.42	27.21	27.03	34.84	34.66	45.14	57.12
11	92.35	92.21	28.40	27.06	33.28	35.06	50.55	54.52
12	88.35	90.55	26.40	27.12	31.17	33.35	51.33	54.61
13	89.97	90.09	28.24	26.32	38.22	32.43	63.17	55.67
14	92.58	91.57	26.55	26.62	30.71	34.50	44.48	52.16
15	90.43	89.89	27.06	26.75	35.87	31.98	64.89	50.76
16	91.45	92.68	27.86	26.55	34.25	33.42	51.82	53.13
17	90.63	89.71	27.27	27.12	31.42	31.21	61.23	55.94
18	90.83	91.98	28.08	26.46	32.58	31.27	52.99	48.39
19	92.65	88.86	26.45	26.87	34.90	32.72	54.04	47.30
20	89.40	88.60	26.59	26.85	35.06	35.83	58.41	61.60
21	91.69	91.30	27.18	26.77	34.55	35.66	59.25	53.71
22	90.56	91.61	26.74	26.92	33.05	33.56	50.13	50.56
23	90.47	90.67	27.69	26.63	34.91	30.82	64.09	48.62
24	92.44	90.50	27.40	27.29	33.59	35.40	55.53	63.88
25	91.94	91.01	27.24	27.04	32.80	33.38	47.47	58.54
26	87.60	92.78	26.55	26.84	34.78	34.72	49.15	54.36
27	92.00	91.56	27.40	26.76	33.70	34.04	52.36	51.02
28	91.63	92.06	27.07	27.45	34.31	32.57	58.75	53.57
29	91.55	92.05	26.91	27.63	35.25	32.34	57.18	50.35
30	89.65	90.31	26.73	26.87	30.80	32.82	50.35	54.06
31	89.95	89.35	26.74	26.93	31.07	34.42	50.72	57.94
32	92.37	90.06	26.72	27.27	24.18	33.93	35.95	57.38
33	92.16	89.76	26.97	27.94	36.08	35.68	56.85	65.54
34	94.80	90.75	28.53	26.74	33.01	34.55	55.14	58.88
35	87.06	90.45	26.40	27.82	35.29	34.16	53.65	55.23
36	89.78	89.43	27.75	27.16	34.41	35.84	54.35	60.60
37	89.93	90.06	27.62	26.94	33.15	32.94	55.41	54.47
38	90.10	90.37	27.66	27.21	34.74	35.60	54.78	59.07

Table 62: Width, depth, thickness and mass before drying of test slices batch II.

Table 63 (1-38) and Table 64 (minimum, maximum, mean, standard deviation, coefficient of variance) show the calculated slope of the load-displacement curves, the related coefficient of

determination R^2 and the modulus of elasticity in tension.

No.	Slope $E_{t,1}$	Slope $E_{t,2}$	R^2 $E_{t,1}$	R^2 $E_{t,2}$	$E_{t,1}$ [N/mm^2]	$E_{t,2}$ [N/mm^2]
1	87.32282	86.63556	0.999758	0.999749	18608	19721
2	67.69377	67.05197	0.999795	0.999776	12222	11130
3	60.98084	69.87739	0.999552	0.999556	17247	16284
4	70.62849	76.84470	0.999807	0.999837	12432	14379
5	91.30480	82.65239	0.999812	0.999756	14727	16255
6	52.92123	55.31700	0.999809	0.999807	13135	13669
7	80.59056	81.09346	0.999700	0.999744	14679	18342
8	73.88381	75.75107	0.999635	0.999684	15841	15072
9	59.17213	64.90493	0.999736	0.999740	14028	14243
10	69.86724	76.28405	0.999850	0.999839	13973	15227
11	64.02338	81.29067	0.999775	0.999776	14073	15820
12	81.98948	91.83758	0.999743	0.999744	11989	12748
13	59.67367	57.68734	0.999839	0.999821	12024	14147
14	68.29636	78.32253	0.999859	0.999862	13157	16414
15	68.68776	74.60871	0.999864	0.999918	12706	19015
16	67.78074	76.94583	0.999752	0.999765	13652	13585
17	63.11577	73.01112	0.999805	0.999761	17545	15848
18	81.96012	86.02430	0.999700	0.999737	16150	15058
19	69.44259	70.67512	0.999703	0.999704	15954	21368
20	86.94287	94.14637	0.999683	0.999301	10109	12319
21	82.26651	90.35295	0.999715	0.999728	12837	13414
22	66.59112	85.04376	0.999718	0.999662	13203	13888
22	66.59112	85.04376	0.999718	0.999662	13203	13888
23	59.42236	64.23401	0.999842	0.999794	10463	11068
24	71.00669	67.61167	0.999764	0.999827	15326	15190
25	-	86.13561	-	0.999770	-	9923
26	-	65.50996	-	0.999872	-	10924
27	-	64.39088	-	0.999794	-	19817
28	-	98.96300	-	0.999497	-	12444
29	-	72.99182	-	0.999495	-	15136
30	-	63.27828	-	0.999463	-	19193
31	-	85.33108	-	0.999693	-	15640
32	-	75.42916	-	0.999869	-	13357
33	-	68.23282	-	0.999841	-	19178
34	-	59.79691	-	0.999878	-	16178
35	-	67.39173	-	0.999587	-	12208
36	-	58.65854	-	0.999806	-	17146
37	-	76.70170	-	0.999669	-	15279
38	-	80.16644	-	0.999767	-	12252

Table 63: Slope load-displacement curve, related R^2 and relative difference slope 1 and 2 of specimens 1-38 batch II.

No.	Slope $E_{t,1}$	Slope $E_{t,2}$	R^2 $E_{t,1}$	R^2 $E_{t,2}$	$E_{t,1}$ [N/mm^2]	$E_{t,2}$ [N/mm^2]
min						9923
max						21368
mean						15076
stdev						2752
COV						0.18

Table 64: Slope load-displacement curve, related R^2 and relative difference slope 1 and 2 batch II.

Table 65 (1-30) and Table 66 (31-38) show the speed of the test set to the control panel, as well as the recorded time to failure, moisture content, density, dynamic modulus of elasticity and finger joint tension strength.

No.	*Speed* [mm/s]	*Time to failure* [s]	part a ω [%]	part b	part a ρ [kg/m^3]	part b	E_{dyn} [N/mm^2]	$f_{t,j}$ [N/mm^2]
1	0.015	200.57	10.9	11.2	702.30	650.50	14927	39.50
2	0.015	250.86	9.4	9.1	550.31	685.84	13987	38.96
3	0.015	150.74	8.3	8.3	660.09	628.33	11900	22.70
4	0.015	277.06	9.7	11.1	719.44	707.90	13713	46.06
5	0.015	251.68	9.8	8.0	692.39	588.93	12276	45.77
6	0.015	255.42	8.9	8.9	687.88	637.10	14927	28.99
7	0.015	240.43	9.8	9.2	657.80	635.19	13987	44.44
8	0.015	187.40	9.4	8.2	651.82	628.10	11900	34.71
9	0.015	247.15	9.3	9.5	630.38	581.92	13713	38.98
10	0.015	228.73	10.4	10.7	611.64	666.92	12276	39.82
11	0.015	240.98	8.2	8.0	579.14	623.15	14927	36.88
12	0.015	42.06	10.9	10.7	706.03	666.80	17035	42.06
13	0.015	45.58	9.3	10.2	650.52	723.96	11466	45.58
14	0.015	44.53	8.4	8.3	589.25	620.24	13832	44.53
15	0.015	48.83	10.3	10.1	739.28	660.10	13454	48.83
16	0.015	33.06	8.1	8.3	593.84	646.07	13542	33.06
17	0.015	39.49	9.7	9.8	788.50	736.71	12964	39.49
18	0.015	44.11	9.8	8.3	637.70	635.84	15749	44.11
19	0.015	31.55	10.1	10.0	631.86	605.44	14391	31.55
20	0.015	41.50	11.2	11.2	700.84	722.70	17672	41.50
21	0.015	37.97	10.5	9.9	688.13	616.25	15614	37.97
22	0.015	40.66	9.8	10.3	626.37	610.90	14070	40.66
23	0.015	47.77	10.4	9.0	732.85	653.35	11366	47.77
24	0.015	36.39	10.5	8.7	652.69	730.65	12833	36.39
25	0.015	47.65	10.0	9.6	577.87	712.64	16171	47.65
26	0.015	44.87	9.5	10.2	607.66	628.73	13191	44.87
27	0.015	39.25	8.1	10.3	616.36	611.73	12773	39.25
28	0.015	48.61	10.1	10.0	690.34	650.86	18862	48.61
29	0.015	34.49	6.7	17.6	658.44	612.15	13976	34.49
30	0.015	31.70	9.1	9.3	682.18	678.79	11484	31.70

Table 65: Testing speed, time to failure, moisture content, density, dynamic modulus of elasticity and finger joint tension strength of specimens 1-30 batch II.

No.	*Speed* [mm/min]	*Time to failure* [s]	part a ω [%]	part b	part a ρ [kg/m³]	part b	E_{dyn} [N/mm²]	$f_{t,j}$ [N/mm²]
31	0.015	32.80	10.7	11.5	678.70	699.58	15877	32.80
32	0.015	44.75	10.3	10.2	602.39	688.59	13164	44.75
33	0.015	35.86	9.8	9.5	633.93	732.44	12409	35.86
34	0.015	40.77	9.5	9.3	617.61	702.28	11607	40.77
35	0.015	33.77	9.6	10.5	661.45	642.53	13699	33.77
36	0.015	40.88	9.3	10.5	633.98	696.13	11082	40.88
37	0.015	35.66	10.4	10.1	672.94	681.56	13697	35.66
38	0.015	41.12	10.9	10.7	632.73	674.78	14603	41.12
min		22.70	6.7	8.0	550.31	581.92	10344	22.70
max		48.83	11.2	17.6	788.50	736.71	18862	48.83
mean		39.54	9.7	9.9	653.88	659.89	13800	39.54
stdev		5.93	1.3	1.6	50.07	42.85	1934	5.93
COV		0.15			0.08	0.06	0.14	0.15

Table 66: Testing speed, time to failure, moisture content, density, dynamic modulus of elasticity and finger joint tension strength of specimens 31-38 batch II.

Table 67 presents a detailed description of the failure mode of all batch II specimens.

No.	Failure mode	No.	Failure mode
1	glue	**20**	glue
2	50% glue 50% finger	**21**	combination
3	glue	**22**	25% glue 75% finger
4	25% glue 75% finger	**23**	25% glue 75% finger
5	wood	**24**	50% glue 50% finger
6	wood	**25**	25% glue 75% finger
7	75% glue 25% finger	**26**	wood
8	50% glue 50% finger	**27**	wood
9	50% glue 50% finger	**28**	wood
10	75% glue 25% finger	**29**	combination
11	wood	**30**	wood
12	glue	**31**	glue
13	finger	**32**	finger
14	combination	**33**	finger
15	50% glue 50% finger	**34**	25% glue 75% finger
16	combination	**35**	wood
17	50% glue 50% finger	**36**	25% glue 75% finger
18	glue	**37**	75% glue 25% finger
19	combination	**38**	wood

Table 67: Detailed failure modes of batch II specimens.

Appendix 8: Data of batch III

This Appendix presents measured and calculated data of batch III; the light grey highlighted data are calculated values. Both measured data and calculated values are shown in Table 68 (1-32) and Table 69 (33-34): maximum, minimum and mean values are given, as well as standard deviations and characteristic values of density and dynamic modulus of elasticity.

No.	l_s [mm]	b [mm]	h [mm]	m [oz]	ω [%]	f_e [Hz]	m [kg]	ρ [kg/m^3]	E_{dyn} [Mpa]
1	3455	100.73	35.68	249.5	8.4	703	7.1	569.6	13442
2	2840	100.60	37.70	237.5	7.0	n/a	6.7	625.1	n/a
3	3550	100.23	34.02	264.5	8.4	673	7.5	619.5	14144
4	3454	100.80	33.16	247.5	7.1	683	7.0	607.7	13529
5	3449	99.70	34.79	278.5	7.3	712	7.9	660.0	15920
6	3453	100.60	32.78	223.5	8.8	722	6.3	556.4	13834
7	3447	99.31	33.63	275.0	6.9	722	7.8	677.2	16778
8	2844	101.50	35.41	254.5	7.0	771	7.2	705.8	13575
9	2844	101.94	33.89	248.5	8.3	722	7.0	717.0	12093
10	2844	100.76	34.68	231.5	7.4	722	6.6	660.4	11138
11	2842	100.88	34.79	228.0	9.2	766	6.5	648.0	12285
12	3454	100.60	34.00	235.5	7.5	722	6.7	565.1	14058
13	3550	100.63	35.16	288.0	6.0	659	8.2	650.0	14231
14	3544	101.08	35.28	265.5	9.2	654	7.5	595.6	12798
15	2831	100.00	39.04	255.5	8.0	800	7.2	655.4	13446
16	2851	100.57	34.90	203.0	7.9	839	5.8	575.1	13162
17	2832	99.70	38.39	247.5	7.8	n/a	7.0	647.3	n/a
18	3453	100.53	34.96	265.5	7.7	703	7.5	620.2	14619
19	3447	99.31	33.26	244.5	6.0	712	6.9	608.8	14668
20	2851	103.22	37.71	218.0	8.3	849	6.2	556.9	13051
21	3466	100.00	35.56	255.0	7.6	673	7.2	586.5	12766
22	3449	98.93	33.10	252.0	7.3	717	7.1	632.6	15473
23	3449	99.09	34.27	259.5	7.4	698	7.4	628.1	14561
24	3457	100.25	34.35	274.5	8.1	698	7.8	653.7	15225
25	3451	98.45	33.28	239.0	7.2	761	6.8	599.2	16532
26	3449	99.65	33.33	245.0	8.9	703	6.9	606.3	14258
27	3447	99.68	33.65	263.0	6.2	717	7.5	644.9	15756
28	3451	97.89	35.33	254.0	7.4	737	7.2	603.3	15611
29	3446	100.25	33.55	231.0	8.0	708	6.5	565.0	13453
30	3451	99.67	34.66	267.5	6.5	708	7.6	636.1	15190
31	3447	99.88	34.92	264.0	7.1	722	7.5	622.5	15423
32	3447	99.95	32.96	272.0	7.6	717	7.7	679.1	16591

Table 68: Data specimens 1-32 batch III.

No.	l_s [mm]	b [mm]	h [mm]	m [oz]	ω [%]	f_e [Hz]	m [kg]	ρ [kg/m^3]	E_{dyn} [Mpa]
33	2852	101.35	34.29	202.0	8.8	834	5.7	577.8	13075
34	2852	101.68	36.98	237.5	8.0	839	6.7	627.9	14379
min	2831	97.89	32.78	202.0	6.0	654	5.7	556.4	11138
max	3550	103.22	39.04	288.0	9.2	849	8.2	717.0	16778
mean	3263	100.3	34.81	249.3	7.7	730	7.1	623.1	14221
stdev	296	1.03	1.58	20.3	0.8	52	0.6	41.1	1377
char								547.1	11676

Table 69: Data specimens 33-34 batch III.

Appendix 9: Data of batch IV

This Appendix presents measured and calculated data of batch IV; the light grey highlighted data are calculated values. Table 70 shows the data of the successive weightings of the specimens, in order to achieve a relative difference of less than 0.1%. The last column shows that this requirement is indeed met.

No.	*m* [kg] 31 Oct	*m* [kg] 7 Nov	*m* [kg] 14 Nov	relative difference 7 and 14 Nov [%]
1	12.900	12.930	12.940	0.077
2	12.675	12.715	12.725	0.079
3	12.240	12.265	12.275	0.082
4	12.325	12.360	12.370	0.081
5	12.930	12.960	12.970	0.077
6	12.530	12.550	12.560	0.080
7	13.225	13.245	13.250	0.038
8	13.150	13.170	13.175	0.038
9	12.560	12.590	12.600	0.079
10	13.105	13.130	13.140	0.076
11	12.820	12.850	12.855	0.039
12	12.855	12.890	12.900	0.078

Table 70: Successive weightings specimens batch IV.

Table 71 shows the measured values of spatial dimensions, mass of specimens, eigen-frequencies and failure loads in bending.

No.	l_s [mm]	*b* [mm]	*h* [mm]	*m* [kg]	f_e [Hz]	$P_{m,g}$ [kN]
1	2101	89.09	108.61	12.920	1113	28.912
2	2101	89.95	109.31	12.700	1161	40.102
3	2097	90.23	109.56	12.250	1122	40.493
4	2102	89.36	108.95	12.350	1142	44.237
5	2102	89.11	108.82	12.950	1108	35.007
6	2102	90.03	109.84	12.535	1171	40.139
7	2096	90.16	108.67	13.235	1166	37.085
8	2101	89.55	109.12	13.150	1152	36.279
9	2093	91.15	109.25	12.585	1142	28.697
10	2097	90.19	109.01	13.130	1161	41.032
11	2097	89.81	108.51	12.835	1152	39.770
12	2100	90.16	108.85	12.885	1166	29.297
min	2093	89.09	108.51	12.250	1108	28.697
max	2102	91.15	109.84	13.235	1171	44.237
mean	2099	89.90	109.04	12.794	1146	36.754
stdev	2.97	0.57	0.40	0.32	22	5.27

Table 71: Spatial dimensions, mass, eigenfrequency, failure load specimens batch IV.

Table 72 shows the data of the successive weightings of the test slices, in order to determine the moisture content of the beams. In the last column it is shown that the relative difference between the last two measurements is less than 0.1%.

No.	m_1 [kg] 28 Nov	m [kg] 30 Nov	m [kg] 3 Dec	m_0 [kg] 5 Dec	relative difference 3 and 5 Dec [%]
1	149.26	136.21	136.34	136.28	0.044027
2	142.68	129.85	129.96	129.89	0.053892
3	145.51	133.38	133.46	133.38	0.059979
4	177.92	161.18	161.34	161.26	0.049609
5	157.02	143.44	143.56	143.47	0.062731
6	183.34	167.29	167.40	167.31	0.053792
7	155.66	142.51	142.60	142.53	0.049113
8	174.02	159.68	159.84	159.77	0.043813
9	176.63	161.87	162.02	161.95	0.043223
10	143.70	131.77	131.91	131.87	0.030333
11	179.23	162.58	162.69	162.62	0.043045
12	150.60	137.15	137.30	137.23	0.051009

Table 72: Successive weightings test slices specimens batch IV.

Table 73 shows the calculated slope of the load-displacement curves, as well as the respective coefficient of determination R^2.

No.	Slope $E_{loc,1}$	Slope $E_{loc,2}$	Slope $E_{glob,1}$	Slope $E_{glob,2}$	R^2 $E_{loc,1}$	R^2 $E_{loc,2}$	R^2 $E_{glob,1}$	R^2 $E_{glob,2}$
1	14.2768	14.0926	1.03273	1.12272	0.999966	0.999982	0.998929	0.999057
2	14.4764	14.8709	1.12342	1.12686	0.999975	0.999868	0.998512	0.998803
3	13.5221	13.9175	1.04026	1.03279	0.999939	0.999941	0.998975	0.998941
4	13.5730	12.6117	1.02876	0.98229	0.999812	0.999941	0.997798	0.998894
5	12.5540	12.4398	1.04157	0.96144	0.999971	0.999973	0.997669	0.998677
6	14.8080	14.9897	1.19520	1.11910	0.999954	0.999963	0.991649	0.996263
7	13.5192	14.4070	1.16198	1.09618	0.999986	0.999990	0.989258	0.997077
8	13.3464	13.6883	1.11544	1.03717	0.999993	0.999994	0.997256	0.997827
9	13.4681	14.0422	1.07963	0.99270	0.999937	0.999945	0.995593	0.995790
10	14.9531	14.8953	1.12584	1.11800	0.999947	0.999956	0.997309	0.999130
11	14.7414	13.7707	1.11663	1.04646	0.999970	0.999962	0.997727	0.998063
12	15.1521	13.9113	1.28149	1.13360	0.999947	0.999937	0.984055	0.996316

Table 73: Slope load-displacement curves and related R^2 specimens batch IV.

Table 74 shows the speed of the test set to the control panel, as well as the recorded time to failure and moisture content, density and bending strength.

No.	*Speed* [mm/min]	*Time to failure* [s]	ω [%]	ρ [kg/m^3]	f_m [N/mm^2]
1	20	90.04	9.5	619.26	52.41
2	20	113.01	9.8	627.10	71.08
3	20	115.00	9.1	603.01	71.22
4	20	152.94	10.3	606.94	79.45
5	20	105.24	9.4	644.10	63.20
6	20	113.57	9.6	587.45	70.40
7	20	104.58	9.2	637.28	66.35
8	20	102.65	8.9	595.80	64.81
9	10	163.43	9.1	620.18	50.25
10	10	214.34	9.0	649.61	72.93
11	10	263.27	10.2	619.87	71.65
12	10	155.90	9.7	627.12	52.24
min		90.04	8.9	587.45	50.25
max		263.27	10.3	649.61	79.45
mean		141.17	9.5	619.81	65.50
stdev				17.9	9.3
COV				0.03	0.14

Table 74: Speed, time to failure, moisture content, density, and bending strength specimens batch IV..

Table 75 shows the dynamic, local and global modulus of elasticity, and their quotients.

No.	E_{dyn} [N/mm^2]	E_{loc} [N/mm^2]	E_{glob} [N/mm^2]	E_{loc} / E_{glob}	E_{loc} / E_{dyn}	E_{glob} / E_{dyn}
1	13901	15394	13816	1.11	1.11	0.90
2	14632	15472	14013	1.10	1.06	0.91
3	13085	14322	12781	1.12	1.09	0.89
4	13910	14034	12731	1.10	1.01	0.91
5	13785	13481	12762	1.06	0.98	0.95
6	14614	15469	14191	1.09	1.06	0.92
7	15397	14949	14279	1.05	0.97	0.96
8	15009	14391	13535	1.06	0.96	0.94
9	13799	14336	12756	1.12	1.04	0.89
10	15100	15824	14051	1.13	1.05	0.89
11	14661	15390	13792	1.12	1.05	0.90
12	14994	15481	15195	1.02	1.03	0.98
min	13085	13481	12731			
max	15397	15824	15195			
mean	14407	14878	13659	1.09	1.03	0.92
stdev	696	738	776			
COV	0.05	0.05	0.06			

Table 75: Dynamic, local, and modulus of elasticity specimens batch IV.

Appendix 10: Load-displacement curves batch I

This Appendix shows all the load-displacement curves of the batch I specimens: see Figure 223 till Figure 260. The results from LVDT 1 and 2 are depicted in dark and light blue, respectively. The red dashed lines depict the area between circa 10% and 40 % of the maximum load, over which the modulus of elasticity in tension is calculated.

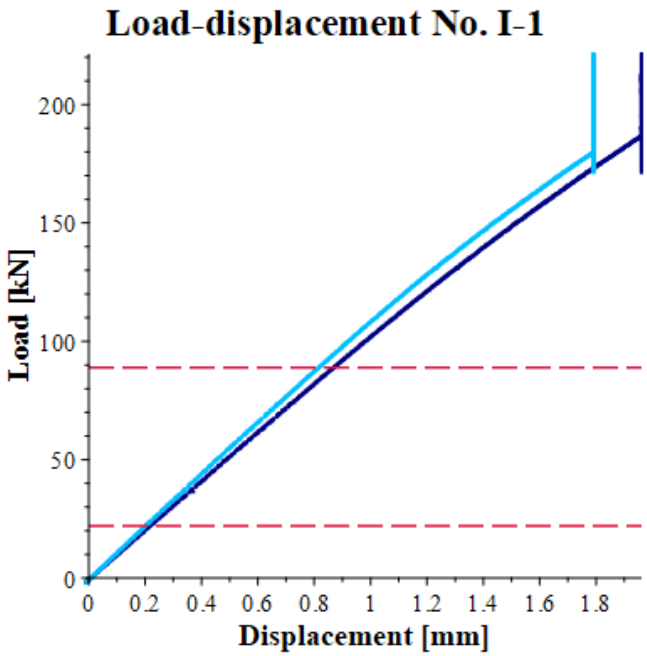

Figure 223: Load-displacement curves specimen I-1.

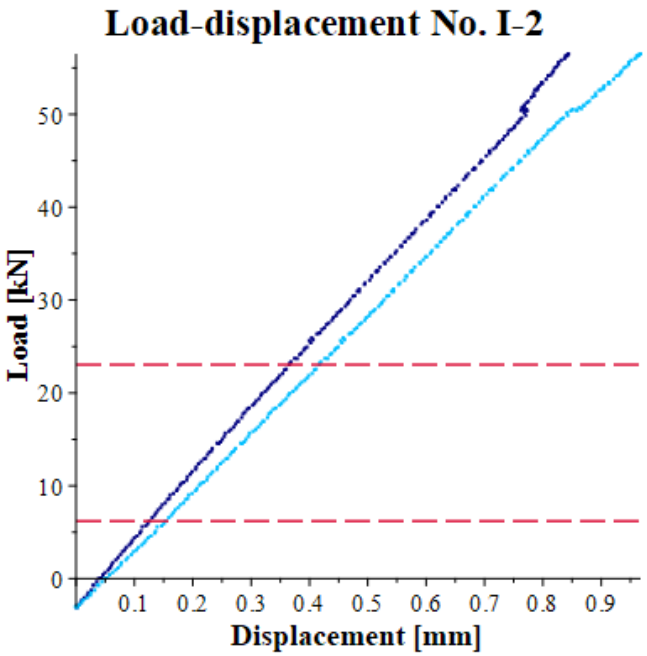

Figure 224: Load-displacement curves specimen I-2.

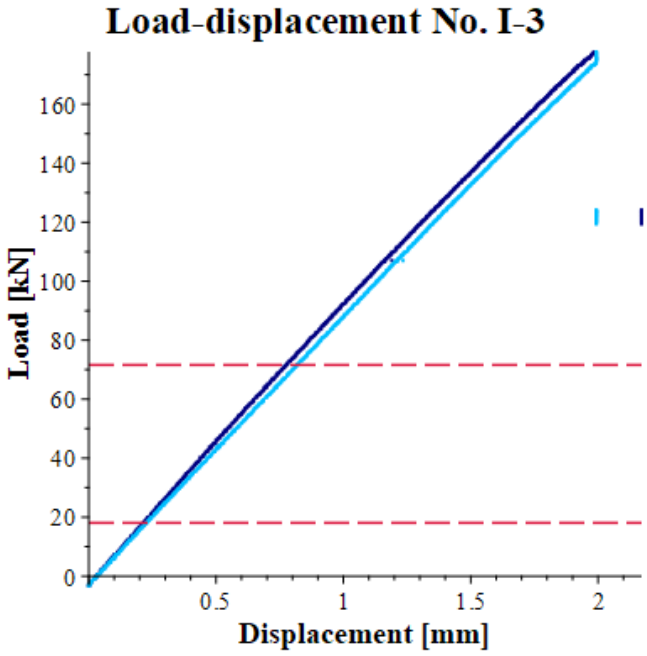

Figure 225: Load-displacement curves specimen I-3.

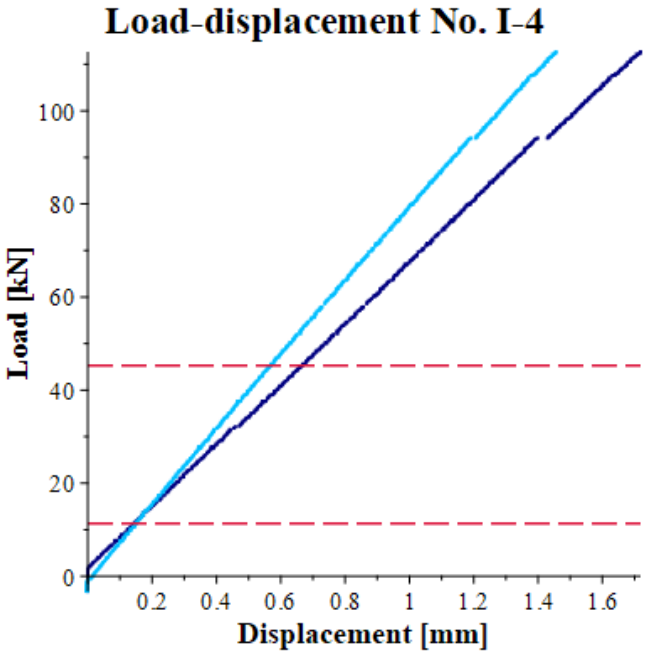

Figure 226: Load-displacement curves specimen I-4.

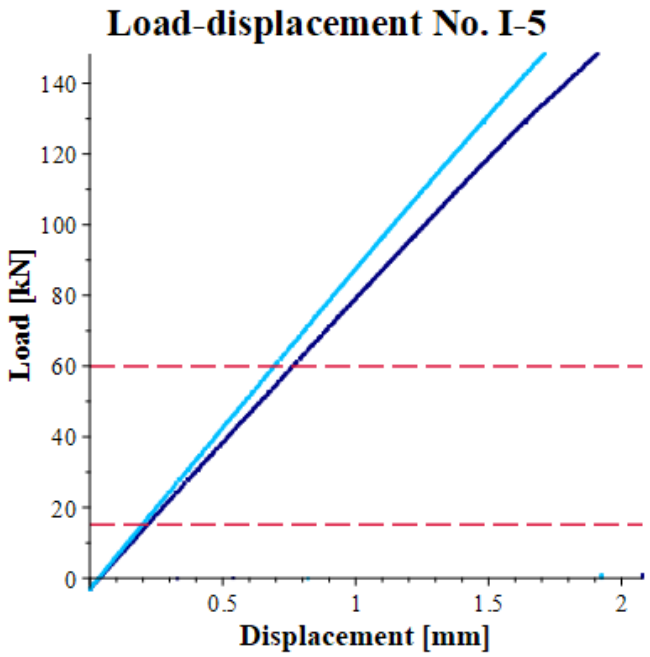

Figure 227: Load-displacement curves specimen I-5.

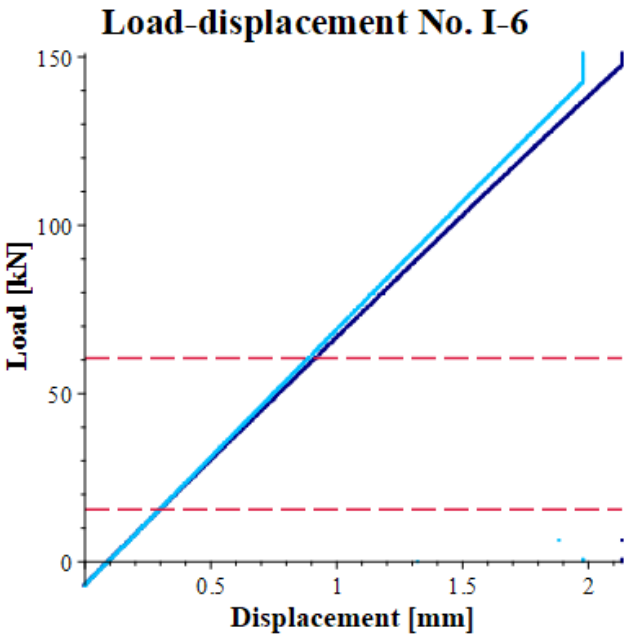

Figure 228: Load-displacement curves specimen I-6.

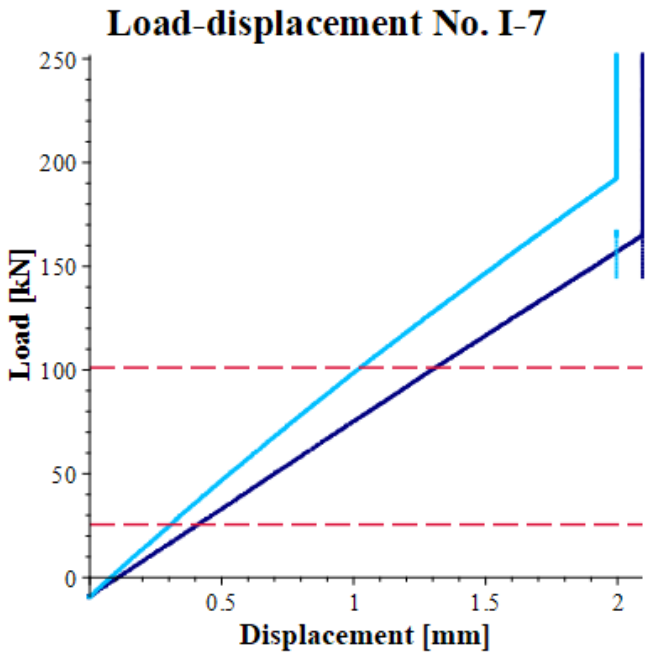

Figure 229: Load-displacement curves specimen I-7.

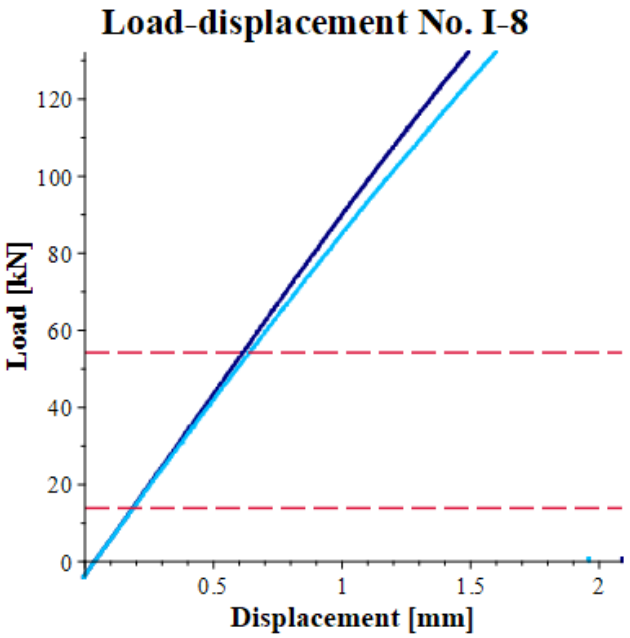

Figure 230: Load-displacement curves specimen I-8.

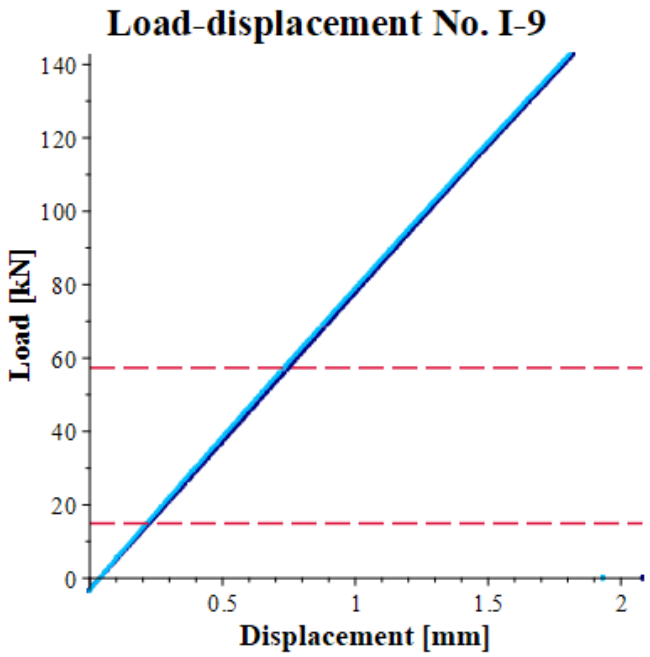

Figure 231: Load-displacement curves specimen I-9.

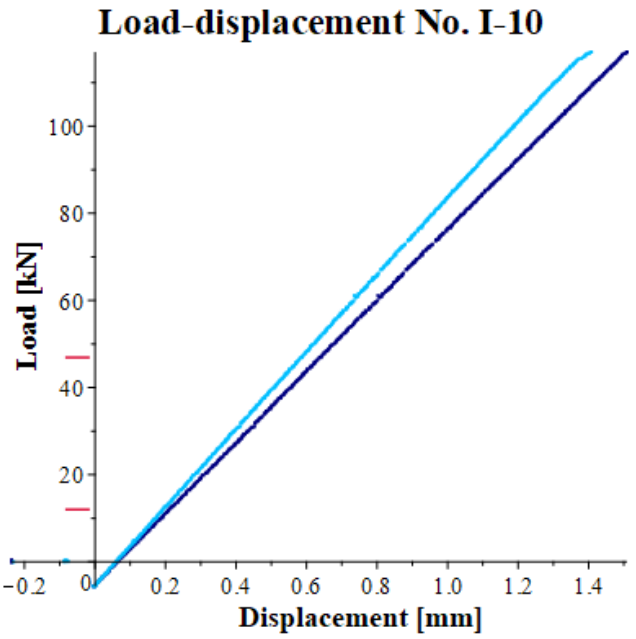

Figure 232: Load-displacement curves specimen I-10.

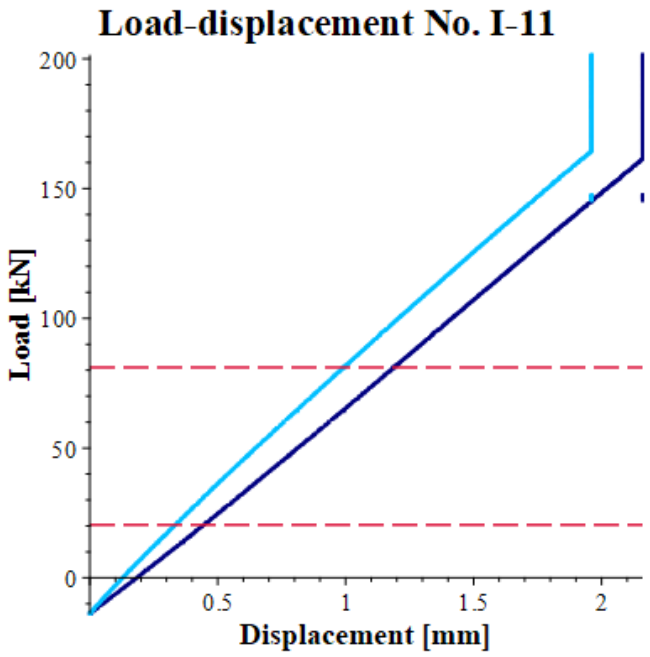

Figure 233: Load-displacement curves specimen I-11.

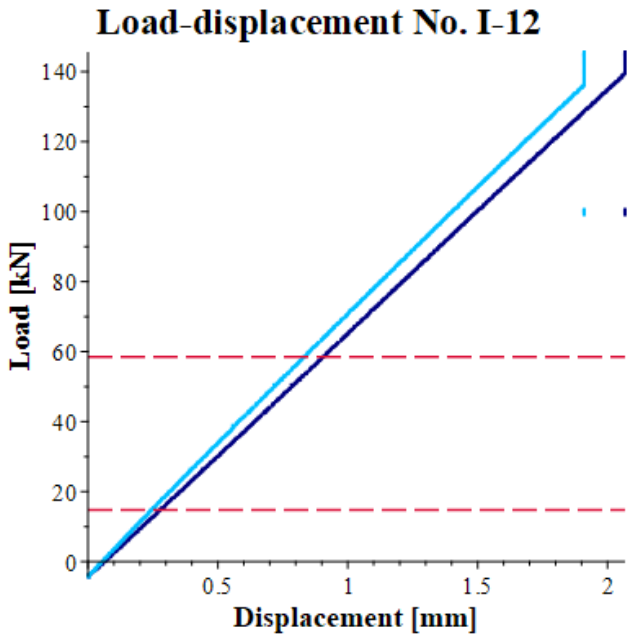

Figure 234: Load-displacement curves specimen I-12.

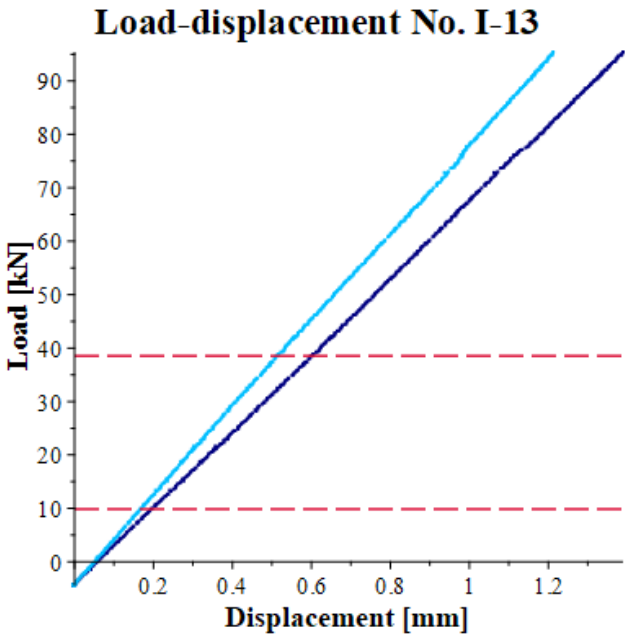

Figure 235: Load-displacement curves specimen I-13.

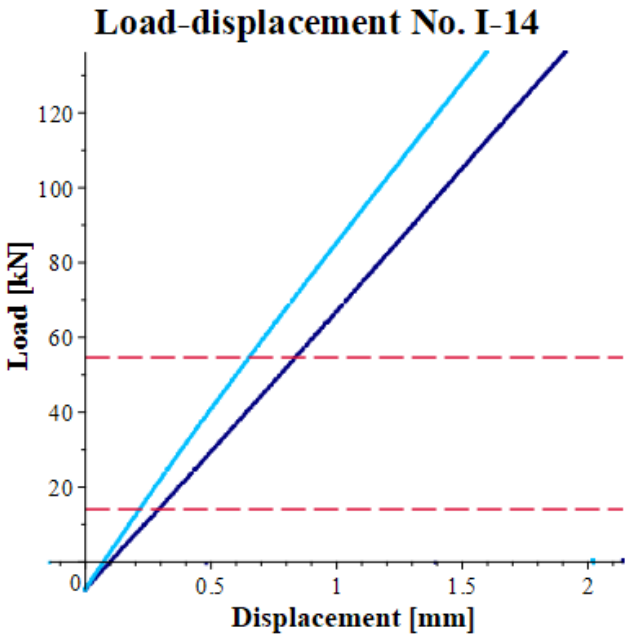

Figure 236: Load-displacement curves specimen I-14.

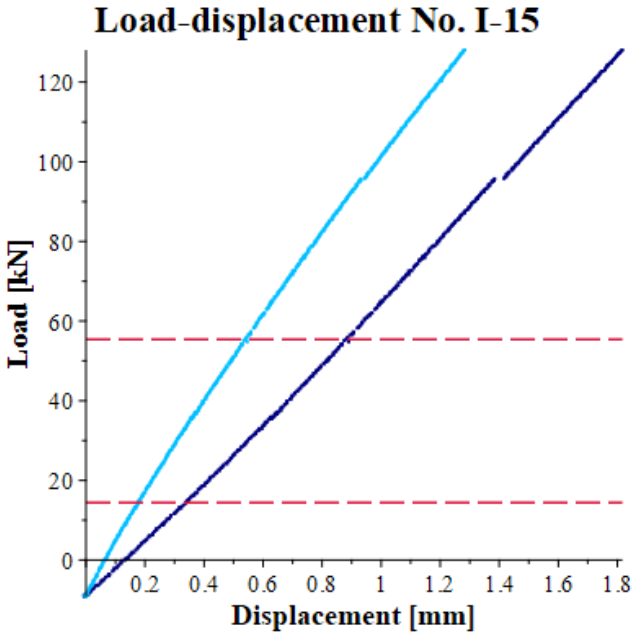

Figure 237: Load-displacement curves specimen I-15.

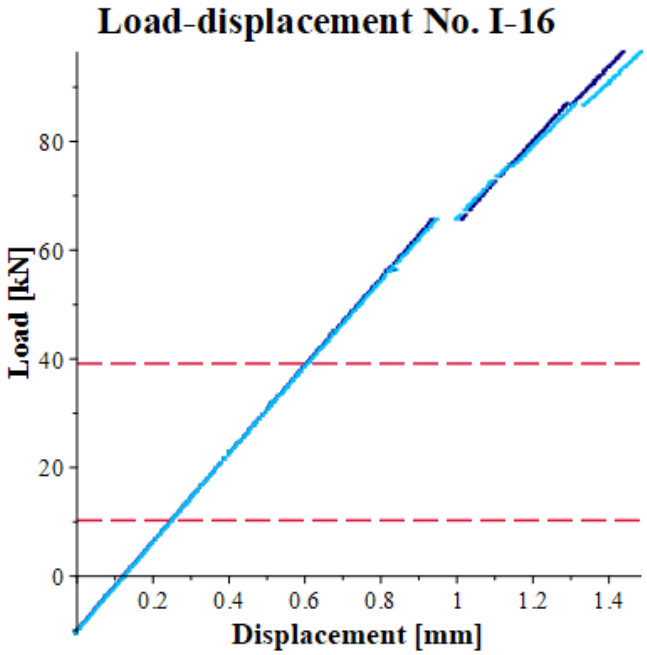

Figure 238: Load-displacement curves specimen I-16.

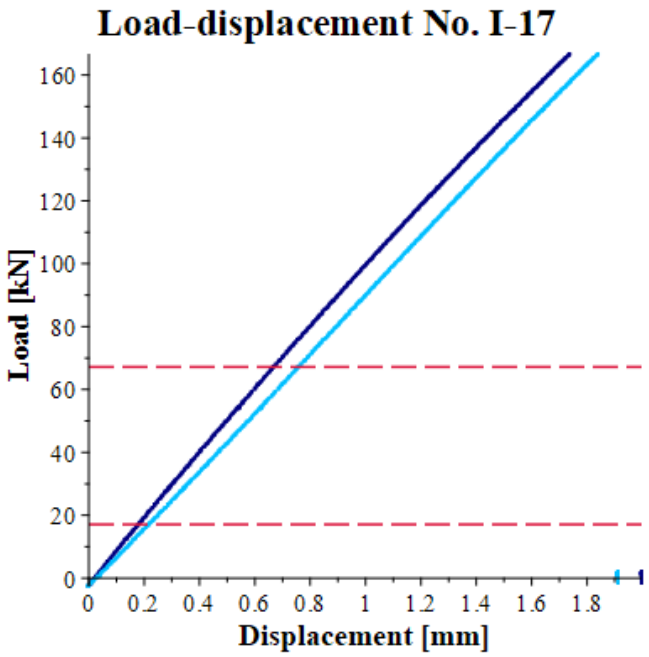

Figure 239: Load-displacement curves specimen I-17.

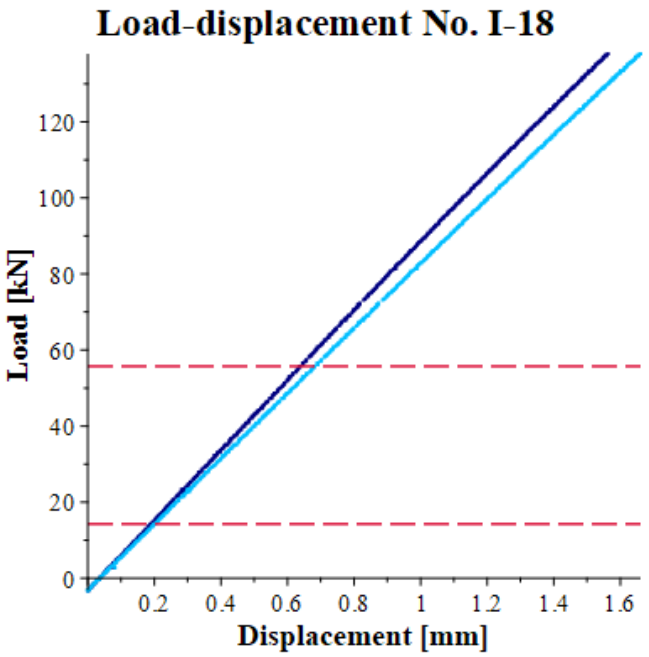

Figure 240: Load-displacement curves specimen I-18.

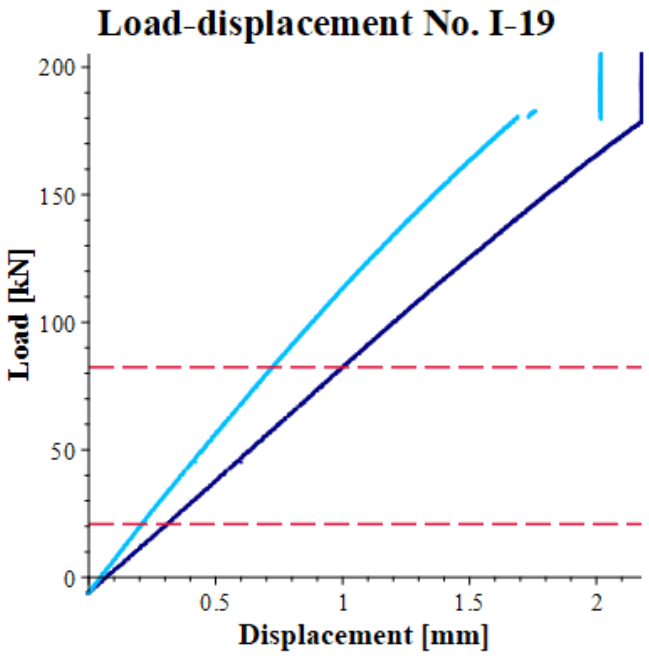

Figure 241: Load-displacement curves specimen I-19.

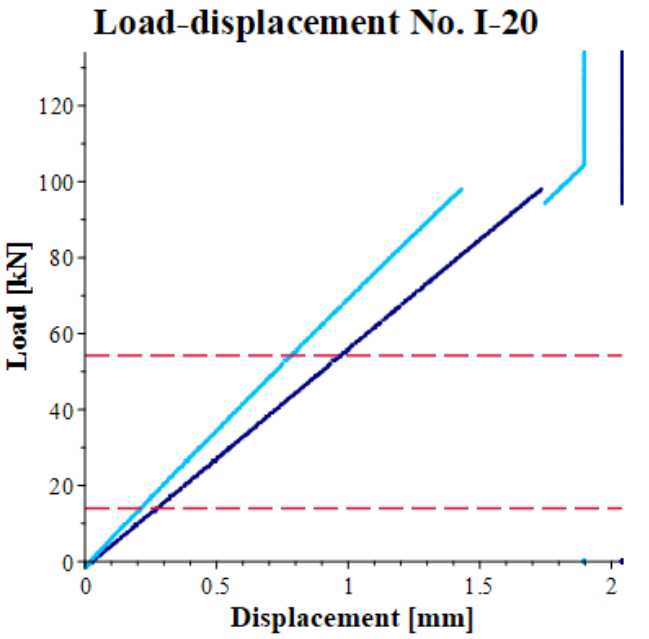

Figure 242: Load-displacement curves specimen I-20.

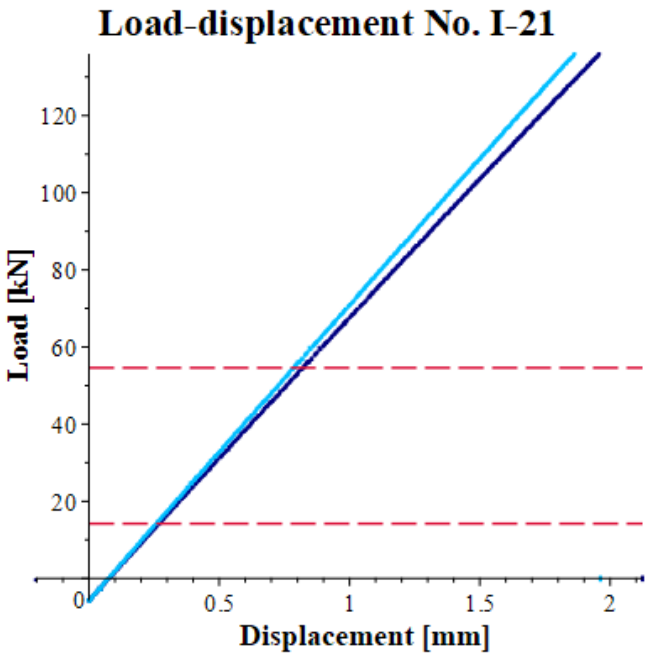

Figure 243: Load-displacement curves specimen I-21.

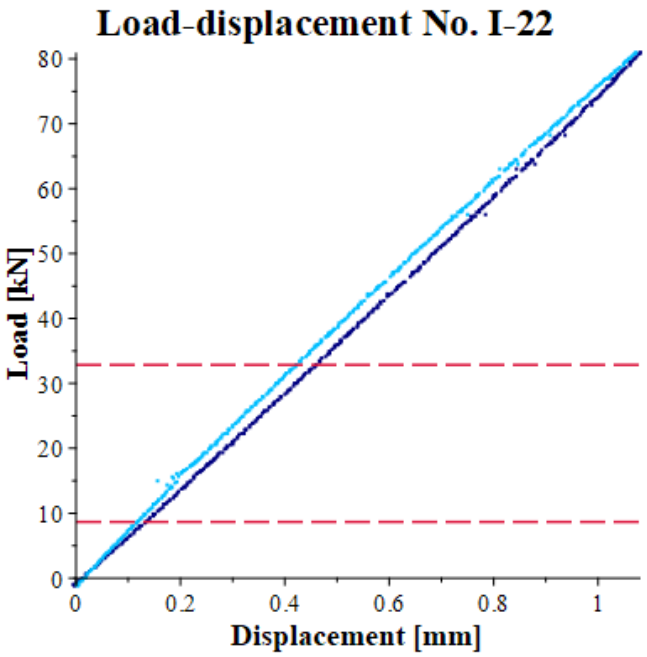

Figure 244: Load-displacement curves specimen I-22.

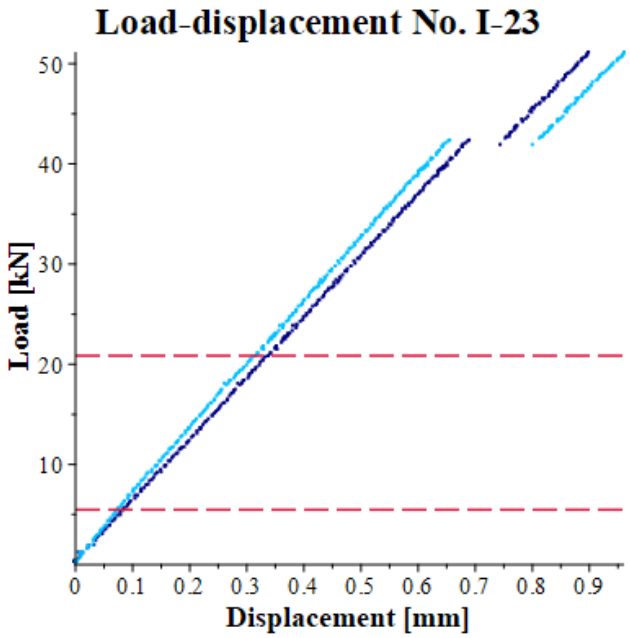

Figure 245: Load-displacement curves specimen I-23.

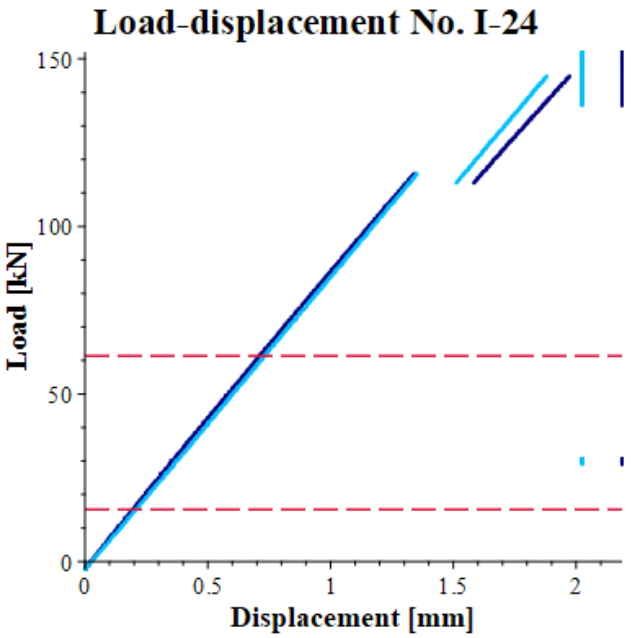

Figure 246: Load-displacement curves specimen I-24.

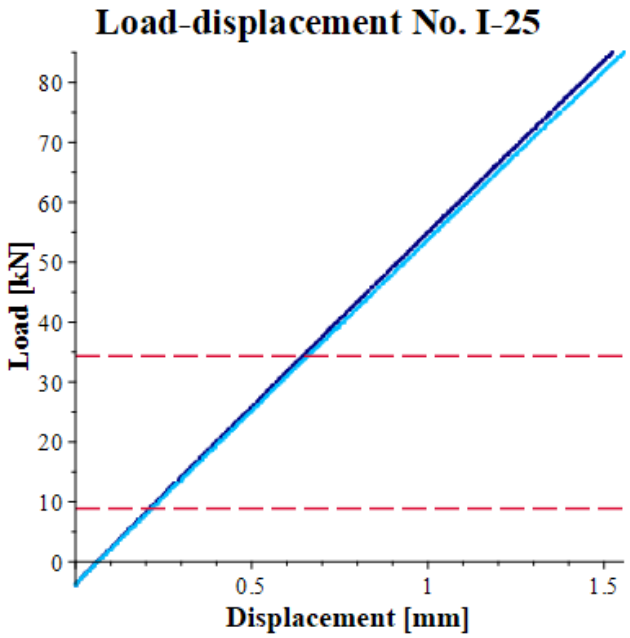

Figure 247: Load-displacement curves specimen I-25.

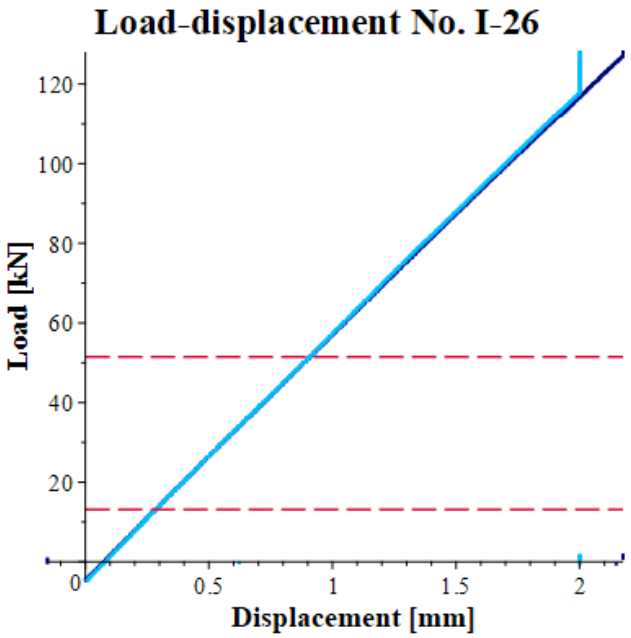

Figure 248: Load-displacement curves specimen I-26.

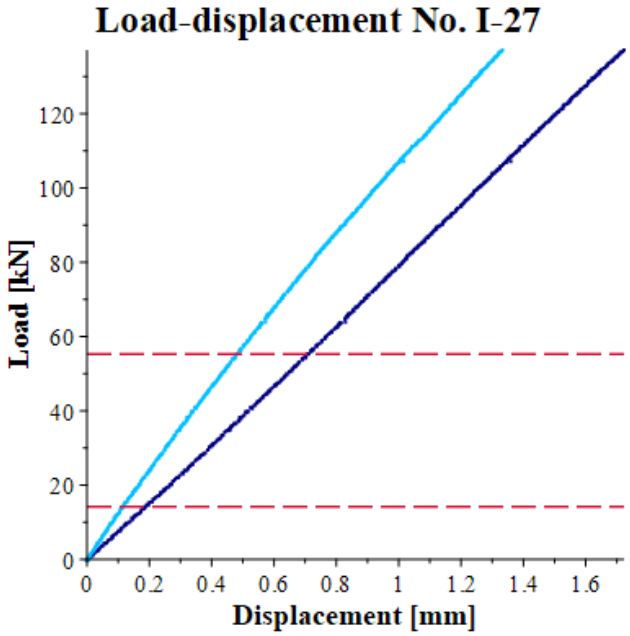

Figure 249: Load-displacement curves specimen I-27.

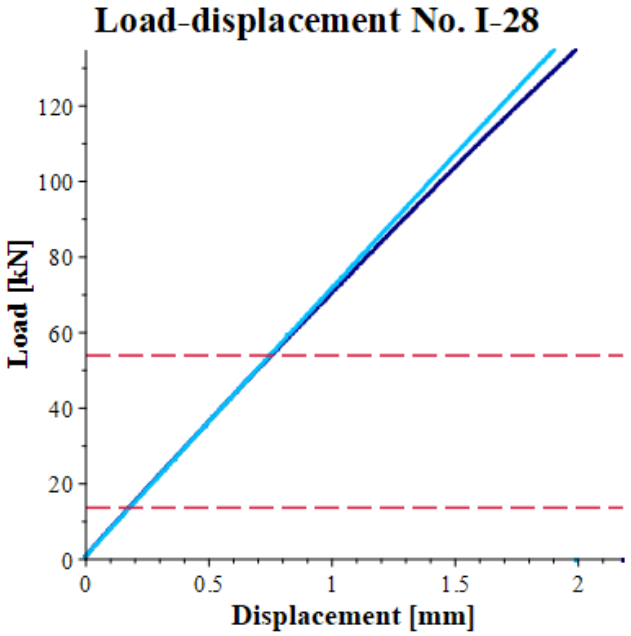

Figure 250: Load-displacement curves specimen I-28.

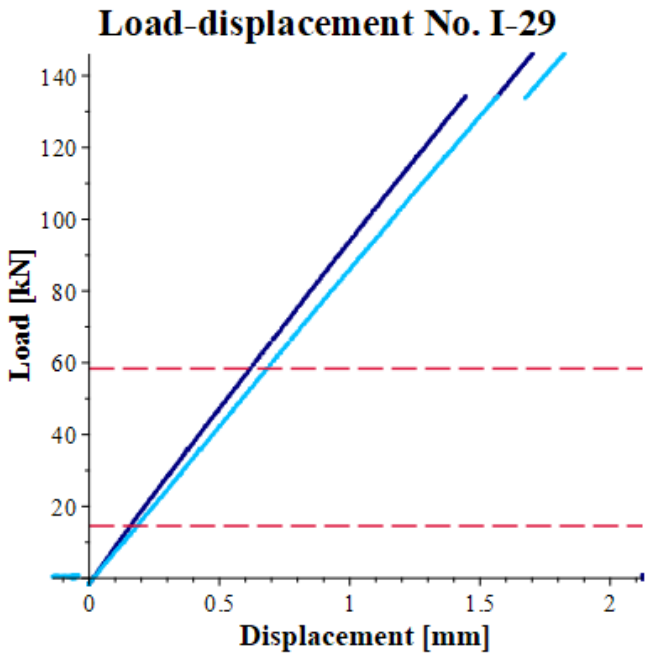

Figure 251: Load-displacement curves specimen I-29.

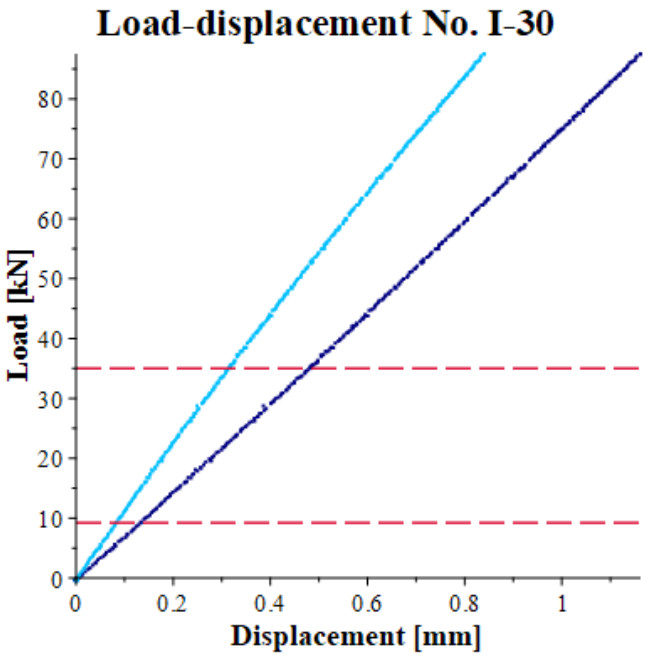

Figure 252: Load-displacement curves specimen I-30.

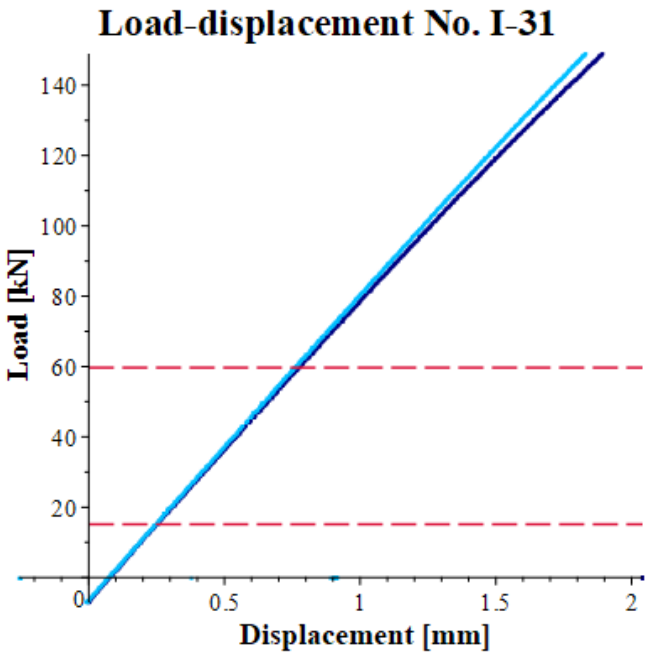

Figure 253: Load-displacement curves specimen I-31.

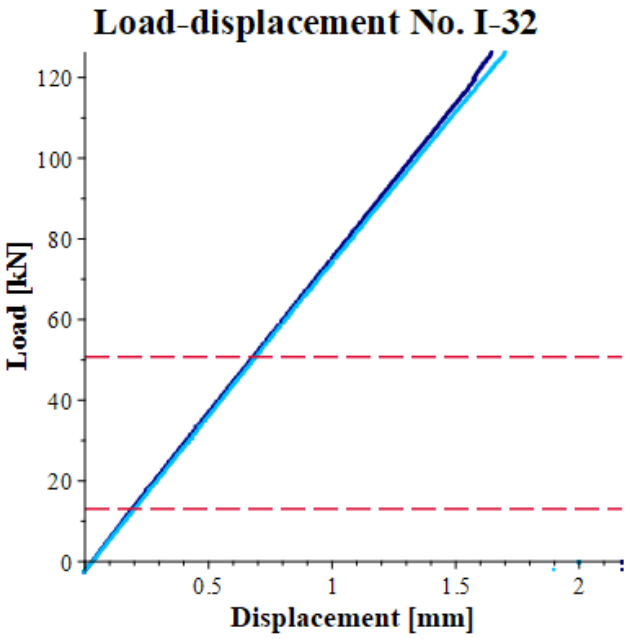

Figure 254: Load-displacement curves specimen I-32.

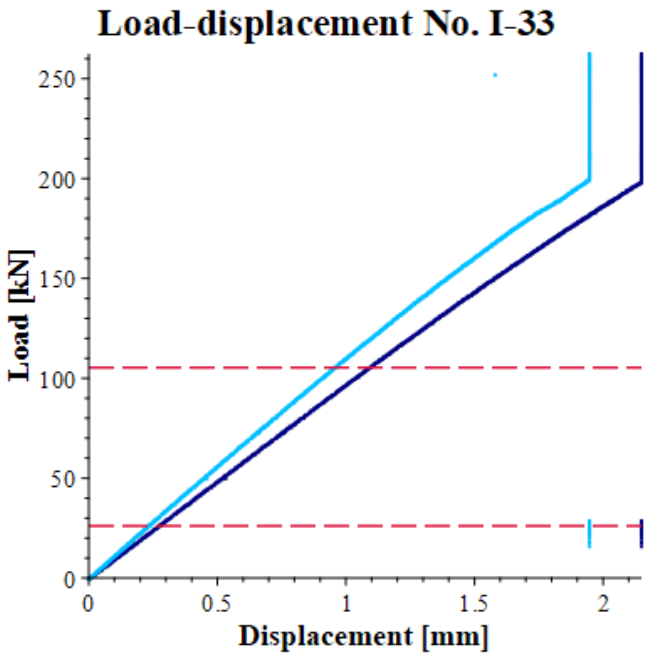

Figure 255: Load-displacement curves specimen I-33.

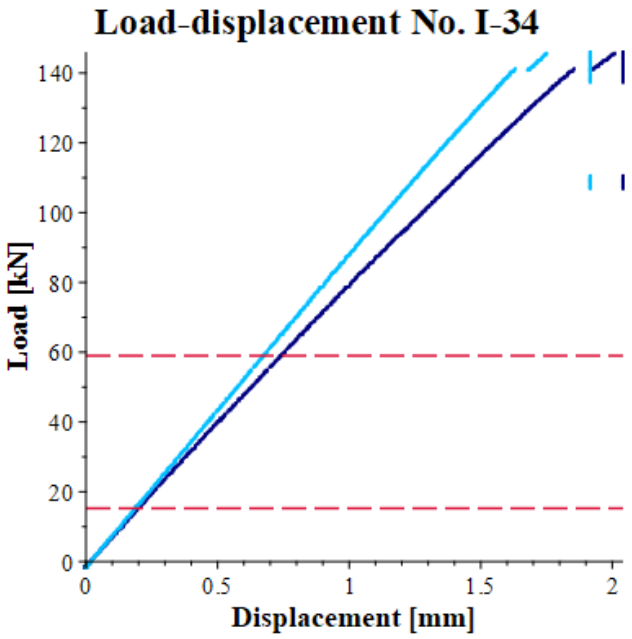

Figure 256: Load-displacement curves specimen I-34.

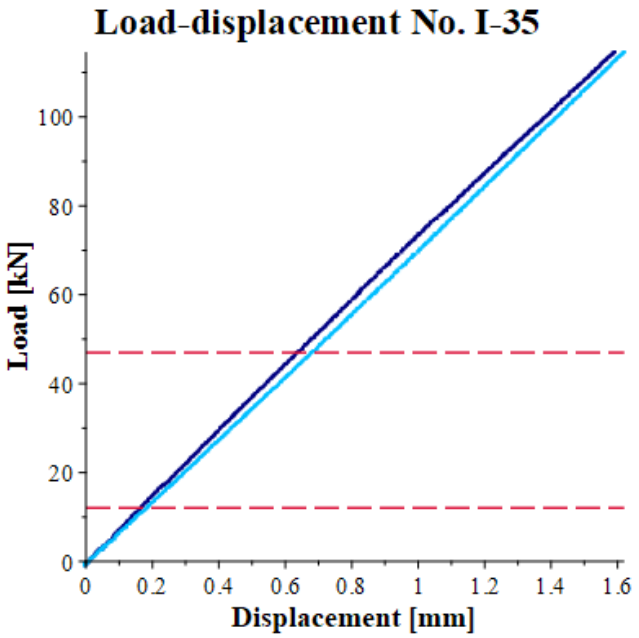

Figure 257: Load-displacement curves specimen I-35.

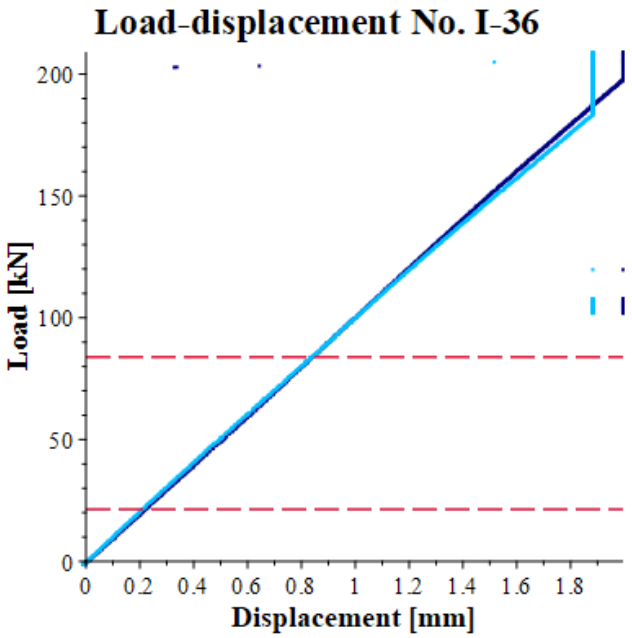

Figure 258: Load-displacement curves specimen I-36.

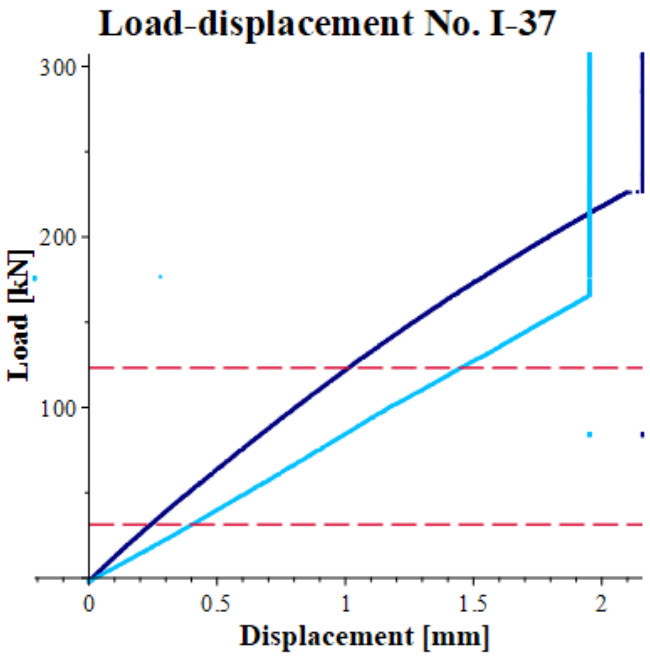

Figure 259: Load-displacement curves specimen I-37.

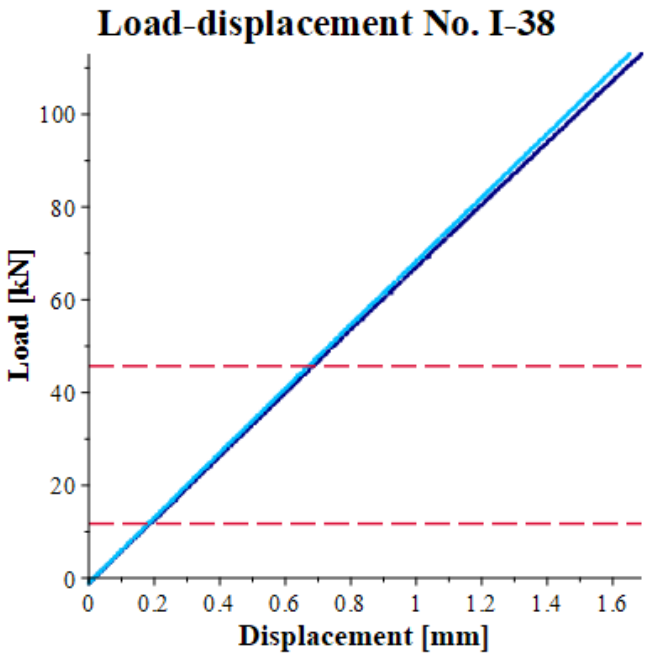

Figure 260: Load-displacement curves specimen I-38.

Appendix 11: Load-displacement curves batch II

This Appendix shows all the load-displacement curves of the batch II specimens: see Figure 261 till Figure 298. The results from LVDT 1 and 2 are depicted in dark and light blue, respectively. The red dashed lines depict the area between circa 10% and 40 % of the maximum load, over which the modulus of elasticity in tension is calculated. Note that data from LVDT 1 for specimens II-25 till II-38 is not included, as this LVDT broke after the test with specimen II-24.

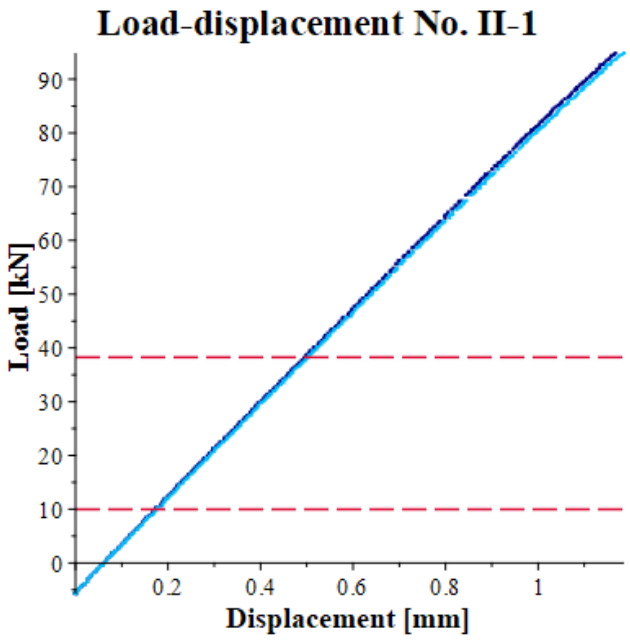

Figure 261: Load-displacement curves specimen II-1.

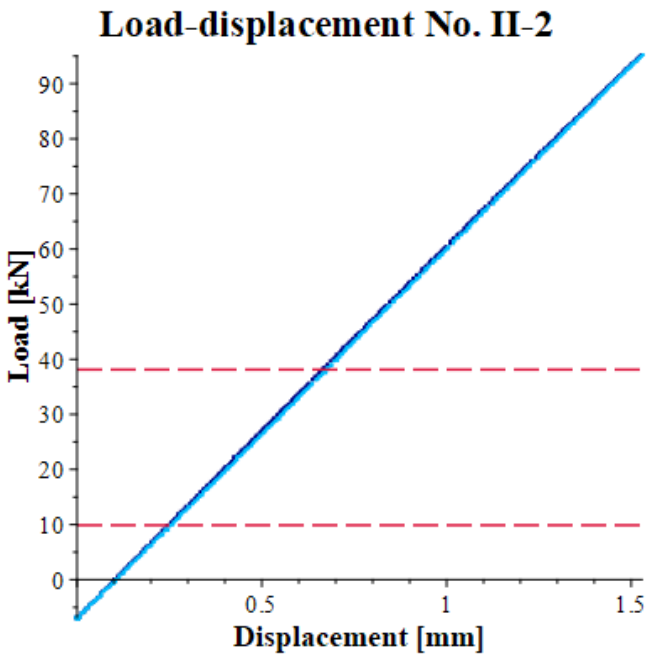

Figure 262: Load-displacement curves specimen II-2.

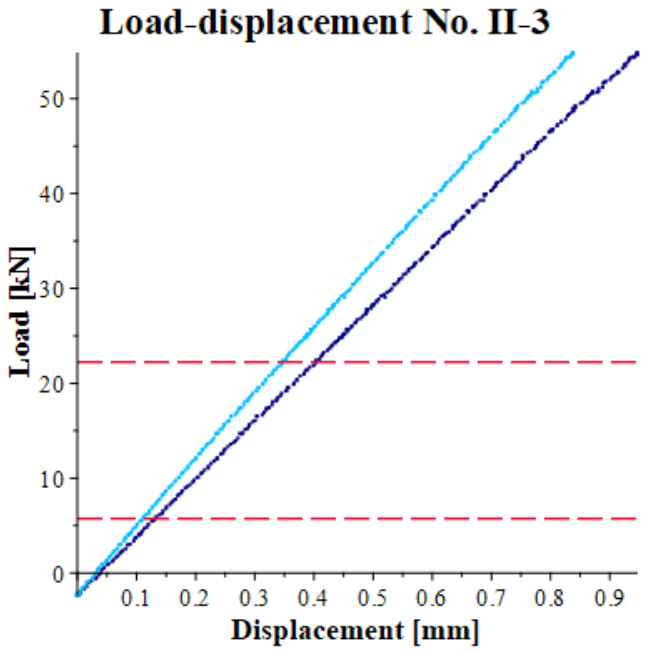

Figure 263: Load-displacement curves specimen II-3.

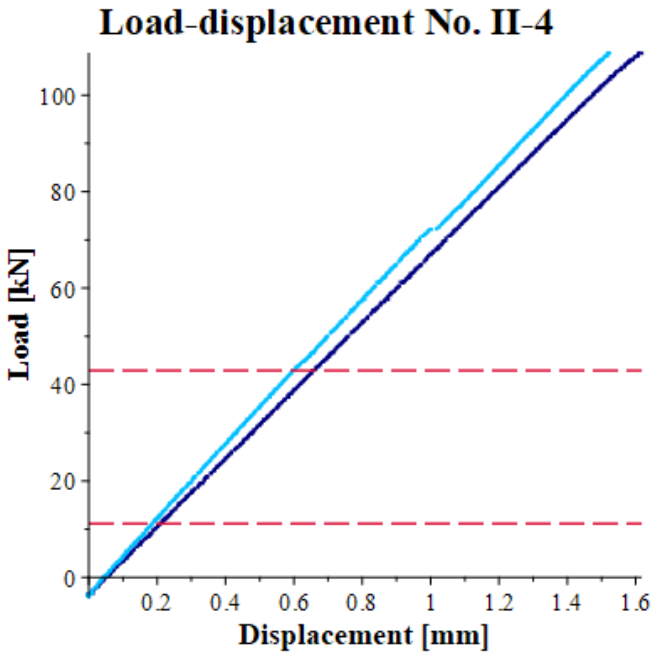

Figure 264: Load-displacement curves specimen II-4.

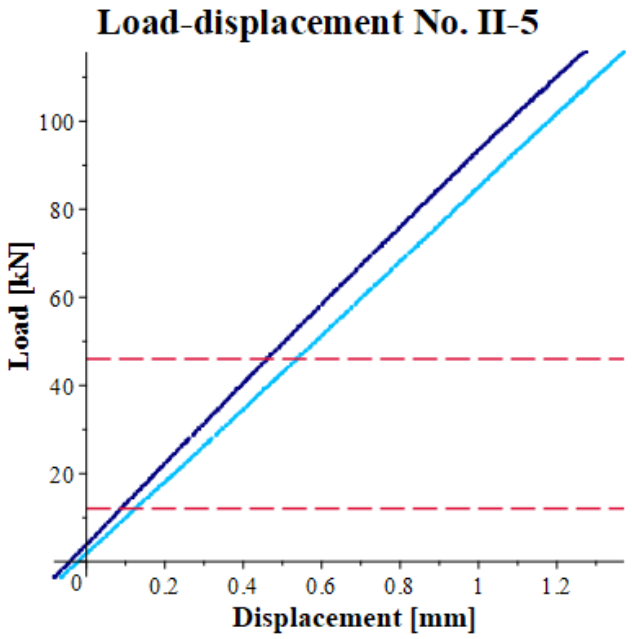

Figure 265: Load-displacement curves specimen II-5.

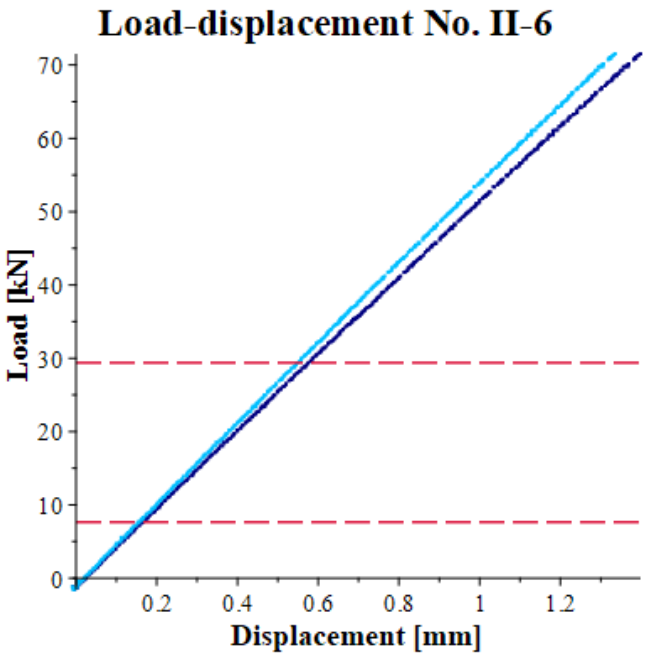

Figure 266: Load-displacement curves specimen II-6.

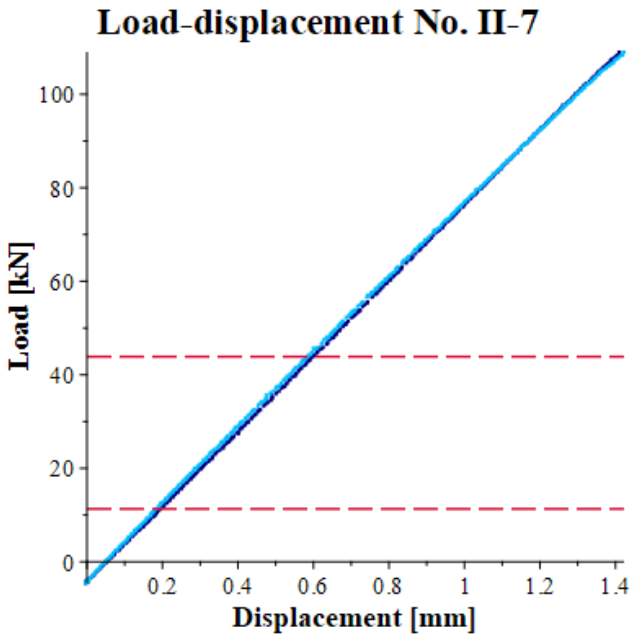

Figure 267: Load-displacement curves specimen II-7.

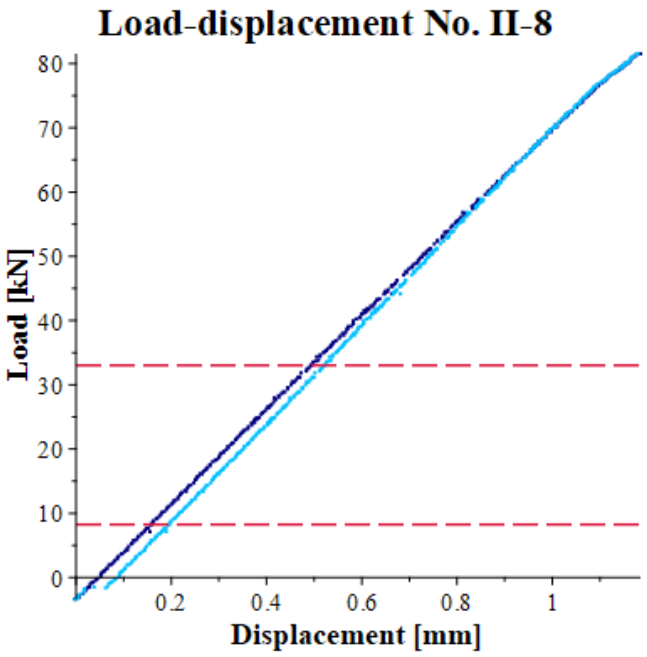

Figure 268: Load-displacement curves specimen II-8.

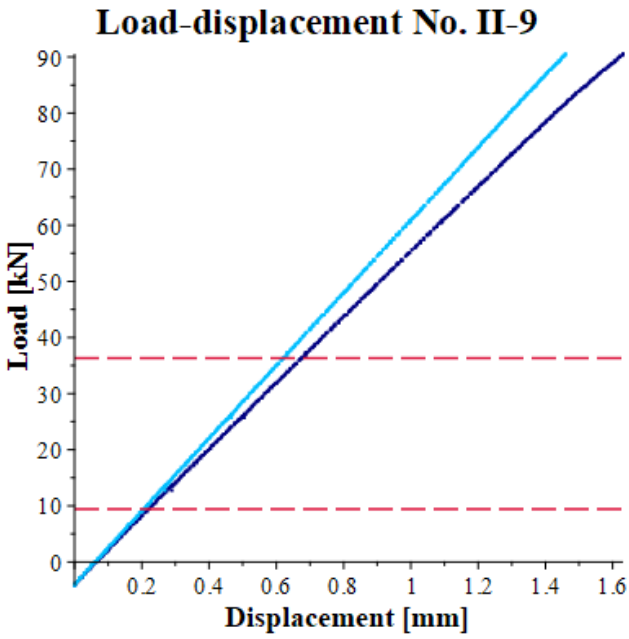

Figure 269: Load-displacement curves specimen II-9.

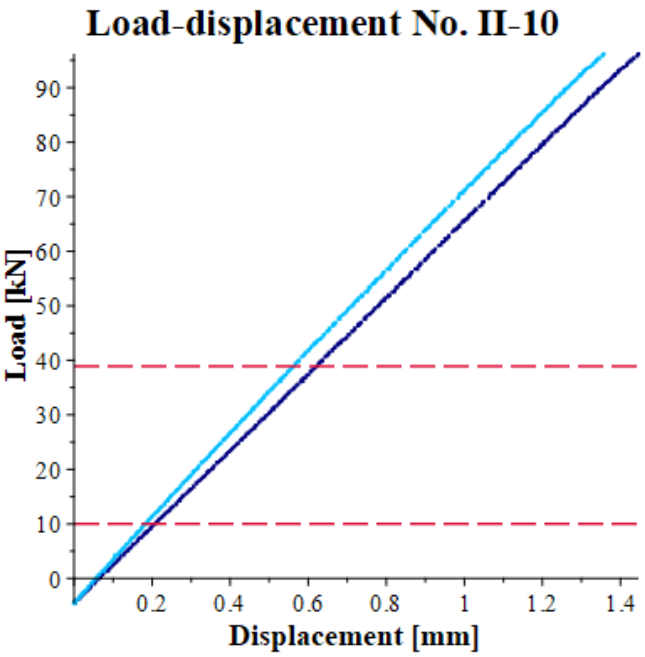

Figure 270: Load-displacement curves specimen II-10.

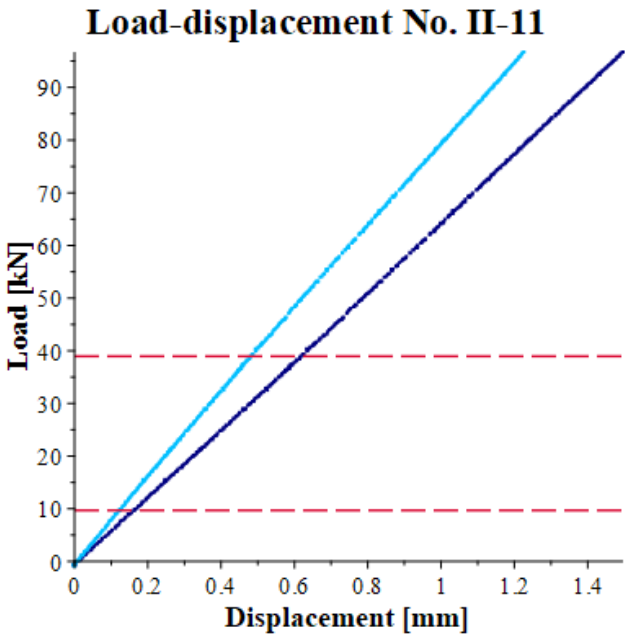

Figure 271: Load-displacement curves specimen II-11.

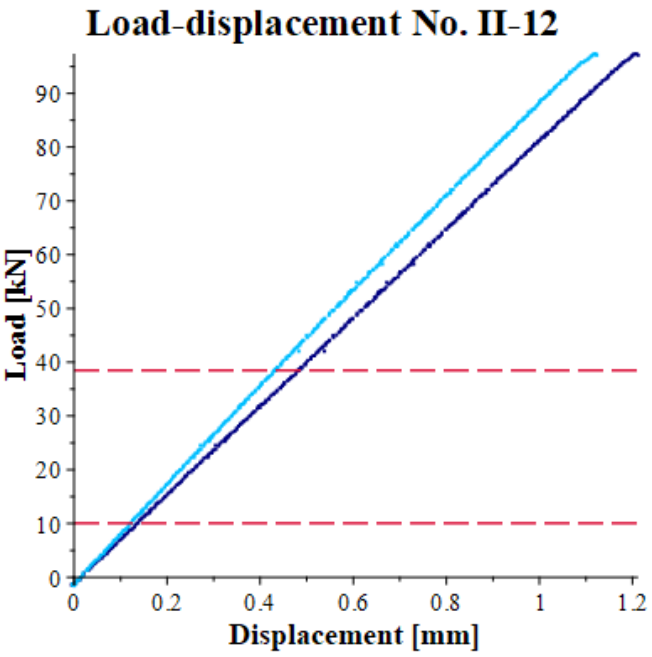

Figure 272: Load-displacement curves specimen II-12.

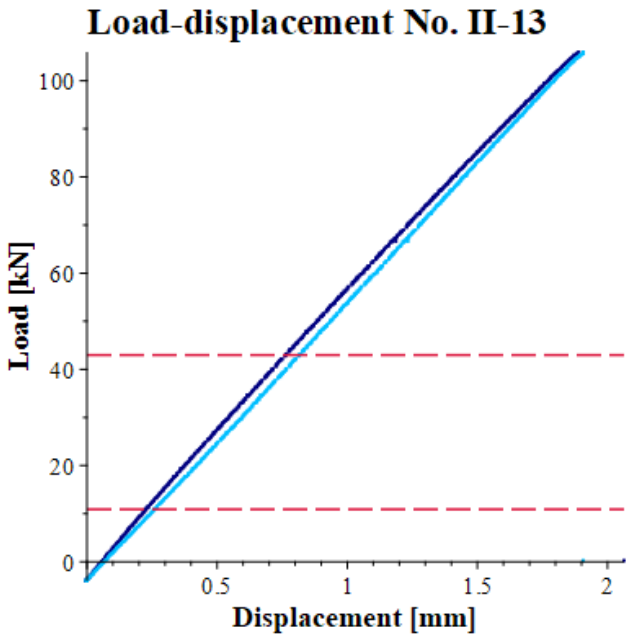

Figure 273: Load-displacement curves specimen II-13.

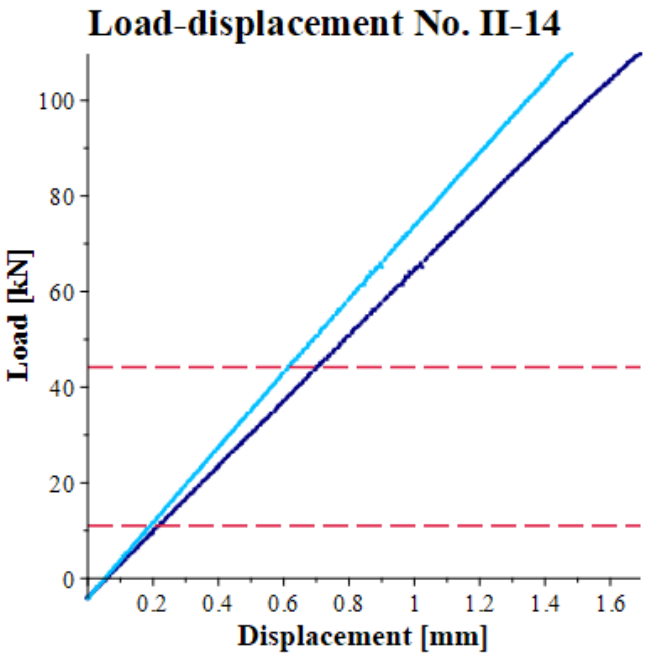

Figure 274: Load-displacement curves specimen II-14.

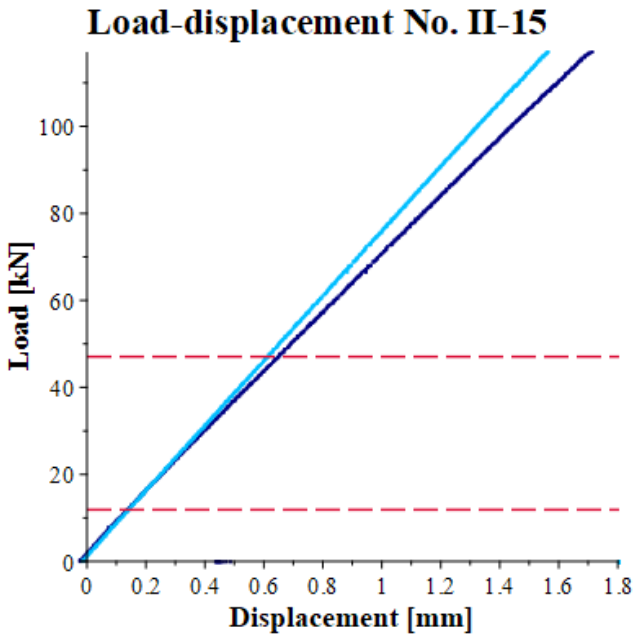

Figure 275: Load-displacement curves specimen II-15.

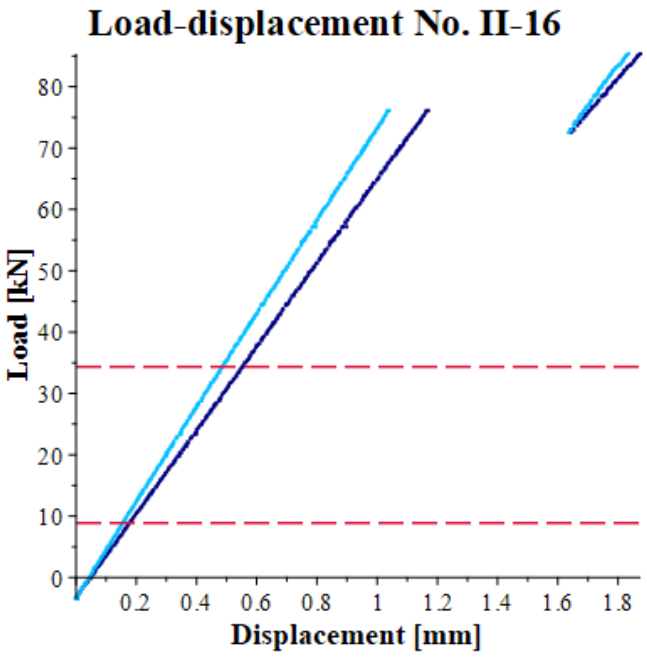

Figure 276: Load-displacement curves specimen II-16.

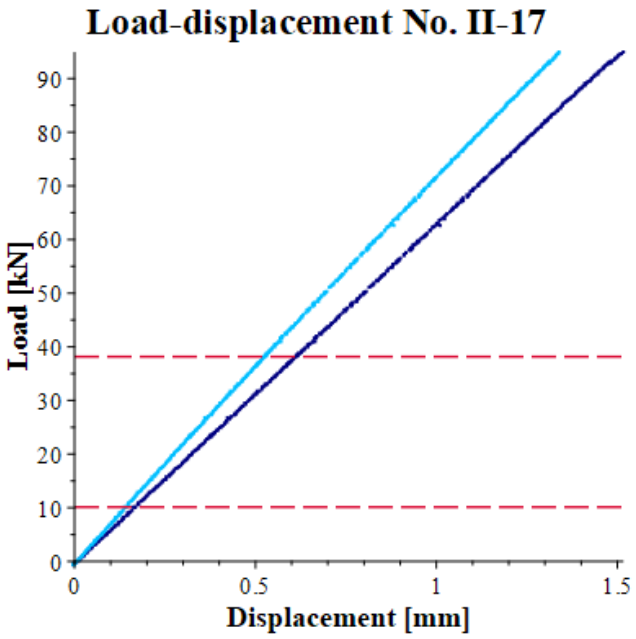

Figure 277: Load-displacement curves specimen II-17.

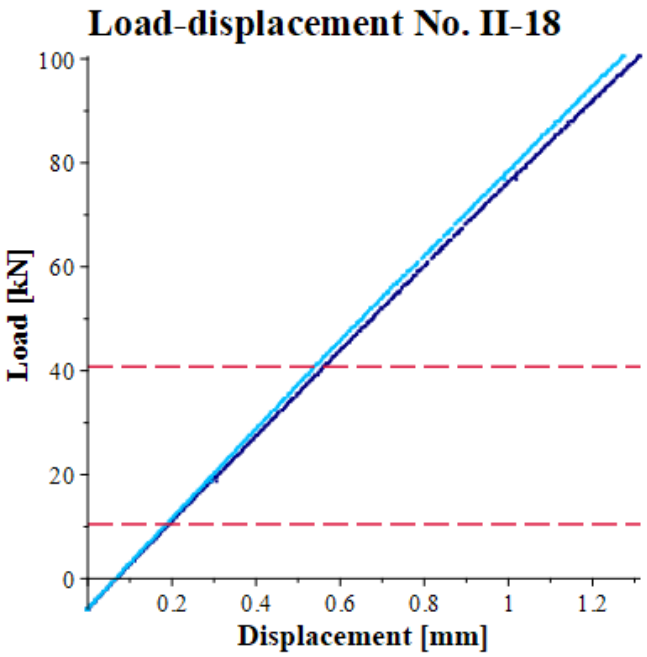

Figure 278: Load-displacement curves specimen II-18.

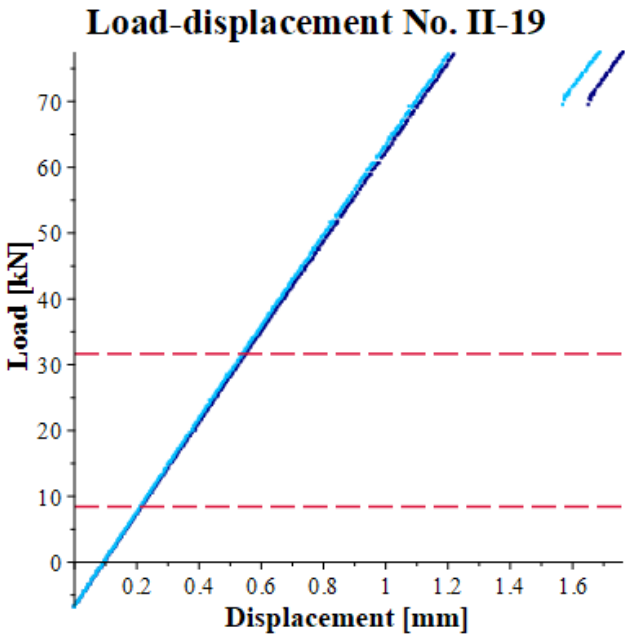

Figure 279: Load-displacement curves specimen II-19.

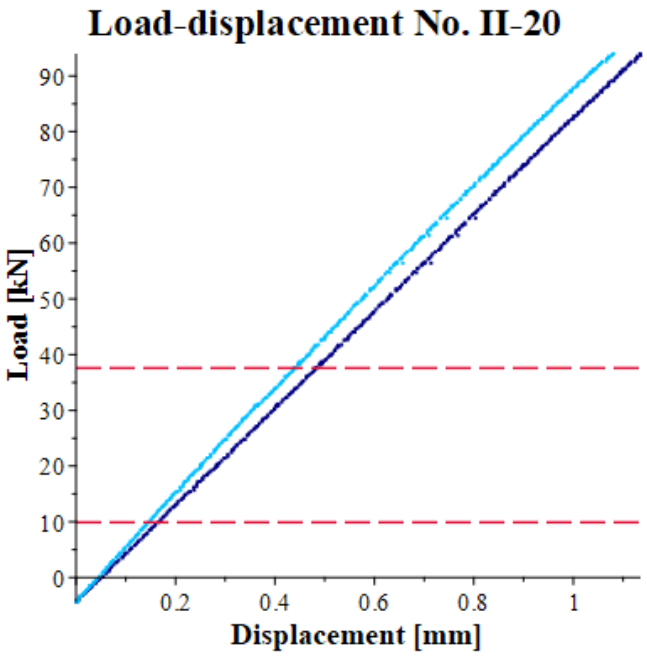

Figure 280: Load-displacement curves specimen II-20.

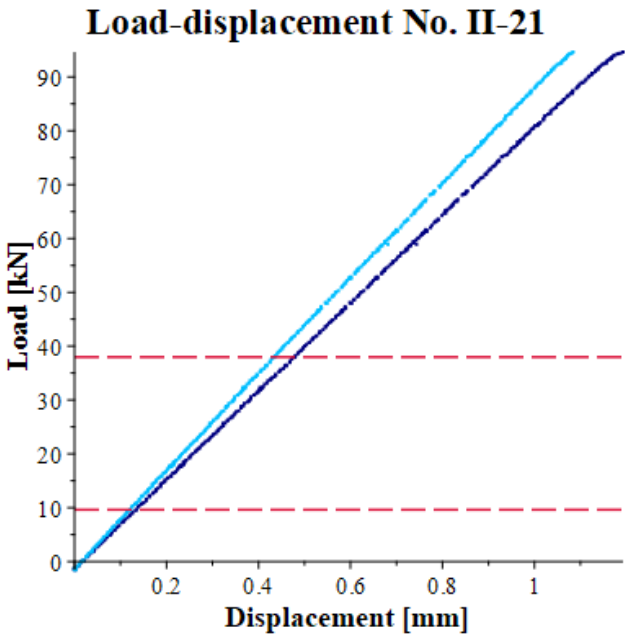

Figure 281: Load-displacement curves specimen II-21.

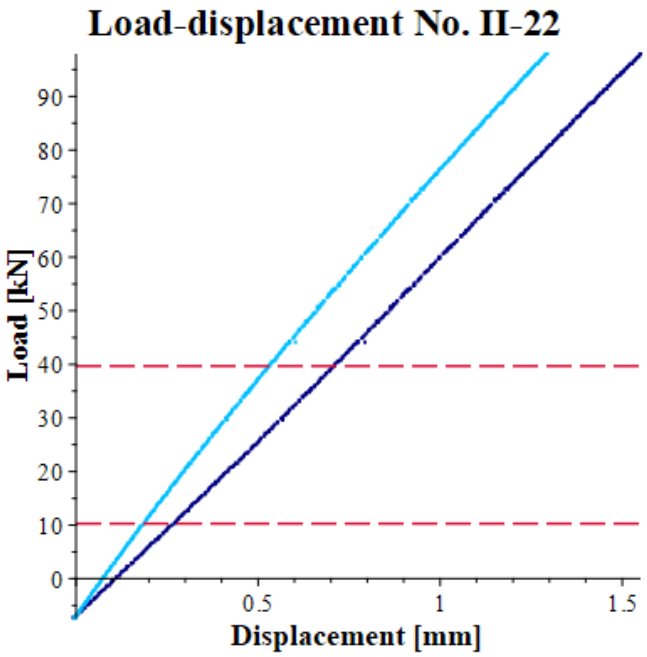

Figure 282: Load-displacement curves specimen II-22.

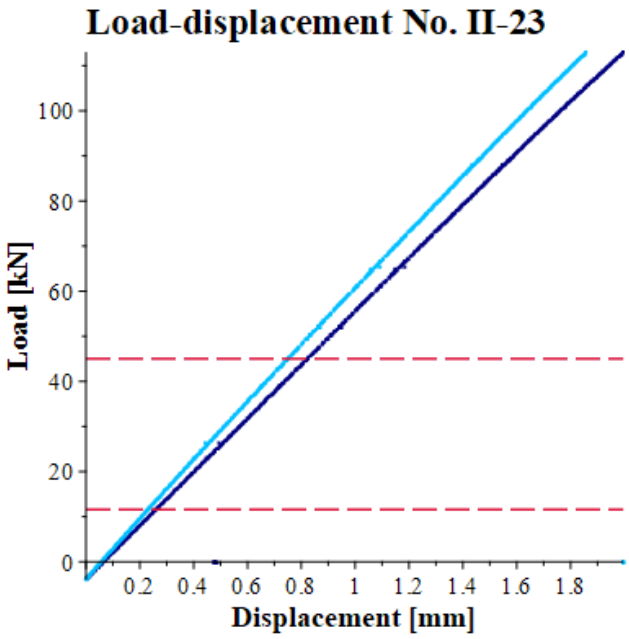

Figure 283: Load-displacement curves specimen II-23.

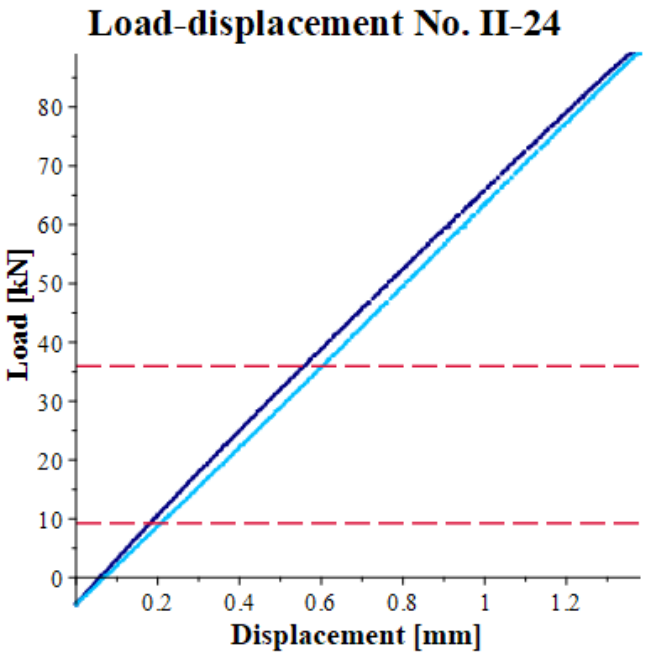

Figure 284: Load-displacement curves specimen II-24.

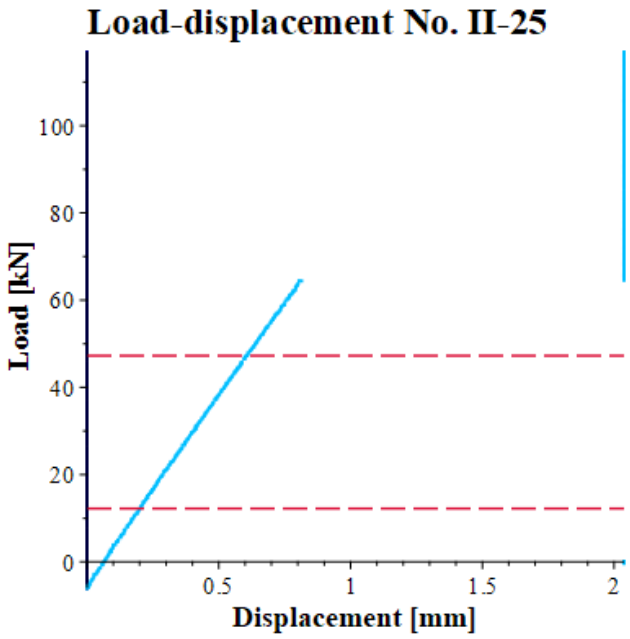

Figure 285: Load-displacement curve specimen II-25.

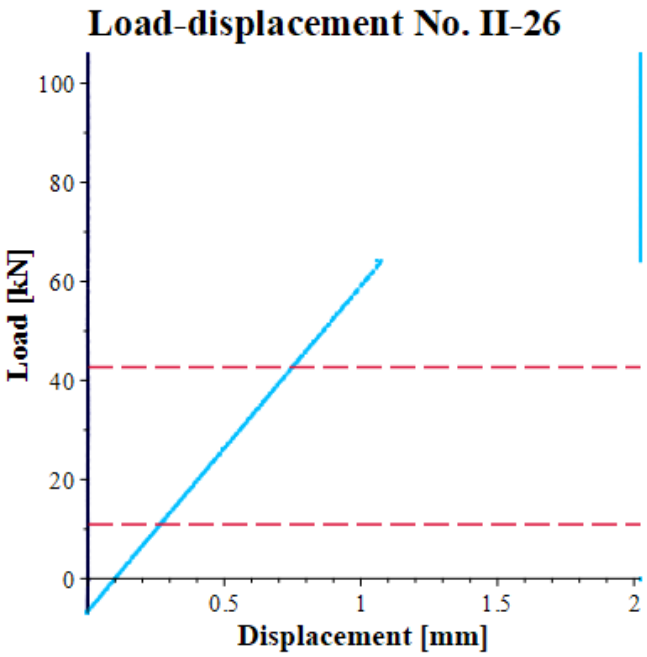

Figure 286: Load-displacement curve specimen II-26.

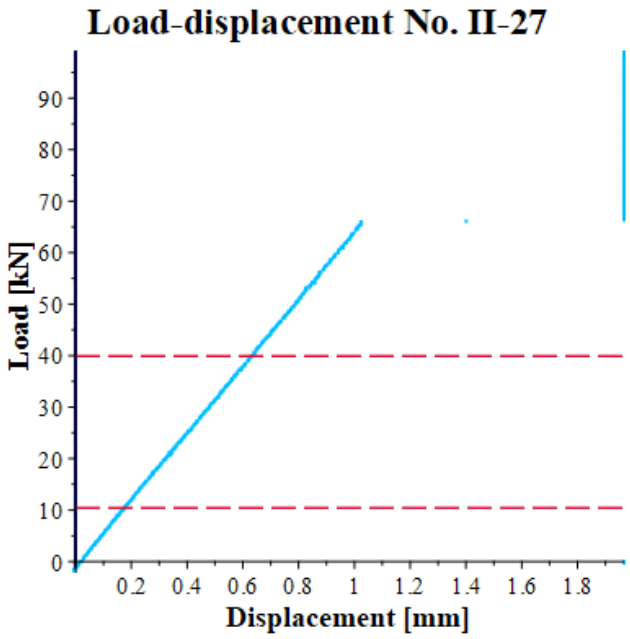

Figure 287: Load-displacement curve specimen II-27.

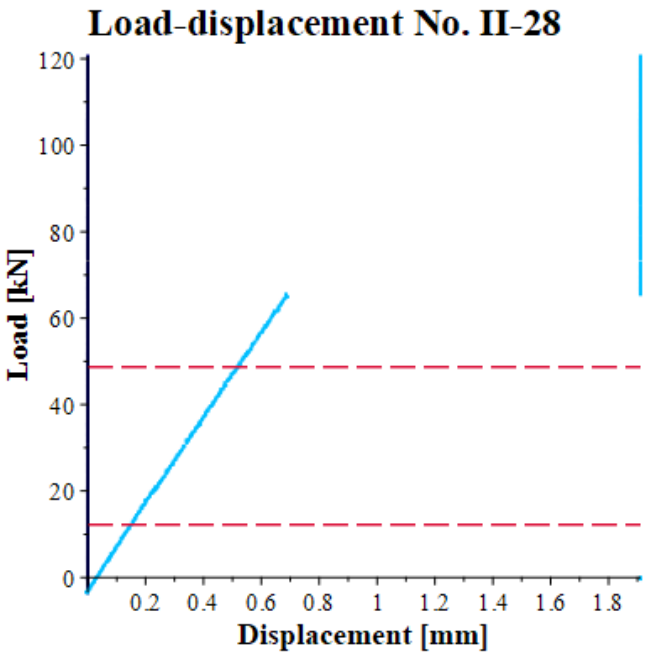

Figure 288: Load-displacement curve specimen II-28.

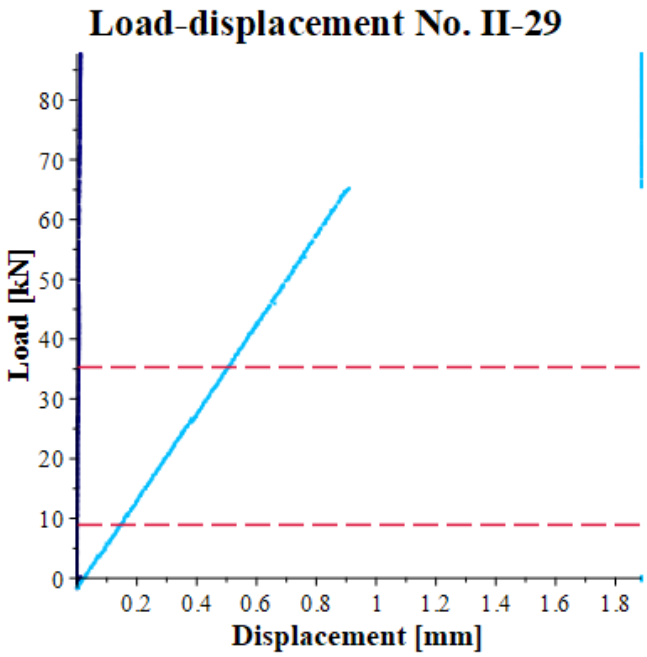

Figure 289: Load-displacement curve specimen II-29.

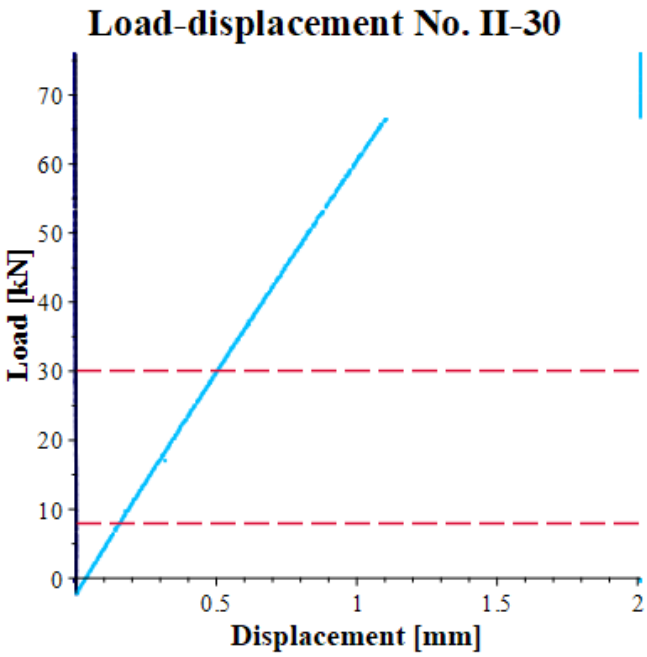

Figure 290: Load-displacement curve specimen II-30.

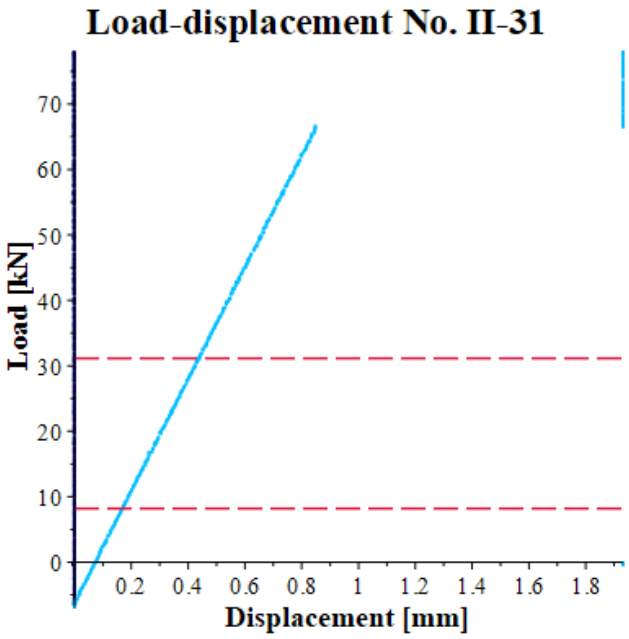

Figure 291: Load-displacement curve specimen II-31.

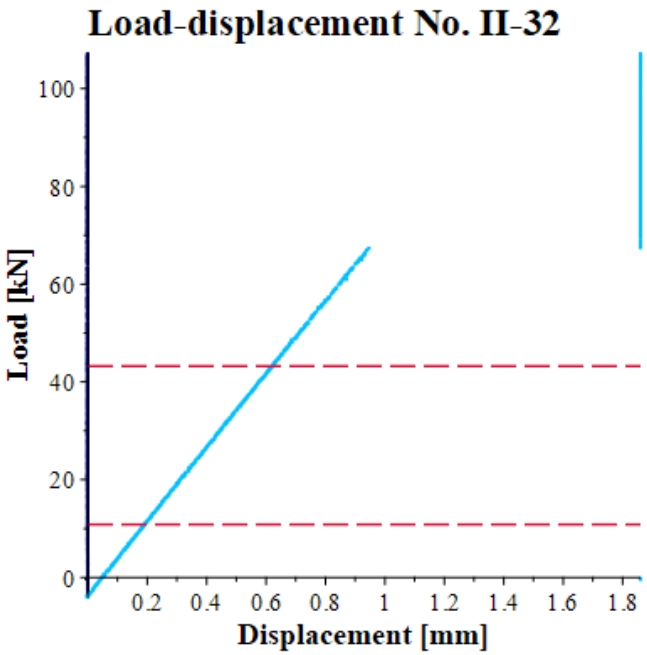

Figure 292: Load-displacement curve specimen II-32.

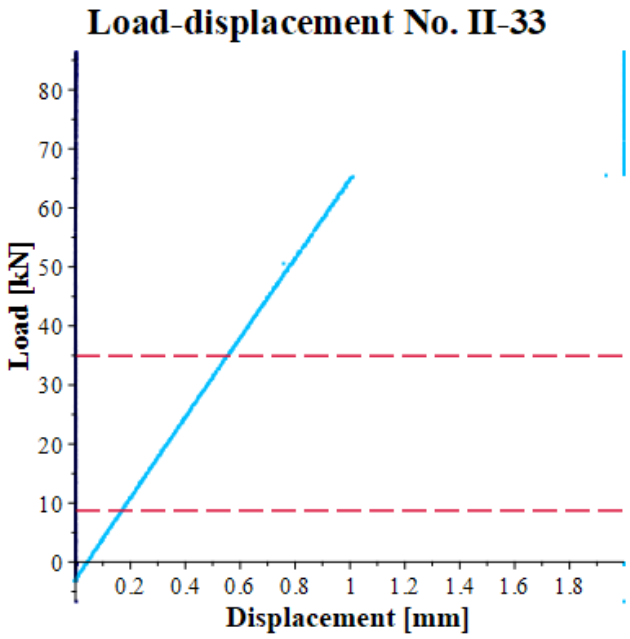

Figure 293: Load-displacement curve specimen II-33.

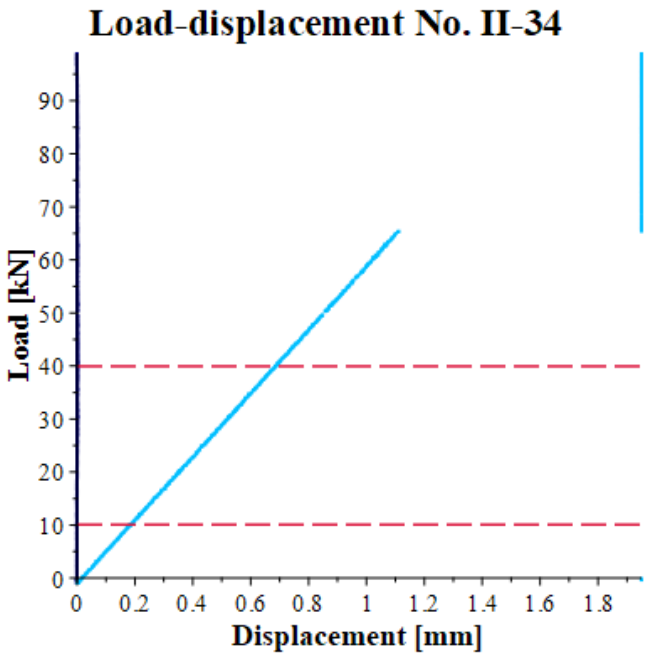

Figure 294: Load-displacement curve specimen II-34.

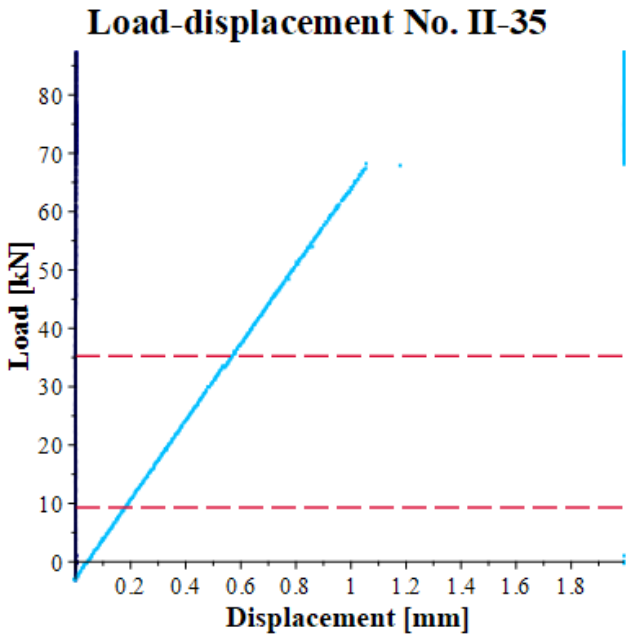

Figure 295: Load-displacement curve specimen II-35.

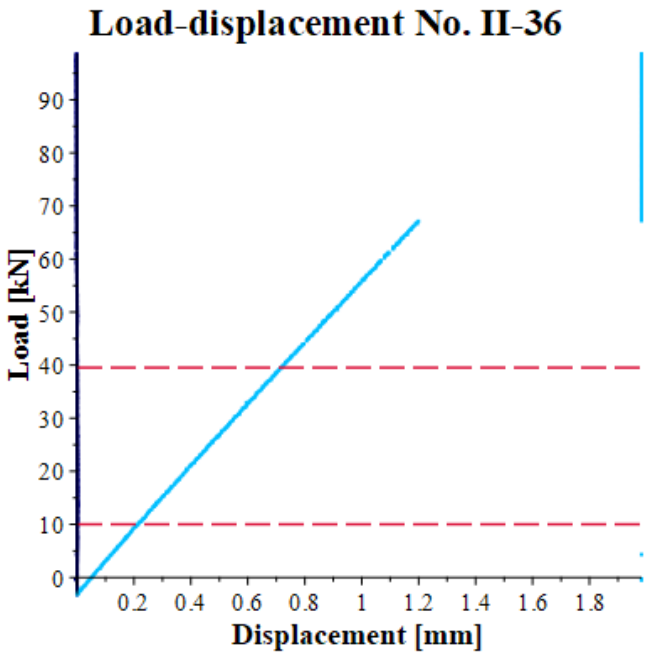

Figure 296: Load-displacement curve specimen II-36.

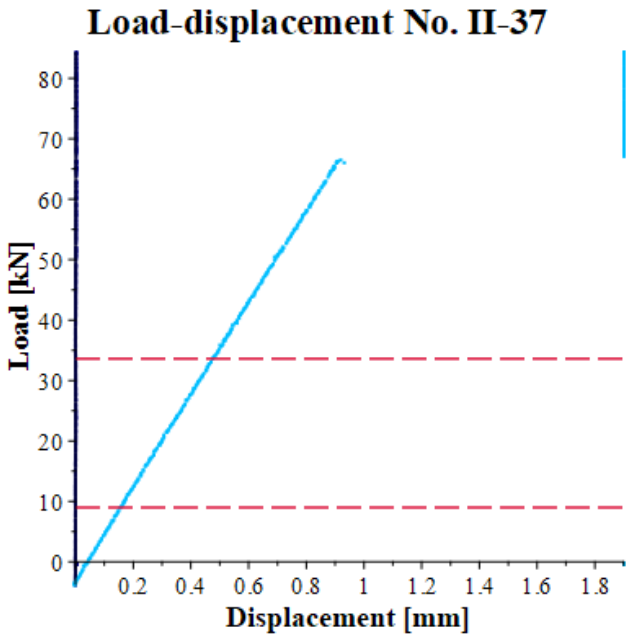

Figure 297: Load-displacement curve specimen II-37.

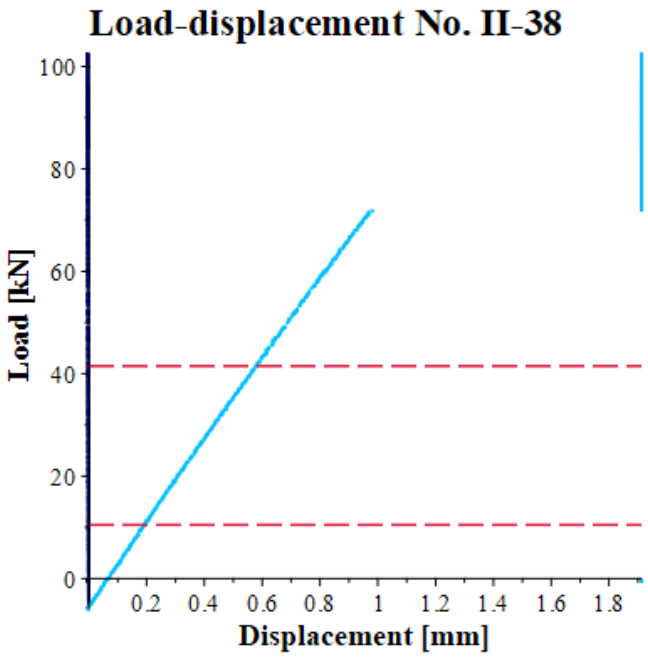

Figure 298: Load-displacement curve specimen II-38.

Appendix 12: Load-displacement curves batch IV

This Appendix shows all the load-displacement curves of the batch IV specimens: see Figure 299 till Figure 310. The results from LVDT 1 and 2 are depicted in dark and light blue, respectively. The results from LASER 1 and 2 are depicted in red and dark yellow, respectively. The purple dashed lines depict the area between circa 10% and 40 % of the maximum load, over which the local and global modulus of elasticity is calculated.

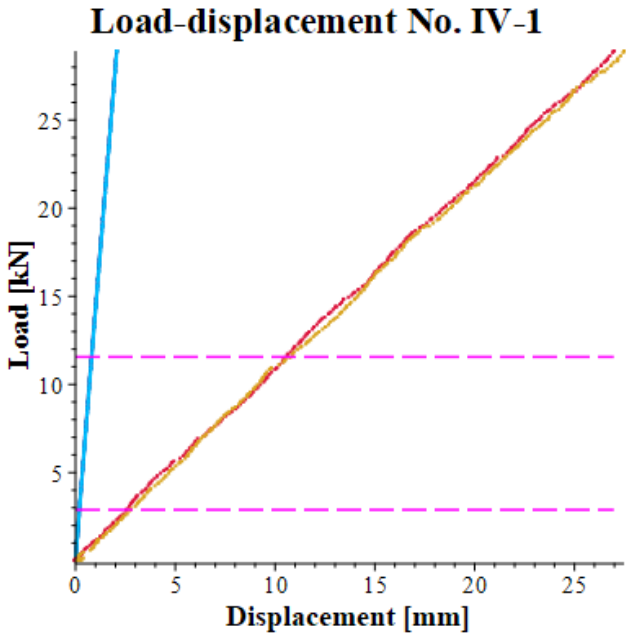

Figure 299: Load-displacement curves specimen IV-1.

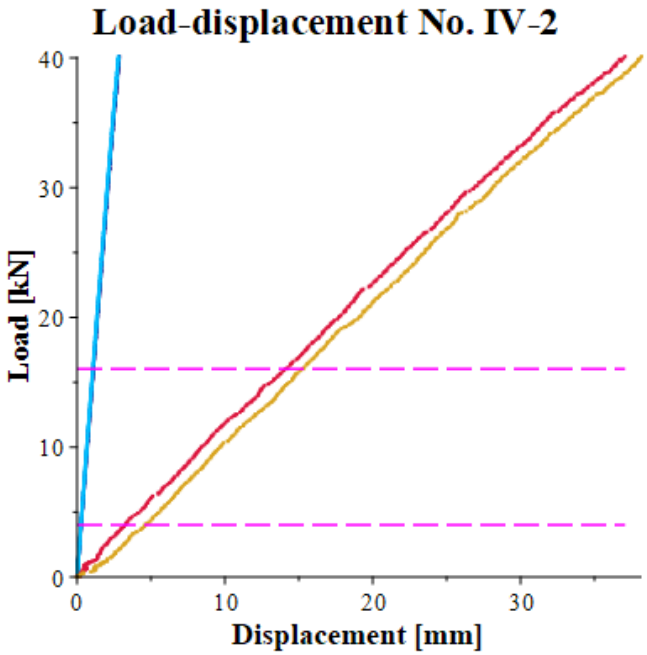

Figure 300: Load-displacement curves specimen IV-2.

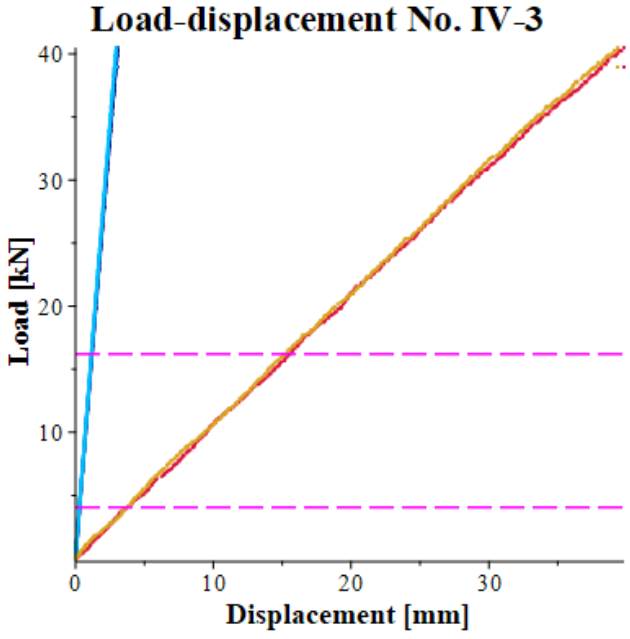

Figure 301: Load-displacement curves specimen IV-3.

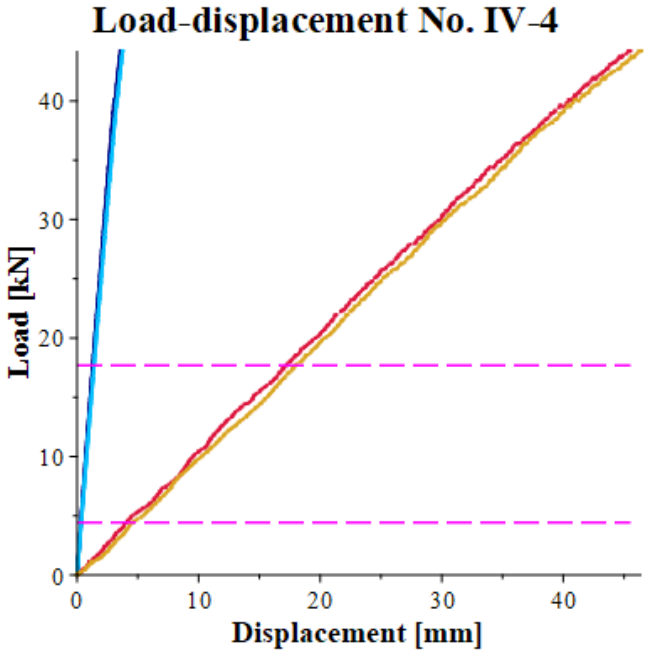

Figure 302: Load-displacement curves specimen IV-4.

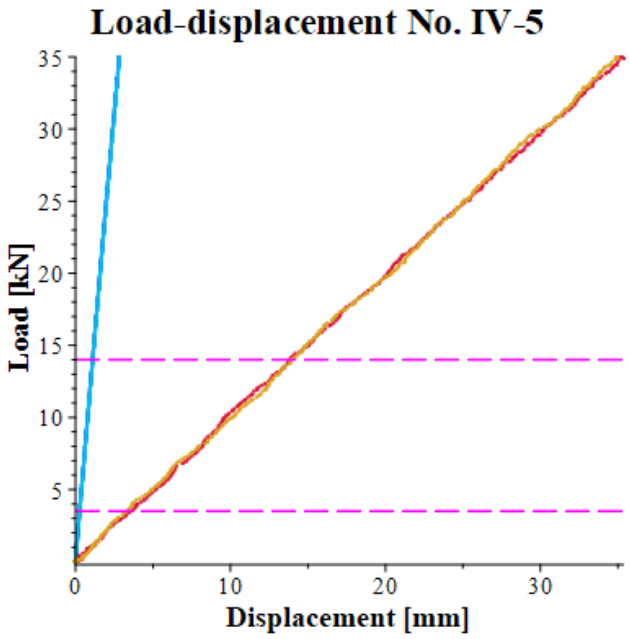

Figure 303: Load-displacement curves specimen IV-5.

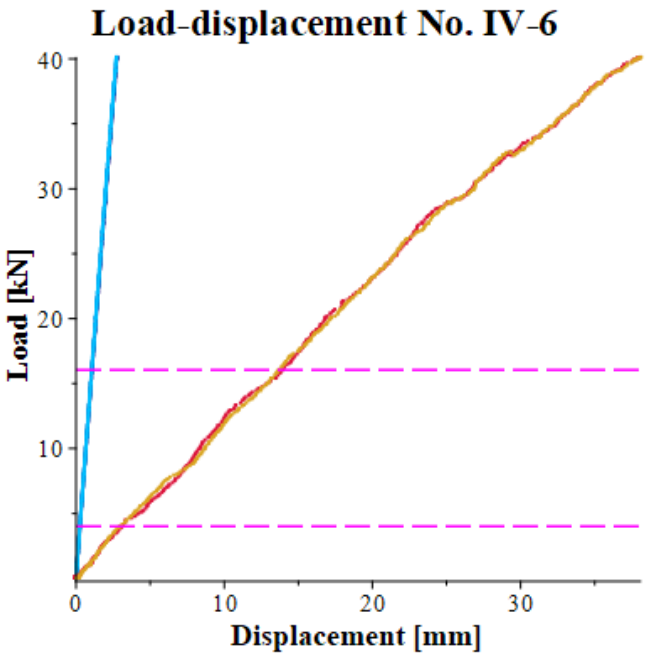

Figure 304: Load-displacement curves specimen IV-6.

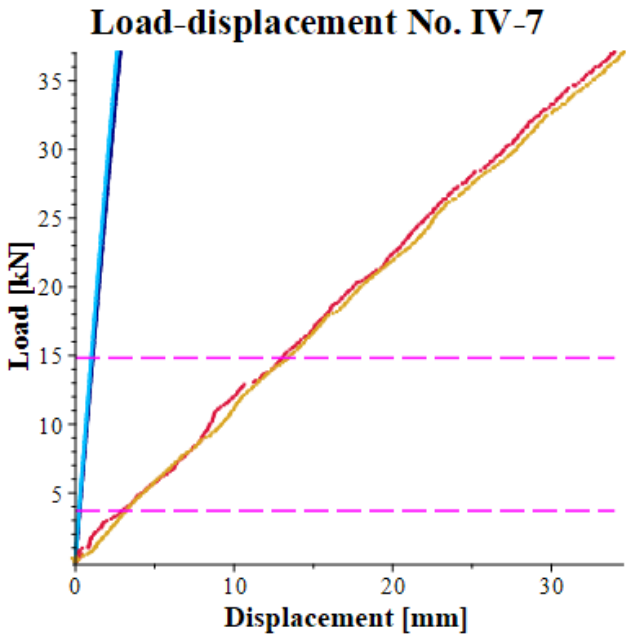

Figure 305: Load-displacement curves specimen IV-7.

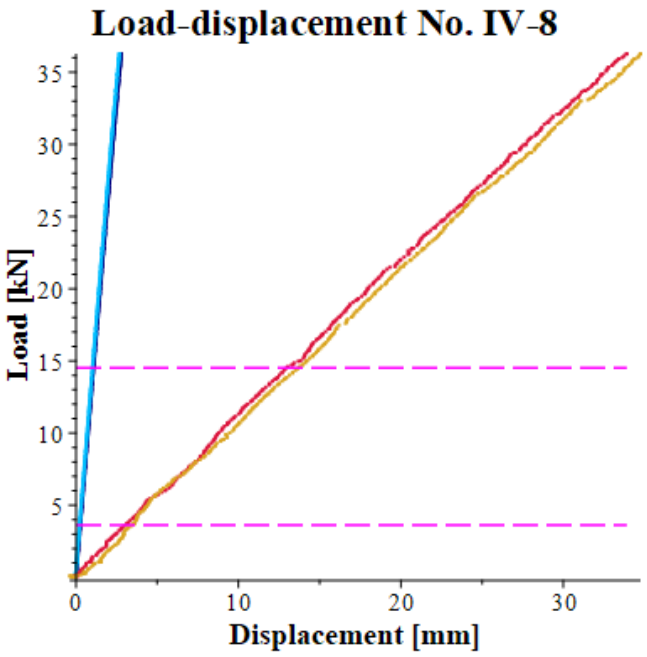

Figure 306: Load-displacement curves specimen IV-8.

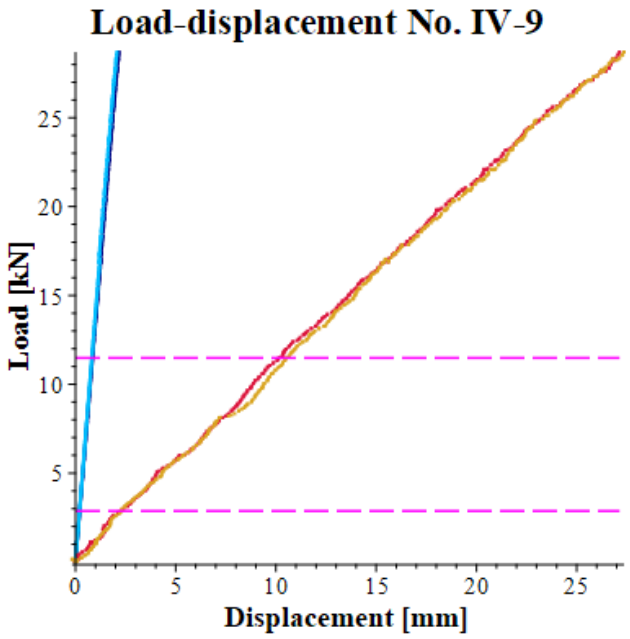

Figure 307: Load-displacement curves specimen IV-9.

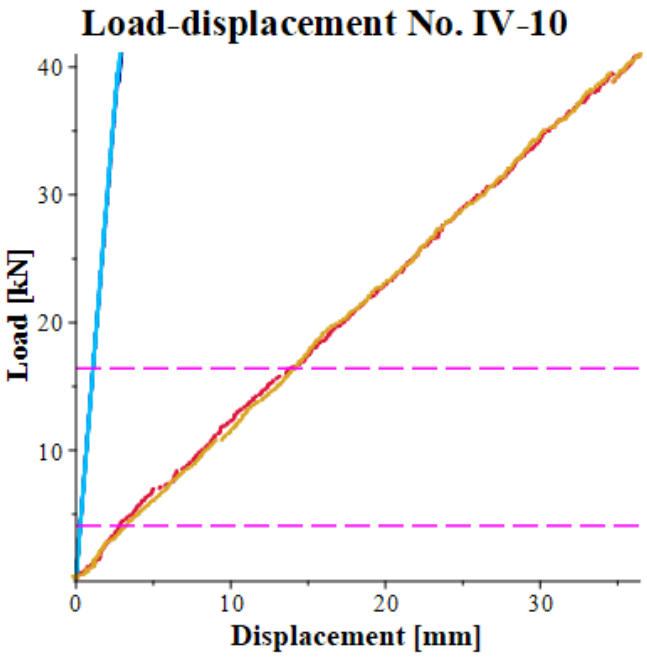

Figure 308: Load-displacement curves specimen IV-10.

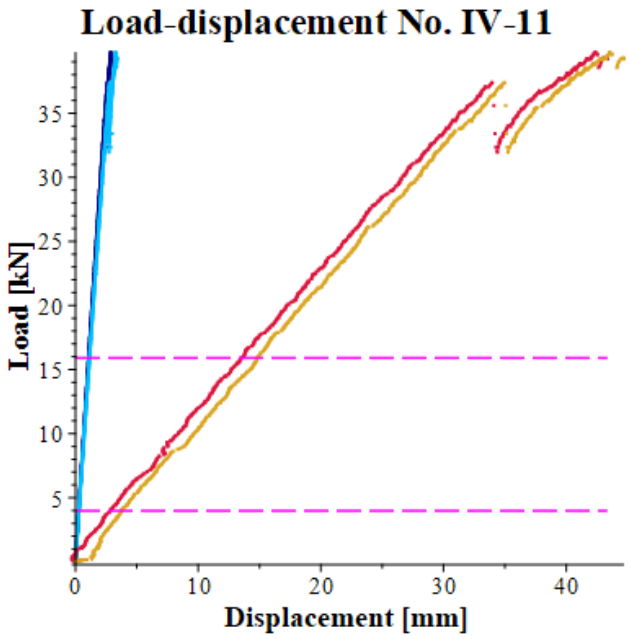

Figure 309: Load-displacement curves specimen IV-11.

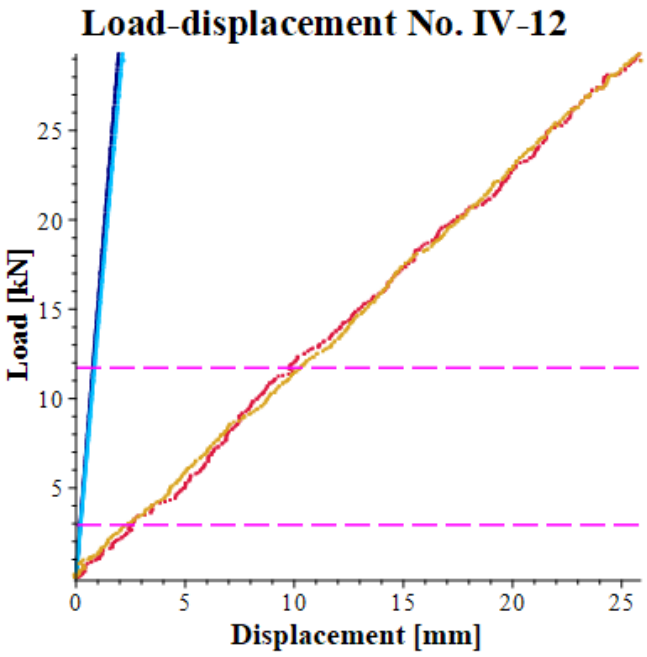

Figure 310: Load-displacement curves specimen IV-12.

Appendix 13: Batch I scatterplots of relationships between mechanical and physical properties

This Appendix shows scatterplots of relationships between mechanical and physical properties, regarding the specimens of batch I: see Figure 311 to Figure 316.

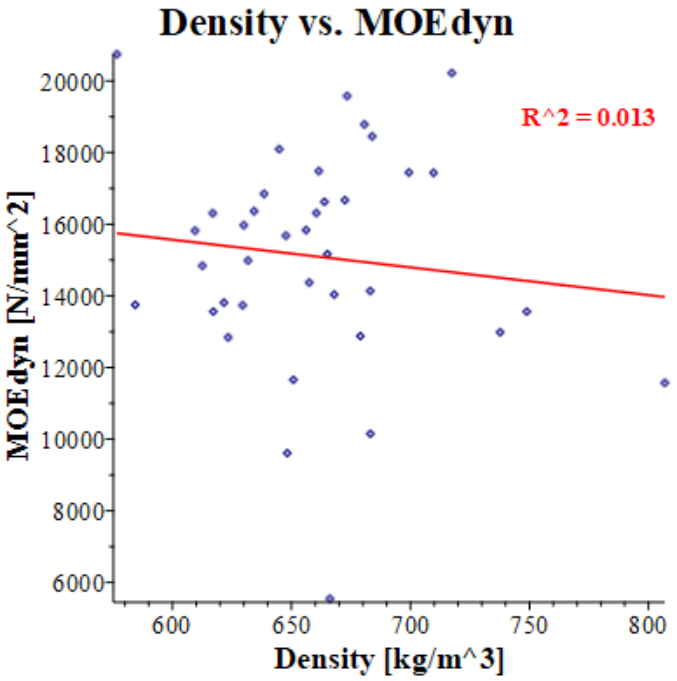

Figure 311: Scatterplot density vs. dynamic modulus of elasticity batch I.

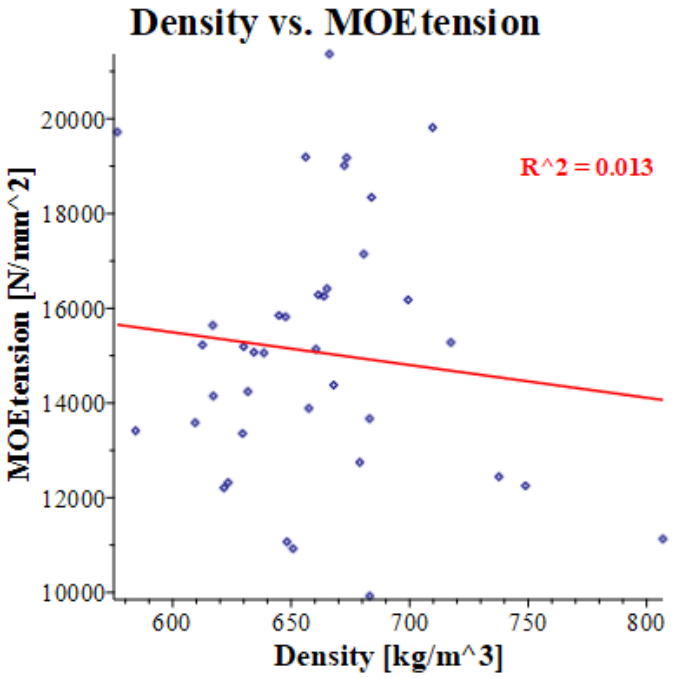

Figure 312: Scatterplot density vs. modulus of elasticity in tension batch I.

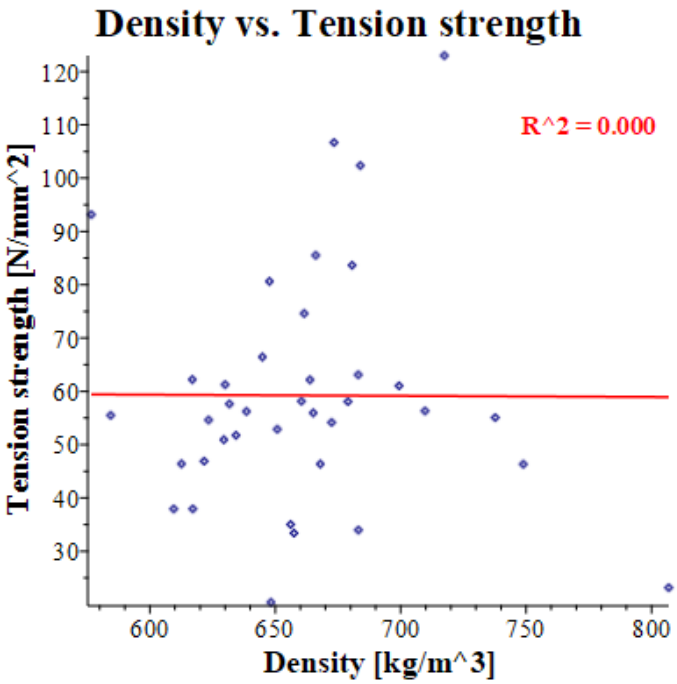

Figure 313: Scatterplot density vs. tension strength batch I.

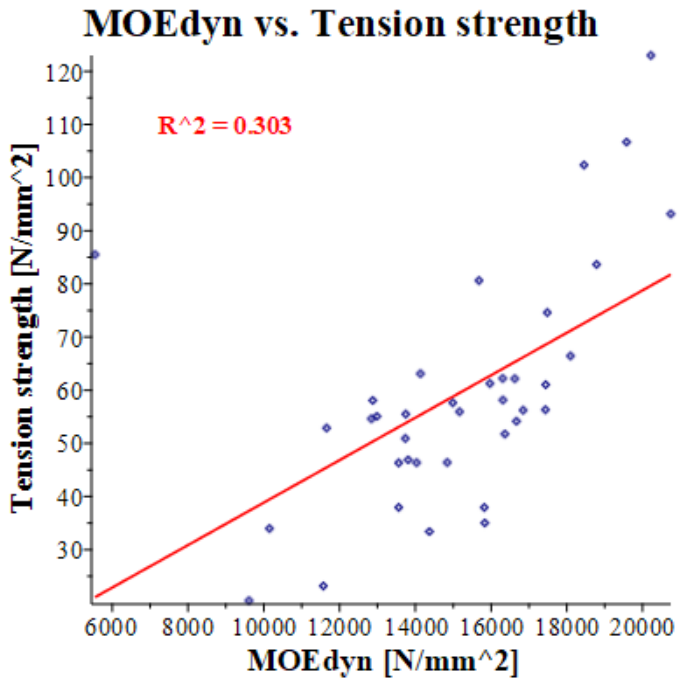

Figure 314: Scatterplot dynamic modulus of elasticity vs. tension strength batch I.

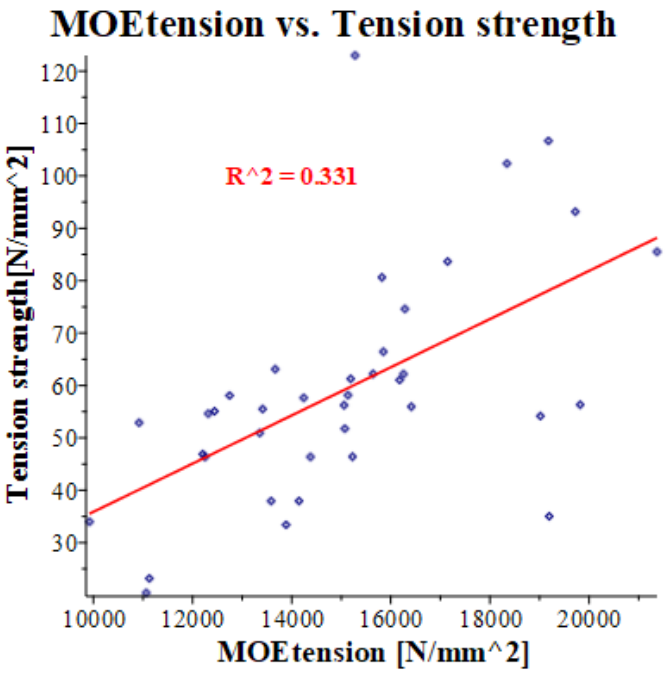

Figure 315: Scatterplot modulus of elasticity in tension vs. tension strength batch I.

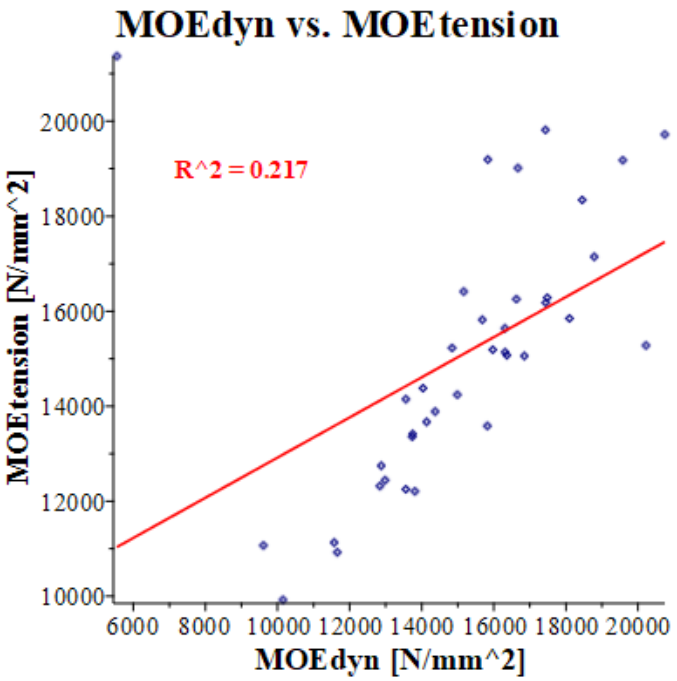

Figure 316: Scatterplot dynamic modulus of elasticity vs. modulus of elasticity in tension batch I.

Appendix 14: Batch II scatterplots of relationships between mechanical and physical properties

This Appendix shows scatterplots of relationships between mechanical and physical properties, regarding the specimens of batch II: see Figure 317 till Figure 328.

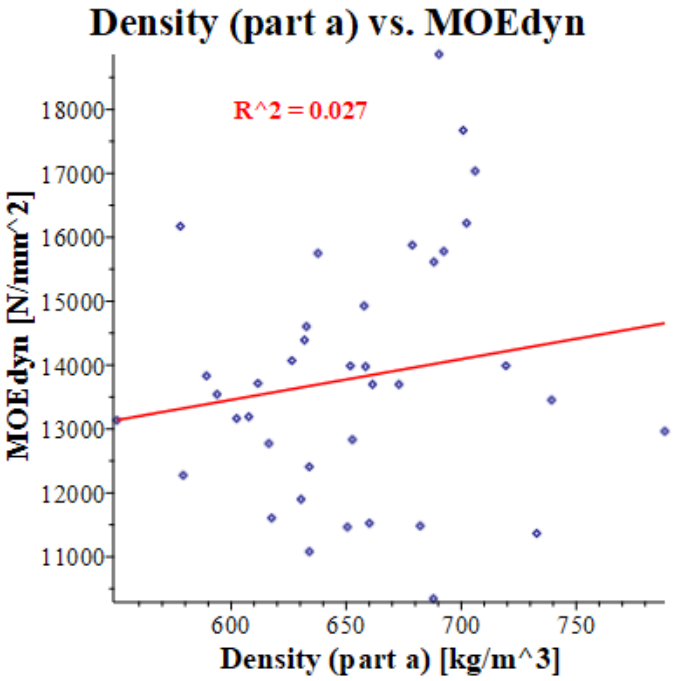

Figure 317: Scatterplot density (part a) vs. dynamic modulus of elasticity batch II.

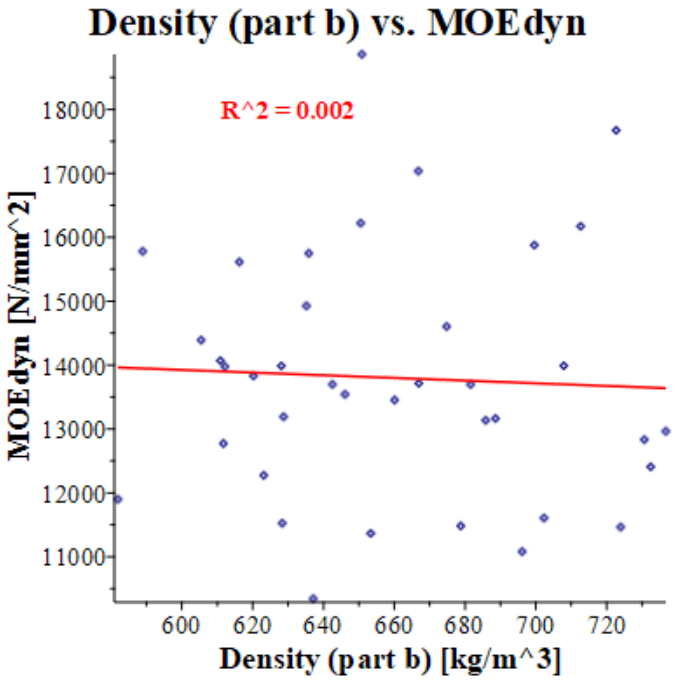

Figure 318: Scatterplot density (part b) vs. dynamic modulus of elasticity batch II.

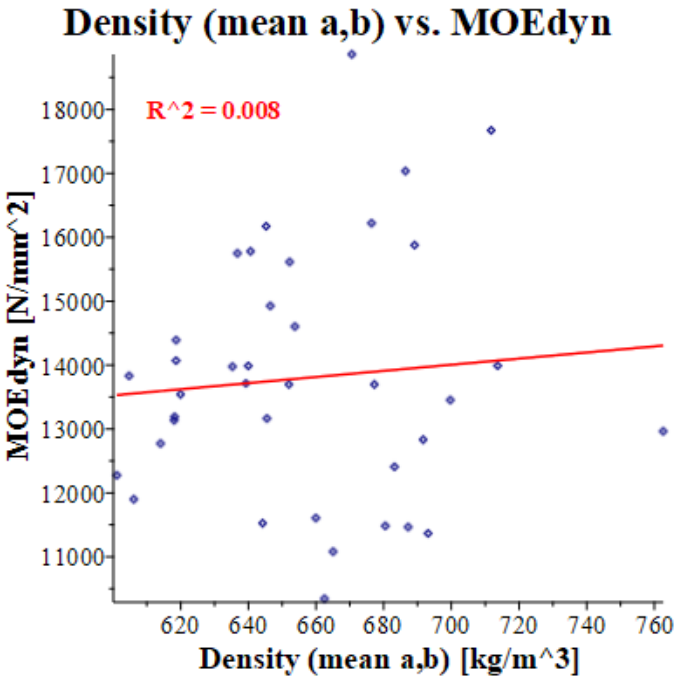

Figure 319: Scatterplot density (mean a,b) vs. dynamic modulus of elasticity batch II.

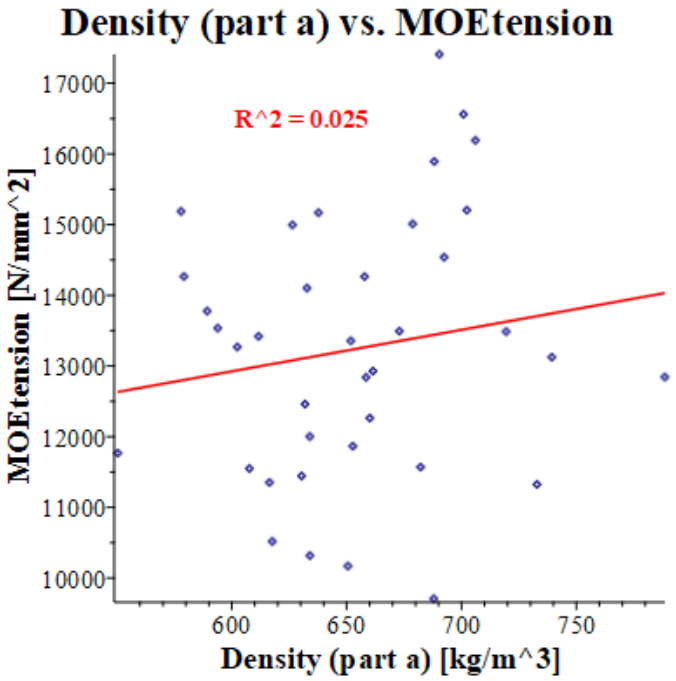

Figure 320: Scatterplot density (part a) vs. modulus of elasticity in tension batch II.

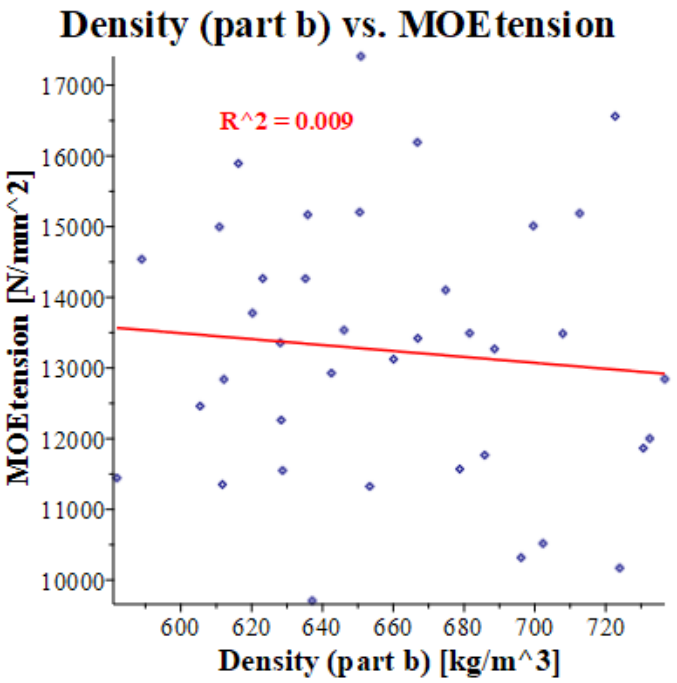

Figure 321: Scatterplot density (part b) vs. modulus of elasticity in tension batch II.

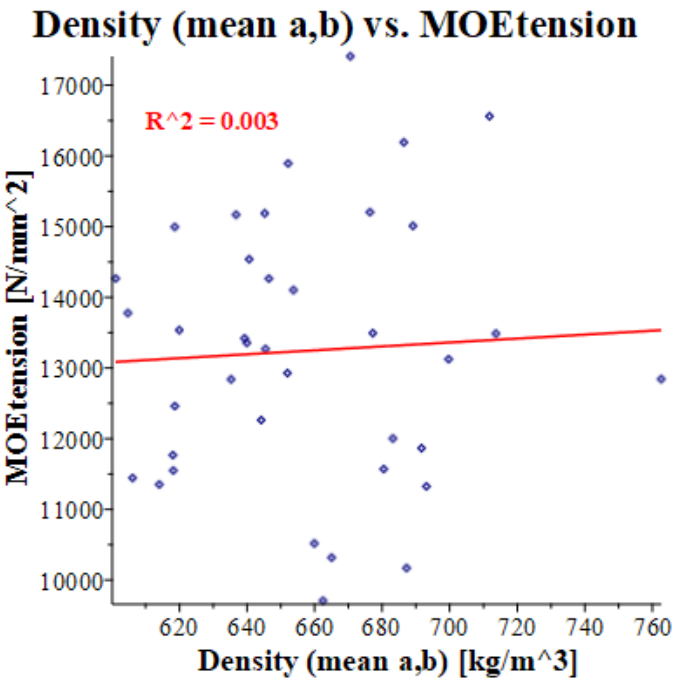

Figure 322: Scatterplot density (mean a,b) vs. modulus of elasticity in tension batch II.

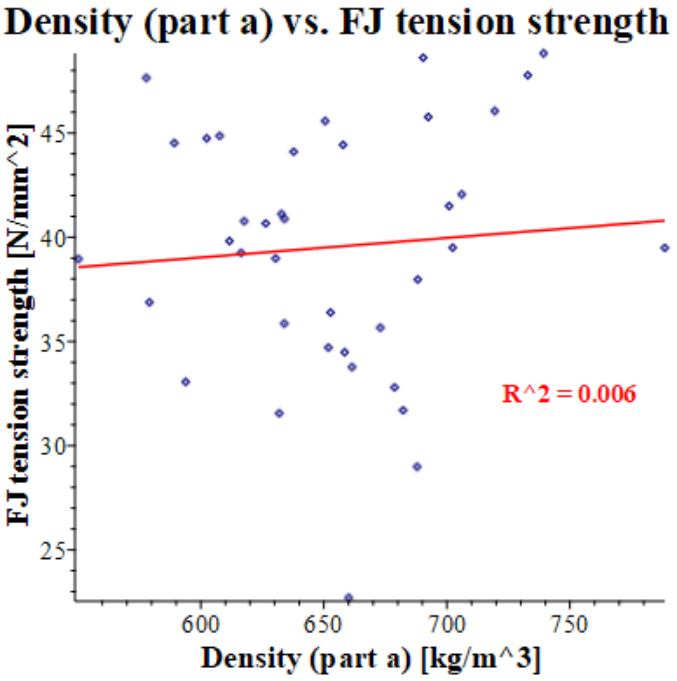

Figure 323: Scatterplot density (part a) vs. finger joint tension strength batch II.

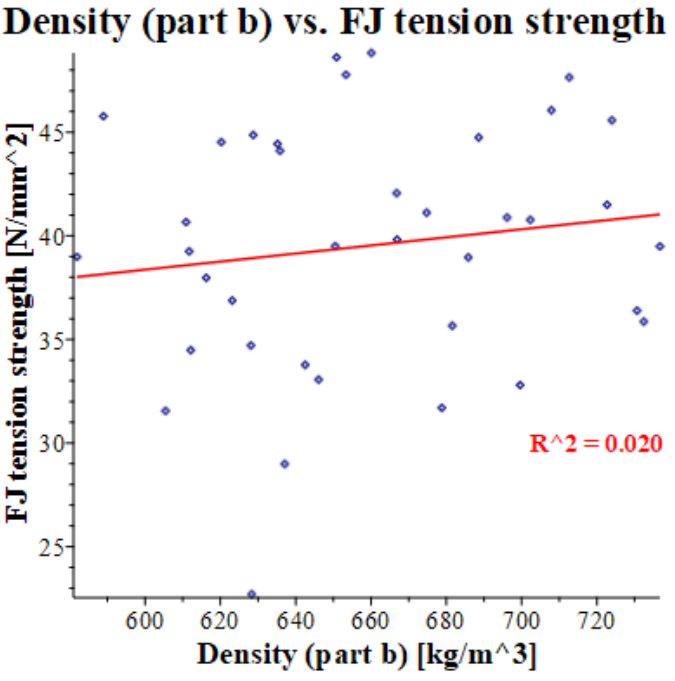

Figure 324: Scatterplot density (part b) vs. finger joint tension strength batch II.

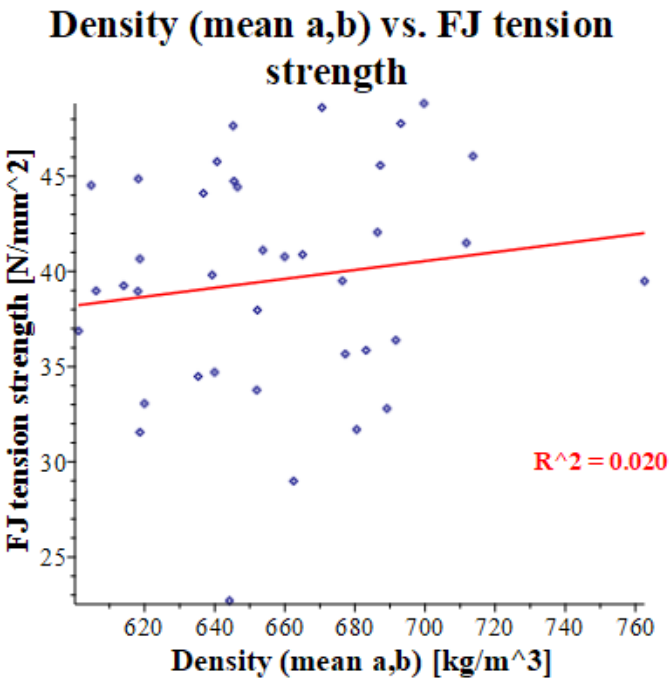

Figure 325: Scatterplot density (mean a,b) vs. finger joint tension strength batch II.

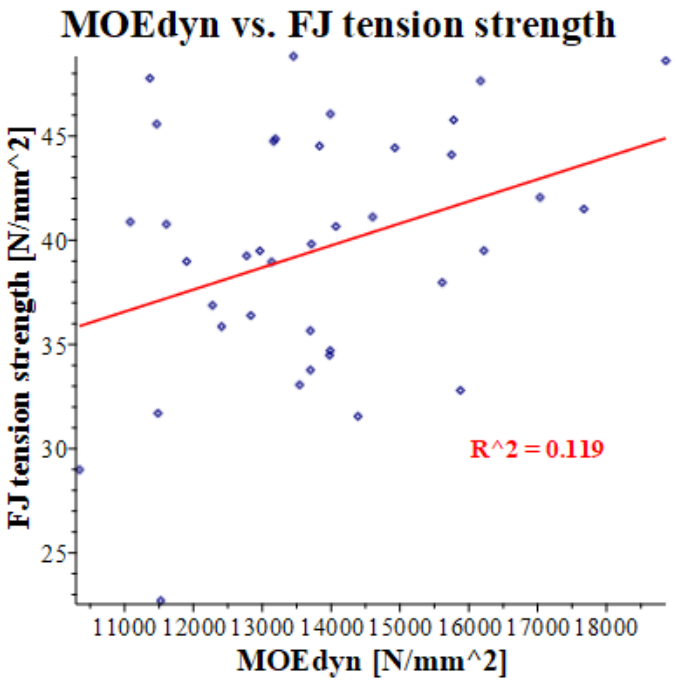

Figure 326: Scatterplot dynamic modulus of elasticity vs. finger joint tension strength batch II.

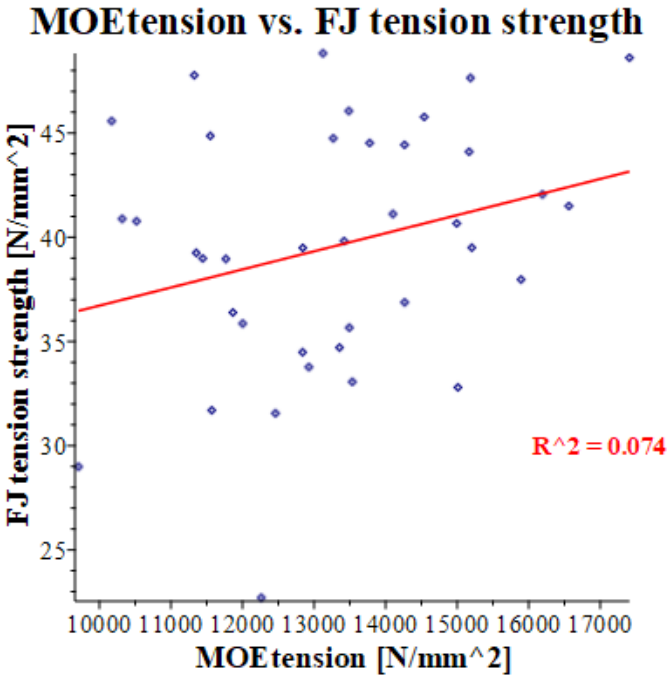

Figure 327: Scatterplot modulus of elasticity in tension vs. finger joint tension strength batch II.

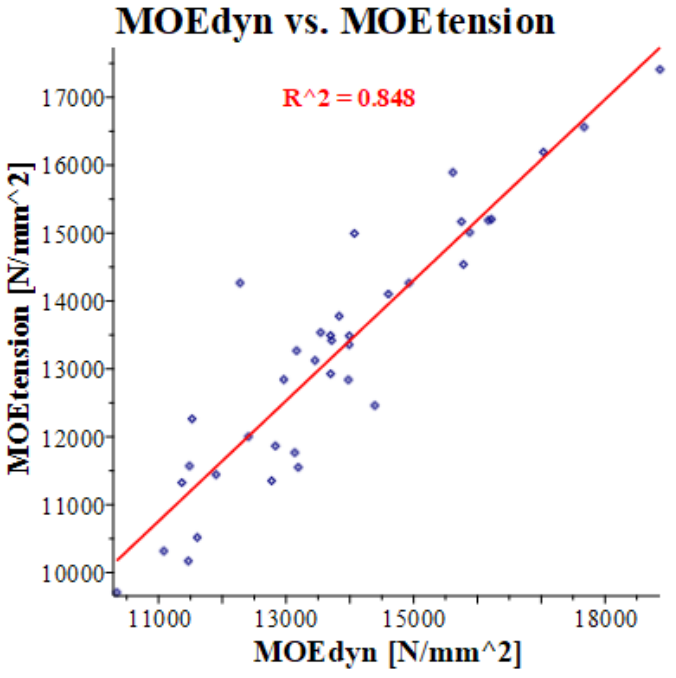

Figure 328: Scatterplot dynamic modulus of elasticity vs. modulus of elasticity in tension batch II.

Appendix 15: Batch IV scatterplots of relationships between mechanical and physical properties

This Appendix shows scatterplots of relationships between mechanical and physical properties, regarding the specimens of batch IV: see Figure 329 to Figure 339.

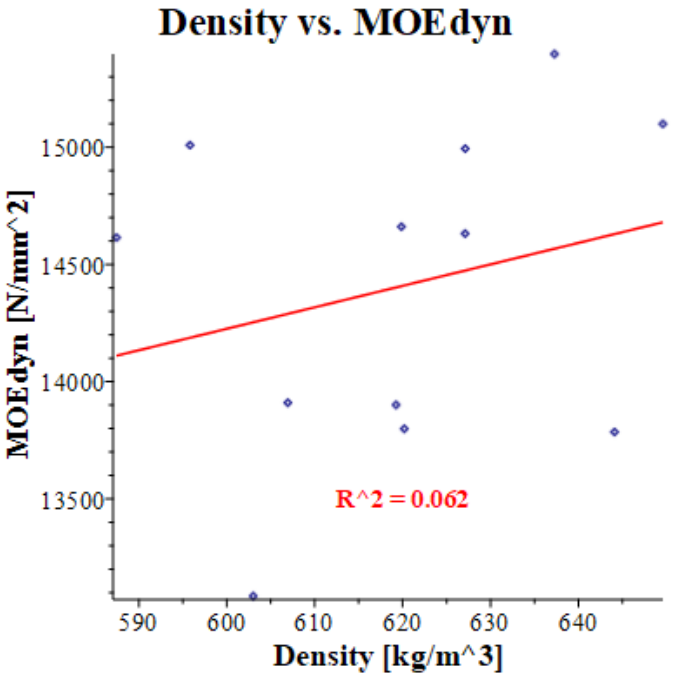

Figure 329: Scatterplot density vs. dynamic modulus of elasticity batch IV.

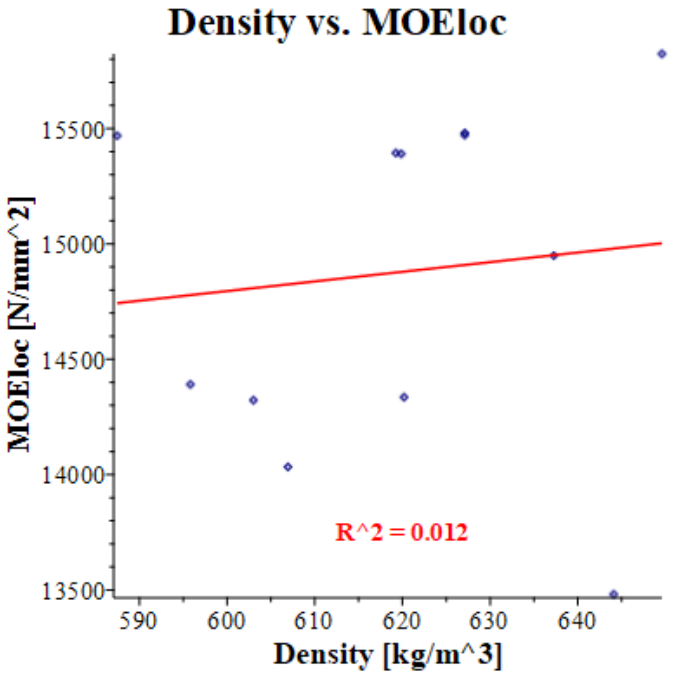

Figure 330: Scatterplot density vs. local modulus of elasticity batch IV.

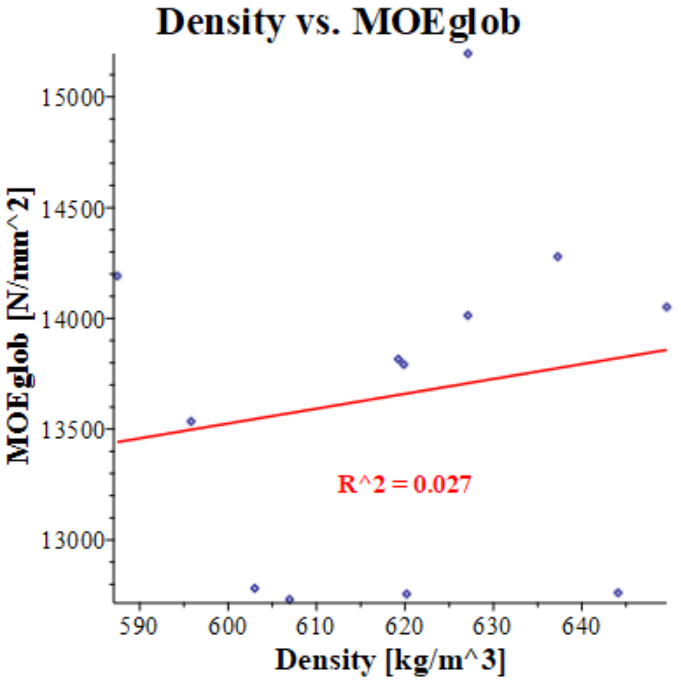

Figure 331: Scatterplot density vs. global modulus of elasticity batch IV.

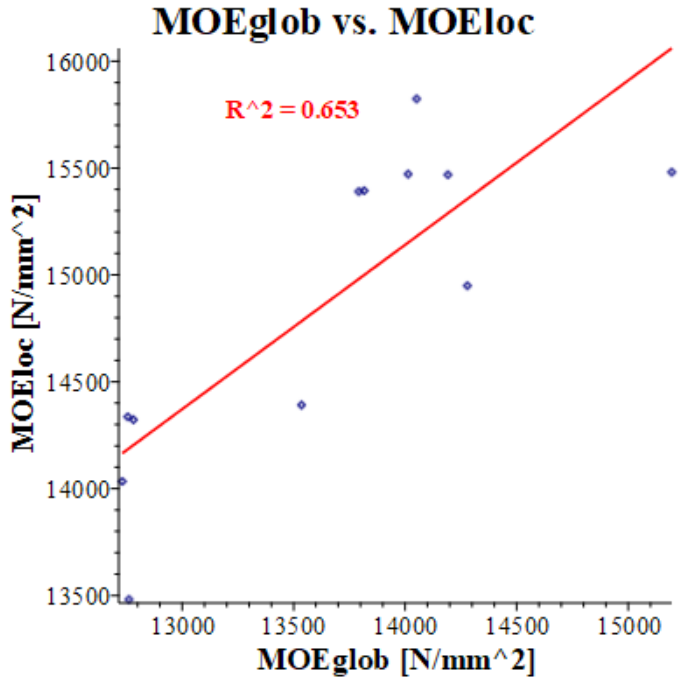

Figure 332: Scatterplot global modulus of elasticity vs. local modulus of elasticity batch IV.

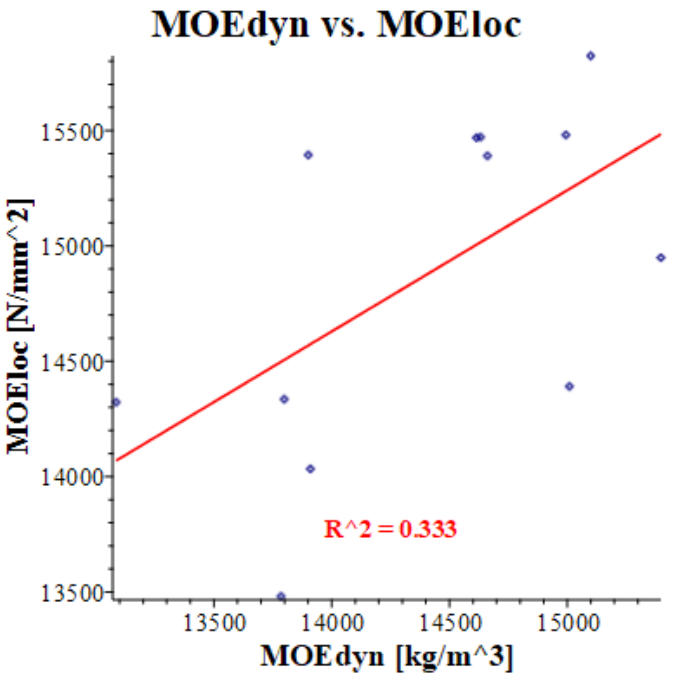

Figure 333: Scatterplot dynamic modulus of elasticity vs. local modulus of elasticity batch IV.

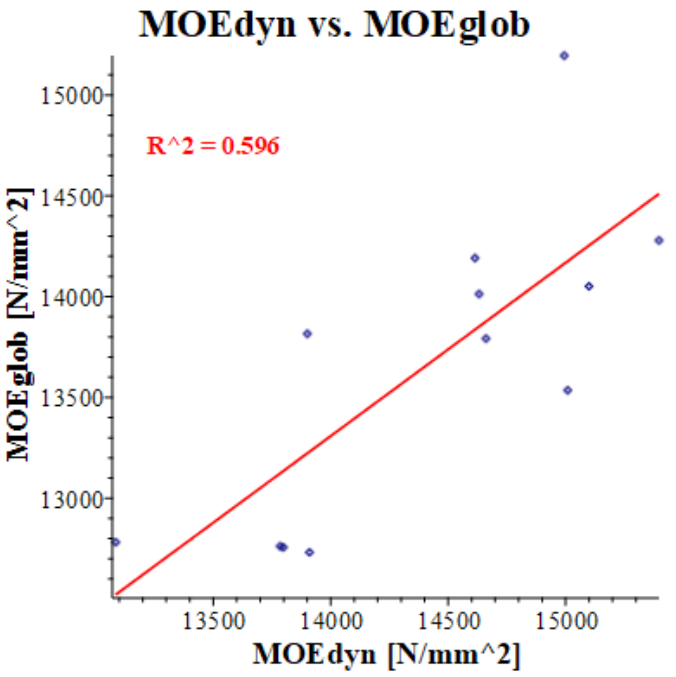

Figure 334: Figure 335: Scatterplot dynamic modulus of elasticity vs. global modulus of elasticity batch IV.

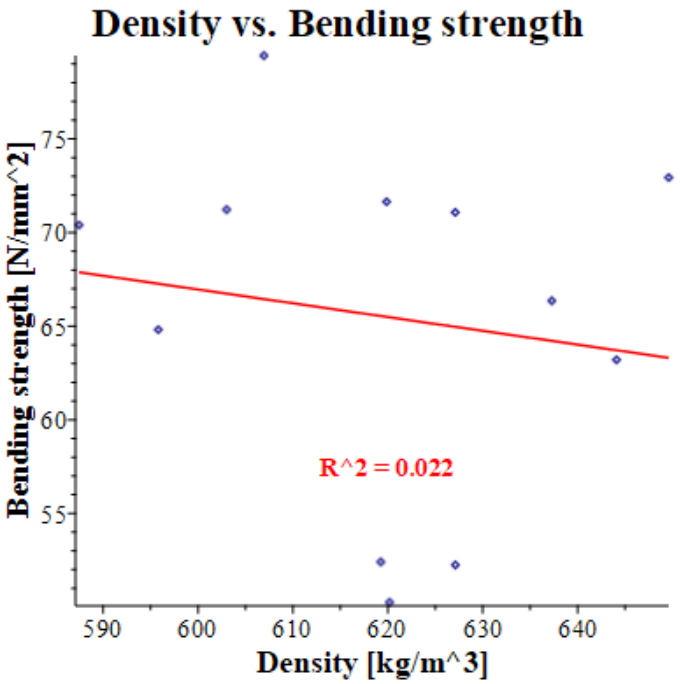

Figure 336: Scatterplot density vs. bending strength batch IV.

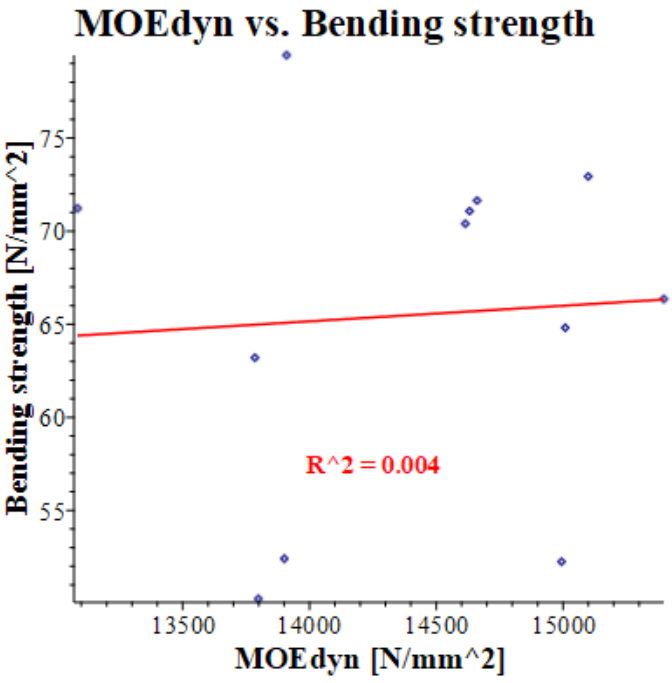

Figure 337: Scatterplot dynamic modulus of elasticity vs. bending strength batch IV.

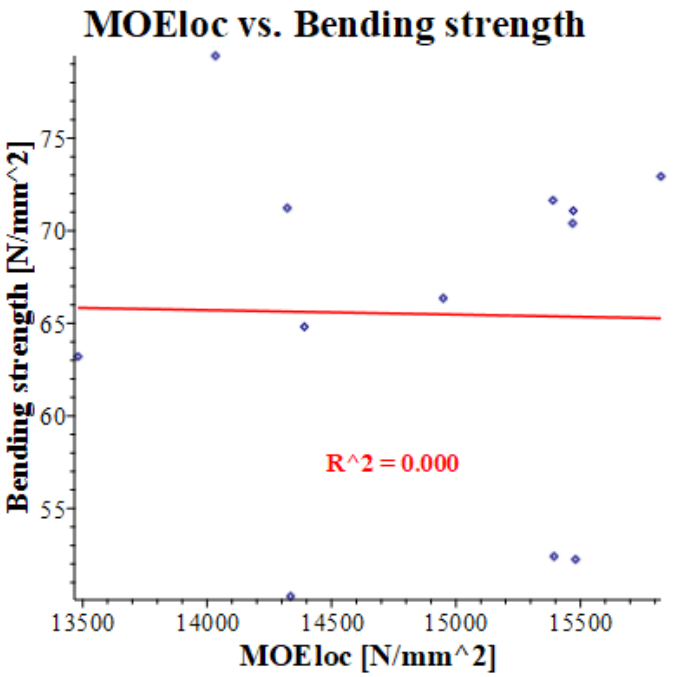

Figure 338: Scatterplot local modulus of elasticity vs. bending strength batch IV.

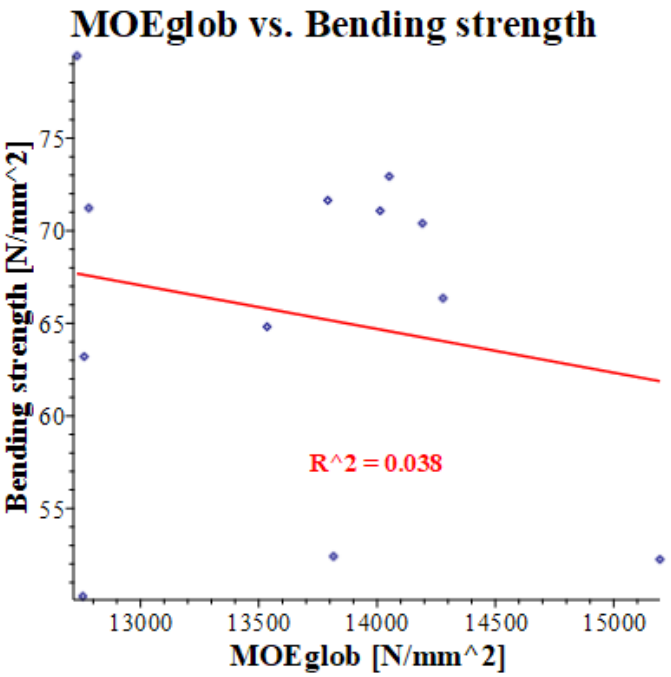

Figure 339: Scatterplot global modulus of elasticity vs. bending strength batch IV.

Soli Dei Gratia